Predicting Drug Disposition during Pregnancy through Modeling and Simulation

Ban Ke

A dissertation

submitted in partial fulfillment of the

requirements for the degree of

Doctor of Philosophy

University of Washington

2013

Reading Committee:

Jashvant D. Unadkat, Chair

Nina Isoherranen

Qingcheng Mao

Program Authorized to Offer Degree:

Pharmaceutics

Abstract

Physiological and ADME changes during pregnancy can significantly affect drug pharmacokinetics and may necessitate dose adjustment. Since it is logistically impossible to delineate the changes in PK of all drugs administered to pregnant women, alternative approaches that can generalize across drugs and predict drug disposition in pregnancy are highly-desirable. We developed and validated a novel PBPK model, which integrates gestational time-dependent changes in maternal physiology and hepatic CYP enzyme activities, preclinical and clinical data, to predict maternal pharmacokinetics of drugs cleared primarily by CYP3A (midazolam, nifedipine, indinavir), CYP1A2 (theophylline), CYP2D6 (metoprolol, paroxetine, dextromethorphan, clonidine), CYP2C9 (phenytoin), and multiple CYP enzymes (glyburide, methadone). We showed that our PBPK model can quantitatively predict the disposition during pregnancy of drugs cleared via single and/or multiple CYP pathways , and allow generalization beyond model drugs studied (e.g. midazolam) to other drugs with well-characterized ADME characteristics (e.g. indinavir). Moreover, our PBPK approach allowed us to bridge knowledge gaps that are difficult to test through clinical studies, for example, discerning the site (hepatic, intestinal, or both) of CYP3A induction in pregnancy. The coupled maternal-fetal physiology imposes additional concerns for both efficacy and safety of treatment. Fetal exposure to drugs not only depends on maternal pharmacokinetics, but also depends on placental passage of drugs. In this research, the gestational time-dependent contribution of the placental efflux transporter, P-glycoprotein, to drug distribution into the fetus, was quantified with PET imaging in a physiologically relevant model, the pregnant macaque. Such knowledge can be incorporated into a comprehensive fetal model in the future to predict fetal exposure to drugs. Taken together, the presented modeling approach can identify drugs whose pharmacokinetics may be altered

during pregnancy, guide rational PK study design, and support dose adjustment for pregnant women.

Dedication

This work is dedicated to my beloved parents, Yuyuan Ke and Zuofang Ren.

Acknowledgement

I owe my gratitude to many individuals whose contributions and support have made this dissertation possible, and because of whom my Ph.D. training experience has been one that I will cherish forever.

First, I must thank all of my committee members. Without their support and active participation in every step of the process, my dissertation project may not be a success. My deepest gratitude is to my advisor, Dr. Jashvant D. Unadkat. I have been extremely fortunate to have an advisor who inspired me to always achieve the best I can in every task, who sought every opportunity to develop my professional skills, who never failed to encourage me to overcome major setbacks during my Ph.D. training. I can never forget all his efforts of going the extra mile to identify a new research project that enabled me to work remotely at FDA in the last two years. I admire Jash's great vision, his willingness to take risks and his pioneering spirit. These qualities will have a profound and lasting impact on my professional career.

I must thank Dr. Nina Isoherranan for her sharp questions and critiques of my work. They have improved the depth of my knowledge and helped prepare me for addressing reviewers' comments on manuscripts. I am also thankful to her for carefully reading and commenting on countless revisions of my manuscripts.

I want to thank Drs. Qingcheng Mao and Gail Anderson for the generosity of their time, for providing their scientific and clinical expertise, and their active participation in shaping the directions of my project.

I must thank the department chair, Dr. Kenneth Thummel. Ken is the most generous person I have known. He always put the student's best interests first. I have benefited tremendously from his long-time support of my academic training in various forms, including covering my tuition expenses during my time at FDA. I am also grateful to the following staff at Department of Pharmaceutics, for their various forms of support during my graduate study—Dima Long, Kathy Hobson and Catherine Cole Rogers.

Part of my dissertation project was an interdisciplinary collaboration between the University of Washington, the Food and Drug Administration and Simcyp Limited. Such three-way collaboration may not be a success without the dedicated, persistent efforts of our co-investigators from FDA and Simcyp. My deep gratitude is to Dr. Srikanth Nallani for his support during my time at FDA, and for his guidance on identifying high-impact areas of model application within the context of regulatory science. I feel extremely fortunate and honored to work with Drs. Shiew Mei Huang and Ping Zhao, the thought leaders and pioneers of the use of PBPK modeling in regulatory science. My interactions with them have inspired me tremendously. I am also thankful to them for their critical review of my manuscripts and providing valuable regulatory perspectives.

I have been privileged to work with Prof. Amin Rostami-Hodjegan from University of Manchester, UK. Amin taught me metabolite kinetics with great patience through hundreds of email exchanges, shared a tremendous amount of data for my modeling need, and joined numerous teleconference for scientific discussions during his after-hours time. I am very much indebted to his generosity in sharing his state-of-the-art knowledge and insights on PBPK modeling.

I learned MATLAB from Simcyp collaborators Drs. Masoud Jamei and Gaohua Lu during the one-week visit at Sheffield, UK at the beginning of 2011. Since then, they have maintained prompt technical support on various aspects of modeling issues despite their busy job schedules. I am thankful to them for their time and attention.

I am indebted to each of these external/internal collaborators, who willingly provided clinical PK data for model validation: Drs. William J. Jusko (SUNY, Buffalo), Timothy Tracy (University of Kentucky), Uwe Fuhr (University of Cologne, Germany), Mia Wadelius (Uppsala University, Uppsala, Sweden) and Mary Hebert (University of Washington, Seattle).

My most sincere gratitude to my former and current labmates—Chris Endres, Huixia Zhang, Hsiao Peng, Brian Kirby, Aaron Moss, Li Liu, Sara Eyal, Faye Zhang and Bhagwat Prasad. I have had the greatest friendship with many of them and I will treasure the memories we had together as a team.

I appreciate the funding source from FDA's Office of Women's Health, and Simcyp visiting fellowship.

Most importantly, none of this would have been possible without the unconditional love and tireless support of my parents. My parents to whom this dissertation is dedicated to, has been a constant source of love, support and strength all these years. I would like to express my heart-felt gratitude to them for always giving me the freedom and encouragement to reach for my dreams, and for all their sacrifices at every stage of my personal and academic life. I deeply appreciate the generosity and understanding of my mother-in-law, Prof. Anna Peck. One of the best outcomes from these past five years is finding my best friend, soulmate, and husband, Maciej. These past five years have not been an easy ride. I truly thank Maciej for staying by my

side through the worst times. I believe that we both learned a lot about life and strengthened our commitment to each other and to live life to the fullest.

Introduction Chapter

Pharmacometrics in Pregnancy: an Unmet Need

* This chapter is to constitute an invited review article in the journal “Annual Review of Pharmacology and Toxicology",volume 54, 2013

Pharmacometrics in Pregnancy: an Unmet Need

1. Current status and need for clinical studies in pregnant women

Pregnant women and their fetuses are orphan populations with respect to the safety and efficacy of drugs. Latest statistics indicate that 64% of pregnant women ingest at least one medication for the treatment of a variety of clinical conditions, including viral (e.g., HIV), fungal or bacterial infections, smoking cessation, epilepsy or pregnancy-induced conditions such as hypertension, depression, and gestational diabetes (1, 2). The use of over-the-counter medications during pregnancy is also common. For example, in rural West Virginia 95.8% of pregnant women were administered prescription medications, 92.6% took over-the-counter medications, and 45.2% used herbal medicines (1). About 5 – 10% of pregnant women receive FDA category D or X drugs which are potential teratogens and the frequency of drug use is higher in early versus late pregnancy (2, 3). Illicit drug use by pregnant women in the United States has increased markedly over the past three decades (4-7). During 2007-2008, about 5.1% of pregnant women in the US reported illicit drug use [http://oas.samhsa.gov/nsduh/2k8nsduh/2k8Results.cfm]. Illicit drug use during pregnancy is a major risk factor for maternal morbidity and neonatal complications and necessitate therapeutic intervention with licit drugs (4). Moreover, a large percent of pregnant women who abuse drugs regularly are HIV positive and therefore need to be treated for this infection (e.g. HIV protease inhibitors) as well as drug abuse (e.g. methadone) (8).

Ethical, legal, and practical considerations often preclude enrollment of pregnant and lactating women in clinical trials. Despite the call to include pregnant women in drug trials in recent

years, there appears to be little movement in that direction. A survey of registered clinical trials at ClinicalTrials.gov, indicates only one drug—Makena (hydroxyprogesterone caproate)—has been approved by the FDA for pregnancy indications in the past five years (9). Drugs used in pregnancy are often developed informally, that is they are used for maternal disease, fetal disease (e.g., digoxin for fetal tachycardia) and placental dysfunction (e.g., malaria), after they are tested in the general population devoid of pregnant participants (10). As a result, although drugs are routinely prescribed during pregnancy, they are invariably prescribed off-label, i.e. without necessary clinical data about the dose, pharmacokinetics (PK), safety, or efficacy of these drugs in pregnant women. PK studies, when conducted in pregnant women, can be generally categorized into two types: opportunistic PK studies of drugs administered for therapeutic intervention purposes, and dedicated PK studies of drugs (e.g probe/model drugs to phenotype activity of a certain enzyme or transporter) for mechanistic understanding of PK changes. Opportunistic studies typically enroll pregnant patients chronically receiving a variety of dosing regimens. Since these studies do not impose additional risks to the study subjects as the subjects receive the drugs as part of clinical care, obtaining IRB approval is relatively easy. Either intensive or sparse PK (amenable to population PK analysis) sampling can be implemented. Dedicated PK studies of (probe) drugs are usually single-dose, intensive sampling PK studies performed in a small number of healthy pregnant women during pregnancy and postpartum, where the drugs are not used for therapeutic purpose. Enrollment can be challenging as subjects are likely more reluctant to participate due to fear of fetal toxicity, especially during the first two trimesters. Therefore, although difficult, such studies are mostly possible during the third trimester. With regard to PK data analysis, opportunistic studies, when

sampling is sparse, are amenable to population PK analysis, while the remaining PK studies, due to the small sample size, are often analyzed by classical non-compartmental analysis.

Considerable data demonstrate that the PK of drugs can be affected by pregnancy to a significant extent. Selective examples are presented in Table 1. Altered drug disposition in this special population may lead to either under-dosing or overdosing of medication with the standard adult dose, with varying consequences for safety and efficacy (11). For example, we found that the oral clearance of the HIV protease inhibitor, indinavir, is 3.8-fold higher during pregnancy than post-partum (or in non-pregnant women or men) (12). This induction resulted in sub-therapeutic indinavir plasma concentrations which could result in breakthrough of resistant virus resulting in progression of disease in the mother, and perhaps higher incidence of maternal-fetal HIV transmission and transmission of resistant virus to the baby. We have also shown that the apparent oral clearance of glyburide (used to treat gestational diabetes) is 2-fold greater in pregnant women with gestational diabetes mellitus than in non-pregnant women with type II diabetes mellitus (13). Thus determining the magnitude of change in PK caused by pregnancy is important to design rationale dosing regimen of drugs for pregnant women. However, it is neither feasible nor desirable to perform extensive PK studies in pregnant women (including fetal exposure) of all the drugs consumed by this vulnerable population. Therefore, alternate approaches are required. One such approach is to conduct focused studies that shed light on the mechanisms by which pregnancy alters maternal drug disposition. Probe drugs (indicated as * in Table 1) are drugs commonly used to probe *in vivo* enzyme or transporter activity, as they are selective substrates of a single enzyme or transporter (either for total clearance or formation clearance of a metabolite excreted in the urine). Therefore, probe drug studies are more

informative in delineating the hepatic enzyme activity during pregnancy, compared to non-probe drugs, and the information generated can be used to predict the anticipated change in systemic exposure to non-probe therapeutic drugs during pregnancy. Of course, this is possible only if the ADME characteristics of the non-probe drugs are well-characterized, such as the fractional contribution of the enzyme or transporter towards the total clearance of the drug. For such predictions to be successful, information on physiological changes that could affect the ADME of the drug also needs to be taken into consideration. Since the latter are multidimensional (e.g. simultaneous and time-dependent changes in volume of distribution, plasma protein binding, cardiac output, renal function; see below under Section 2), the most efficient methodology for incorporating such prior knowledge to predict appropriate dosing regimens of drugs during pregnancy is through physiologically-based pharmacokinetic (PBPK) modeling (see below under Section 4.3) .

The coupled maternal-fetal physiology imposes additional concerns for both efficacy and safety of treatment. Recommendation of dose adjustment in this population should also be carefully evaluated in terms of assessing the risk of fetal exposure to drugs administered to the mother. This is because the teratogenic or fetal toxicity potential of the drug is usually not known. Therefore treatment should also target to minimize fetus exposure to drugs, except in the cases such as treating fetal conditions or HIV infection, where fetal exposure to drugs is important for therapeutic reasons (14).

2. Review of physiological changes during pregnancy

Pregnancy is associated with a multitude of temporal physiological and metabolic changes. The mean change of physiological parameters in each trimester, based on a comprehensive meta-analysis of literature data obtained from adult healthy women (15), are summarized in Table 2. The causative mechanism of these changes is poorly understood and most of them are believed to be regulated by pregnancy-related hormones. A number of these changes in maternal physiology can have a direct effect on drug absorption, distribution, metabolism and excretion as discussed in greater detail below.

Absorption

Intestinal absorption of drugs may be affected, theoretically, in pregnancy by alterations in gastric motility and gastric pH. However, limited data in literature do not appear to support a significant reduction in gastric motility or increase in gastric pH (15). Moreover, the rate of drug absorption does not appear to be altered to a significant extent as a result of any of these changes in pregnant women, as suggested by similar antepartum vs. postpartum/non-pregnant T_{max} values and none-to-modest changes in the half-lives of drugs (12, 16, 17). However, the extent of pre-systemic elimination (by enzymes or transporters) might be greater or lower, depending on the contributing pathway towards elimination of the drug (e.g. CYPs or transporters), which then results in a lower (more likely) or higher C_{max} in this population. Distinguishing changes in intestinal metabolism/transport (or overall bioavailability of the drug) from changes in systemic elimination is difficult unless the drug can be administered by both IV and the oral route to the pregnant and postpartum woman. Most pharmacokinetic studies in pregnant women are conducted after only oral administration of drugs.

Table 1. Summary of pregnancy-induced effects on pharmacokinetics of clinically used drugs

Drugs/probes	Indication	Effect on oral clearance (%) [a]			Metabolizing enzyme activity changes	Ref
		1st Trimester	2nd Trimester	3rd Trimester		
Caffeine *	CNS stimulant	↓ 33	↓ 48	↓ 65	↓ CYP1A2	(18)
Theophylline	Asthma	↔	↔	↓ 34		(19)
Nicotine	Smoking cessation	NA	↑ 54	↑ 54	↑ CYP2A6	(20)
Phenytoin *[b]	Antiepileptic	↑ 43	↑ 51	↑ 61	↑ CYP2C9	(21)
Proguanil	Antimalarial	NA	↓ 60	↓ 60	↓ CYP2C19	(22)
Metoprolol *	Antihypertensive	NA	NA	↑ 459	↑ CYP2D6	(23)
Dextromethorphan [b]	Antitussive	↑ 26	↑ 35	↑ 48		(18)
Midazolam *	Anxiolytic	NA	NA	↑ 99	↑ CYP3A4	(16)
Indinavir	Antiretroviral	NA	NA	↑ 277		(12)
Glyburide	Antidiabetic	NA	NA	↑ 106		(13)
Methadone	Addiction	NA	↑ 101	↑ 65	↑ CYP2B6	(24)
Labetalol	Antihypertensive	NA	↑ 30	↑ 30	↑UGT 1A1	(25)
Lamotrigine	Antiepileptic	↑ 200	↑ 200	↑ 300	↑UGT 1A4	(26)
Zidovudine [c]	Antiretroviral	NA	NA	↔	↔ UGT2B7	(27)
Amoxicillin	Bacterial infection	NA	↑ 23	↑ 20	↑ Renal CL	(28)
Metformin *	Antidiabetic	↑ 22	↑ 28	↑ 11		(29)
Digoxin *	Cardiac diseases	NA	NA	↑ 19		(16)

a: Mean percentage change relative to postpartum value.
↓ indicates decrease; ↑ indicates increase; ↔ indicates no effect; NA: data not available
*: indicates probe drug commonly used to measure specific hepatic enzyme activity or transporter activity *in vivo*
b: Phenytoin data is based on plasma trough concentration (total). Dextromethorphan data is based on urinary metabolic ratio (dextromethorphan/dextrorphan).
c: Morphine IV clearance (mediated by UGT2B7), determined at time of delivery, was found to ↑ 59% compared to non-pregnant control data (30), suggesting increased UGT2B7 activity and/or increased hepatic blood flow.

Table 2. Summary of pregnancy-induced changes in maternal physiology

Parameters	1st Trimester [a]	2nd Trimester [a]	3rd Trimester [a]
Total body weight (kg)	↑ 6%	↑ 16%	↑ 23%
Total fat mass (kg)	↑ 11%	↑ 16%	↑ 32%
Total body water (L)	↑ 11%	↑ 27%	↑ 41%
Cardiac output (L)	↑ 18%	↑ 28%	↑ 33%
Plasma volume (L)	↑ 7%	↑ 42%	↑ 50%
Red Blood Cell Volume (L)	↑ 4%	↑ 20%	↑ 28%
Hematocrit (%)	↓ 3%	↓ 8%	↓ 14%
Albumin (g/L)	↓ 5%	↓ 16%	↓ 31%
α1-acid glycoprotein (g/L)	↓ 1%	↓ 22%	↓ 19%
Glomerular filtration rate (mL/min)[b]	↑ 19%	↑ 37%	↑ 40%
Effective renal plasma flow (L/h)	↑ 38%	↑ 48%	↑ 31%
Creatinine clearance (mL/min)	↑ 28%	↑ 58%	↑ 26%
Uterine blood flow (L/h)	↑ 923%	↑ 1567%	↑ 2771%
Hepatic blood flow (L/h) [c]	↔	↔	↔

a: Mean percentage change (%) relative to pre-pregnancy level.
↓ indicates decrease; ↑ indicates increase; ↔ indicates no effect.
b: GFR measurement is based on inulin clearance
c: literature data on hepatic blood flow is contradictory, hence no effect is assumed.
Data sources are provided in reference (15).

Distribution

Various pregnancy-related hemodynamic changes lead to increased plasma volume (up to 50%) and decreased plasma protein binding, which can alter the apparent volume of distribution (V_d) of drugs (31). Serum albumin and α1-AGP concentrations decrease up to 31% and 19% during late pregnancy (15). Consequently, the change of unbound plasma fraction of highly-bound drugs during pregnancy can be as much as ~30% (e.g. phenytoin) (32). Pregnancy-related changes in activity of transporters expressed in various tissues/organs (liver, kidney, brain, placenta, etc) may also affect V_d of drugs. However such changes, with the exception of renal transporters, are extremely difficult to quantify *in vivo*. Most mechanistic studies are restricted

to placental transporters such as P-glycoprotein and breast cancer resistance protein (33). These placental transporters can modulate the exposure of the fetus to drugs even when the exposure of the mother to the drug is not affected. However, given the small size of the fetus, distribution of drugs into the fetus is not expected to alter maternal PK significantly. It is important to note that, in the literature, the reported change in apparent V_d (V_d /F) of oral drugs during pregnancy may result from the physiological changes of pregnancy affecting V_d or oral bioavailability. The two effects cannot be easily dissociated (except when the drug is administered IV) and data should be interpreted with caution. Through changes in V_d and clearance, pregnancy can cause an increase or a decrease in the terminal elimination half-life of drugs.

Clearance

Changes in IV clearance of drugs may result from changes in hepatic blood flow, protein binding, or hepatic intrinsic clearance. Based on well-stirred model of hepatic elimination, an increase in hepatic blood flow would result in increased clearance after intravenous administration for a high extraction-ratio drug. Despite a marked one third increase of cardiac output during pregnancy, little is known about changes in hepatic blood flow and the existing data in literature, using various techniques such as indocyanine green clearance and Doppler ultrasonography are contradictory (15). Due to this inconsistency in literature data, we have assumed pregnancy has no effect on hepatic blood flow, as shown in Table 2. Since most drugs administered to pregnant women are given orally, changes in oral clearance of drugs are likely due to altered hepatic enzyme/transporter activity and/or decreased plasma protein binding of drugs. The majority of PK studies in pregnant women have focused on CYP activity (see Table 1). The change in maternal hepatic enzyme activity is CYP isoform specific. Several groups

have utilized model (probe) drugs that report CYP enzyme activities to delineate the magnitude of change in activity of major CYP enzymes, mostly during the third trimester (e.g. caffeine for CYP1A2, midazolam for CYP3A, metoprolol for CYP2D6, phenytoin for CYP2C9) (31) (see Table 1) For example, the metabolism of drugs catalyzed by selective CYP isoenzymes (i.e. CYP3A4, 2D6 and 2C9) and UGT isoenzymes (i.e. UGT1A4 and 1A1) is increased during pregnancy. In contrast, CYP1A2 and 2C19 activity is decreased during pregnancy (31). The magnitude of pregnancy-related induction in drug metabolizing enzyme activities can be as high as 300% as suggested by lamotrigine PK (26).

The renal excretion of unchanged drugs is increased during pregnancy due to increased glomerular filtration rate and also possibly increased renal secretion via transporters (31). Renal secretion clearance mediated by organic cation transporter and P-glycoprotein is increased by 50% and 120% during T_3, based on metformin $CL_{secretion}$ (29) and digoxin $CL_{secretion}$ (16). However, it is important to point out that despite these significant increases in renal clearance of drugs, they do not always translate into a significant increase in apparent oral clearance as secretion is not the only route of elimination of the drug. For example, the reported increase in oral clearance of metformin and digoxin is less than 30% throughout pregnancy (Table 1).

3. Mechanistic basis of changes in CYP and UGT activity

The underlying mechanism for the hepatic isoform-specific and gestational state specific induction of CYP or UGT enzymes during pregnancy is not fully understood. Generally speaking, the increased or decreased enzyme expression/activity is through regulation of the respective transcript level, as opposed to protein stabilization. Activation of nuclear receptors

and transcriptional factors, possibly mediates these effects, in a manner similar to enzyme induction by xenobiotics (31). Further, the transcriptional regulation of drug metabolizing enzymes during pregnancy is linked to drastically-elevated concentrations of various hormones up to 100-fold in maternal blood, including placental growth hormone (PGH), progesterone, corticosteroids and estrogens (Jeong, 2010). Specifically, in human hepatocytes, estradiol enhances the expression and activity of CYP2A6, CYP2B6, CYP2C9 and CYP3A4. Progesterone can enhance CYP2B6, CYP3A4, CYP2A6 and CYP2C8 expression, but to a smaller extent compared to estradiol (Choi et al., 2012; Dickmann and Isoherranen, 2012). In a study from our laboratory, the combined treatment with all the pregnancy-related hormones, at their unbound plasma concentrations during the third trimester, induced CYP3A activity by ~2-fold, a value that matches the observed *in vivo* (midazolam clearance) (34). Estradiol down-regulates CYP2C19 mRNA expression by ~ 30% in human hepatocytes (35). Interestingly, incubating estradiol and progesterone, with human and rat hepatocytes does not affect CYP1A2 mRNA expression or activity (36, 37). Alternatively, CYP1A2 may be down-regulated by cytokines. The increase in CYP2D6 activity during pregnancy is intriguing because 2D6 is not inducible by xenobiotics. Until recently, the mechanisms for CYP2D6 induction during pregnancy remained unknown. Mouse data suggest the changes of CYP2D6 activity observed during human pregnancy could be replicated in the mouse, and the transcriptional regulation of Cyp2d in mice could be mediated by retinoic acid signaling (38). The up-regulation of UGT1A1 and 1A4 may potentially be mediated by estradiol and progesterone (39). Taken together, these mechanistic studies provide a potential explanation for the mechanisms by which certain CYP and UGT activities are increased and certain CYP activities are decreased during pregnancy. Once the concentration-dependent induction or suppression relationship (i.e. EC_{50}

and E_{max}) is established *in vitro* for these CYP and UGT isoforms, the prediction of the magnitude of enzyme induction or suppression *in vivo* at gradually rising concentration of specific hormones in plasma in each trimester will be possible. Of course, if a combination of hormones is required for induction, the studies will need to be more complex.

Mechanistic studies of pregnancy related hormones and their impact on transporter expression is limited. One study reported decreased level of expression of the rat multidrug resistance protein 2 (MRP2) on the canalicular membrane of hepatocytes during pregnancy and following the administration of ethinyl estradiol (40). The oral absorption and hepatobiliary elimination of azithromycin are mediated in part by efflux transporters, MRP2 and P-glycoprotein. This mechanistic study suggests a role for MRP2 in the hormone-mediated changes in the hepatobiliary clearance of azithromycin observed *in vivo* (see section 4.2).

4. Modeling and Simulation Methodology

In consideration of the ethical and logistical barrier to include pregnant women in clinical trials, modeling and simulation (M&S) to study the disposition of xenobiotics in mother-fetus has emerged as a promising approach to guide dose adjustment in pregnancy to ensure adequate efficacy and to prevent undesirable toxicity (28, 41). The pharmacometric tools that support PK analysis most applied to the special population of pregnant women include noncompartmental analysis (NCA), population PK analysis (PPK), physiologically-based pharmacokinetic modeling (PBPK) and semi-mechanistic modeling (SMPK). The role of each of these tools in study design and analysis is described, as well as the pros and cons of each methodology. The impact of each methodology is illustrated using a range of case examples.

4.1. Non-compartmental analysis (NCA)

NCA is a data-driven method of analysis that requires densely sampled PK data in order to empirically calculate integral measures (moments) such as the area-under-the-concentration-time curve (AUC). These can then be used to obtain estimates for valuable PK parameters such as clearance (CL or CL/F), volume of distribution (V_d or V_d/F) and half-life. The peak concentration (C_{max}), trough concentration (C_{min}), and the time at which the peak concentration occurs (T_{max}) are usually determined by direct inspection of data. NCA-based methods work mainly for dedicated PK study in pregnant women such that the PK data are dense enough to reliably estimate the above parameters for each individual. Moreover, few prior assumptions are made in the calculation of PK parameters.

The majority of PK studies conducted in pregnant women to date are dedicated PK study with intensive sampling and data are analyzed by NCA approach. For example, collective efforts between academicians, clinicians and industrial scientists have made significant progress in understanding the disposition of antiretrovirals for the prevention of mother-to-child HIV transmission during pregnancy and after birth (42). Almost all studies assessed steady-state 24-hour pharmacokinetic profiles during the third trimester and/or second trimester and during postpartum. Maternal and umbilical cord blood samples are usually also obtained at delivery to assess placental transfer of these drugs. All protease inhibitors (PIs) studied to date show decreased exposure during pregnancy, compared with nonpregnant adults, including atazanavir, fosamprenavir, indinavir, lopinavir, nelfinavir, ritonavir, and saquinavir, when standard doses of these drugs are administered (42). Among these PIs, lopinavir (50% prescription rate) and atazanavir (25%) are the most frequenty prescribed to HIV infected pregnant women (14). For

example, the plasma AUC of unboosted indinavir is 68% lower during pregnancy compared to postpartum (12), although when indinavir is boosted with ritonavir, trough concentrations during pregnancy appear adequate (43). Saquinavir plasma AUC, C_{min} and C_{max} with use of a ritonavir boosted regimen (saquinavir 1200 mg/ritonavir 100 mg once daily are reduced during pregnancy compared to nonpregnant women, but adequate saquinavir trough concentrations are achieved in 93% of pregnant subjects (44). Lopinavir plasma AUC is reduced by 50% when administered during the third trimester as capsules at standard dosing (lopinavir 400 mg/ritonavir 100 mg twice daily) and that administration during the third trimester of an increased dose as either capsules (lopinavir 533 mg/ritonavir 133 mg twice daily) or tablets (lopinavir 600 mg/ritonavir 150 mg twice daily) results in lopinavir AUC equivalent to that seen in nonpregnant adults with standard dosing (45). During the third trimester, atazanavir median plasma AUC and C_{min} are reduced by 30-34 % at standard dosing (atazanavir 300 mg/ritonavir 100 mg once daily) compared with postpartum and are reduced both during pregnancy and postpartum by an additional 25% when coadministered with tenofovir (46). Lastly, several studies have shown that nelfinavir (1250 mg) plasma AUC and C_{min} are reduced during the second and third trimester (47).

For many of these PIs, there is an established relationship between AUC or C_{min} of the PIs and virologic response. Therefore, achieving equivalent AUC and/or C_{min} of PIs in pregnant women is the primary goal of therapeutic drug monitoring programs in pregnant women. Many of these PIs share common PK characteristics including: mainly metabolized by CYP3A4, with lesser contributions by CYP2C9, 2C19, 2D6; plasma protein binding of >85% for the available protease inhibitors (except indinavir); highly-variable bioavailability due to poor absorption

(solubility, active transport in enterocytes), and complex DDI due to induction, inhibition and inactivation of CYPs (42). Pregnancy may reduce exposure of a PI by a direct effect on its disposition, by an indirect effect through reduction of exposure to the booster, ritonavir, and therefore its inactivation of PI's metabolism, or by a combination of both mechanisms. Given these complications, it is not surprising that pregnancy effect on the disposition of PIs is highly variable. Quantitative prediction of the pregnancy's effect on the disposition of PIs, in the presence of ritonavir, is difficult. Nevertheless, mechanistic modeling such as PBPK approach can be useful in predicting the disposition of a PI when given without ritonavir, as illustrated for indinavir (48) (see chapter 1).

4.2. Population PK analysis (PPK)

When a dedicated PK study in pregnant women is logistically difficult to conduct, population PK approach offers a less restricted study design such as sparse sampling. The advantage of sparse-sampling strategy is that missed clinic visit or time limitations have less impact on study integrity. PPK models allow simultaneous estimation of mean population PK parameters, as well as between-subject variability and residual unexplained variability (e.g. assay variation) (49). The structural (base) model used in PPK analysis is usually one-, two- or three-compartmental models. Once the structural (base) model is identified, covariates can be incorporated to understand the influence of demographic and clinical information including body size measures (total or lean body weight, body mass index, etc), categorical variables (such as pregnancy state, concurrent medication, disease state, etc), and continuous variables (gestational age, creatinine clearance, serum albumin, dose, etc) on PK parameters (40). Model validation is usually achieved by bootstrap analysis and visual predictive check. A limitation of PPK

analysis, is that because PPK study conditions are less controlled (compared to dedicated PK studies), the reported time for subjects to take their doses and recorded blood sampling time may not be as accurate as one may wish. Also since PK samples are usually collected during clinic visit, they tend to cluster around certain time windows (such as in the morning) but not enough PK samples in other time windows. PPK analysis can be employed prospectively or retrospectively to analyze PK samples collected according to a sparse sampling strategy from pregnant women and/or from non-pregnant women receiving the same drug treatment. In literature, PPK approach has been widely used for anti-malaria drugs (see below) and sometimes for anti-viral drugs (50). The studies of anti-malarials are usually conducted in the remote areas where study conditions are challenging. Previous studies reported that artesunate, artemether, dihydroartemisinin, sulfadoxine, atovaquone, progunanil, cycloguanil, pyrimethamine and lumefantrine concentrations and cure rates are lower in pregnant women compared with non-pregnant adults of child bearing age (11). A meta-analysis by McGready *et al* (51) showed that 9 out of 12 included PK studies recommended dose-optimization in pregnant women with malaria.

One interesting case is azithromycin (AZ), an azalide antibiotic with antimalarial activity that is considered safe in pregnancy. AZ is also among 15 most frequently prescribed drugs to pregnant women and is commonly administered for community acquired respiratory, skin and gynecological infections (2). AZ has incomplete oral absorption (34%), extensively distributes into tissues, and is eliminated by hepatobiliary excretion mediated in part by P-glycoprotein and multidrug resistance protein-2 (MRP-2) (40). The understanding of pregnancy effect on these hepatic transporters is limited. In one study, two 2 g doses were given 24 h apart to 31 pregnant and 29 age-matched nonpregnant Papua New Guinean women. The only significant relationship

between the PK of the drugs and a range of potential covariates, including malarial parasitemia, was with pregnancy, which accounted for an 86% increase in the apparent volume of distribution of the central compartment (V_c/F). The plasma $AUC_{0-\infty}$ was similar for pregnant and nonpregnant subjects. Based on this study no dose adjustment was proposed for pregnant women (41). In a more recent study conducted in an urban population in the US, the population analysis included 53 pregnant and 25 nonpregnant women. Lean body weight, pregnancy, ethnicity, and the coadministration of oral contraceptives were covariates identified as significantly influencing the oral clearance of AZ. Compared to nonpregnant women not receiving oral contraceptives, a 21% to 42% higher dose-adjusted AZ AUC occurred in non-African American women who were pregnant or receiving oral contraceptives. The authors proposed that although higher levels of maternal and fetal AZ exposure suggest that lower doses be administered to non-African American women during pregnancy, consideration of AZ pharmacodynamics during pregnancy should guide any dose adjustments. Potential immunological changes in pregnant women (which may alter the bacterial responsiveness to AZ) and a limited understanding of safety of fetal AZ exposure warrant further studies to determine the clinical implications of the observed PK differences. These two examples illustrate the utility of PPK approach in providing appropriate estimates of pharmacokinetic parameters as well as identifying important covariates contributing to pharmacokinetic variability in women of childbearing age.

4.3. Physiologically-based PK modeling (PBPK)

While the above two methods are used to analyze PK data from studies conducted in pregnant or non-pregnant women, they cannot efficiently predict an appropriate dosing regimen of a drug to

use during pregnancy. This is because they do not readily incorporate the multidimensional changes in physiology produced by pregnancy that can affect the ADME of a drug (e.g. volume of distribution, renal function). In contrast, PBPK models can. PBPK models are multi-compartmental models that aim to describe major human tissues and organs in a mechanistic manner. Under the overarching umbrella of "Systems Pharmacology", PBPK modeling has the advantage of incorporating both physiological parameters (such as tissue blood flow, tissue composition, glomerular filtration rate, etc) that are important for the absorption, distribution, metabolism and elimination (ADME) processes and drug-specific parameters (e.g. physico-chemical and drug disposition characteristics) into a quantitative predictive model (52, 53). PBPK has been used in drug development and regulatory review (54). The separation of drug and system-dependent variables (53) offers many advantages in comparison to other M&S platforms in that the structural model and system-specific parameters are "generic" as they remain the same for a given population while drug-specific parameters are over-laid onto the system model (52) making "extrapolation" from one drug to another drug possible; the structural model is mechanistic and integrative and users can incorporate the effect of multiple "extrinsic" or "intrinsic" patient factors on drug disposition (54), making this approach particularly useful in the case of pregnant population when a multitude of pregnancy-related physiological changes on the ADME of drugs is expected.

Because of the complexity of PBPK models, they require rich experimental data and often rely on *in silico* prediction tools to obtain required physiochemical or ADME parameters. Since drug-specific parameters may not always be available, assumptions are often made based on general knowledge. Thus it is important to validate model predictions with available data. For example,

validation of the drug-specific parameters using i.v. and p.o. data obtained in the non-pregnant population is necessary to demonstrate adequacy of the model in non-pregnant adults. It is also necessary to assess the sensitivity of model predictions to changes in system model key parameters.

Many of the existing PBPK models developed to model maternal-fetal disposition have typically focused on toxicokinetics and risk assessment of environmental chemicals. Lu et al. provided a systematic review of the existing human or animal PBPK models in literature (55). These models considered the dynamic changes of physiological parameters including tissue volume, blood flow rate in the maternal body and the growth of the placental-fetal unit. However, few models accounted for pregnancy-induced changes in ADME of drugs (55). As reviewed previously, pregnancy effect on the ADME processes of drugs, particularly the metabolism and elimination of drugs can be profound and therefore cannot be neglected. For example, the midazolam model developed by Andrew et al., sought to account for time-dependent physiological changes due to gestation (56). The developed model consists of 20 maternal compartments and 16 fetal compartments. Due to lack of data on fetal physiology, many assumptions were made to incorporate a detailed fetal structure. By assigning intrinsic clearance calculated from reported midazolam IV clearance in non-pregnant and postpartum subjects, the authors demonstrated the feasibility of their PBPK model in assessment of midazolam disposition during pregnancy.

More recently, a meta-analysis of literature data on the pregnancy-induced physiological and metabolic change in healthy pregnant woman was carried out (15). Based on this work, Lu et al. proposed to extend the perfusion-limited form of a 13-compartment PBPK model used for the

non-pregnant population to the pregnancy population, by applying known maternal physiological changes to all model components (57) (Fig. 1). These included gestational weight gain, plasma protein and lipid concentration, individual organ/tissue volumes and blood flows, glomerular filtration rates, and hepatic enzyme activity changes (CYP1A2, 2D6 and 3A). A lumped placental-fetal component was added to the model to represent the placenta, fetal organs and the amniotic fluid. Such simplification reduces the uncertainty stemming from fetal physiological parameters. Changes in these CYP activities were described based on urinary metabolic ratio (UR) of dextromethorphan (DEX; CYP3A and 2D6) and salivary caffeine clearance (CYP1A2). While DEX UR is an acceptable measure of CYP2D6/3A for the non-pregnant population, it is not an adequate measure of these activities in the presence of CYP induction such as during pregnancy (58). This is because metabolic ratios are known to be dependent on changes in the renal function (59), which is likely to be induced during pregnancy alongside any induction of CYP2D6 and 3A. For the reasons outlined, it is important to rigorously validate the presumed changes in specific CYP activity in the developed PBPK model through model prediction for multiple drugs cleared by the respective CYP. Therefore, the PBPK model of Lu et al. (57) needs to be expanded to incorporate pregnancy-induced change in other major CYP activity such as CYP2C9, CYP2B6 and CYP2C19 (see section 6). Further *in vitro* and *in vivo* studies of drug metabolism and transport during pregnancy are also required to fully populate the model (see section 6).

Fig. 1

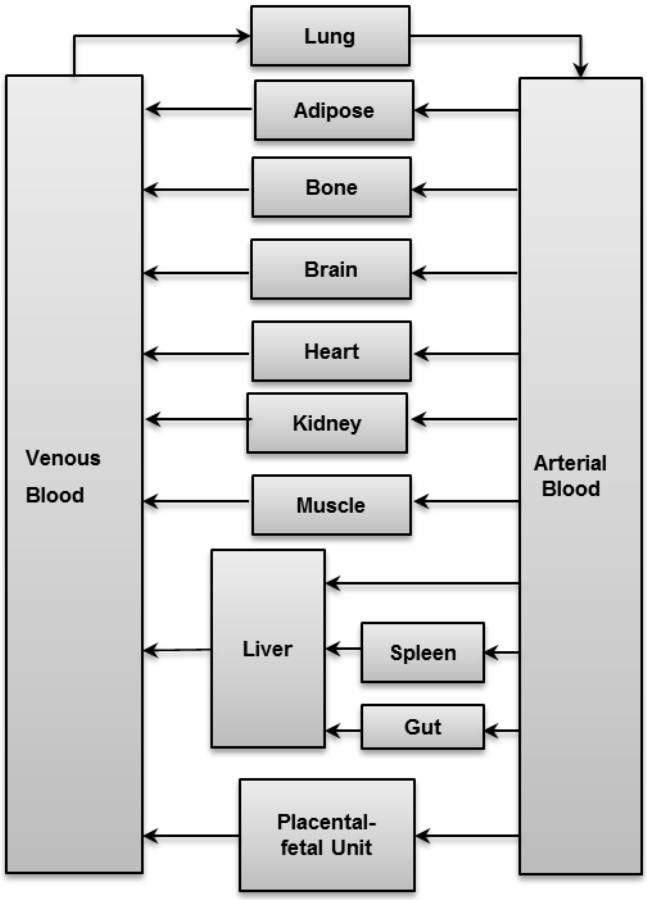

4.4. Semi-mechanistic pharmacokinetic Modeling (SMPK)

Semi-mechanistic pharmacokinetic model is usually based on standard one- or two compartment models, while incorporating both hepatic and/or intestinal metabolism. This approach uses compartmental pharmacokinetic parameters available from the literature or derived from clinical study data (60). Metabolic enzyme activity can be estimated from *in vitro* rate constants or from clinical data. In essence, the SMPK is a minimal PBPK model incorporating the key organs involved in the absorption, distribution and clearance of drugs: intestine, liver, portal circulation, and systemic circulation. Other physiologic compartments are usually collapsed into the central

and peripheral compartments. Such models are easier to implement using standard pharmacometric platforms compared to PBPK models. This approach has been successfully used in drug-drug interaction predictions of CYP3A substrates (60), and has also been adopted to incorporate certain physiologic changes associated with pregnancy, such as change in CYP3A enzyme activity to predict drug disposition of CYP3A substrates (61). Validation of SMPK is similar to that of the PBPK models, i.e. demonstrate adequacy of model in non-pregnant adults and assess the sensitivity of model predictions for multiple drugs, for the pregnant population, to key model parameters.

5. Additional considerations

5.1. Pharmacodynamic (PD) considerations

PD modeling has been applied in the assessment of the commonly used oral hypoglycemic agent, glyburide, in the treatment of women with gestational diabetes (GDM). Normal pregnancy is characterized by insulin resistance with compensatory augmentation of insulin production, particularly in the 3rd trimester. GDM is characterized by more severe insulin resistance and impaired beta-cell compensation. The authors observed significant gestational augmentation of glyburide oral clearance, compared to non-pregnant patients with type 2 diabetes mellitus (13). In addition, insulin sensitivity was estimated from glucose and insulin concentrations using the minimal model of glucose kinetics following a mixed meal tolerance test**.** They found that although insulin secretion was significantly enhanced, the effects of glyburide were still not enough to compensate for the degree of insulin resistance exhibited by the women with GDM, as demonstrated by the significantly lower beta-cell response to glucose concentration corrected for the insulin sensitivity. These results suggest that patients with inadequate glucose control might

benefit from increased glyburide dosage. Other PD alterations including known changes in hemodynamics, cardiac output, peripheral resistance during pregnancy may have an impact on the PD response to antihypertensive drugs such as clonidine (62). Immunosuppression during pregnancy may impact the PD response to antibiotics (40). Disease activity changes in pregnancy may also occur. For example, improvement in rheumatoid arthritis disease, i.e. reduced disease activity, is noted in pregnancy (63). Because the efficacy of drugs will be influenced by alteration in the PK and PD of drugs, the latter should also guide dose adjustment in pregnancy.

5.2. Study design issue

As described earlier, dedicated PK studies in pregnant women often include volunteers unaffected by the clinical condition being treated, which allow the investigator to test a given drug dose. This is the case for many of the probe (model) drug studies (such as midazolam, digoxin) conducted in pregnant, healthy subjects during the third trimester (16). However, such study is not always possible to conduct in pregnant women, when potential fetal harm of the probe drug is unknown. Alternatively, opportunistic PK studies in pregnant women enroll subjects receiving drugs as part of clinical care. These studies typically receive a variety of dosing regimens, and subjects are afflicted with a disease. The ideal study would include a longitudinal pharmacokinetics assessment of drugs during each trimester and postpartum, especially for drugs that are administered chronically or given for several treatment cycles during pregnancy (64). This allows for intensive PK studies in pregnant women conducted serially so that each woman serves as her own control, therefore minimizes interindividual variability across gestational ages. It is not expected that PK will change back to the non-pregnant baseline

instantaneously as illustrated in a number of examples including theophylline (19). Therefore, postpartum assessment should be planned beyond the immediate postpartum, i.e. >6 weeks post-delivery. If postpartum assessment is not possible because the treatment is discontinued during postpartum, such as the case of pregnancy-induced hypertension, the study should include sufficient numbers of pregnant and non-pregnant women to allow a robust comparison of pharmacokinetics among all 3 trimesters of pregnancy compared to non-pregnant state. In addition, there would be equivalent diversity of demographic and clinical characteristics between the various study groups (65). Plasma concentration-time profile in pregnant subjects is preferred to single time-point assessment of plasma sample or urine sample. The latter is susceptive to much variability and reflects a multitude of factors, hence can complicate the interpretation of study results. Lastly, efficacy/safety assessment should also be included as part of the study design. In the absence of established exposure targets, a reasonable goal for a pregnancy dosing regimen has been to achieve exposure equivalent to that obtained in non-pregnant adults receiving the standard dosing (65). Efficacy measures and fetal outcomes measures will greatly enhance the confidence of making a safe recommendation for dosing adjustment.

5.3. Fetal exposure to drugs

The coupled maternal-fetal physiology imposes additional concerns for both efficacy and safety of treatment. Recommendation of dose adjustment in this population should also be carefully evaluated in terms of assessing the risk of fetal exposure to drugs administered to the mother. Although it is important to determine the fetal exposure to a drug administered to the pregnant mother, due to logistical and ethical reasons such exposure cannot be determined except at the

time of birth when a single cord blood sample can be obtained. Fetal exposure to drugs not only depends on maternal pharmacokinetics, but also depends on placental passage of drugs. The high abundance of efflux transporters (P-glycoprotein and breast cancer resistance protein) expressed at the blood-placental barrier protects the fetus by minimizing fetal exposure to their substrate drugs in the treatment of maternal conditions (e.g. glyburide). Conversely, these transporters also limit drug delivery for treating fetal conditions (e.g. protease inhibitors)(66). Understanding the contribution of these placental efflux transporters to drug distribution into the fetus *in vivo* is the first step towards quantitative prediction of fetal exposure to drugs. Only recently it has become possible to evaluate P-gp activity *in vivo* when positron emission tomography (PET) imaging probe [^{11}C]-verapamil was developed. Although the noninvasive measurement by PET of placental P-gp function in humans is not possible due to fetal radiation exposure, the pregnant macaque provides a physiologically relevant model for studying the contribution of P-gp to drug distribution into the fetus. We have assessed, in the pregnant macaque, P-gp activity at the blood-placental barrier and its gestational age-dependency using PET imaging (chapter 4).

6. Key knowledge gaps required for PBPK modeling of maternal-fetal drug disposition

Since cytochrome P450 enzymes are arguably the most important route of drug elimination. Of these enzymes, CYP3A, 1A2, 2D6, 2C9, 2C19 and 2B6 are likely more important than other CYPs in terms of metabolism of drugs that are administered to pregnant women. For these reasons, my dissertation is focused on predicting the disposition of drugs during pregnancy that are metabolized by these enzymes. Quantitative predictions of dosing regimen of CYP metabolized drugs for pregnant women necessitates that a validated model be available. To this

end, we utilized the PBPK modeling and simulation approach because of its numerous advantages over other approaches (see section 4.3). Because of the complexity of PBPK models, model validation entails a two-step procedure: first to demonstrate adequacy of the model for the non-pregnant population; and second for the pregnant population. For the first-step, we selected a set of validating drugs associated with well-characterized ADME characteristics, and validated the drug-specific parameters using i.v. and p.o. data obtained in the non-pregnant adults. To globally validate the presumed changes in specific CYP activity in the prototype PBPK model developed for the pregnant population by Lu et al.(57), model prediction for multiple drugs cleared by the respective CYP needs to be generated. We populated the PBPK model with probe drug data (for CYP2B6 *in vitro* data) delineating hepatic CYP3A, 1A2, 2D6, 2C9, 2B6 and 2C19 enzyme activity during pregnancy, and validated the model performance for well-characterized non-probe drugs cleared primarily by the same CYP enzyme as the probe drug. These studies are described in detail in chapters 1-3.

Chapter 1 focuses on predicting dosing regimens of drugs primarily metabolized by CYP3A enzymes. Specifically, the refined PBPK model, assuming 99% induction of hepatic CYP3A during the third trimester (T_3) based on midazolam data, was used to predicte T_3- induced change in the disposition of other CYP3A-metabolized drugs, nifedipine and indinavir. Distinguishing changes in intestinal metabolism from changes in systemic elimination (hepatic metabolism) is important because for the drugs predominantly cleared by CYP3A, the site of CYP3A induction during pregnancy is expected to have differential impact on pregnancy induced change in AUC. Since this is difficult to assess definitely through clinical studies in pregnant women (because for this population administering drugs IV and PO is challenging), we performed a sensitivity

analysis to assess the relative contribution by intestinal CYP3A induction and hepatic CYP3A induction, to the change in systemic exposure to midazolam, nifedipine and indinavir (chapter 1).

Chapter 2 focuses on predicting dosing regimens of drugs primarily cleared by CYP1A2 and CYP2D6 respectively. The PBPK model assuming 65% suppression of hepatic CYP1A2 during T_3 based on caffeine data, was used to predicted theophylline disposition during T_3. The PBPK model assuming 200% induction of hepatic CYP2D6 during T_3 based on metoprolol data, was used to predict paroxetine, dextromethorphan/dextrorphan and clonidine disposition during pregnancy (chapter 2).

Since the majority of drugs administered to pregnant women are metabolized by multiple CYP enzymes, it is important to determine if the above data can be synthesized to predict the disposition of these drugs. Therefore, in chapter 3, we expanded the pregnancy PBPK model by incorporating hepatic CYP2B6 induction (based on *in vitro* data), CYP2C9 induction (based on phenytoin PK), and CYP2C19 suppression (based on proguanil PK), into the model. For verification, the pregnancy-related changes in the disposition of drug cleared by multiple CYPs, such as methadone (cleared by CYP2B6, 3A and 2C19), and glyburide (cleared by CYP3A, 2C9 and 2C19), was predicted (chapter 3).

However, to fully populate the PBPK model, further probe drug studies to delineate the longitudinal changes of other CYPs and UGTs are warranted. For example, there are currently no studies evaluating the effect of pregnancy on CYP2C8 and CYP2E1 activity *in vivo*. PK studies of repaglinide (antidiabetic) and chlorzoxazone (muscle relaxer), can be conducted to

assess the pregnancy effect. For the majority of the probe drug studies conducted in pregnant women, data is obtained only in the third trimester. This issue stems from the limitation that some probe drugs cannot be safely administered to pregnant women during early gestation if they are not used for therapeutic purposes. Opportunistic PK studies in pregnant women are also likely restricted to certain phase of pregnancy during which the patients are afflicted with the disease. In both cases, extrapolating the magnitude of change in CYP enzyme activity from one trimester to other trimesters is difficult. We propose an alternative approach to predict the magnitude of enzyme induction or suppression *in vivo* at gradually rising concentration of specific hormones in plasma in each trimester, utilizing human hepatocytes (34). This approach has been shown to successfully predict CYP3A induction in the third trimester, and can be expanded to study other CYP isoforms. Last but not the least, pregnancy effect on certain physiological parameters, such as hepatic blood flow, should be further evaluated given the inconsistency in literature data as described earlier.

Currently, we have some knowledge of pregnancy effect on renal transporter organic cation transporter 2 (OCT2) and intestinal/renal transporter P-gp, based on metformin and digoxin data (16, 29). Future studies should extend to other important renal transporters such as organic anion transporter. Understanding pregnancy effect on the expression/activity of hepatic transporters, organic anion-transporting polypeptide 1B1 and 1B3 (OATP), is important when uptake of the drug into hepatocytes is the rate-limiting step of its clearance. To date, established probe drugs for OATPs are statins but they are contraindicated in pregnancy. In future, newly-identified probe drugs for OATPs that are not contraindicated in pregnancy can be evaluated in pregnant women. Finally, increased knowledge base of gestational-dependent

changes in placental transporter activity of drugs would be especially helpful in the utility of PBPK models in further exploration of fetal exposure *in silico.* In this regard, we have made some progress with respect to assessing gestational-dependent placental P-gp activity in the nonhuman primates using PET imaging (chapter 4). With such knowledge, as well as the fetal physiological parameters, a comprehensive fetal model can be developed and linked to the maternal PBPK model in the future to predict fetal exposure to drugs.

7. Conclusions

We have discussed the specific challenges related to the design, conduct and analysis of clinical studies in pregnant women, underlining the unmet need for pharmacometric analysis approaches. This research is focused on PBPK approach, as we believe with the established knowledge base of the profound physiological changes during pregnancy, and significant advances in PBPK approaches applied in special populations such as pediatrics (67), the PBPK approach offers added advantage in comparison to other approaches. By integrating physiological data, preclinical and clinical data to quantify anticipated changes in PK, this approach allows extrapolation beyond model drugs studied to other drugs with well-characterized ADME characteristics. Further, the coupled maternal-fetal physiology imposes additional concerns for both efficacy and safety of treatment. To assess fetal exposure to drugs administered to the mother, PBPK method is considered to be the most appropriate methodology to provide quantitative predictions for these events. Using such systems pharmacology approach can potentially allow us to identify drugs whose maternal-fetal PK, and therefore their efficacy and toxicity for the mother and/or the fetus, are likely to be affected by pregnancy.

References

(1) Glover, D.D., Amonkar, M., Rybeck, B.F. & Tracy, T.S. Prescription, over-the-counter, and herbal medicine use in a rural, obstetric population. *Am J Obstet Gynecol* **188**, 1039-45 (2003).

(2) Andrade, S.E., Gurwitz, J.H., Davis, R.L., Chan, K.A., Finkelstein, J.A., Fortman, K. *et al.* Prescription drug use in pregnancy. *Am J Obstet Gynecol* **191**, 398-407 (2004).

(3) Andrade, S.E., Raebel, M.A., Morse, A.N., Davis, R.L., Chan, K.A., Finkelstein, J.A. *et al.* Use of prescription medications with a potential for fetal harm among pregnant women. *Pharmacoepidemiol Drug Saf* **15**, 546-54 (2006).

(4) Keegan, J., Parva, M., Finnegan, M., Gerson, A. & Belden, M. Addiction in pregnancy. *J Addict Dis* **29**, 175-91 (2010).

(5) Kuczkowski, K.M. The effects of drug abuse on pregnancy. *Curr Opin Obstet Gynecol* **19**, 578-85 (2007).

(6) Taylor, P., Zaichkin, J., Pilkey, D., Leconte, J., Johnson, B.K. & Peterson, A.C. Prenatal screening for substance use and violence: findings from physician focus groups. *Matern Child Health J* **11**, 241-7 (2007).

(7) Williamson, S., Jackson, L., Skeoch, C., Azzim, G. & Anderson, R. Determination of the prevalence of drug misuse by meconium analysis. *Arch Dis Child Fetal Neonatal Ed* **91**, F291-2 (2006).

(8) Kapetanovic, S., Christensen, S., Karim, R., Lin, F., Mack, W.J., Operskalski, E. *et al.* Correlates of perinatal depression in HIV-infected women. *AIDS Patient Care STDS* **23**, 101-8 (2009).

(9) Endicott, S. & Haas, D.M. The current state of therapeutic drug trials in pregnancy. *Clin Pharmacol Ther* **92**, 149-50.

(10) Anger, G.J. & Piquette-Miller, M. Pharmacokinetic studies in pregnant women. *Clin Pharmacol Ther* **83**, 184-7 (2008).

(11) van Hasselt, J.G., Andrew, M.A., Hebert, M.F., Tarning, J., Vicini, P. & Mattison, D.R. The Status of Pharmacometrics in Pregnancy: Highlights from the 3(rd) American Conference on Pharmacometrics. *Br J Clin Pharmacol*, (2012).

(12) Unadkat, J.D., Wara, D.W., Hughes, M.D., Mathias, A.A., Holland, D.T., Paul, M.E. *et al.* Pharmacokinetics and safety of indinavir in human immunodeficiency virus-infected pregnant women. *Antimicrob Agents Chemother* **51**, 783-6 (2007).

(13) Hebert, M.F., Ma, X., Naraharisetti, S.B., Krudys, K.M., Umans, J.G., Hankins, G.D. *et al.* Are we optimizing gestational diabetes treatment with glyburide? The pharmacologic basis for better clinical practice. *Clin Pharmacol Ther* **85**, 607-14 (2009).

(14) Guidelines for the Use of AntiretroviralAgents in HIV-1-Infected Adults and Adolescents: January 10, 2011. http://www.aidsinfo.nih.gov/contentfiles/AdultandAdolescentGL.pdf

(15) Abduljalil, K., Furness, P., Johnson, T.N., Rostami-Hodjegan, A. & Soltani, H. Anatomical, physiological and metabolic changes with gestational age during normal pregnancy: a database for parameters required in physiologically based pharmacokinetic modelling. *Clin Pharmacokinet* **51**, 365-96 (2012).

(16) Hebert, M.F., Easterling, T.R., Kirby, B., Carr, D.B., Buchanan, M.L., Rutherford, T. *et al.* Effects of pregnancy on CYP3A and P-glycoprotein activities as measured by

disposition of midazolam and digoxin: a University of Washington specialized center of research study. *Clin Pharmacol Ther* **84**, 248-53 (2008).

(17) Bryson, Y.J., Mirochnick, M., Stek, A., Mofenson, L.M., Connor, J., Capparelli, E. *et al.* Pharmacokinetics and safety of nelfinavir when used in combination with zidovudine and lamivudine in HIV-infected pregnant women: Pediatric AIDS Clinical Trials Group (PACTG) Protocol 353. *HIV Clin Trials* **9**, 115-25 (2008).

(18) Tracy, T.S., Venkataramanan, R., Glover, D.D. & Caritis, S.N. Temporal changes in drug metabolism (CYP1A2, CYP2D6 and CYP3A Activity) during pregnancy. *Am J Obstet Gynecol* **192**, 633-9 (2005).

(19) Gardner, M.J., Schatz, M., Cousins, L., Zeiger, R., Middleton, E. & Jusko, W.J. Longitudinal effects of pregnancy on the pharmacokinetics of theophylline. *Eur J Clin Pharmacol* **32**, 289-95 (1987).

(20) Dempsey, D., Jacob, P., 3rd & Benowitz, N.L. Accelerated metabolism of nicotine and cotinine in pregnant smokers. *J Pharmacol Exp Ther* **301**, 594-8 (2002).

(21) Tomson, T., Lindbom, U., Ekqvist, B. & Sundqvist, A. Disposition of carbamazepine and phenytoin in pregnancy. *Epilepsia* **35**, 131-5 (1994).

(22) McGready, R., Stepniewska, K., Edstein, M.D., Cho, T., Gilveray, G., Looareesuwan, S. *et al.* The pharmacokinetics of atovaquone and proguanil in pregnant women with acute falciparum malaria. *Eur J Clin Pharmacol* **59**, 545-52 (2003).

(23) Hogstedt, S., Lindberg, B., Peng, D.R., Regardh, C.G. & Rane, A. Pregnancy-induced increase in metoprolol metabolism. *Clin Pharmacol Ther* **37**, 688-92 (1985).

(24) Pond, S.M., Kreek, M.J., Tong, T.G., Raghunath, J. & Benowitz, N.L. Altered methadone pharmacokinetics in methadone-maintained pregnant women. *J Pharmacol Exp Ther* **233**, 1-6 (1985).

(25) Hardman, J., Endres, L., Fischer, P. & Fischer, J. Pharmacokinetics of labetalol in pregnancy. *Pharmacotherapy* **25**, 1493 (2005).

(26) Fotopoulou, C., Kretz, R., Bauer, S., Schefold, J.C., Schmitz, B., Dudenhausen, J.W. *et al.* Prospectively assessed changes in lamotrigine-concentration in women with epilepsy during pregnancy, lactation and the neonatal period. *Epilepsy Res* **85**, 60-4 (2009).

(27) RETROVIR® (zidovudine) Tablets Product Label. http://www.accessdata.fda.gov/drugsatfda_docs/label/2011/019655s052,019910s039,020518s022lbl.pdf.

(28) Andrew, M.A., Easterling, T.R., Carr, D.B., Shen, D., Buchanan, M.L., Rutherford, T. *et al.* Amoxicillin pharmacokinetics in pregnant women: modeling and simulations of dosage strategies. *Clin Pharmacol Ther* **81**, 547-56 (2007).

(29) Eyal, S., Easterling, T.R., Carr, D., Umans, J.G., Miodovnik, M., Hankins, G.D. *et al.* Pharmacokinetics of metformin during pregnancy. *Drug Metab Dispos* **38**, 833-40 (2010).

(30) Gerdin, E., Salmonson, T., Lindberg, B. & Rane, A. Maternal kinetics of morphine during labour. *J Perinat Med* **18**, 479-87 (1990).

(31) Anderson, G.D. Pregnancy-induced changes in pharmacokinetics: a mechanistic-based approach. *Clin Pharmacokinet* **44**, 989-1008 (2005).

(32) Tomson, T., Lindbom, U., Ekqvist, B. & Sundqvist, A. Epilepsy and pregnancy: a prospective study of seizure control in relation to free and total plasma concentrations of carbamazepine and phenytoin. *Epilepsia* **35**, 122-30 (1994).

(33) Mathias, A.A., Hitti, J. & Unadkat, J.D. P-glycoprotein and breast cancer resistance protein expression in human placentae of various gestational ages. *Am J Physiol Regul Integr Comp Physiol* **289**, R963-9 (2005).
(34) Papageorgiou, I., Grepper, S. & Unadkat, J.D. Induction of Hepatic CYP3A Enzymes by Pregnancy-related Hormones: Studies in Human Hepatocytes and Hepatic Cell Lines. *Drug Metab Dispos* **41**, (2013).
(35) Mwinyi, J., Cavaco, I., Pedersen, R.S., Persson, A., Burkhardt, S., Mkrtchian, S. *et al.* Regulation of CYP2C19 expression by estrogen receptor alpha: implications for estrogen-dependent inhibition of drug metabolism. *Mol Pharmacol* **78**, 886-94 (2010).
(36) Choi, S.Y., Koh, K.H. & Jeong, H. Isoform-specific Regulation of Cytochromes P450 Expression by Estradiol and Progesterone. *Drug Metab Dispos*, (2012).
(37) Walker, A.A., Dickmann, L. & Isoherranen, N. Pregnancy decreases rat CYP1A2 activity and expression. *Drug Metab Dispos* **39**, 4-7 (2011).
(38) Topletz, A., Le, H.N., Lee, N., Chapman, J., Kelly, E.J., Wang, J. *et al.* Hepatic Cyp2d and Cyp26a1 mRNAs and Activities are Increased During Mouse Pregnancy. *Drug Metab Dispos* **41**, (2013).
(39) Jeong, H. Altered drug metabolism during pregnancy: hormonal regulation of drug-metabolizing enzymes. *Expert Opin Drug Metab Toxicol* **6**, 689-99 (2010).
(40) Fischer, J.H., Sarto, G.E., Habibi, M., Kilpatrick, S.J., Tuomala, R.E., Shier, J.M. *et al.* Influence of body weight, ethnicity, oral contraceptives, and pregnancy on the pharmacokinetics of azithromycin in women of childbearing age. *Antimicrob Agents Chemother* **56**, 715-24 (2012).
(41) Salman, S., Rogerson, S.J., Kose, K., Griffin, S., Gomorai, S., Baiwog, F. *et al.* Pharmacokinetic properties of azithromycin in pregnancy. *Antimicrob Agents Chemother* **54**, 360-6 (2010).
(42) Mirochnick, M., Best, B.M. & Clarke, D.F. Antiretroviral pharmacology: special issues regarding pregnant women and neonates. *Clin Perinatol* **37**, 907-27, xi.
(43) Ghosn, J., De Montgolfier, I., Cornelie, C., Dominguez, S., Perot, C., Peytavin, G. *et al.* Antiretroviral therapy with a twice-daily regimen containing 400 milligrams of indinavir and 100 milligrams of ritonavir in human immunodeficiency virus type 1-infected women during pregnancy. *Antimicrob Agents Chemother* **52**, 1542-4 (2008).
(44) Lopez-Cortes, L.F., Ruiz-Valderas, R., Rivero, A., Camacho, A., Marquez-Solero, M., Santos, J. *et al.* Efficacy of low-dose boosted saquinavir once daily plus nucleoside reverse transcriptase inhibitors in pregnant HIV-1-infected women with a therapeutic drug monitoring strategy. *Ther Drug Monit* **29**, 171-6 (2007).
(45) Best, B.M., Stek, A.M., Mirochnick, M., Hu, C., Li, H., Burchett, S.K. *et al.* Lopinavir tablet pharmacokinetics with an increased dose during pregnancy. *J Acquir Immune Defic Syndr* **54**, 381-8.
(46) Mirochnick, M., Best, B.M., Stek, A.M., Capparelli, E.V., Hu, C., Burchett, S.K. *et al.* Atazanavir pharmacokinetics with and without tenofovir during pregnancy. *J Acquir Immune Defic Syndr* **56**, 412-9.
(47) Fang, A., Valluri, S.R., O'Sullivan, M.J., Maupin, R., Jones, T., Delke, I. *et al.* Safety and pharmacokinetics of nelfinavir during the second and third trimesters of pregnancy and postpartum. *HIV Clin Trials* **13**, 46-59 (2012).
(48) Ke, A.B., Nallan, S.C., Zhao, P., Rostami-Hodjegan, A. & Unadkat, J.D. A PBPK Model to Predict Disposition of CYP3A-metabolized Drugs in Pregnant Women: Verification

and Discerning the Site of CYP3A Induction. *Clin Pharmacol Ther: Pharmacometrics & Systems Pharmacology* **1**, http://www.nature.com/psp/journal/v1/n9/index.html (2012).

(49) Johnson, T.N., Kerbusch, T., Jones, B., Tucker, G.T., Rostami-Hodjegan, A. & Milligan, P.A. Assessing the efficiency of mixed effects modelling in quantifying metabolism based drug-drug interactions: using in vitro data as an aid to assess study power. *Pharm Stat* **8**, 186-202 (2009).

(50) Benaboud, S., Hirt, D., Launay, O., Pannier, E., Firtion, G., Rey, E. *et al.* Pregnancy-related effects on tenofovir pharmacokinetics: a population study with 186 women. *Antimicrob Agents Chemother* **56**, 857-62 (2012).

(51) McGready, R., White, N.J. & Nosten, F. Parasitological efficacy of antimalarials in the treatment and prevention of falciparum malaria in pregnancy 1998 to 2009: a systematic review. *BJOG* **118**, 123-35.

(52) Rowland, M., Peck, C. & Tucker, G. Physiologically-based pharmacokinetics in drug development and regulatory science. *Annu Rev Pharmacol Toxicol* **51**, 45-73 (2011).

(53) Jamei, M., Dickinson, G.L. & Rostami-Hodjegan, A. A framework for assessing inter-individual variability in pharmacokinetics using virtual human populations and integrating general knowledge of physical chemistry, biology, anatomy, physiology and genetics: A tale of 'bottom-up' vs 'top-down' recognition of covariates. *Drug Metab Pharmacokinet* **24**, 53-75 (2009).

(54) Zhao, P., Zhang, L., Grillo, J.A., Liu, Q., Bullock, J.M., Moon, Y.J. *et al.* Applications of physiologically based pharmacokinetic (PBPK) modeling and simulation during regulatory review. *Clin Pharmacol Ther* **89**, 259-67 (2011).

(55) Lu, G., Abduljalil, K., Jamei, M., Johnson, T.N., Soltani, H. & Rostami-Hodjegan, A. Physiologically-based pharmacokinetic (PBPK) models for assessing the kinetics of xenobiotics during pregnancy: achievements and shortcomings. *Curr Drug Metab* **13**, 695-720 (2012).

(56) Andrew, M.A., Hebert, M.F. & Vicini, P. Physiologically based pharmacokinetic model of midazolam disposition during pregnancy. *Conf Proc IEEE Eng Med Biol Soc* **2008**, 5454-7 (2008).

(57) Lu, G., Abduljalil, K., Jamei, M., Johnson, T.N. & Rostami-Hodjegan, A. A Pregnancy Physiologically-Based Pharmacokinetic (p-PBPK) Model for Disposition of Drugs Metabolized by CYP1A2, CYP3A4 and CYP2D6. *British Journal of Clinical Pharmacology* **74**, 873-85 (2012).

(58) Kirby, B.J., Collier, A.C., Kharasch, E.D., Dixit, V., Desai, P., Whittington, D. *et al.* Complex drug interactions of HIV protease inhibitors 2: in vivo induction and in vitro to in vivo correlation of induction of cytochrome P450 1A2, 2B6, and 2C9 by ritonavir or nelfinavir. *Drug Metab Dispos* **39**, 2329-37 (2011).

(59) Rostami-Hodjegan, A., Kroemer, H.K. & Tucker, G.T. In-vivo indices of enzyme activity: the effect of renal impairment on the assessment of CYP2D6 activity. *Pharmacogenetics* **9**, 277-86 (1999).

(60) Quinney, S.K., Zhang, X., Lucksiri, A., Gorski, J.C., Li, L. & Hall, S.D. Physiologically based pharmacokinetic model of mechanism-based inhibition of CYP3A by clarithromycin. *Drug Metab Dispos* **38**, 241-8.

(61) Quinney, S.K., Mohamed, A.N., M.F., H., Haas, D.M., Clark, S., Umans, J.G. *et al.* A Semi-Mechanistic Metabolism Model of CYP3A Substrates in Pregnancy: Predicting

Changes in Midazolam and Nifedipine Pharmacokinetics. *Clin Pharmacol Ther: Pharmacometrics & Systems Pharmacology* **1**, (2012).

(62) Rothberger, S., Carr, D., Brateng, D., Hebert, M. & Easterling, T.R. Pharmacodynamics of clonidine therapy in pregnancy: a heterogeneous maternal response impacts fetal growth. *Am J Hypertens* **23**, 1234-40.

(63) Ostensen, M., Villiger, P.M. & Forger, F. Interaction of pregnancy and autoimmune rheumatic disease. *Autoimmun Rev* **11**, A437-46.

(64) US Department of Health and Human Services, Food and Drug Administration, Center for Drug Evaluation and Research (CDER). 2004. Guidance for Industry Pharmacokinetics in Pregnancy -Study Design, Data Analysis, and Impact on Dosing and Labeling. *US FDA webiste* [online]: http://www.fda.gov/downloads/Drugs/GuidanceComplianceRegulatoryInformation/Guidances/ucm072133.pdf.

(65) Mirochnick, M. & Clarke, D. Oseltamivir pharmacokinetics in pregnancy: a commentary. *Am J Obstet Gynecol* **204**, S94-5.

(66) Unadkat, J.D., Dahlin, A. & Vijay, S. Placental drug transporters. *Curr Drug Metab* **5**, 125-31 (2004).

(67) Leong, R., Vieira, M.L., Zhao, P., Mulugeta, Y., Lee, C.S., Huang, S.M. *et al.* Regulatory experience with physiologically based pharmacokinetic modeling for pediatric drug trials. *Clin Pharmacol Ther* **91**, 926-31.

Chapter One

A PBPK Model to Predict Disposition of CYP3A-metabolized Drugs in Pregnant Women: Verification and Discerning the Site of CYP3A Induction

* This chapter has been published in CPT: Pharmacometrics & Systems Pharmacology: 1, 2012, and is formatted according to the requirements of the journal.

A PBPK Model to Predict Disposition of CYP3A-metabolized Drugs in Pregnant Women: Verification and Discerning the Site of CYP3A Induction

A.B. Ke[1,2], S.C. Nallani[2], P. Zhao[2], A. Rostami-Hodjegan[3,4], J. D. Unadkat[1]

[1] Department of Pharmaceutics, University of Washington, Seattle, Washington, USA.

[2] Office of Clinical Pharmacology, Office of Translational Sciences, Center for Drug Evaluation and Research, Food and Drug Administration, Silver Spring, Maryland, USA.

[3] School of Pharmacy and Pharmaceutical Sciences, University of Manchester, Manchester, UK.

[4] Simcyp Limited, Sheffield, UK.

Running title: PBPK Prediction of PK Changes during Pregnancy

Corresponding author:

Dr. Jashvant D. Unadkat

Department of Pharmaceutics

University of Washington

Box 357610

Seattle, WA 98195

Telephone: 206-543-9434

Fax: 206-543-3204

E-mail: jash@u.washington.edu

Tables: 2

Figures: 5

Abstract: 150

Introduction: 943

Total word count: 4297

References: 43

Abbreviations: ADME: absorption, distribution, metabolism and excretion; ADAM: Advanced Dissolution, Absorption and Metabolism model; AUC, area under the curve; AUCR: AUC ratio; B/P: blood to plasma concentration ratio; CL: clearance; CL_r: renal clearance; $CL_{int,u}$: unbound intrinsic clearance; C_{max}: maximum plasma concentration; C_{min}: minimum plasma concentration; CYP: cytochrome P450; $f_{m,\ CYP3A}$: fraction metabolized by CYP3A; $f_{u,p}$: fraction unbound in plasma; F: bioavailability; F_a: fraction absorbed; F_g: intestinal bioavailability; F_h: hepatic bioavailability; HLM, human liver microsomes; k_a: fist order absorption rate constant; K_p, tissue-to-plasma partition coefficient; Q_{Gut}, hybrid parameter of blood flow and drug permeability; P_{app}, apparent permeability; PBPK model: physiologically-based pharmacokinetic model; PP: postpartum; T_1, T_2 and T_3: 1st, 2nd and 3rd trimester; V_{ss}: volume of distribution at steady state.

Abstract

Besides logistical and ethical concerns, evaluation of safety and efficacy of medications in pregnant women is complicated by marked changes in PK of drugs. For example, CYP3A activity is induced during the 3rd trimester (T_3). We explored whether a previously published physiologically-based pharmacokinetic (PBPK) model could quantitatively predict PK profiles of CYP3A-metabolized drugs during T_3, and discern the site of CYP3A induction (i.e. liver, intestine or both). The model accounted for gestational age-dependent changes in maternal physiological function and hepatic CYP3A activity. For model verification, mean plasma AUC, C_{max} and C_{min} of midazolam, nifedipine and indinavir were predicted and compared with published studies. The PBPK model successfully predicted midazolam, nifedipine and indinavir disposition during T_3. A sensitivity analysis suggested that CYP3A induction in T_3 is most likely hepatic and not intestinal. Our PBPK model is a useful tool to evaluate different dosing regimens during T_3 for drugs cleared primarily via CYP3A metabolism.

Key words: Pregnancy, Disposition, PBPK, CYP3A, Induction, Model verification

Introduction

Pregnant women and their fetuses are orphan populations with respect to the safety and efficacy of drugs. Latest statistics indicate that 64% of pregnant women ingest at least one medication for the treatment of a variety of clinical conditions, including viral (e.g., HIV), fungal or bacterial infections, smoking cessation, epilepsy or pregnancy-induced conditions such as hypertension, depression and diabetes (1, 2). For the large majority of drugs used during pregnancy, there is limited or no information available regarding whether pregnant women have altered pharmacokinetics or dosage requirement (3). Therefore, prescription drugs are routinely used off-label during pregnancy, i.e. without the necessary clinical data about the dose, maternal-fetal pharmacokinetics (PK) or efficacy of the drug in pregnant women. Determining the magnitude of change in PK caused by pregnancy is important to design evidence-based dosing regimen of drugs for pregnant women.

To avoid surveying all the drugs consumed by pregnant women, one can study the magnitude of changes, induced by various stages of pregnancy, in the processes of drug absorption (e.g., gastric pH, transporters), distribution (e.g., plasma protein binding and transporters), metabolism (e.g. cytochrome P450 (CYP) metabolism) and excretion (e.g., renal secretion via transporters) (ADME) of drugs. Specifically, the rate of absorption of drugs does not appear to be altered to a significant extent in pregnant women, as suggested by similar antepartum vs. postpartum/non-pregnant T_{max} values and none-to-modest changes in the half-lives of drugs (4-6). However the extent of pre-systemic elimination might be greater or lower, depending on the contributing pathway of elimination (e.g. CYPs or transporters), which then results in a lower (more likely) or higher C_{max} in this population. Increased plasma volume and decreased plasma protein binding

can alter the apparent volume of distribution (V_d) of drugs. Through changes in V_d and clearance, pregnancy can cause increases or decreases in the terminal elimination half-life of drugs. The renal excretion of unchanged drugs is increased during pregnancy due to increased glomerular filtration rate and also possibly increased renal secretion via transporters (7). On the other hand, the change in maternal hepatic enzyme activity is CYP isoform specific. Several groups have utilized model (probe) drugs that report CYP enzyme activities to delineate the magnitude of change in activity of major CYP enzymes, mostly during the third trimester (e.g. caffeine for CYP1A2, midazolam for CYP3A, metoprolol for CYP2D6, phenytoin for CYP2C9) (7). However, this approach has limitations in that some probe drugs (eg. midazolam) cannot be safely and logistically administered to pregnant women during early gestational age if they are not of therapeutic benefit to the woman.

In consideration of the ethical and logistical barrier to include pregnant women in clinical trials, PBPK modeling and simulation (M&S) based on mechanistic studies has begun to gain attention as a promising approach to predict drug disposition in this population (8, 9). Under the overarching umbrella of "Systems Pharmacology", PBPK modeling has the advantage of incorporating both physiological parameters that are important for ADME processes and drug-specific parameters (e.g. physico-chemical and drug disposition characteristics) into a quantitative predictive model (8, 10) and has been used in drug development and regulatory review (11). In comparison to a static approach, a dynamic approach, i.e. PBPK modeling, has added benefits in that it can a) handle drugs with non-linear kinetics (e.g. indinavir), b) quantitatively predict C_{max} and $C_{min,}$ which are sometimes correlated with the pharmacodynamic effects (safey/efficacy) of drugs, c) make it possible to predict, in the future, time-dependent fetal

drug exposure; and d) provide an integrative platform to evaluate drug dosing regiments for pregnant women since the only required input is drug-specific parameters.

Despite the advantages of PBPK models outlined above, until recently, no model existed that allowed prediction of maternal-fetal disposition of drugs that is drug- and gestational age-independent. Abduljalil et al. and Lu et al. recently proposed a maternal PBPK model, incorporating known physiological parameters as well as maternal hepatic CYP activity in each trimester (12-14). Changes in these CYP activities were described based on urinary metabolic ratio (UR) of dextromethorphan (DEX; CYP3A and 2D6) and salivary caffeine clearance (CYP1A2). While DEX UR is an acceptable measure of CYP2D6/3A for the non-pregnant population, it is not an adequate measure of these activities in the presence of CYP induction such as during pregnancy (15). This is because metabolic ratios are known to be dependent on changes in the renal function (16), which is likely to be induced during pregnancy alongside any induction of CYP2D6 and 3A. Therefore, we replaced the 3rd trimester (T_3) DEX data with more reliable CYP3A activity data based on oral clearance (CL_{PO}) of the validated probe drug, midazolam (MDZ) (4). However, the use of MDZ is also complicated by the fact that it reflects a combination of both hepatic and intestinal CYP3A activity. The site (hepatic, intestinal, or both) of CYP3A induction during pregnancy is expected to have differential impact on the bioavailability and disposition of various orally administered drugs which are metabolized by CYP3A. For example, if only intestinal CYP3A is induced during pregnancy, then only the disposition of those drugs significantly extracted by the intestine will be affected (i.e. low-intermediate intestinal bioavailability, F_g). In contrast, if hepatic CYP3A activity is induced, the disposition of all CYP3A drugs will be affected by pregnancy due to increased metabolic

clearance and decreased hepatic bioavailability (F_h). However, the site of CYP3A induction cannot be inferred from *in vivo* studies in pregnant women, due to the fact that almost all PK studies conducted in this population are conducted after oral dosing.

The aims of our study were two-fold: first, to test whether the refined PBPK model populated with CYP3A activity change based on CL_{PO} of MDZ, could accurately predict the T_3 disposition of other CYP3A-metabolized drugs, namely nifedipine (NIF) and indinavir (IDV). Second, to utilize PBPK modeling to discern the site of CYP3A induction in pregnancy. This was possible because the drugs included in the verification set, MDZ, NIF and IDV, are associated with different extent of CYP3A metabolism in the intestine and the liver.

Results

Midazolam The disposition kinetics of MDZ following a single oral dose of 2 mg was evaluated in thirteen women during T_3 and postpartum (4). The initial model based on DEX data (12), predicted mean AUC ratio (AUCR, PP:T_3) of 1.6, mean C_{max} ratio (PP:T_3) of 1.8 and mean C_{min} ratio (PP:T_3) of 1.6 , whereas the observed ratios were 1.9 ,1.5 and 2.7 respectively (Fig. 2A) (4). The initial-model prediction of AUCR (PP:T_3) and C_{max} ratio (PP:T_3), but not C_{min} ratio (PP:T_3), passed the pre-defined verification criterion ($0.80 \leq$ pred./obs. ≤ 1.25, see Methods) (Fig. 4). Based on reported change in 1'-hydroxymidazolam unbound formation clearance assessed during T_3 and postpartum (4), the initial model was refined to account for 99% induction of hepatic 3A activity during T_3. The refined model predicted mean AUCR (PP:T_3) of 2.3, mean C_{max} ratio (PP:T_3) of 2.3 and mean C_{min} ratio (PP:T_3) of 2.3 (Fig. 2A). Prediction of AUCR (PP:T_3) and C_{min} ratio (PP:T_3) passed the verification criterion (Fig. 4). However, the refined model failed the verification criterion when predicting C_{max} ratio (PP:T_3) (Fig. 4).

Nifedipine Prevost et al. studied steady-state NIF disposition (10mg p.o. q.i.d.) during T_3 in fifteen pregnant women with pregnancy-induced hypertension (17). PK assessment was not conducted in the same group of subjects during postpartum as NIF treatment was discontinued after delivery. When comparing to historical control data (18), mean oral clearance at steady state in pregnant women was almost doubled (145.7 L/hr vs. 74.4 L/hr). The initial model (based on DEX data) (12, 13) predicted mean steady-state AUCR (PP:T_3) of 1.3, C_{max} ratio (PP:T_3) of 1.5 and C_{min} ratio (PP:T_3) of 1.3, whereas the observed ratios were 2.0, 1.8 and 3.1 respectively (Fig. 2B). Moreover, the initial model failed the verification criterion for AUCR and C_{min} ratio (Fig. 4). The refined model (based on MDZ data) predicted mean steady-state

AUCR of 2.1, C_{max} ratio of 2.1 and C_{min} ratio of 2.4. With the exception of C_{min} ratio, the rest of the predictions passed the verification criterion (Fig. 2B and 4).

Indinavir We first constructed a "drug file" for IDV within Simcyp and populated the simulator with necessary drug-specific parameters for IDV (Table 2). Then, the constructed PBPK model was verified against the disposition kinetics following the administration of a tracer dose of 16 mg IDV via 30-min i.v. infusion to non-pregnant healthy volunteers (19). Predicted population mean $AUC_{0\text{-}24h}$, C_{max} and C_{min} values reasonably matched observed mean values (Fig. 3A). The IDV model, accounting for CYP3A saturation at both hepatic and intestinal levels (see Methods), predicted disproportional increase in AUC (3.0-fold predicted vs. 3.2-fold observed) following a single oral dose of 800mg vs. 400mg in non-pregnant healthy volunteers (Fig. 3B). Taken together, with the exception of C_{max} following 400mg p.o. dose and C_{min} following 800mg p.o. dose, the model-predicted AUC, C_{max} and C_{min}, following either i.v. dosing or p.o. dosing in non-pregnant healthy volunteers, passed verification criterion.

These parameters were then used in conjunction with the pregnancy PBPK model to replicate the study report by Unadkat et al. (5). In this report, the disposition of IDV in fifteen human immunodeficiency virus-infected women receiving IDV (800 mg q8h) plus zidovudine plus lamivudine was assessed during T_3 and postpartum. The initial PBPK model (12-14) predicted mean AUCR (PP:T_3) of 1.8, mean C_{max} ratio (PP:T_3) of 1.6 and mean C_{min} ratio (PP:T_3) of 2.3, compared with the observed values of 3.1, 2.1 and 6.3 respectively (5) (Fig. 3C). The initial model (based on DEX data) did not pass the verification criterion for AUCR, C_{max} and C_{min} ratio (Fig. 4). On the other hand, the refined model (based on MDZ data) predicted mean AUCR

(PP:T_3) of 2.6, mean C_{max} ratio (PP:T_3) of 1.9 and mean C_{min} ratio (PP:T_3) of 3.4 (Fig. 3C). With the exception of C_{min} ratio, the model-predicted AUCR and C_{max} ratio met verification criterion (Fig. 4).

Sensitivity Analysis To gain additional insights into the site of CYP3A induction during pregnancy, we conducted a sensitivity analysis to assess the relative contribution of induction of hepatic and intestinal CYP3A activity towards changes in MDZ, NIF or IDV AUC by varying CYP3A induction in the range of 0-200% in each organ (see Methods). As expected, 90-100% increase in hepatic CYP3A activity alone could universally explain the T_3 –induced AUCR (PP:T_3) for all three CYP3A substrates (Fig. 5). On the other hand, induction of intestinal CYP3A alone, by as much as 200%, could not explain the AUCR (PP:T_3) for all three CYP3A substrates. Simultaneous induction of hepatic 3A (40-50%) and intestinal 3A (40-100%) could explain the AUCR (PP:T_3) for MDZ and NIF, but under-predicted AUCR (PP:T_3) of IDV (pred./obs. ratio<0.80). One hundred percent induction of hepatic 3A and 50% induction of intestinal 3A could explain the AUCR (PP:T_3) of IDV, but over-predicted the AUCR (PP:T_3) of MDZ or NIF (pred./obs. ratio>1.25).

Discussion

This manuscript describes the use of PBPK modeling approach for evaluating the effect of pregnancy on system-dependent parameters that are critical for ADME of CYP3A-eliminated compounds. Three clinically-used model drugs, MDZ, NIF and IDV, are either exclusively ($f_{m,CYP3A}$=92% for MDZ and 99% for NIF) or predominantly (85% for IDV) eliminated by CYP3A. The disposition kinetics are well-characterized in the non-pregnant population, and well-designed clinical PK studies in pregnant women are readily available in the literature to allow comparison to model predictions. The main objective of PBPK simulations was to determine if the refined PBPK model, populated with CYP3A activity change based on probe drug study (MDZ), accurately predicts T_3- induced change in the disposition of other CYP3A-metabolized drugs, NIF and IDV. To our knowledge, data on PK of other drugs studied during pregnancy are for those that are not predominately metabolized by CYP3A enzymes, or if they are, their PK is complicated by mechanism-based inactivation of CYP3A enzymes (e.g. ritonavir/lopinavir/atazanavir).

Verification of our refined PBPK model was based on AUC because achieving equivalent drug exposure in pregnant and non-pregnant women was our primary focus. In addition, prediction of C_{max} and $C_{min,}$ were considered because achieving similar drug C_{max} and C_{min} may be important for some drugs where these measures are related to drug efficacy and/or toxicity. In the absence of (proper guidance), we arbitrarily chose criterion of PK bioequivalence to assess if the predicted exposure measures (PP:T_3) fall within 80% to 125% of the observed value, i.e. $0.80 \leq pred/obs \leq 1.25$.

The initial model was built on Tracy et al. study, which reported that, relative to postpartum, maternal hepatic CYP3A4 activity increased by 35%, 35%, 38% during 1^{st}, 2^{nd} and 3^{rd} trimesters respectively (20). These changes in enzyme activity during pregnancy were based on urinary parent/metabolite ratios (UR) of dextromethorphan (DEX), an indirect marker of enzyme activity (16). Deconvolution of intrinsic hepatic clearance from UR is possible, however this requires the assumption of the change in renal clearance of DEX during pregnancy (12). Indeed, as discussed above, further simulation results using MDZ as the model CYP3A drug, confirmed the speculation that the magnitude of 3A induction during T_3 from the report by Tracy et al., was significantly underestimated (Fig. 4).

Before evaluating the performance of the refined PBPK model in the pregnant population, we ensured that the drug disposition of MDZ, NIF and IDV was adequately described in the non-pregnant population. Simulations using MDZ and NIF drug file provided in Simcyp in non-pregnant healthy volunteers showed comparable PK profiles to the observed data, as gauged by visual inspection, obtained in either non-pregnant healthy or postpartum subjects (Fig. 2). For IDV, we established a drug file that captured the nonlinearity of its disposition, as was observed in non-pregnant healthy subjects (see Discussion below). Overall the initial model systematically under-predicted the AUCR for three drugs but the refined model did not. From a model validation perspective, MDZ might be best described as a model training compound. However, because PBPK model accounted for altered maternal physiology (renal function, plasma protein binding, blood flow, etc), in addition to CYP activity changes, MDZ prediction could still be viewed as verifications of the above-mentioned, system-dependent variables. MDZ C_{max} ratio (PP:T_3) obtained using the refined model did not pass verification criterion (Fig.

2A and Fig. 4). This could be due to the model assumption of no significant change in the rate of drug absorption or time lag. For the C_{min} ratio (PP:T_3), the refined model noticeably improved the model predictions for all three drugs, despite the fact that NIF and IDV C_{min} ratio (PP:T3) predictions did not meet verification criterion. Because C_{max} prediction for all three compounds met verification criterion (except for MDZ T3 C_{max}), it is possible that inadequate prediction of tissue distribution (hence the $t_{1/2}$ of drugs) resulted in inadequate prediction of C_{min}. Overall, the refined model was found to be superior to the initial model in predicting pregnancy-induced systemic exposure changes of drugs primarily metabolized by CYP3A.

At first sight the marked magnitude of effect of T_3 on IDV AUC (~200% change or 3.1-fold PP:T_3) is surprising since we observed only a ~100% increase in CYP3A activity as measured by oral MDZ clearance. However, on closer examination, this difference can be completely explained by the nonlinear PK of IDV caused by saturation of CYP3A metabolism. To test this hypothesis, we constructed and qualified a "drug file" for IDV within Simcyp. Then, this drug file was applied to the refined PBPK model, and the resulting predicted PK parameters, including AUC and C_{max}, during T_3 and postpartum met verification criterion. However, the predicted mean IDV C_{min} ratio (PP:T_3) was considerably lower than the observed ratio. We suspect that the large inter-individual variability in the observed C_{min} (reported geometric mean [95% CI] C_{min} ratio of 3.80 [1.03, 13.99]) contributed to the discrepancy between predicted and observed values (5). The discrepancy between the predicted and observed mean postpartum profiles (Fig. 3C) may also be due to fact that the observed postpartum $AUC_{0\text{-}8h}$ (23.8± 11.8 mg/L*hr) is 27% higher than reported $AUC_{0\text{-}8h}$ in non-pregnant HIV-positive female subjects (18.7± 9.0 mg/L*hr) (5). In contrast, the predicted postpartum $AUC_{0\text{-}8h}$ (16.7 mg/L*hr) is in good agreement with the

reported $AUC_{0\text{-}8h}$ in non-pregnant HIV-positive female subjects. This IDV case study illustrates two advantages of PBPK modeling. First, the capability of simultaneously considering the impact of concentration-dependent metabolism, changes in volume of distribution, and induction of CYP enzymes in prediction of disposition of drugs; and second, the separation of drug and system-dependent variables (10). In the absence of information on nonlinear PK of IDV (drug-dependent), one would not be able to correctly predict the change in IDV exposure in pregnant women during T_3 from MDZ and NIF T_3 data (~100% increase in hepatic CYP3A activity, system-dependent).

The placental-fetal component of the current model is considered as a peripheral compartment and may affect the overall drug disposition in the pregnant woman. As expected, given the small size of the placental-fetal unit, the presence or absence of this unit did not alter maternal PK of the three model drugs (contributed to <2% change in AUC). A more mechanistic fetal model describing maternal-fetal transfer and fetal disposition requires extensive fetus physiology (system-dependent) data, some of which are not available. Such comprehensive fetal model could be incorporated into this PBPK model in the future to predict fetal exposure to drugs. However, as has been documented by us and others, unless there is extensive distribution or irreversible clearance of the drugs from the fetal compartment (unlikely because of the smaller size of the fetal organs and lower abundance of metabolizing enzymes), incorporation of a comprehensive fetal model is unlikely to significantly affect the PK of drugs in the maternal compartment (21, 22).

For drugs predominantly cleared by CYP3A, the site (hepatic, intestinal, or both) of CYP3A induction during pregnancy is expected to have differential impact on AUCR ($PP:T_3$), as the latter is determined by CYP3A activity (i.e. CL_{int}) change in each organ, fraction metabolized by CYP3A ($f_{m,\ CYP3A}$) and basal intestinal extraction ($1-F_g$) (23). The vastly-different intestinal extraction of MDZ (F_g =0.51), NIF (F_g =0.73) and IDV (F_g =0.93) (Table 1-2) allowed us to assess, through a sensitivity analysis, the relative impact of hepatic vs. intestinal 3A induction on AUCR ($PP:T_3$). Although, without experimental verification we cannot completely exclude the possibility that a certain combination of hepatic and intestinal activity induction can also explain the observed change in AUCR, our sensitivity analysis suggests that the observed change in systemic exposure was mostly driven by an induction of hepatic 3A activity, with modest to little contribution from intestinal 3A induction (Fig. 5). Based on this finding, and our observation that hepatic, but not intestinal, luciferase activity is increased by pregnancy in the CYP3A4-promoter-luciferase transgenic mice (24), we propose that human pregnancy induces hepatic, and not intestinal, CYP3A activity. This conclusion needs to be supported by definitive studies such as i.v. and oral administration of midazolam during T_3. The underlying mechanism for this hepatic CYP3A induction during pregnancy remains unknown. It is possibly due to rising concentrations of various hormones in maternal blood, including placental growth hormone (PGH), progesterone, corticosteroids and estrogens (25).

Ethical issues are important when conducting drug studies in pregnant women. Hence, *in silico* methods offer a great promise for leveraging existing knowledge to better plan and conduct studies in pregnant women. Per FDA guidance, "in single-dose trials, the same adult dose usually can be administered to all women in the trial" and "The dosage regimen can be adjusted

based on the best available pre-trial estimates of the pharmacokinetics of the drug and its active metabolites and what is known about drug elimination" (26). To arrive at a rational pre-trial estimates, one can employ the M&S approach to simulate systemic exposure of approved drugs in the three trimesters and postpartum, and based on this one can optimize design of "first in pregnancy" PK study including prioritizing study period and dosage selection. Compared with conventional compartmental models, PBPK offers added advantages in trial simulation supporting "first in pregnancy" PK studies. The established PBPK model captures changes in system-dependent parameters and describes tissue distribution of drug molecule in much greater details. The latter may play a vital role in study design because one may be interested in tissue exposure or unbound plasma exposure of the approved drug in pregnant women. These exposure measures are more relevant to dosage adjustment (if any) than is measurement of total plasma concentration of a drug.

Conclusion

With a thorough knowledge and understanding of drug-dependent parameters, combined with system parameters describing physiological and biological changes in the pregnant population, the proposed PBPK approach is capable of quantitatively predicting disposition of CYP3A substrate drugs during T_3. At present, verification of the model for predicting drug PK during earlier trimesters is not possible due to lack of reliable probe drug studies during these periods. However, CYP3A induction in human hepatocytes incubated with pregnancy-related hormones at their unbound plasma concentrations observed during T_3 is virtually identical to that observed *in vivo* (27). Therefore, CYP3A induction in hepatocytes incubated with pregnancy-related hormones at unbound plasma concentrations observed during T_1 and T_2 may be able to fill this

knowledge gap. Future expansion of the refined PBPK model could also include incorporating variability in the predicted drug exposure measures, when necessary data on the variability (and covariance) in the system- and drug-dependent parameters are better defined. As described here for CYP3A substrate drugs, PBPK prediction of the disposition of drugs cleared by other major CYPs, including CYP1A2, CYP2D6, CYP2B6 and CYP2C9, based on probe drug studies, are currently in progress. Once completed, it should be possible to utilize the predictive model, prior to clinical investigations, to evaluate different dosing regimens in pregnant women for drugs cleared primarily via single or mixed CYP metabolism.

Method

General pregnancy PBPK model structure and verification methodology

Known maternal physiological, anatomical and biological differences between pregnant and non-pregnant populations, based on meta-analysis of literature data, were incorporated in the virtual population as reported (12). These included gestational weight gain, plasma protein and lipid concentration, individual organ/tissue volumes and blood flows, glomerular filtration rates, and hepatic enzyme activity changes (CYP1A2, 2D6 and 3A). A time-varying full PBPK model constructed in Matlab v. 7.10® (2010) was utilized (14). Briefly, the PBPK model is an extension of the Simcyp 13-compartment full-PBPK model, by adding a lumped compartment to represent the placenta, fetal organs and the amniotic fluid (Fig. 1). Systemic clearance was considered to occur in the maternal liver and kidney and pre-systemic metabolism was considered to occur in both maternal small intestine and the liver. Key model assumptions and governing equations of the PBPK model are provided in Supplementary Methods. The Matlab model is available for scientific research and can be obtained by contacting Dr. Amin Rostami-Hodjegan (amin.rostami@manchester.ac.uk).

Mean plasma AUC, C_{max} and C_{min} were predicted and compared with published studies in pregnant and non-pregnant women. Midazolam and Indinavir observed data were obtained directly from the authors. Nifedipine observed data was captured using "digitize", a Matlab tool for digitizing images that is freely available on http://www.mathworks.com/matlabcentral/. An arbitrary criterion for successful verification of the model was prediction of pregnancy-induced fold-changes in mean population PK parameters of the drug (i.e. AUC ratio (PP:T_3), C_{max} ratio

(PP:T_3) and C_{min} ratio (PP:T_3)) within 80% to 125% of the observed value, i.e. $0.80 \leq pred/obs \leq 1.25$.

Midazolam PBPK model

Physiochemical and protein binding parameters (B/P ratio, $f_{u,p}$), absorption (F_a, F_g), distribution (K_p, tissue-to-plasma partition coefficient) and elimination ($CL_{int,h,u}$) were obtained from Simcyp® Population-based Simulator (Version 10). k_a (=2.5 hr^{-1}) was estimated (see Table 1) in the reported range of 2-4.2 hr^{-1} (28, 29) in Simcyp to match the absorption kinetics from selected clinical studies conducted in non-pregnant or postpartum subjects (4, 30, 31). Log $P_{o:w}$ (=3.1) was further optimized through manual sensitivity analysis in the range of 3.0-4.0 in order to match predicted V_{ss} (=1.49 L/kg) to reported V_{ss} (= 1.1 L/kg) (28) and to improve C_{max} prediction. The drug-dependent parameters of MDZ are outlined in Table 1.

Nifedipine PBPK model

Physiochemical and protein binding parameters (B/P ratio, $f_{u,p}$), absorption (F_a, F_g), distribution (K_p) and elimination ($CL_{int,h,u}$) were obtained from Simcyp (Version 10). Log $P_{o:w}$ (=2.53) was optimized in the range of 2.0-3.0 in order to match predicted V_{ss} (=0.60 L/kg) to reported V_{ss} (= 0.79 L/kg) (28) and to improve C_{max} prediction. k_a (=1.91 hr^{-1}) was estimated (see Table 1) in Simcyp to match the absorption kinetics from selected clinical studies conducted in non-pregnant subjects (18, 32-34). The drug-dependent parameters of NIF are outlined in Table 1.

Indinavir PBPK model

Drug-specific parameters for IDV, including physiochemical and protein binding parameters (B/P ratio, $f_{u,p}$), absorption (F_a, k_a, F_g), were extracted from literature. Non-pregnant CL_r of 8.6 L/hr was the average literature value (19, 35). Log $P_{o:w}$ was optimized in Simcyp through manual sensitivity analysis in the range of 1.5-3.0 (36) to improve V_{ss} and C_{max} prediction (see Table 2). To capture the more-than-proportional increase in AUC following a single p.o. dose in the dose range of 400mg-800mg in healthy volunteers, *in vivo* K_m was estimated via sensitivity analysis in Simcyp with a starting value of 0.1 µM obtained in HLM (37). During the optimization process, V_{max} was adjusted accordingly so as to maintain a constant ratio of V_{max}/K_m to equal the maximum $CL_{int,h,u}$ determined in HLM (37). The drug-dependent parameters of IDV are outlined in Table 2.

Sensitivity analysis to discern site of CYP3A induction

First the change in intestinal bioavailability (F_g) of these drugs as a result of intestinal CYP3A induction in the range of 0-200% (20% increment per step) was predicted using either Q_{gut} model or ADAM model (See Supplementary Methods). Then the newly-obtained F_g value was incorporated into the pregnancy PBPK model. Subsequently, induction of hepatic CYP3A in the range of 0-200% (20% increment per step) and its impact on pre-systemic as well as systemic elimination of these drugs was considered in the pregnancy-PBPK model.

Study Highlights

What is the current knowledge on the topic: During pregnancy, changes in physiology and ADME processes can significantly affect the disposition of drugs which may necessitate adjustment of drug dosing regimens.

What question this study addressed: We verified a novel physiologically-based model which incorporates gestational age-dependent changes in maternal physiology and hepatic CYP3A activity, to predict the disposition of CYP3A-metabolized drugs during the third trimester

What this study adds to our knowledge: The PBPK model successfully predicted the disposition of CYP3A-metabolized drugs, midazolam, nifedipine and indinavir, during the third trimester and suggested that CYP3A induction is likely hepatic and not intestinal.

How this might change clinical pharmacology and therapeutics: The proposed PBPK model can be used to optimize the dosing regimens of CYP3A-metabolized approved drugs and design "first in pregnancy" PK study including dosage selection of approved drugs during the third trimester.

Acknowledgements

The authors acknowledge funding from FDA Office of Women's Health and visiting fellowship from SimCYP (A.B. Ke). The authors would also like to thank Dr. Shiew Mei Huang (OCP, CDER, FDA) for her critical review of the manuscript and Drs. Masoud Jamei and Gaohua Lu (SimCYP®Ltd,UK) for their technical support on Matlab models.

Conflict of Interest/Disclosure

The authors declared no conflict of interest. CPT:PSP Associate Editor Prof. Amin Rostami-Hodjegan was not involved in the review or decision process for this article.

Author Contributions

Participated in research design: A.B. Ke, S.C. Nallani, P. Zhao, A. Rostami-Hodjegan, J. D. Unadkat

Conducted experiments: A.B. Ke

Contributed new reagents or analytical tools: A. Rostami-Hodjegan

Performed data analysis: A.B. Ke

Wrote or contributed to the writing of the manuscript: A.B. Ke, S.C. Nallani, P. Zhao, A. Rostami-Hodjegan, J. D. Unadkat

References

(1) Glover, D.D., Amonkar, M., Rybeck, B.F. & Tracy, T.S. Prescription, over-the-counter, and herbal medicine use in a rural, obstetric population. *Am J Obstet Gynecol* **188**, 1039-45 (2003).

(2) Andrade, S.E., Gurwitz, J.H., Davis, R.L., Chan, K.A., Finkelstein, J.A., Fortman, K. *et al.* Prescription drug use in pregnancy. *Am J Obstet Gynecol* **191**, 398-407 (2004).

(3) Anderson, G.D. & Carr, D.B. Effect of pregnancy on the pharmacokinetics of antihypertensive drugs. *Clin Pharmacokinet* **48**, 159-68 (2009).

(4) Hebert, M.F., Easterling, T.R., Kirby, B., Carr, D.B., Buchanan, M.L., Rutherford, T. *et al.* Effects of pregnancy on CYP3A and P-glycoprotein activities as measured by disposition of midazolam and digoxin: a University of Washington specialized center of research study. *Clin Pharmacol Ther* **84**, 248-53 (2008).

(5) Unadkat, J.D., Wara, D.W., Hughes, M.D., Mathias, A.A., Holland, D.T., Paul, M.E. *et al.* Pharmacokinetics and safety of indinavir in human immunodeficiency virus-infected pregnant women. *Antimicrob Agents Chemother* **51**, 783-6 (2007).

(6) Bryson, Y.J., Mirochnick, M., Stek, A., Mofenson, L.M., Connor, J., Capparelli, E. *et al.* Pharmacokinetics and safety of nelfinavir when used in combination with zidovudine and lamivudine in HIV-infected pregnant women: Pediatric AIDS Clinical Trials Group (PACTG) Protocol 353. *HIV Clin Trials* **9**, 115-25 (2008).

(7) Anderson, G.D. Pregnancy-induced changes in pharmacokinetics: a mechanistic-based approach. *Clin Pharmacokinet* **44**, 989-1008 (2005).

(8) Rowland, M., Peck, C. & Tucker, G. Physiologically-based pharmacokinetics in drug development and regulatory science. *Annu Rev Pharmacol Toxicol* **51**, 45-73 (2011).

(9) Andrew, M.A., Hebert, M.F. & Vicini, P. Physiologically based pharmacokinetic model of midazolam disposition during pregnancy. *Conf Proc IEEE Eng Med Biol Soc* **2008**, 5454-7 (2008).

(10) Jamei, M., Dickinson, G.L. & Rostami-Hodjegan, A. A framework for assessing inter-individual variability in pharmacokinetics using virtual human populations and integrating general knowledge of physical chemistry, biology, anatomy, physiology and genetics: A tale of 'bottom-up' vs 'top-down' recognition of covariates. *Drug Metab Pharmacokinet* **24**, 53-75 (2009).

(11) Zhao, P., Zhang, L., Grillo, J.A., Liu, Q., Bullock, J.M., Moon, Y.J. *et al.* Applications of physiologically based pharmacokinetic (PBPK) modeling and simulation during regulatory review. *Clin Pharmacol Ther* **89**, 259-67 (2011).

(12) Abduljalil K, F.P., Johnson TN, Rostami-Hodjegan A, Soltani H. Physiological, Anatomical and Metabolic Changes with Gestational Age during Normal Pregnancy; A Database for Parameters Required in Physiologically Based Pharmacokinetic Modelling. *Clinical Pharmacokinetics*, (2012).

(13) Lu, G., Abduljalil, K., Jamei, M., Johnson, T.N., Soltani, H. & Rostami-Hodjegan, A. Physiologically-based Pharmacokinetic (PBPK) Models for Assessing the Kinetics of Xenobiotics during Pregnancy: Achievements and Shortcomings. *Curr Drug Metab*, (2012).

(14) Lu, G., Abduljalil, K., Jamei, M., Johnson, T.N. & Rostami-Hodjegan, A. A Pregnancy Physiologically-Based Pharmacokinetic (p-PBPK) Model for Disposition of Drugs

Metabolized by CYP1A2, CYP3A4 and CYP2D6. *British Journal of Clinical Pharmacology*, (2012).

(15) Kirby, B.J., Collier, A.C., Kharasch, E.D., Dixit, V., Desai, P., Whittington, D. *et al.* Complex drug interactions of HIV protease inhibitors 2: in vivo induction and in vitro to in vivo correlation of induction of cytochrome P450 1A2, 2B6, and 2C9 by ritonavir or nelfinavir. *Drug Metab Dispos* **39**, 2329-37 (2011).

(16) Rostami-Hodjegan, A., Kroemer, H.K. & Tucker, G.T. In-vivo indices of enzyme activity: the effect of renal impairment on the assessment of CYP2D6 activity. *Pharmacogenetics* **9**, 277-86 (1999).

(17) Prevost, R.R., Akl, S.A., Whybrew, W.D. & Sibai, B.M. Oral nifedipine pharmacokinetics in pregnancy-induced hypertension. *Pharmacotherapy* **12**, 174-7 (1992).

(18) Foster, T.S., Hamann, S.R., Richards, V.R., Bryant, P.J., Graves, D.A. & McAllister, R.G. Nifedipine kinetics and bioavailability after single intravenous and oral doses in normal subjects. *J Clin Pharmacol* **23**, 161-70 (1983).

(19) Yeh, K.C., Stone, J.A., Carides, A.D., Rolan, P., Woolf, E. & Ju, W.D. Simultaneous investigation of indinavir nonlinear pharmacokinetics and bioavailability in healthy volunteers using stable isotope labeling technique: study design and model-independent data analysis. *J Pharm Sci* **88**, 568-73 (1999).

(20) Tracy, T.S., Venkataramanan, R., Glover, D.D. & Caritis, S.N. Temporal changes in drug metabolism (CYP1A2, CYP2D6 and CYP3A Activity) during pregnancy. *Am J Obstet Gynecol* **192**, 633-9 (2005).

(21) Tuntland, T., Nosbisch, C. & Unadkat, J.D. Effect of pregnancy, mode of administration and neonatal age on the pharmacokinetics of zalcitabine (2', 3'-dideoxycytidine) in the pigtailed macaque (Macaca nemestrina). *J Antimicrob Chemother* **40**, 687-93 (1997).

(22) Tuntland, T., Odinecs, A., Nosbisch, C. & Unadkat, J.D. In vivo maternal-fetal-amniotic fluid pharmacokinetics of zidovudine in the pigtailed macaque: comparison of steady-state and single-dose regimens. *J Pharmacol Exp Ther* **285**, 54-62 (1998).

(23) Fahmi, O.A., Hurst, S., Plowchalk, D., Cook, J., Guo, F., Youdim, K. *et al.* Comparison of different algorithms for predicting clinical drug-drug interactions, based on the use of CYP3A4 in vitro data: predictions of compounds as precipitants of interaction. *Drug Metab Dispos* **37**, 1658-66 (2009).

(24) Zhang, H., Wu, X., Wang, H., Mikheev, A.M., Mao, Q. & Unadkat, J.D. Effect of pregnancy on cytochrome P450 3a and P-glycoprotein expression and activity in the mouse: mechanisms, tissue specificity, and time course. *Mol Pharmacol* **74**, 714-23 (2008).

(25) Jeong, H. Altered drug metabolism during pregnancy: hormonal regulation of drug-metabolizing enzymes. *Expert Opin Drug Metab Toxicol* **6**, 689-99 (2010).

(26) US Department of Health and Human Services, Food and Drug Administration, Center for Drug Evaluation and Research (CDER). 2004. Guidance for Industry Pharmacokinetics in Pregnancy -Study Design, Data Analysis, and Impact on Dosing and Labeling. *US FDA webiste* [online]: http://www.fda.gov/downloads/Drugs/GuidanceComplianceRegulatoryInformation/Guidances/ucm072133.pdf.

(27) Papageorgiou, I. & Unadkat, J.D. Mechanisms by which hepatic CYP3A enzymes are induced during pregnancy *ISSX, 17th North American Meeting Atlanta, Georgia*, (2011).

(28) Obach, R.S., Lombardo, F. & Waters, N.J. Trend analysis of a database of intravenous pharmacokinetic parameters in humans for 670 drug compounds. *Drug Metab Dispos* **36**, 1385-405 (2008).
(29) Gertz, M., Harrison, A., Houston, J.B. & Galetin, A. Prediction of human intestinal first-pass metabolism of 25 CYP3A substrates from in vitro clearance and permeability data. *Drug Metab Dispos* **38**, 1147-58 (2010).
(30) Thummel, K.E., O'Shea, D., Paine, M.F., Shen, D.D., Kunze, K.L., Perkins, J.D. *et al.* Oral first-pass elimination of midazolam involves both gastrointestinal and hepatic CYP3A-mediated metabolism. *Clin Pharmacol Ther* **59**, 491-502 (1996).
(31) Gorski, J.C., Jones, D.R., Haehner-Daniels, B.D., Hamman, M.A., O'Mara, E.M., Jr. & Hall, S.D. The contribution of intestinal and hepatic CYP3A to the interaction between midazolam and clarithromycin. *Clin Pharmacol Ther* **64**, 133-43 (1998).
(32) Reitberg, D.P., Love, S.J., Quercia, G.T. & Zinny, M.A. Effect of food on nifedipine pharmacokinetics. *Clin Pharmacol Ther* **42**, 72-5 (1987).
(33) Smith, S.R., Kendall, M.J., Lobo, J., Beerahee, A., Jack, D.B. & Wilkins, M.R. Ranitidine and cimetidine; drug interactions with single dose and steady-state nifedipine administration. *Br J Clin Pharmacol* **23**, 311-5 (1987).
(34) Odou, P., Ferrari, N., Barthelemy, C., Brique, S., Lhermitte, M., Vincent, A. *et al.* Grapefruit juice-nifedipine interaction: possible involvement of several mechanisms. *J Clin Pharm Ther* **30**, 153-8 (2005).
(35) Balani, S.K., Woolf, E.J., Hoagland, V.L., Sturgill, M.G., Deutsch, P.J., Yeh, K.C. *et al.* Disposition of indinavir, a potent HIV-1 protease inhibitor, after an oral dose in humans. *Drug Metab Dispos* **24**, 1389-94 (1996).
(36) Lin, J.H., Chen, I.W., Vastag, K.J. & Ostovic, D. pH-dependent oral absorption of L-735,524, a potent HIV protease inhibitor, in rats and dogs. *Drug Metab Dispos* **23**, 730-5 (1995).
(37) Gertz, M., Houston, J.B. & Galetin, A. Physiologically-based pharmacokinetic modeling of intestinal first-pass metabolism of CYP3A substrates with high intestinal extraction. *Drug Metab Dispos*, (2011).
(38) Ito, K., Ogihara, K., Kanamitsu, S. & Itoh, T. Prediction of the in vivo interaction between midazolam and macrolides based on in vitro studies using human liver microsomes. *Drug Metab Dispos* **31**, 945-54 (2003).
(39) Kirby, B.J., Collier, A.C., Kharasch, E.D., Whittington, D., Thummel, K.E. & Unadkat, J.D. Complex drug interactions of HIV protease inhibitors 1: inactivation, induction, and inhibition of cytochrome P450 3A by ritonavir or nelfinavir. *Drug Metab Dispos* **39**, 1070-8 (2011).
(40) Lin, J.H., Chiba, M., Balani, S.K., Chen, I.W., Kwei, G.Y., Vastag, K.J. *et al.* Species differences in the pharmacokinetics and metabolism of indinavir, a potent human immunodeficiency virus protease inhibitor. *Drug Metab Dispos* **24**, 1111-20 (1996).
(41) Product label for CRIXIVAN (indinavir sulfate) oral capsule. <http://www.accessdata.fda.gov/drugsatfda_docs/label/2010/020685s073lbl.pdf>.
(42) Yang, J., Jamei, M., Yeo, K.R., Tucker, G.T. & Rostami-Hodjegan, A. Prediction of intestinal first-pass drug metabolism. *Curr Drug Metab* **8**, 676-84 (2007).
(43) Darwich, A.S., Neuhoff, S., Jamei, M. & Rostami-Hodjegan, A. Interplay of metabolism and transport in determining oral drug absorption and gut wall metabolism: a simulation

assessment using the "Advanced Dissolution, Absorption, Metabolism (ADAM)" model. *Curr Drug Metab* **11**, 716-29 (2010).

Figure legends:

Fig. 1 A schematic representation of the pregnancy PBPK model. The PBPK model is an extension of the Simcyp 13-compartment full-PBPK model, and includes a lumped compartment to represent placental-fetal organs including the fetus, placenta and the amniotic fluid. Reproduced from Lu et al., 2012 (13).

Fig. 2 A) Simulated and observed plasma concentration-time profiles of midazolam (MDZ) after a single oral dose of 2mg during 3rd trimester (T_3) and postpartum (PP). The solid black line represents predicted mean postpartum profile. The grey dashed line represents predicted mean T_3 profile using initial model based on DEX UR data, and the black dashed line represents predicted mean T_3 profile using the refined model based on MDZ oral clearance data. Mean observed data (4) are overlaid (filled circles: postpartum profile; closed circles: T_3 profile). Error bars represent standard deviations. In the inset, predicted and observed PK profiles are plotted on a logarithmic scale.

B) Simulated and observed plasma concentration-time profiles of nifedipine (NIF) at steady state (10mg p.o. q.i.d.) during 3rd trimester (T_3) and postpartum (PP). The solid black line represents predicted mean postpartum profile. The grey dashed line represents predicted mean T_3 profile using the initial model, and the black dashed line represents predicted mean T_3 profile using the refined model. Mean observed data are overlaid (filled circles: historical control profile taken from ref. 18, 32-34; closed circles: T_3 profile taken from ref. 17). Error bars represent standard deviations. In the inset, predicted and observed PK profiles are plotted on a logarithmic scale.

Fig. 3: A) Simulated and observed plasma concentration-time profiles of indinavir (IDV) after an i.v. dose of 16mg administered to non-pregnant healthy volunteers (M=6, F=6). The black solid line represents predicted mean profile following an i.v. dose of 16mg. Mean observed data (19) are overlaid. In the inset, predicted and observed PK profiles are plotted on a logarithmic scale.

B) Simulated and observed plasma concentration-time profiles of IDV after administration of a single oral dose of 400mg or 800mg to non-pregnant healthy volunteers (M=6, F=6). The black solid line represents predicted mean profile following 800mg p.o. dose. The black dashed line represents predicted mean profile following 400mg p.o. dose. Mean observed data (19) are overlaid (filled circles: 800mg p.o. dose profile; open circles: 400mg p.o. dose profile). In the inset, predicted and observed PK profiles are plotted on a logarithmic scale.

C) Simulated and observed plasma concentration-time profiles of IDV following 800mg q8h p.o. dose administered during 3rd trimester (T_3) and postpartum (PP). The black solid line represents predicted mean profile during postpartum. The grey dashed line represents predicted mean T_3 profile using the initial model and the black dashed line represents predicted mean profile during T_3 using the refined model. Mean observed data (5) are overlaid (filled circles: postpartum profile; open circles: T_3 profile). Considerable inter-individual variability in C_{min} of IDV was observed across the fifteen patients and for clarification, the observed variability in the data is omitted. In the inset, predicted and observed PK profiles are plotted on a logarithmic scale.

Fig. 4: Comparison of initial (based on DEX data) vs. refined (based on MDZ data) model performance as gauged by predicted (pred.)/observed (obs.) ratio of mean AUCR (PP:T_3), mean

C_{max} ratio (PP:T_3) and mean C_{min} ratio (PP:T_3). A) The grey bars represent predicted AUCR, C_{max} ratio and C_{min} ratio using the initial model and the black bars represent predicted AUCR, C_{max} ratio and C_{min} ratio using the refined model. The white bars represent observed AUCR, C_{max} ratio and C_{min} ratio.

B) The grey bars represent pred./obs. ratio using the initial model and the black bars represent pred./obs. ratio using the refined model. The dashed grey lines bracket the range of values that fall within the verification criterion. MDZ: observed mean AUCR, C_{max} ratio and C_{min} ratio (sample taken at last time-point) calculated from ref. 4. NIF: observed mean AUCR, C_{max} ratio and C_{min} ratio calculated from mean T_3 $AUC_{0\text{-}tau}$, C_{max} and C_{min} from ref. 17, and weighted mean $AUC_{0\text{-}tau}$, C_{max} and C_{min} in non-pregnant historical controls from refs. 18, 32-34. IDV: observed mean AUCR, C_{max} ratio and C_{min} ratio extracted from ref. 5.

Fig. 5: Changes in midazolam, nifedipine and indinavir AUCR (AUC_{PP}/AUC_{T3}) as a function of hepatic and intestinal CYP3A activity induction during pregnancy. Observed mean AUCR is represented by horizontal plane in dark grey. Two horizontal planes in light grey show AUCR range between 80-120% of observed mean AUCR. Arrows indicate the intersections corresponding to 100% increase in hepatic CYP3A activity, 200% increase in intestinal CYP3A and simultaneous induction of hepatic 3A (50%) and intestinal 3A (50%). Figures were generated using SigmaPlot™ (Version 12.0, San Jose, CA).

List of Tables:

Table 1: Summary of midazolam (MDZ) and nifedipine (NIF) drug-dependent parameters

Parameter	MDZ Value	Methods/ reference	NIF Value	Methods/ reference
Molecular Weight	325.8	Library [a]	346.3	Library
Log $P_{o:w}$	3.13	Optimized [b]	2.53	Optimized [f]
pKa	10.95,6.2	Library	2.82	Library
B/P Ratio	0.663	Library	0.73	Library
$f_{u,p}$	0.032	Library	0.04	Library
F_a	0.88	Library	0.88	Library
k_a (h^{-1})	2.5	Parameter estimation [c]	1.91	Parameter estimation [g]
F_g	0.58	Predicted by Q_{gut} model [d]	0.69	Predicted by Q_{gut} model [h]
Predicted V_{ss} (L/Kg)	1.49	Reported V_{ss} is 1.1 [e]	0.60	Reported value is ~ 0.79 [f]
CL_{iv}(L/h)	23.0	Library	33.3	Library
CL_r(L/h)	0.085	Library	0.0	Library
$CL_{int,u}$(L/h)	1672.3	Library	938.5	Library

[a]: refers to Simcyp compound library (version 10).

[b]: optimized through manual sensitivity analysis in the range of 3.0-4.0 to match predicted V_{ss} (=1.49 L/kg) to reported V_{ss} (= 1.1 L/kg, range 0.76-1.86 L/kg) (28, 30, 31) and predicted C_{max} to reported C_{max} following i.v. infusion (30, 31); experimentally-determined Log $P_{o:w}$ value is 3.53 (Simcyp compound library).

[c]: parameter estimation of k_a (i.e. by fitting the PBPK model to the observed data) in the range of reported values of 1.2-4.2 h^{-1} (37, 38) using "maximum likelihood" algorithm, to match the absorption kinetics from selected clinical studies conducted in non-pregnant or postpartum subjects (4, 30, 31).

[d]: reported F_g ranges from 0.32 to 0.87 with an average of 0.51 (30, 31, 39).

[e]: extracted from (28).

[f]: optimized through manual sensitivity analysis to match predicted V_{ss} (=0.60 L/kg) to reported V_{ss} value of 0.79 (L/Kg) (28) in literature and predicted C_{max} to reported C_{max} following i.v. infusion (18); experimentally-determined Log $P_{o:w}$ value is 2.69 (Simcyp compound library).

[g]: parameter estimation of k_a in Simcyp using "maximum likelihood" algorithm, to match the absorption kinetics from selected clinical studies conducted in non-pregnant subjects (18, 32-34).

[h]: reported F_g value in literature is 0.73 (29).

Table 2: Summary of indinavir drug-dependent parameters

Parameter	Value	Methods/reference
Molecular Weight	613.79	a
Log $P_{o:w}$	2.0	Optimized [g]
pKa	5.90, 3.70	a
B/P Ratio	0.84	b
$f_{u,p}$	0.36	c,e
F_a	0.8	d,e
k_a (h^{-1})	1.8	b
F_g	0.98	Predicted by ADAM model, reported F_g is 0.93 [c]
P_{app} MDCK (10-6 cm/s)	1.9	b
Predicted V_{ss} (L/Kg)	1.29	~0.85 L/kg [g]
CL_{iv}(L/h)	77.3	f
CL_r(L/h)	8.6	d,e,f
$CL_{int,u}$(µl/min/mg)	582	b
K_{mCYP3A}(uM)	0.2	Sensitivity Analysis, *in vitro* value obtained in HLM is 0.1 µM [b]
$V_{maxCYP3A}$(pmol/min/mg protein)	116.4	Calculated by taking the product of $CL_{int,u}$ and K_{mCYP3A}

[a]: literature value(40).

[b]: literature value (37)

[c]: literature value (29)

[d]: literature value (35)

[e]: Product label for CRIXIVAN (41)

[f]: literature value (19)

[g]: Log $P_{o:w}$ was optimized through manual sensitivity analysis in the reported range of 1.5-3.0 (36) to match predicted V_{ss} (=1.29 L/kg) to reported V_{ss} (= 0.85 L/kg) estimated from i.v. PK data (19) using Phoenix WinNonlin version 6.2, and to match predicted C_{max} to reported C_{max} following i.v. infusion (19).

Fig. 1

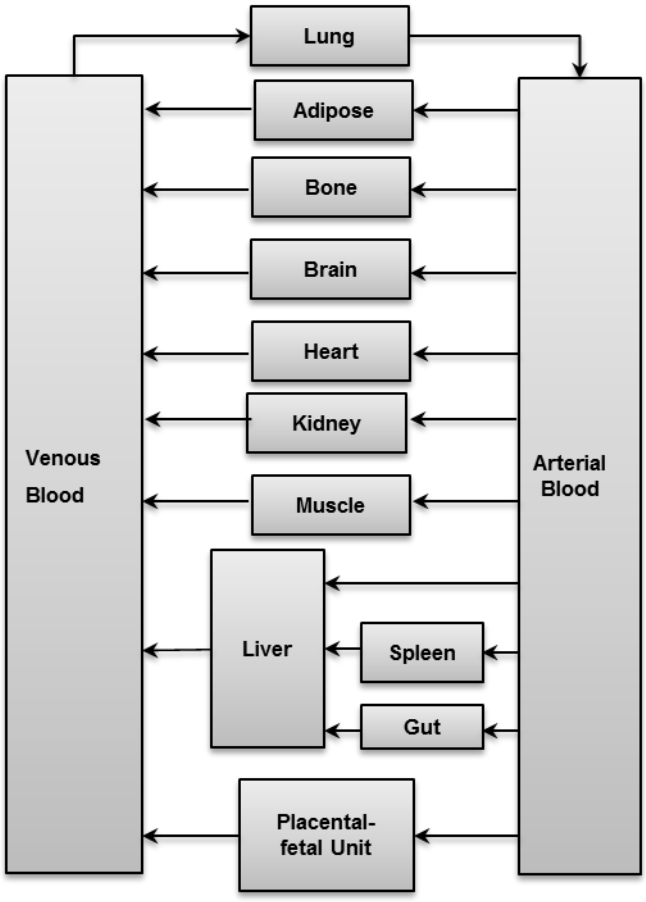
Lung
Adipose
Bone
Brain
Heart
Kidney
Muscle
Liver
Spleen
Gut
Placental-
fetal Unit
Venous
Blood
Arterial
Blood

Fig. 2

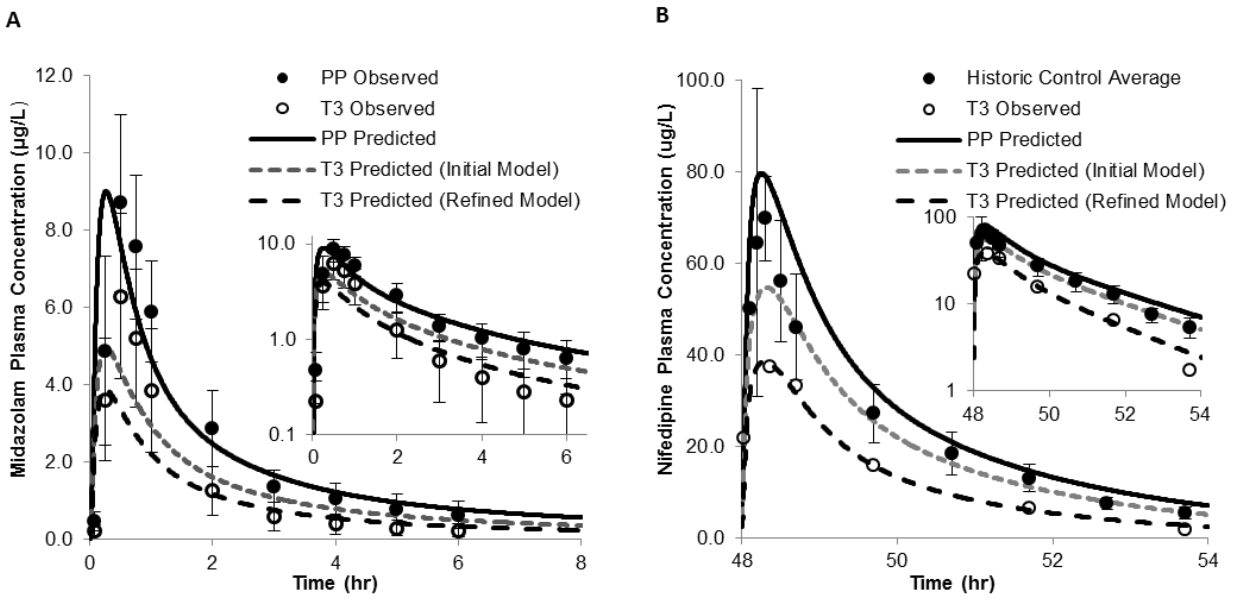
A
Midazolam Plasma Concentration (µg/L)
Time (hr)
PP Observed
T3 Observed
PP Predicted
T3 Predicted (Initial Model)
T3 Predicted (Refined Model)
B
Nifedipine Plasma Concentration (ug/L)
Time (hr)
Historic Control Average
T3 Observed
PP Predicted
T3 Predicted (Initial Model)
T3 Predicted (Refined Model)

Fig. 3

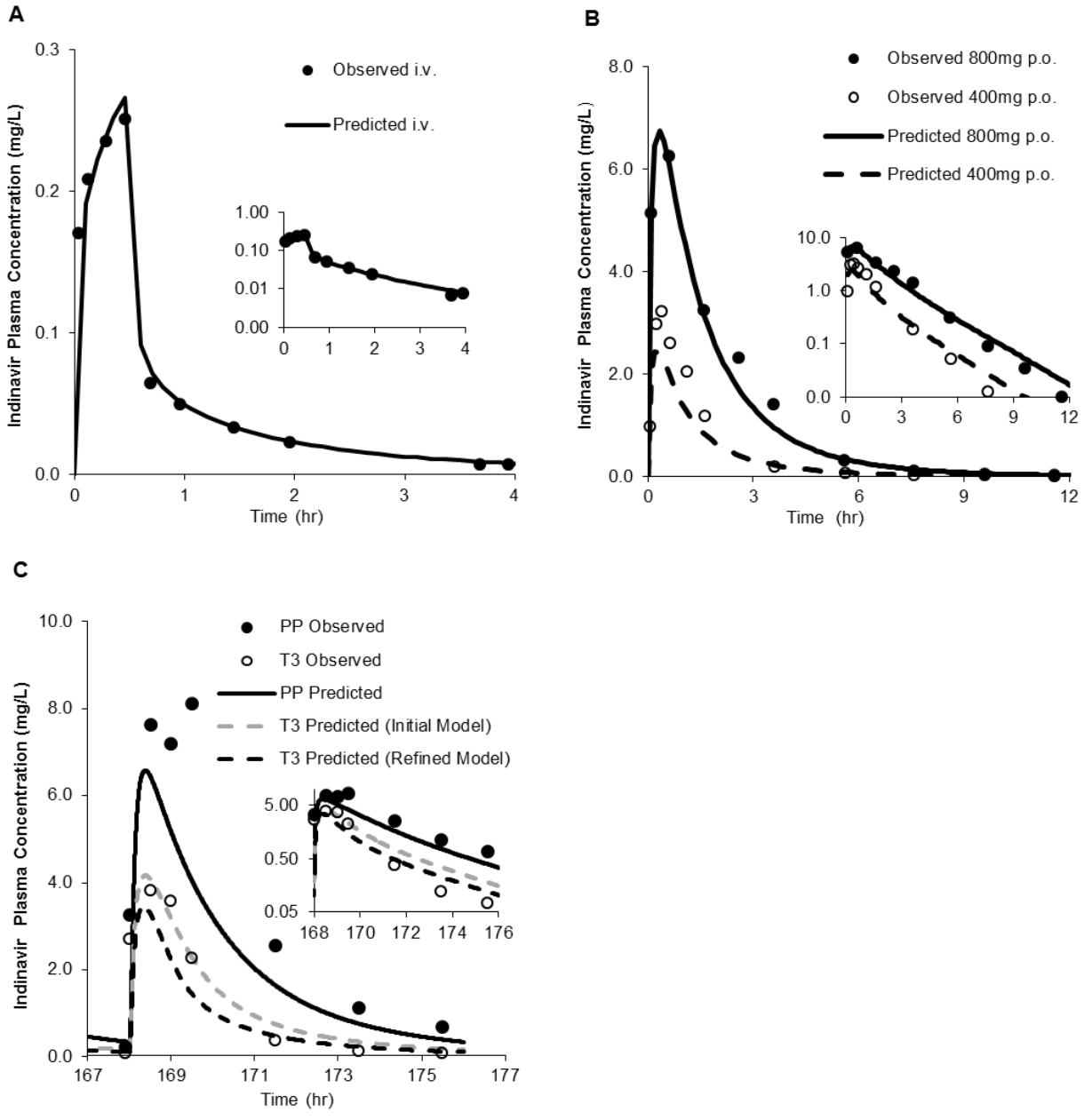
A
Indinavir Plasma Concentration (mg/L)
Time (hr)
Observed i.v.
Predicted i.v.
B
Indinavir Plasma Concentration (mg/L)
Time (hr)
Observed 800mg p.o.
Observed 400mg p.o.
Predicted 800mg p.o.
Predicted 400mg p.o.
C
Indinavir Plasma Concentration (mg/L)
Time (hr)
PP Observed
T3 Observed
PP Predicted
T3 Predicted (Initial Model)
T3 Predicted (Refined Model)

Fig. 4

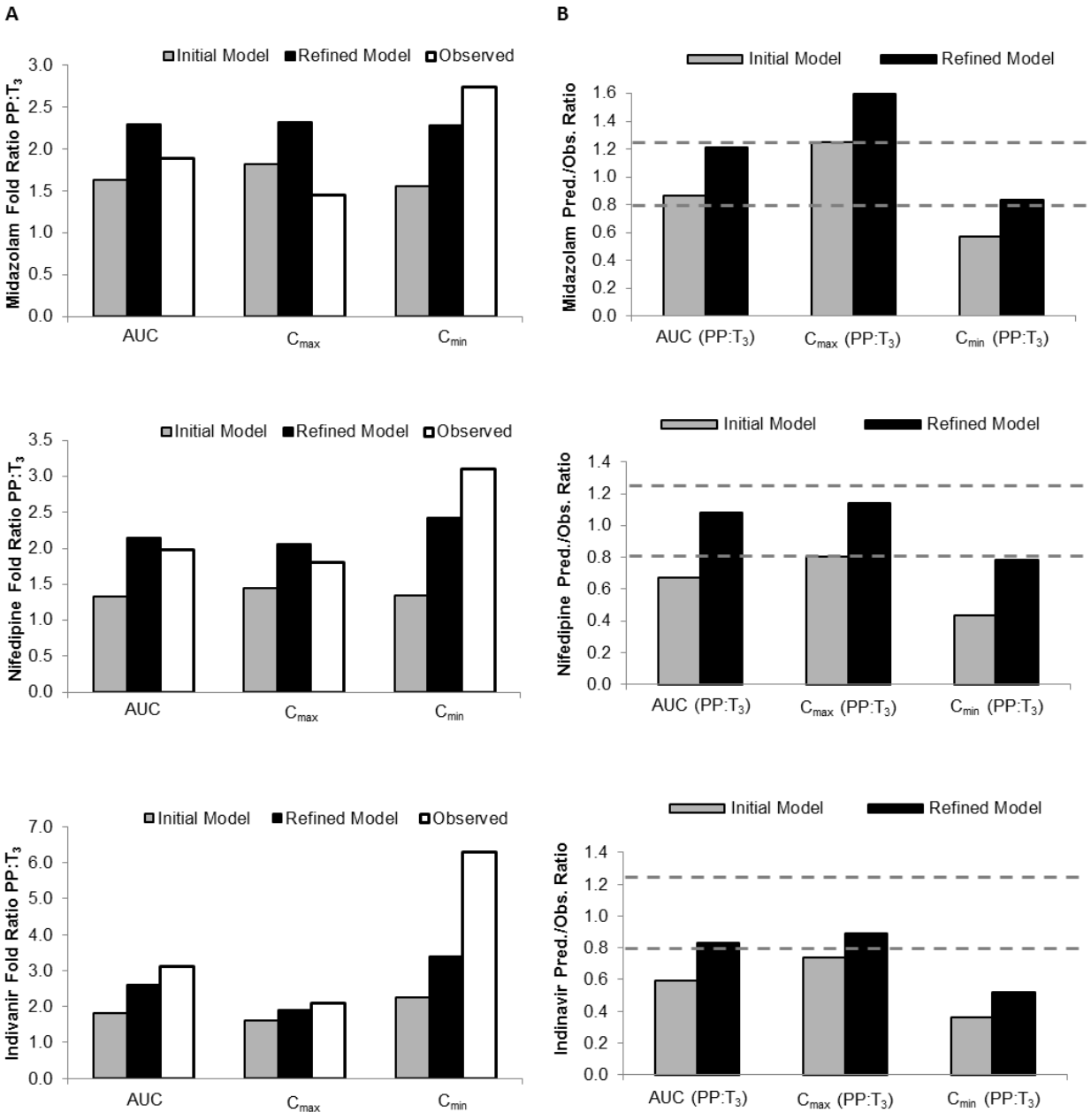
A
B
Initial Model
Refined Model
Observed
Midazolam Fold Ratio PP:T3
Midazolam Pred./Obs. Ratio
Nifedipine Fold Ratio PP:T3
Nifedipine Pred./Obs. Ratio
Indivanir Fold Ratio PP:T3
Indinavir Pred./Obs. Ratio
AUC
Cmax
Cmin
AUC (PP:T3)
Cmax (PP:T3)
Cmin (PP:T3)

Fig. 5

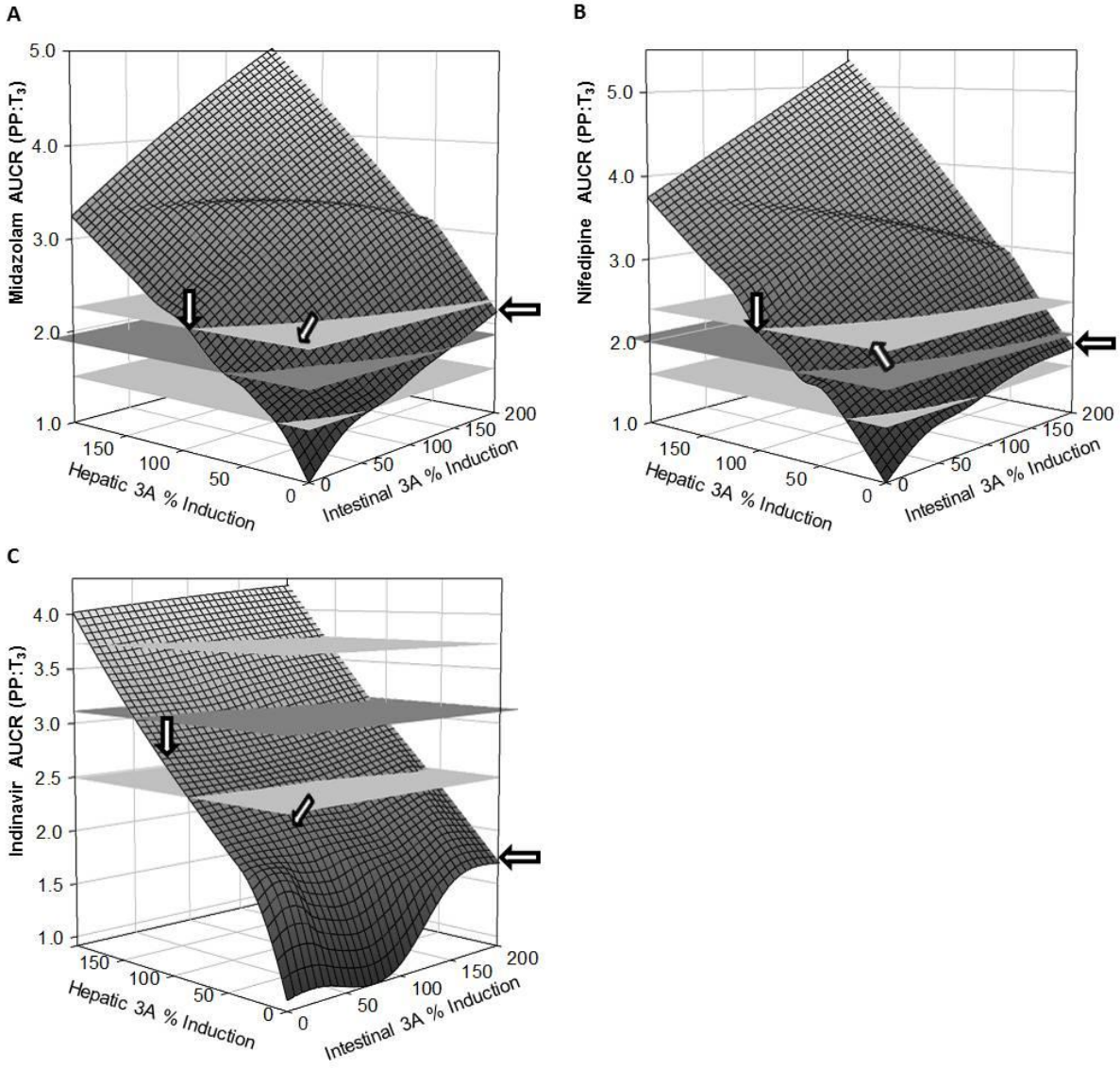
A
Midazolam AUCR (PP:T3)
5.0
4.0
3.0
2.0
1.0
150
100
50
0
Hepatic 3A % Induction
0
50
100
150
200
Intestinal 3A % Induction
B
Nifedipine AUCR (PP:T3)
5.0
4.0
3.0
2.0
1.0
150
100
50
0
Hepatic 3A % Induction
0
50
100
150
200
Intestinal 3A % Induction
C
Indinavir AUCR (PP:T3)
4.0
3.5
3.0
2.5
2.0
1.5
1.0
150
100
50
0
Hepatic 3A % Induction
0
50
100
150
200
Intestinal 3A % Induction

Supplementary Methods

General pregnancy PBPK model structure and key assumptions

Key assumptions of the PBPK model include:

1. Perfusion-limited process prevails in all organs and tissue-to-plasma partition coefficient (K_p) remains constant during pregnancy. K_p of the placental-fetal unit was set to equal to predicted K_p of the brain, based on the similarity shared between the blood-brain barrier and blood-placental barrier.
2. First-order absorption prevails and k_a, F_a and F_g remain constant during pregnancy.
3. In the original model, maternal hepatic CYP3A activity increased by 35%, 35%, 38% (DEX UR) during T_1, T_2 and T_3 respectively (20). Here, CYP3A activity was further refined to increase by 99% (1'-hydroxymidazolam unbound formation clearance) during T_3 (4). Reliable assessments of the magnitude of CYP3A induction in earlier trimesters are not available in literature.
4. Maternal glomerular filtration rate (GFR) increases during pregnancy by 19%, 40% and 37% during T_1, T_2 and T_3 trimesters respectively (12). CL_R is defined as below: $CL_R=(f_{u,p}*GFR+CL_{secretion})*(1\text{-Fraction\_reabsorbed})$. P-gp mediated $CL_{secretion}$ is assumed to increase by 107% during T_3 (digoxin $CL_{secretion}$) (4). Fraction_reabsorbed was assumed to remain constant through gestation. Serum albumin and α1-AGP concentrations decrease during pregnancy by 1%, 4%, 27%, and 1%, 22%, 19% during T_1, T_2 and T_3 respectively (12). Consequently, the change of $f_{u,p}$ during pregnancy as a function of serum albumin concentration was accounted for in the model.
5. The dynamic changes of individual tissue blood flow and volume during gestation were described by polynormial or exponential equation as described by Abduljalil et al.(12).

The pitfalls of making the model assumptions outlined above are well-recognized, as the validity of some of these assumptions has not been tested. For example, whether tissue-to-plasma partition coefficient K_p and the extent of absorption (F_a) are altered during pregnancy is unknown. Yet these assumptions were made for simplification purpose.

Governing equations

All tissues were considered to be well-stirred compartments, i.e. that the unbound tissue concentration is at equilibrium with the unbound concentration in the emergent blood (Eq. 1) (37).

$$\frac{d(VC)}{dt} = QC_{ab} - Q\frac{C}{K_p / B:P} \qquad \text{Eq. 1}$$

where V, Q and C denote the tissue volume, tissue blood flow rate and tissue drug concentration, respectively. K_p is the partition coefficient of tissue:plasma and B:P is the blood-plasma partition coefficient . The subscript 'ab' denotes arterial blood.

For drug-eliminating organ, namely the maternal liver, Eq.2 was used. Eq.3 was used to describe the apparent intrinsic clearance.

$$V_h \frac{dC_h}{dt} = (Q_h - Q_g - Q_{sl})C_{ab} + Q_g C_{vbg} + Q_{sl} C_{vbsl} - Q_h C_{vbh} - CLu_{int-H} f_u \frac{C_h}{K_p / B:P}$$

$$CLu_{int-H} = \frac{V_{max} * A_{CYP}}{K_m + f_{u,h} * C_h}$$

where C_{ab}, C_h, C_{vbsl}, C_{vbg} and C_{vbh} represent the concentrations in the arterial blood, liver, spleen-blood, gut-blood and hepatic outlet (or liver-blood), respectively; Q_h, Q_g and Q_{sl} represent the blood flows of the liver, gut and spleen respectively; f_u and $f_{u,h}$ represents the fractions unbound

in blood and liver ($f_{u,h}=f_u/(K_p$/B:P) for drugs with no active uptake or efflux). $CL_{u,int-H}$, V_{max} and K_m represent the unbound hepatic intrinsic clearance, maximum velocity and the Michaelis-Menten constant for metabolism, respectively; A_{CYP} represents the total hepatic amount of CYP isoform. Pregnancy-induced change, either induction or suppression of CYP enzyme activity was reflected in unbound hepatic intrinsic clearance $CL_{u,int-H}$ for drugs with linear kinetics, or A_{CYP} for drugs associated with saturable hepatic metabolism.

General PBPK modeling workflow

A general workflow of PBPK modeling and simulation consisted of the following steps: 1) comparison of mean plasma concentration-time (C-T) profiles simulated using Simcyp with those obtained from *in vivo* studies in non-pregnant subjects including i.v. dosing, single and multiple oral dosing (to qualify the drug-specific parameters); 2) refinement of the drug-specific parameters (e.g. f_m) if the prediction in (1) above deviates significantly from that observed. Such refinements were often based on changes in mean AUC and mean C-T profiles in non-pregnant subjects in the presence of inhibitors or genetic polymorphism of the enzymes clearing the drug; 3) populating the PBPK model with these qualified drug-specific parameters and pregnancy-induced CYP activity changes.

Sensitivity analysis

In order to reflect its impact on F_g as a result of intestinal CYP3A induction, we considered two predictive models available in Simcyp, namely Q_{Gut} model (42) and ADAM model (43). Briefly, Q_{gut} model retains the form of the "well-stirred" liver model, but the flow term (Q_{Gut}) is a hybrid of both permeability through the enterocyte membrane and villous blood flow (42).

ADAM, short for Advanced Dissolution, Absorption and Metabolism, represents GI tract in nine segments that are heterogeneous in terms of size, enzyme and transporter abundance, transit time, pH and bile salt concentration (43). The simpler Q_{Gut} is generally preferred for drugs with low-to-medium intestinal extraction (29). ADAM model is utilized when formulation-specific data (e.g., dissolution, solubility) need to be taken account into the model. Q_{Gut} model-predicted F_g matched the observed value for MDZ and NIF in the clinically-relevant dose range (Table 1 and 2), whereas ADAM model appeared to be much superior in predicting IDV F_g . Specifically, the ADAM-projected fold decrease in AUC of IDV following rifampin (RIF) treatment was 15.7-fold, compared to reported AUCR (control: RIF) of 12.5-fold (41). In contrast, Q_{gut} model projected AUCR (control:RIF) of 28.9-fold (data not shown). A RIF drug model readily available in Simcyp was used by others previously (11) and was used here in simulations without modifications. The drastic over-prediction of AUCR from Q_{gut} model is thought to be attributable to the difference in operational concentration exposed to gut CYP enzymes specified in two models: ADAM model assumes the enterocyte concentration, whereas in Q_{gut} model the portal vein concentration is used as a surrogate. Further, IDV exhibits pH-dependent solubility (36) and its impact on F_g was accounted for in the ADAM model. Our finding concerning the choice of model for predicting first-pass intestinal metabolism of IDV is also consistent with others (29, 37).

Chapter Two

A PBPK Model to Predict Disposition of P450 2D6 and P450 1A2 Metabolized Drugs in Pregnant Women

* This chapter has been accepted for publication in the journal titled “Drug Metabolism and Disposition”, and is formatted according to the requirements of the journal.

A PBPK Model to Predict Disposition of P450 2D6 and P450 1A2 Metabolized Drugs in Pregnant Women

A.B. Ke[1,2], S.C. Nallani[2], P. Zhao[2], A. Rostami-Hodjegan[3,4], N Isoherranen[1], J. D. Unadkat[1]

[1] Department of Pharmaceutics, University of Washington, Seattle, Washington, USA.

[2] Office of Clinical Pharmacology, Office of Translational Sciences, Center for Drug Evaluation and Research, Food and Drug Administration, Silver Spring, Maryland, USA.

[3] School of Pharmacy and Pharmaceutical Sciences, University of Manchester, Manchester, UK.

[4] Simcyp Limited, Sheffield, UK.

Running title: PBPK Prediction of PK Changes during Pregnancy

Corresponding author:

Dr. Jashvant D. Unadkat

Department of Pharmaceutics

University of Washington

Box 357610

Seattle, WA 98195

Telephone: 206-543-9434

Fax: 206-543-3204

E-mail: jash@u.washington.edu

Tables: 5

Figures: 6

Abstract: 249 (250 limit)

Introduction: 708 (750 limit)

Discussion: 1605 (1500 limit)

Abbreviations: ADME: absorption, distribution, metabolism and excretion; AUC, area under the curve; AUCR: AUC ratio; B/P: blood to plasma concentration ratio; CL: clearance; CL_r: renal clearance; $CL_{int,u}$: unbound intrinsic clearance; C_{max}: maximum plasma concentration; C_{min}: minimum plasma concentration; C_{ss}: steady-state plasma concentration; P450 : cytochrome P450; ER: extraction ratio; $f_{m,\ P450}$: fraction metabolized by a specific P450 isoform; $f_{u,p}$: fraction unbound in plasma; F: bioavailability; F_a: fraction absorbed; F_g: intestinal bioavailability; F_h: hepatic bioavailability; HLM, human liver microsomes; k_a: fist order absorption rate constant; K_p, tissue-to-plasma partition coefficient; Q_{Gut}, hybrid parameter of blood flow and drug permeability; PBPK model: physiologically-based pharmacokinetic model; PP: postpartum; T_1, T_2 and T_3: 1st, 2nd and 3rd trimester; UR: urinary metabolic ratio; V_{ss}: volume of distribution at steady state.

Abstract

Conducting PK studies in pregnant women is challenging. Therefore, we asked if a physiologically-based pharmacokinetic (PBPK) model could be used to evaluate different dosing regimens for pregnant women. We refined and verified our previously published pregnancy PBPK model by incorporating P450 1A2 suppression (based on caffeine PK) and P450 2D6 induction (based on metoprolol PK), into the model. This model accounts for gestational age-dependent changes in maternal physiology and hepatic P450 3A activity. For verification, the disposition of P450 1A2-metabolized drug theophylline (THEO), and P450 2D6-metabolized drugs paroxetine (PAR), dextromethorphan (DEX) and clonidine (CLO) during pregnancy was predicted. Our PBPK model successfully predicted THEO disposition during T_3. Predicted mean postpartum to 3rd trimester (PP:T_3) ratios of THEO AUC, C_{max} and C_{min} were 0.76, 0.95 and 0.66, vs. observed values 0.75, 0.89 and 0.72, respectively. Predicted mean PAR C_{ss} ratio (PP:T_3) was 7.1 vs. the observed value 3.7. Predicted mean DEX urinary ratio (UR) (PP:T_3) was 2.9 vs. the observed value 1.9 (Tracy et al., 2005). Predicted mean CLO AUCR (PP:T_3) was 2.2 vs. the observed value 1.7 (Buchanan et al., 2009). Sensitivity analysis suggested that a 100% induction of P450 2D6 during T_3 was required to recover the observed PP:T_3 ratios of PAR C_{ss} , DEX UR and CLO AUC. Based on these data, it is prudent to conclude that the magnitude of hepatic P450 2D6 induction during T_3 ranges from 100 to 200%. Our PBPK model can predict the disposition of CYP1A2, 2D6 and 3A drugs during pregnancy.

Introduction

Pregnancy can affect drug absorption (e.g., gastric pH, transporters), distribution (e.g., plasma protein binding and transporters), metabolism (e.g. cytochrome P450 metabolism) and excretion (e.g., renal secretion via transporters) (ADME) of drugs. Such changes can result in reduced efficacy (eg. antiepileptics, antivirals), or increased toxicity of a drug. Considerable clinical data in the literature suggests that the magnitude of change in maternal hepatic enzyme activity, as reflected in the change in exposure to probe drugs, is P450 isoform specific and gestational age dependent (Hodge and Tracy, 2007). Many of these studies have utilized model (probe) drugs that report P450 enzyme activities to delineate the magnitude of change in activity of major P450 enzymes, mostly during the third trimester (e.g. caffeine for P450 1A2, metoprolol for P450 2D6, midazolam for P450 3A, phenytoin for P450 2C9) (Anderson, 2005).

Hepatic P450 1A2 enzyme activity as measured by caffeine salivary clearance, is suppressed throughout pregnancy, with the greatest suppression of up to ~65% observed in the third trimester (T_3) vs. postpartum (Tracy et al., 2005). Consistent with these data, the oral clearance (CL_{ORAL}) of another P450 1A2 probe substrate, theophylline (THEO), is reduced by ~30% during T_3 vs. postpartum (PP), but the CL_{ORAL} during the first (T_1) and the second (T_2) trimesters is not affected (Gardner et al., 1987). In contrast, the activity of hepatic CYP2D6 appears to be increased during pregnancy. In pregnant women, the mean CL_{ORAL} of metoprolol (MET) (100 mg p.o.) during T_3 was almost 4-fold of that during postpartum (Hogstedt et al., 1985). However the IV clearance or the plasma protein binding of MET (10 mg) is not affected by pregnancy. Subsequently, two studies assessed CYP2D6 activity during pregnancy using the dextromethorphan/dextrorphan (DEX/DXO) metabolic ratio in pregnant

women. The plasma DEX/DXO metabolic ratio (2 hrs post dose, ~T_{max}) during T_3 is significantly reduced (~ 2.3-fold PP:T_3) among extensive metabolizers (EMs), indicating increased P450 2D6 activity (Wadelius et al., 1997). Similarly, the 24-hr DEX urinary metabolic ratio (UR: DEX/DXO) was significantly reduced throughout pregnancy in subjects phenotyped as EMs with the greatest reduction (~ 1.9-fold PP:T_3) observed during T_3 (Tracy et al., 2005). In accordance with the increased P450 2D6 activity during pregnancy, paroxetine (PAR) plasma concentrations steadily decrease over the course of pregnancy in women genotyped as P450 2D6 EMs (Ververs et al., 2009). The most pronounced effect (73% reduction compared to postpartum) on PAR steady-state plasma concentrations is observed during T_3. Finally, the CL_{ORAL} of Clonidine (CLO) is 1.7-fold of that in the nonpregnant subjects (Buchanan et al., 2009). This increase in CLO CL_{ORAL} is most likely due to increased P450 2D6 activity as P450 2D6 plays a major role in *in vitro* CLO metabolism (Claessens et al., 2010) and the renal clearance (CL_r) of clonidine appears not to be affected by pregnancy.

The above-described changes in P450 activities during pregnancy are postulated to reduce the efficacy or enhance the toxicity of drugs during pregnancy. Since it is logistically impossible to delineate the changes in PK of all drugs administered to pregnant women, alternative approaches that can generalize across drugs and predict drug disposition in pregnancy are highly-desirable. Physiologically-based pharmacokinetic (PBPK) modeling has the advantage of incorporating both physiological parameters that are important for ADME processes and drug-specific parameters (e.g. physico-chemical and drug disposition characteristics) into a quantitative predictive model (Jamei et al., 2009; Rowland et al., 2011).

A maternal PBPK model, incorporating known physiological parameters as well as maternal hepatic P450 activity in each trimester was recently developed (Abduljalil et al., 2012; Lu et al., 2012a; Lu et al., 2012b). We refined this PBPK model and showed that the PBPK model populated with P450 3A activity change, based on CL_{ORAL} of midazolam, could accurately predict the T_3 disposition of other P450 3A-metabolized drugs, nifedipine and indinavir (Ke et al., 2012). A sensitivity analysis suggested that P450 3A induction in T_3 is most likely hepatic and not intestinal. In the current study, we expanded and verified the established PBPK model, by incorporating P450 1A2 suppression and P450 2D6 induction based on disposition of caffeine (Tracy et al., 2005) and metoprolol data (Hogstedt et al., 1985). The model was then used to predict the disposition during pregnancy of P450 1A2-metabolized drug, THEO, and P450 2D6-metabolized drugs PAR, DEX and CLO.

Methods

General workflow of PBPK model development and verification criterion

A general workflow of PBPK modeling and simulation of test compounds in non-pregnant subjects consisted of the following steps: 1) comparison of mean plasma concentration-time (C-T) profiles simulated using Simcyp® Population-based Simulator (Version 11.1, Simcyp Limited, Sheffield, UK) with those obtained from *in vivo* studies including i.v. dosing, single and multiple oral dosing. The 13-compartment full-PBPK model was used; 2) refinement (hence referred to as modified model) of the drug-specific parameters (e.g. f_m) if the prediction in (1) above deviates significantly (<0.8-fold or >1.25-fold) from that observed. Such refinements were often based on changes in mean AUC and mean concentration-time profiles in the presence of inhibitors or genetic polymorphism of the enzymes clearing the drug; 3) populating the time-varying full PBPK model constructed in Matlab v. 7.10® (2010, Mathworks®, Natick, MA) with these qualified drug-specific parameters and pregnancy-induced P450 activity changes (see below).

Verification of the established PBPK model was primarily based on AUC (for DEX data urinary data were used as AUC data were not available) because achieving equivalent drug exposure in pregnant and non-pregnant women was our primary focus. The term "verification" is used in place of "validation" to acknowledge the complexity of PBPK model that requires more than plasma data to accomplish proper validation. As secondary criteria, prediction of C_{max} and $C_{min,}$ were considered because achieving similar drug C_{max} and C_{min} may be important for some drugs where these measures are related to drug efficacy and/or toxicity. For model verification, 1) mean AUC, C_{max} and C_{min} of THEO; 2) average steady-state concentration (C_{ss}) of PAR; 3) mean DEX/Dextrorphan (DXO) urinary metabolic ratio (UR); 4) mean steady-state AUC of

CLO during pregnancy were predicted and compared with published studies in pregnant, P450 2D6 EM subjects. We chose the criterion of PK bioequivalence as the criterion for successful verification of the model, namely, the predicted mean population PK parameters of the drug (as described above), should fall within 80% to 125% of the observed value, i.e. $0.80 \leq pred/obs \leq 1.25$.

General pregnancy PBPK model structure and key assumptions

The general pregnancy PBPK model structure and key assumptions were described in detail previously (Ke et al., 2012; Lu et al., 2012a). Briefly, the gestational age dependent changes in physiological parameters (e.g., cardiac output, glomerular filtrate rate, etc) were incorporated into an existing PBPK scheme (Jamei et al, 2009). Maternal glomerular filtration rate (GFR) was assumed to increase during pregnancy by 19%, 40% and 37% during T_1, T_2 and T_3 respectively (Abduljalil et al., 2012). Renal secretion clearance mediated by organic cation transporter was assumed to increase by 50% during T_3 (metformin $CL_{secretion}$) (Eyal et al., 2010). Fraction reabsorbed was assumed to remain constant through gestation. The change in drug unbound fraction in plasma ($f_{u,p}$) during pregnancy, as a function of serum albumin or α1-AGP concentrations, was accounted for in the model as described previously (Ke et al., 2012). The established PBPK model also assumed that hepatic P450 3A activity increased by 99% (measured by midazolam CL_{ORAL}) during T_3 (Ke et al., 2012).

The PBPK model was further expanded to incorporate pregnancy-induced P450 1A2 suppression and P450 2D6 induction as described below. Maternal hepatic P450 1A2 was assumed to decrease during pregnancy by 33%, 48%, 65% (salivary caffeine clearance) during 1st (T_1), 2nd

(T_2), and 3rd trimesters respectively (Tracy et al., 2005). Maternal P450 2D6 activity was assumed to increase by 200% (reported by metoprolol CL_{ORAL}) during T_3 (Hogstedt et al., 1985). This value of 200% was obtained through sensitivity analysis by varying P450 2D6 activity in the range of 50%-350% induction to recover the observed metoprolol data. Reliable assessment of the magnitude of P450 2D6 induction in earlier trimesters has not been conducted. All other maternal hepatic P450 activities were assumed to remain constant throughout pregnancy. These changes were accomplished in Matlab v7.10®.

THEO PBPK model construction

THEO physiochemical and protein binding parameters (Log $P_{o:w}$, pK_a, B/P ratio), absorption (F_a, F_g), distribution (K_p, tissue-to-plasma partition coefficient) were obtained from Simcyp (Version 11.1). Initial scaling of *in vitro* metabolic data to metabolic clearance (CL_H) over-predicted THEO CL_H observed *in vivo.* Therefore $CL_{int,u}$ was back-calculated from observed CL_H using well-stirred liver model. The contributions from individual P450 to total metabolic clearance of THEO obtained *in vitro* were 91.7%, 8% and 0.06% for 1A2, 2E1 and 3A, respectively (Tjia et al., 1996). However, *in vivo* DDI studies using diltizem and verapamil as the perpetrator (both are mechanism-based inactivator of P450 3A) reported AUC % change of 12-18% (Sirmans et al., 1988; Stringer et al., 1992), suggesting that P450 3A plays a greater role in THEO metabolism *in vivo*. Therefore, the *in vivo* P450 1A2 contribution to total metabolic clearance was reduced to 80% and *in vivo* P450 3A contribution was increased to 12%. The drug-dependent parameters of THEO are listed in Table 1.

MET PBPK model construction

MET is mainly eliminated via hepatic metabolism (~84% by P450 2D6, ~7% by P450 3A4), with a minor contribution from renal elimination (~9%) (Brown et al., 2005; Ito et al., 2005). After administration of a single dose of 100mg in healthy volunteers, there is a 4.5-fold difference in AUC of poor metabolizers (PMs) and extensive metabolizers (EMs) of P450 2D6 (Hamelin et al., 2000; Sharma et al., 2005). MET physiochemical and protein binding parameters (Log $P_{o:w}$, pK_a, B/P ratio, $f_{u,p}$), absorption (F_a, F_g, k_a), distribution (K_p, tissue-to-plasma partition coefficient) and elimination (V_{max}, $K_{m,u}$) were obtained from Simcyp (Version 11.1). Initial scaling using *in vitro* V_{max} determined in HLM significantly under-predicted CL_{IV} and CL_{ORAL} by a factor of 2.2 and 2.3 in non-pregnant, P450 2D6 EMs. This under-prediction was also evident in non-pregnant, P450 2D6 PMs (by a factor of 3.2 and 1.4, for CL_{IV} and CL_{ORAL} respectively). To improve IVIVE prediction of CL_H, *in vivo* V_{max} for P450 2D6 and P450 3A4 was optimized by multiplying *in vitro* V_{max} by a factor of 2 (Table 2). The optimized drug model showed comparable AUC, C_{max} and C_{min} following 100mg single p.o. dosing in non-pregnant, 2D6 EM and PM subjects to reported literature values. DDI prediction for the victim-perpetrator pair MET (100mg single p.o.) and quinidine (100 mg q.d for 6 days) was evaluated to qualify drug-specific parameters, specifically $f_{m,2D6}$. Perpetrator drug model (quinidine, Qd) readily available in Simcyp was used in all simulations without modifications. The drug-dependent parameters of MET are listed in Table 2.

PAR PBPK model construction

PAR is extensively metabolized in humans and exhibits nonlinear kinetics during single and multiple dosing (Kaye et al., 1989). After the administration of a single dose of PAR, there is a 7-fold difference in the median total clearance in PMs and EMs of P450 2D6, which is then

reduced to 2-fold at steady state (Sindrup et al., 1992a; Sindrup et al., 1992b). The nonlinear PK of PAR is much more pronounced in EMs than PMs, mainly due to time-dependent inhibition of the P450 2D6-mediated metabolism (Venkatakrishnan and Obach, 2005).

A previously published PAR PBPK model (Jornil et al., 2010) was modified as described below. Jornil et al. showed that, in addition to P450 2D6, P450 3A and P450 1A2 are involved in the metabolism of PAR. The authors then used prior *in vitro* and *in vivo* information on the metabolism of PAR to predict the exposure in EM and PM individuals receiving single and multiple dosing regimens using SimCYP. However, IVIVE approach significantly under-predicted single-dose and steady-state median CL_{oral} for P450 2D6 PM subjects by a factor of 2.9 and 3.5 respectively (Jornil et al., 2010). It is worth noting that even though PAR has been identified, *in vitro*, as a P450 3A mechanism-based inhibitor (MBI) (Venkatakrishnan and Obach, 2005), the *in vivo* importance of P450 3A inactivation by PAR may be limited (Jornil et al., 2010). When such inactivation was considered, the predicted mean percent of active P450 3A enzyme remaining at steady-state, was 97% and 93% in P450 2D6 EMs and PMs, respectively. In contrast, 34% of P450 2D6 activity was predicted to remain in EMs. Sensitivity analysis showed that varying maximal inactivation rate constant ($K_{inact,3A}$) and inactivation constant ($K_{I,3A}$) in the range of 0.1-10 fold of reported values had minimal impact (<10%) on AUC and C_{max} of PAR in PM population, in which P450 3A is expected to be the major elimination pathway of PAR. Based on these analyses, it has been speculated that, there is a non-P450 3A, non-renal pathway responsible for PAR elimination in P450 2D6 PMs. Therefore, we modified the PBPK model established by Jornil et al. by incorporating an un-identified pathway ($CL_{int,other}$) ($f_{m,other}$ =9.7 % in 2D6 EMs) into the IVIVE model. The optimized drug model was verified by comparing the predicted mean AUC, C_{max} and C_{min}

following single or chronic p.o. dosing in non-pregnant, P450 2D6 EM and PM subjects to reported literature values. The drug-dependent parameters of PAR are listed in Table 3.

DEX and DXO PBPK model construction

The DEX/DXO metabolic ratio, such as plasma concentration of the parent/metabolite (C_p/C_m) or urinary concentration ratio (UR) is commonly used in drug-drug interaction and pharmacogenetic studies as an *in vivo* measure of P450 2D6 activity (Borges et al., 2005; Lutz and Isoherranen, 2011). DEX is extensively *O*-demethylated to dextrorphan by P450 2D6. The formation of dextrorphan (DXO) by P450 2D6 is responsible for approximately 97% of the oral clearance of dextromethorphan (DEX) in EMs (Capon et al., 1996; Gorski et al., 2004). Dextrorphan then undergoes glucuronidation mostly by UGT2B7 (Lutz and Isoherranen, 2011) . *N*-demethylation to 3-methoxymorphinan also occurs, largely by P450 3A4 (Yu and Haining, 2001). Both dextrorphan and 3-methoxymorphinan are further metabolized to 3-hydroxy-morphinan, by P450 3A4 and 2D6, respectively (Yu and Haining, 2001; Lutz and Isoherranen, 2011).

DEX physiochemical and protein binding parameters (Log $P_{o:w}$, pK_a, B/P ratio, $f_{u,p}$), absorption (F_a, F_g), distribution (K_p, tissue-to-plasma partition coefficient) and hepatic elimination (P450 3A-mediated unbound intrinsic clearance, or $CL_{int,h,u,3A}$) were from Simcyp compound library (Version 11.1). $CL_{int,u,2D6}$ was estimated in Simcyp by simultaneously fitting observed plasma concentration-time (C-T) profiles extracted from previous publications (Abdul Manap et al., 1999; Moghadamnia et al., 2003) (see Table 4). Optimization of $CL_{int,u,2D6}$ was necessary to match predicted bioavailability ($F_a*F_h*F_g$ ~7%) to that reported (<5%) (Capon et al., 1996). CL_r of DEX was assumed to approximate $f_{u,p}$ *GFR (see footnote to Table 4). The optimized drug

model was verified by comparing predicted mean AUC, C_{max} and C_{min} following single p.o. dosing, or in the presence of quinidine, in non-pregnant 2D6 EM and PM subjects, to reported literature values.

Then, to predict cumulative amount of DXO in urine, we constructed a semi-PBPK model with the following assumptions and/or simplifications: 1) we assumed that the metabolite distributed homogeneously into nonmetabolic tissues/organs and that these tissues can be combined into an apparent plasma compartment; 2) the metabolite formed in gut and liver was available for further metabolism by P450 3A; 3) glucuronidation of DXO was not incorporated due to lack of appropriate scaling factors for UGT enzymes in hepatic and extra-hepatic tissues, therefore quantitative prediction of plasma concentration-time profiles of free or total DXO was not possible. DXO physiochemical and protein binding parameters (Log $P_{o:w}$, pK_a, $f_{u,p}$) and elimination ($CL_{int,h,u,3A}$) were obtained from the literature (Table 4). Apparent CL_r (= 5 L/h) of DXO was determined through sensitivity analysis by comparing simulated $A_{e,DXO,0\text{-}24h}$ values to those reported (Jones et al., 1996; Abduljalil et al., 2010)(see footnotes to Table 4). Given the wide range of reported DXO recovery in urine (f_e=40-91%), in addition to apparent CL_r of DXO and P450 3A-mediated clearance, biliary excretion of DXO conjugates was incorporated into the DXO model (see footnote to Table 4). The combination that best recovered the observed $A_{e,DXO}$ was used in the final model. In addition, the DXO PBPK model accounted for pregnancy-induced changes including a decrease in plasma protein binding of DXO, increase in apparent renal clearance of DXO, and increase in P450 3A-mediated clearance of DXO. The drug-dependent parameters of DEX and DXO are listed in Table 4.

CLO PBPK model construction

CLO has dose-proportional kinetics following i.v. administration, single or multiple dosing in the clinical dose range (Arndts et al., 1983). In nonpregnant subjects, approximately 41-62% of orally administered CLO is cleared unchanged by the kidney (Frisk-Holmberg et al., 1981; Arndts et al., 1983), with the remainder undergoing hepatic metabolism to produce inactive metabolites, mainly 4-hydroxyclonidine. Selective inhibition studies in human liver microsomes have shown that P450 2D6 plays a major role in clonidine metabolism, followed by P450 3A and P450 1A2 (Claessens et al., 2010).

Physiochemical and protein binding parameters (Log $P_{o:w}$, pK_a, $f_{u,p}$), absorption (F_a), distribution (K_p, tissue-to-plasma partition coefficient), and elimination (CL_{IV}, CL_r, f_e) were obtained from literature. B/P ratio and F_g were predicted in SimCYP (Version 11.1). The contribution from individual P450 to the metabolic clearance (67%, 22% and 11% for P450 2D6, 3A and 1A2, respectively) were obtained in HLM (Claessens et al., 2010). Then, $CL_{int,h,u}$ for P450 2D6, 3A and 1A2 were back-calculated from hepatic CL (=CL-CL_r), f_m for individual P450 , and 'average' population values for liver weight and hepatic P450 enzyme abundance for P450 3A, 1A2 and 2D6, respectively. The drug-dependent parameters of CLO are listed in Table 5.

Results

1. Prediction of THEO PK in pregnancy using PBPK model incorporating P450 1A2 suppression based on caffeine data

The disposition of THEO, following multiple p.o. dose during T_3 and postpartum (PP) was predicted (Gardner et al., 1987). Briefly, the disposition of THEO was assessed in ten pregnant, non-smoking asthmatic women, who had been chronically maintained on sustained release theophylline. Twenty-four hrs preceding the study, all subjects were switched to immediate release theophylline tablets and the last dose was given before mid-night of the study day. After overnight fasting, a single oral dose of theophylline (Somophyllin liquid, 259 mg) was administered. Compared to PP (range of 14-58 wks PP), THEO CL_{ORAL} during T_1 (13-19 wks) and T_2 (23-28 wks) was not significantly altered. THEO CL_{ORAL} during T_3 (range of 34-39 wks) was reduced and remained suppressed during immediate PP period (9-13 wks PP) (Gardner et al., 1987). Hence, systemic exposures of THEO obtained during 14-58 wks PP was considered to represent baseline levels and those obtained during immediate PP period (9-13 wks PP) were excluded. Predicted mean Theo AUCR (PP:T_3), C_{max} ratio (PP:T_3) and C_{min} ratio (PP:T_3) were 0.76, 0.95 and 0.66, compared to the observed values of 0.75, 0.89 and 0.72, respectively (Fig. 1 and Supplemental. Table 1). All predictions met verification criterion (i.e. the pred./obs. of mean AUC, C_{max} and C_{min} were in the range of 0.9-1.1). Predicted mean Theo AUCR (PP:T_1) and (PP:T_2) were 0.79 and 0.77, compared to observed values of 0.99 and 0.95 respectively (Supplemental. Table 1). THEO plasma unbound fraction was predicted to be modestly increased from 58% during postpartum to 66% in T_3, consistent with observed values (59% PP vs. 68% T_3). THEO CL_r was predicted to be increased from 0.45 L/hr during postpartum to 0.68 L/hr in T_3, a 52% increase that is comparable to the observed 48% reported by Frederiksen et al., 1986.

2. Prediction of PK for P450 2D6 substrates in pregnancy

2.1. MET prediction to inform P450 2D6 induction in pregnancy

The mean AUC of MET (100 mg single p.o.) in non-pregnant, P450 2D6 EM and PM subjects, or in the presence of inhibitor (quinidine) were quantitatively predicted by the modified (see Methods) MET model (i.e., pred./obs. in the range of 0.9-1.2, Fig. 2 and Supple. Table 2). Specifically, the predicted AUC_{PM}/AUC_{EM} of 4.1 matched well with the observed ratio of 4.5 (Hamelin et al., 2000; Sharma et al., 2005). The predicted mean AUC_I/AUC for victim-perpetrator pair MET (100 mg single p.o.) and quinidine (100 mg q.d. for 6 days) is 3.3-fold, compared to observed AUCR of 3.2-fold (Johnson and Burlew, 1996). The corresponding pred./obs. of mean C_{max} and C_{min} were in the range of 0.7-0.9 and 1.3-1.4, respectively.

MET exposure in pregnant women was assessed (Hogstedt et al., 1985) and the observed increase in $CL_{ORAL,}$ during pregnancy, was used to deconvolute the magnitude of increase in P450 2D6 activity after accounting for other pregnancy related components of MET CL_{ORAL} (P450 3A-mediated CL, CL_r and protein binding). In this study, the disposition of MET following i.v. and oral dosing was studied in five women who developed hypertension during pregnancy and after delivery. The change in systemic clearance following i.v. dosing of MET (10 mg) during pregnancy vs. postpartum was insignificant, although there was a trend towards higher CL_{IV} during T_3 (T_3 vs. PP: 82.8±15.6 L/hr vs. 39± 4.8 L/hr, n=5). The mean CL_{ORAL} following a single oral dose of 100 mg during pregnancy was almost quadrupled (range 2-13 fold). Although P450 2D6 genotype of the five study subjects was not determined, comparison of reported individual AUC values following oral dosing to literature values (Johnson and Burlew, 1996; Hamelin et al., 2000; Sharma et al., 2005) confirmed that the systemic exposures of all five subjects were comparable to those of EM subjects and were significantly lower than

those of PM subjects (Hamelin et al., 2000; Sharma et al., 2005) (Fig. 2A). The PBPK model incorporating 200% induction of P450 2D6 during T_3, predicted mean AUCR (PP:T_3) of 3.0, mean C_{max} ratio (PP:T_3) of 2.8, mean C_{min} ratio (PP:T_3) of 3.5, compared to the observed ratios of 3.6±2.3, 2.4±1.3 and 2.0±2.5, respectively (Fig. 2B). With the exception of C_{min} ratio, the model-predicted AUCR and C_{max} ratio met verification criterion (Supple. Table 2). The predicted MET plasma unbound fraction was 88% during PP vs. 90.7% in T_3, consistent with the observed values (89% ± 11% PP vs. 90.7% ± 17% T_3).

2.2 PAR PK prediction in pregnancy

We modified a previously published PAR PBPK model (see Methods) and predicted single-dose (30 mg SD) and steady-state (SS, 30 mg QD) PAR AUC in both EM and PM, non-pregnant individuals. The mean $AUC_{0\text{-}inf}$ or $AUC_{ss,0\text{-}tau}$ in non-pregnant, P450 2D6 EM and PM subjects, was quantitatively predicted by the modified PAR model (i.e., pred./obs. in the range of 0.8-1.2, Fig. 3A and Supple. Table 3). The model-predicted mean SD and SS C_{max} and C_{min} in EMs met verification criterion. In PMs, the pred./obs. values of mean SD and SS C_{max} and C_{min} were in the range of 1.0-1.3 (Supple. Table 3). PAR exposure in pregnant women was predicted based on the study design described by Ververs et al. (Ververs et al., 2009). In this study, subjects were genotyped and steady-state ($C_{ss,ave}$) PAR plasma concentrations were examined in each of the three trimesters but not during postpartum. Women who were genotyped as EM showed steadily decreasing plasma paroxetine concentrations during the course of pregnancy. During T_3, the median $C_{ss,ave}$ plasma concentration declined to 5 ng/mL (range 0.6-19.6 ng/mL) following the daily dose of 19.9±8.8 mg (range 3–40 mg), compared to median $C_{ss,ave}$ plasma concentration of 18.4 ng/mL (range 3.3-66 ng/mL) in historical controls receiving 20 mg daily (Sindrup et al.,

1992a). These observations correspond to median $C_{ss,ave}$ ratio (PP:T_3) of 3.7 (Fig. 3B). The PBPK model incorporating 200% induction of 2D6 during T_3, predicted mean PAR $C_{ss,ave}$ ratio (PP:T_3) of 7.1 following 20 mg daily (14 days). Sensitivity analysis suggested that a 100% induction of P450 2D6 during T_3 was required to recover the observed change in PAR $C_{ss,ave}$ ratio (PP:T_3) (pred. value 4.1; Fig. 3B and Supple. Table 4). Furthermore, P450 2D6 activity was induced modestly by 10% and 25% in T_1 and T_2, respectively, to recover the observed changes in median PAR C_{ss} ratio (PP:T_1) and C_{ss} ratio (PP:T_2) of 1.6 and 1.9, respectively (data not shown).

2.3 DEX PBPK model prediction

The modified (see Methods) DEX model-predicted mean AUC in non-pregnant, P450 2D6 EM and PM subjects following the administration of a single oral dose of 30 mg DEX, met verification criterion (i.e. pred./obs. values within the range 0.9-1.0, Fig. 4 and Supple. Table 5). Specifically, the predicted AUC_{PM}/AUC_{EM} of 65.0 was comparable to the observed ratio of 73.5 (pred./obs. ratio of 0.9). In addition, the predicted mean AUC_I/AUC for the victim-perpetrator pair DEX (30 mg single p.o.) and quinidine (50 mg single p.o. given 1-hr prior the DEX dose) was 15.9-fold, compared to observed mean AUC_I/AUC of 20.8-fold (pred./obs. ratio of 0.8) (Capon et al., 1996; Abdul Manap et al., 1999). The model-predicted mean C_{max} in the presence/absence of quinidine in non-pregnant, P450 2D6 EMs, met verification criterion (i.e. pred./obs. values within the range 0.9-1.1 (Fig. 4 and Supple. Table 5). Mean C_{max} in non-pregnant, P450 2D6 PMs was slightly over-predicted (pred./obs. of 1.3). Mean C_{min} in the presence and absence of quinidine in non-pregnant, P450 2D6 EMs was under-predicted (pred./obs. of 0.2 and 0.5, respectively). However model-predicted mean C_{min} in non-pregnant,

P450 2D6 PMs, met verification criterion (pred./obs. of 0.8). Furthermore, the predicted mean cumulative amount (0.06 mg) of DEX (30 mg p.o.) excreted in urine ($A_{e,0\text{-}24h}$) in EMs was also in reasonable agreement with the observed data: 0.075±0.167 mg (Abduljalil et al., 2010) and 0.153±0.155 mg (Jones et al., 1996) (Fig. 5A).

Since plasma concentration-time data for DEX are not available in pregnant subjects, a semi-PBPK model to predict the cumulative amount of DXO excreted in urine was constructed (see Methods). The model-predicted $A_{e,0\text{-}24h}$ of DXO in EMs, following the administration of a single oral dose of 30 mg, was within the range of the observed values (9.6 mg pred. vs. 1.3-15.3 mg obs. (Jones et al., 1996; Abduljalil et al., 2010) (Fig. 5A). Further, the predicted PP $UR_{0\text{-}24h}$ (DEX/DXO) of 0.0065 in 2D6 EMs matched the reported median PP $UR_{0\text{-}24h}$ of 0.0063 (90% CI: 0.0037-0.027) (n=25) (Tracy et al., 2005) and the reported $UR_{0\text{-}72h}$ (mean: 0.0082; range 0.0007-0.028) in non-pregnant, 2D6 EMs (n=11) (Borges et al., 2005). The observed median T_3 DEX $UR_{0\text{-}24h}$ was 0.0033 (90% CI: 0.0015-0.0086), compared to median PP DEX $UR_{0\text{-}24h}$ of 0.0063 (90% CI: 0.0037-0.027). These observations correspond to median DEX UR (PP:T_3) of 1.9±1.2. The PBPK model incorporating 200% induction of 2D6 during T_3, predicted mean DEX UR (PP:T_3) of 2.9. Sensitivity analysis by varying P450 2D6 activity in the range of 50-250% suggested that a 100% induction of P450 2D6 during T_3 was required to recover the observed change in DEX UR (pred. value 1.9, Fig. 5B and Supple. Table 6). The reported median DEX UR (PP:T_1) and DEX UR (PP:T_2) are 1.6 and 1.9, respectively, suggesting the magnitude of P450 2D6 induction during T_1 and T_2 are similar to that of T_3.

2.4 CLO PBPK model prediction

The constructed CLO PBPK model was first verified by comparing the predicted vs. the observed disposition kinetics of an i.v. dose of 1.79-2.35 µg/Kg to non-pregnant healthy volunteers (Frisk-Holmberg et al., 1981). The pred./obs. $AUC_{0\text{-}inf}$ was in the range of 1.1-1.2 (Supple. Table 7). The pred./obs. $C_{min,\ 24h}$ was 0.4 (2.35 µg/Kg) and 1.0 (1.79 g/Kg). The PBPK model was also verified against the disposition kinetics following the administration of a single oral dose of 0.1-0.3 mg to non-pregnant healthy volunteers. Model-predicted $AUC_{0\text{-}inf}$, C_{max} and $C_{min,\ 24h}$ all met verification criterion (Fig. 6A and Supple. Table 7). The PBPK model incorporating 200% induction of 2D6 during T_3, predicted mean AUCR (PP:T_3) of 2.2 (observed value 1.7) (Buchanan et al., 2009). Sensitivity analysis suggested that a 100% induction of P450 2D6 during T_3 better recovered the observed AUCR (PP:T_3) (pred. value 1.8, Fig. 6B and Supple. Table 8). Because clonidine is a substrate of renal transporter OCT, the current PBPK model accounted for pregnancy-induced increase in GFR and OCT-mediated secretion (measured by metformin $CL_{secretion}$) (Eyal et al., 2010), and predicted that CLO CL_r increased from 116.8 mL/min to 182.7 mL/min. If CL_r was kept constant during T_3, both 100% and 200% induction of P450 2D6 during T_3 could recover (1.48 and 1.84, respectively, Supple. Table 8) the observed AUCR (PP:T_3) of 1.7.

Discussion

The pregnancy PBPK model populated with P450 1A2 activity change based on caffeine salivary clearance, quantitatively predicted THEO disposition during T_3. The pregnancy effect on THEO is smaller than the decrease in P450 1A2 activity (reported by caffeine) as THEO has significant renal clearance (15%) and minor P450 3A-mediated clearance (7%), both of which increase during T_3 and counteracts the decrease in 1A2 activity. Based on the 1A2 decrease during T_1 and T_2 reported by the caffeine data, a modest increase (<23%) in THEO AUC during T_1 and T_2 was predicted. Such a modest decrease may not be detectable in the clinic or be clinically significant. Indeed, the observed data shows a lack of pregnancy effect on THEO disposition during these periods. Additional pregnancy PK data on other 1A2 substrates are needed to confirm or refute whether the assumed 1A2 activity suppression based on caffeine data during T_1 and T_2 can recover the disposition of other 1A2 substrates (such as clozapine).

The increase in P450 2D6 activity during pregnancy is intriguing because 2D6 is not inducible by xenobiotics, and only HNF4α has been shown to have a role in regulating 2D6 transcription (Corchero et al., 2001). Given that MET has linear PK and is a well-accepted 2D6 probe drug ($f_{m,2D6}$ =84 %) with minor involvement from other clearance pathways (P450 3A-mediated CL and CL_r), the pregnancy PBPK model was populated with 2D6 activity change based on CL_{ORAL} of MET. The lack of significant pregnancy-induced effect following i.v. dosing is not surprising. MET is an intermediate-to-high ER drug, and CL_{IV} is reflective of both the magnitude of hepatic blood flow and 2D6-mediated intrinsic clearance. The lack of pregnancy-induced effect on CL_{IV} suggests that hepatic blood flow does not increase significantly during T_3.

This is consistent with the conclusion drawn from meta-analysis of literature data on the direct assessment of hepatic blood flow in pregnant women (Abduljalil et al., 2012).

Because *in vitro* PAR metabolic data did not recover observed metabolic clearance in non-pregnant EM and PM individuals, we modified a published PAR model by incorporating an un-identified pathway ($CL_{int,other}$) into the IVIVE model. At steady-state (20 mg QD), this $CL_{int,other}$ contributes <10% of PAR clearance in EMs and ~50% in PMs (see Table 3). $CL_{int,other}$ was assumed not to be affected by pregnancy. Under this assumption, the magnitude of 2D6 induction would be slightly over-estimated by assuming this $CL_{int,other}$ pathway is not induced . However, if the contrary is true and $CL_{int,other}$ is suppressed (more likely, see below), the impact of this minor pathway on estimating the magnitude of 2D6 induction would be minimal in 2D6 EMs (<10%). 2D6 induction of 100% as opposed to 200%, recovered the observed C_{ss} (PP:T_3) in EMs. Interestingly, in PMs, the median PAR C_{ss} was 48, 65, and 71 µg/L during T_1, T_2 and T_3, respectively (n=2) (Ververs et al., 2009). In comparison, the reported C_{ss} in non-pregnant PMs is 80±16 µg/L (n=3) (Sindrup et al., 1992a). From this very limited data set, we speculate that in PMs where $CL_{int,other}$ and P450 3A contribute equally to PAR clearance, $CL_{int,other}$ is suppressed during pregnancy, similar to 1A2. This suppression counteracts the effect of P450 3A induction.

DEX is the most sensitive P450 2D6 probe substrate with the highest $f_{m,2D6}$ amongst all the drugs included in the model verification set. Therefore, we would expect that the systemic exposure of DEX to be reduced substantially in pregnant women. However, such evaluation of DEX plasma concentration-time profiles in pregnant women is not available in literature.

Nonetheless, Wadelius et al. reported a change in DEX plasma concentration (2 hrs post dose, ~ T_{max}) of 2.3-fold (PP:T_3, range 1.5 to 4.9-fold) in 2D6 EMs (n=13) (Wadelius et al., 1997). Despite the expected variability associated with C_{max}, this change in DEX concentration is in line with ~100% induction of 2D6: model-predicted DEX AUCR (PP:T3) and C_{max} (PP:T3) were 2.4 and 3.0 in 2D6 EMs (data not shown). Two-hundred percent induction of 2D6 would over-predict C_{max} (PP:T_3) by 91%.

Since the pregnancy effect on DEX $UR_{0\text{-}24h}$ was evaluated, we developed a semi-PBPK model of DXO to predict this UR. Construction of a fully-mechanistic DXO model is not possible, mainly because once DXO is formed by 2D6, significant glucuronidation of DXO in hepatic and extra-hepatic tissues occurs, and the appropriate scaler for IVIVE of this clearance is not available (Lutz and Isoherranen, 2011). However, this limitation is not expected to impact our ability to predict DEX $UR_{0\text{-}24h}$, as the latter is based on total DXO amount excreted in urine, and free and conjugated DXO are mostly recovered in urine (range of recovery 40.2-85%) (Rostami-Hodjegan et al., 1999). The developed model quantitatively predicted mean $A_{e,DEX,}$ $A_{e,DXO}$ and mean DEX $UR_{0\text{-}24h}$, in non-pregnant, 2D6 EMs. It is important to note that the inter-individual and inter-study variability in observed $A_{e,DEX}$ and $A_{e,DXO}$ in non-pregnant, 2D6 EMs is substantial, possibly due to the heterogeneity of 2D6 EM population (i.e. allelic variant-specific 2D6 activity) and urine pH-dependency of DEX CL_r (Abduljalil et al., 2010). The PBPK model incorporating 200% induction of 2D6 during T_3, over-predicted mean DEX UR (PP:T_3) by 50%. To recover the observed change, 2D6 activity would need to be induced less than 200% or the CL_r of DEX would need to be increased by 2.5-fold. In the current PBPK model, DEX CL_r is assumed to be mainly filtration clearance as DEX has not been identified as a

substrate of major renal transporters. Recent evidence suggests DEX may be secreted by the kidneys (unpublished data, Lutz and Isoherranen). Nevertheless, until confirmed, we concluded that 100% induction of 2D6 during T_3 was required to recover the observed change in DEX UR.

In pregnant women, CL_r (=153±67 ml/min) of CLO (Buchanan et al., 2009) did not deviate significantly , from that obtained in Japanese male population (183±55 ml/min) (Fujimura et al., 1994). Therefore, the authors attributed the increase in apparent oral clearance of clonidine during pregnancy to a change in its nonrenal clearance (i.e. 2D6). On closer examination, the reported CL_r in pregnant women is higher than calculated CL_r (= f_e*CL_{IV}) based on mean f_e and mean CL_{IV} in literature (116.8 ml/min, see Table 5). Nevertheless, if CL_r was kept constant during T_3, both 100% and 200% induction of 2D6 during T_3 could recover the observed AUCR (PP:T_3). This finding is not surprising, because CLO AUCR (PP:T_3) is not a sensitive reporter of changes in 2D6 activity ($f_{m,2D6}$=30%) when the latter is masked by a change or lack of change in CL_r, the major elimination pathway of CLO (f_e =41-62%).

The above analyses suggest that P450 2D6 induction during pregnancy could range from 100% to 200%. To determine if this range could be narrowed, we expanded our sensitivity analysis to recover possible range of 2D6 induction that bracket 80%-125% of the observed MET, PAR, DEX and CLO data in pregnancy. We found these ranges did not overlap, indicating the drugs evaluated reported different magnitude of P450 2D6 induction, even after accounting for inter-study variability. The reason for these discrepancies is not clear, although we suspect it may be related to the study design being less than optimal. For e.g., the MET study has limited sample

size, and the inter-individual variability of the observed data is large; the PAR dose used varied from 3-40 mg in the PAR study, and the reported PAR concentrations normalized to the mean dose of 20 mg can be misleading for a drug with non-linear kinetics. Additional limitations include the lack of concentration-time profile (PAR and DEX) or the use of urinary metabolic ratio as an index of enzyme activity (DEX) in the published reports. Therefore, to definitively assess the magntidue of CYP2D6 induction during pregnancy, we propose that a PK study with the most sensitive 2D6 probe DEX, where the plasma concentration-time profile of DEX is measured, be conducted during various stages of pregnancy and postpartum. In the absence of such data, we can only conclude that the P450 2D6 induction during the 3rd trimester ranges from 100% to 200%.

The underlying mechanism for the hepatic isoform-specific and gestational state specific induction during pregnancy is not fully understood. Data from human hepatocyte incubation with pregnancy-related hormones suggest that the rising concentrations of various hormones in maternal blood, including placental growth hormone (PGH), progesterone, corticosteroids and estrogens, contribute to induction of some of these isoforms (Jeong, 2010; Papageorgiou and Unadkat, 2011; Dickmann and Isoherranen, 2012). In contrast, suppression of 1A2 activity during pregnancy may be due to the increase in circulating concentration of cytokines (e.g. IL-1ß and IL-6) which suppress 1A2 mRNA expression in human hepatocytes (Dickmann et al., 2011). However, the mechanisms for P450 2D6 induction during pregnancy still remains unknown and further mechanistic studies are warranted to fill this knowledge gap.

In summary, we have shown that our PBPK model: 1) can quantitatively predict the disposition of P450 1A2 drug, THEO, during T_3; 2) defined the range of 2D6 induction during T_3 to be 100% to 200% through modeling MET, PAR, DEX and CLO disposition during pregnancy; 3) allows extrapolation beyond model drugs studied (e.g. caffeine and metoprolol) to other drugs with well-characterized ADME characteristics (e.g. THEO, PAR). Previously, we have shown that such extrapolation can also be made for P450 3A metabolized drugs (Ke et al., 2012). Our study also highlights the importance of further mechanistic and probe drug studies pertaining to P450 2D6 induction during pregnancy. Since conducting PK studies in pregnant women is challenging, we propose that this refined PBPK model be used to evaluate different dosing regimens of P450 3A4, 1A2 and 2D6-metabolized drugs during pregnancy.

Acknowledgements

The authors acknowledge funding from FDA Office of Women's Health and visiting fellowship from SimCYP (A.B. Ke). The authors would also like to thank Drs. William J. Jusko (SUNY, Buffalo), Uwe Fuhr (University of Cologne, Cologne, Germany) and Mia Wadelius (Uppsala University, Uppsala, Sweden) for providing clinical PK data used for model validation. The clonidine PK study in pregnancy was supported in part by grant number U10HD047892 from the Eunice Kennedy Shriver National Institute of Child Health & Human Development, National Institutes of Health. The content is solely the responsibility of the authors and does not necessarily represent the official views of the Eunice Kennedy Shriver National Institute of Child Health & Human Development or the National Institutes of Health.

Authorship Contributions

Participated in research design: A.B. Ke, S.C. Nallani, P. Zhao, A. Rostami-Hodjegan, N Isoherranen, J. D. Unadkat

Conducted experiments: A.B. Ke

Contributed new reagents or analytical tools: A. Rostami-Hodjegan

Performed data analysis: A.B. Ke

Wrote or contributed to the writing of the manuscript: A.B. Ke, S.C. Nallani, P. Zhao, A. Rostami-Hodjegan, N Isoherranen, J. D. Unadkat

Figure Legends

Figure 1. Predicted and observed plasma concentration-time profiles of theophylline (THEO) following multiple p.o. dose during during 3rd trimester (T_3) and postpartum (PP). The solid line represents predicted mean postpartum profile. The dashed line represents predicted mean T_3 profile. Mean observed data are overlaid (●: postpartum profile; ○: T_3 profile) (Gardner et al., 1987). Error bars represent standard deviations.

Figure 2. A) Predicted and observed plasma concentration-time profiles of metoprolol (MET) after administration of a single oral dose of 100 mg to non-pregnant, P450 2D6 EMs and PMs. The solid line represents predicted mean profile in EMs. The dashed line represents predicted mean profile in PMs. Mean observed data in non-pregnant EMs (● and ■) and PMs (▲ and ♦) (Hamelin et al., 2000; Sharma et al., 2005) are overlaid, as are mean observed data in postpartum women (○) (Hogstedt et al., 1985).

B) Predicted and observed plasma concentration-time profiles of MET (100 mg p.o.) during 3rd trimester (T_3) and postpartum (PP). The solid line represents predicted mean postpartum profile. The dashed line represents predicted mean T_3 profile. Mean observed data are overlaid (●: postpartum profile; ○: T_3 profile) (Hogstedt et al., 1985). Error bars represent standard deviations.

Figure 3 A) Predicted and observed plasma concentration-time profiles of paroxetine (PAR) following single and chronic dosing of 30 mg (p.o.) to non-pregnant, P450 2D6 EMs and PMs.

Mean observed data in non-pregnant EMs (○ and ●) and PMs (□ and ■) are overlaid (● and ■: steady-state or SS; ○ and □: single-dose or SD) (Sindrup et al., 1992b).

B) Predicted and observed steady-state (C_{ss}) PAR plasma concentrations following 20 mg Q.D. during 3rd trimester (T_3) and postpartum (PP). The grey bars represent predicted C_{ss} and C_{ss} ratio (PP:T_3) assuming 200% induction of P450 2D6, and the black bars represent predicted C_{ss} and C_{ss} ratio (PP:T_3) assuming 100% induction of P450 2D6. The white bars represent observed median C_{ss} in non-pregnant historical controls (Sindrup et al., 1992b), in pregnant women during T_3 (Ververs et al., 2009), and calculated C_{ss} ratio (PP:T_3) based on observed median C_{ss}.

Figure 4. A) Predicted and observed plasma concentration-time profiles of dextromethorphan (DEX) after administration of a single oral dose of 30 mg to non-pregnant, P450 2D6 EMs and PMs, or in the presence of a strong P450 2D6 inhibitor quinidine (Qd, 50 mg q.d.). The black and grey solid line represents predicted mean profile in EMs and in PMs, respectively. The dashed line represents predicted mean profiles in EMs in the presence of quinidine. Mean observed data in non-pregnant EMs (■: Abdul Manap et al., 1999; ♦: Gorski et al., 2004; ▲: Abduljalil et al., 2010) and PMs (○: Capon et al., 1996; ◊: Gorski et al., 2004) are overlaid. Mean observed data (+, X) in non-pregnant EMs in the presence of quinidine (Qd) are overlaid (+: Abdul Manap et al., 1999; X: Capon et al., 1996).

Figure 5. A) Predicted mean time course of the amount (mg) of A) DEX (solid line) and dextrorphan (DXO) (dashed line) excreted in urine after administration of a single oral dose of 30 mg to to non-pregnant, P450 2D6 EMs. Average observed DEX (○: Jones et al., 1996; ●:

Abduljalil et al., 2010) and DXO (◊: Jones et al., 1996; ♦: Abduljalil et al., 2010) data in non-pregnant EMs are overlaid. Error bars represent standard deviations.

B) Predicted and observed UR (DEX/DXO) (PP:T_3) following 30 mg (p.o.). The black bar represent predicted UR (PP:T_3) assuming 200% induction of P450 2D6, and the grey bar represent predicted UR (PP:T_3) assuming 100% induction of P450 2D6. The white bars represent observed UR (PP:T_3) (Tracy et al., 2005).

Figure 6. A) Observed (symbols) and predicted (lines) plasma concentration-time profiles of clonidine after administration of a single oral dose of 0.1, 0.2 and 0.3 mg to non-pregnant, P450 2D6 EMs. Grey filled circles: observed data (0.1 mg); open symbols: observed data (0.2 mg) (Porchet et al., 1992); Black filled circles: observed data (0.3 mg) (Cunningham et al., 1994). B) Observed and/or simulated and plasma concentration-time profiles of clonidine 0.15 mg (p.o.) during 3rd trimester (T_3) and postpartum (PP). The black solid line represents predicted mean postpartum profile. The grey dashed lines represents predicted mean T_3 profile assuming 200% induction of P450 2D6, and the black dashed line represents predicted mean T_3 profile assuming 100% induction of P450 2D6. Observed (dose-normalized to 0.15 mg) mean T_3 profile (symbols) is overlaid (Buchanan et al., 2009). Error bars represent standard deviations.

List of Tables

Table 1: Summary of theophylline (THEO) drug-dependent parameters

Parameter	Value	Methods/reference
Molecular Weight	180.2	Library[a]
Log $P_{o:w}$	-0.02	Library
pKa	8.8,0.99	Library
B/P Ratio	0.815	Library
$f_{u,p}$	0.58	b
F_a	0.97	Predicted [c]
k_a (h^{-1})	0.154(SR), 1.98(IR)	Predicted [d]
F_g	1	Predicted by Q_{gut}[e]
V_{ss} (L/Kg)	0.39	Predicted [f]
CL_{IV} (L/h)	3.0	g
CL_r (L/h)	0.45	h
$CL_{int,u}$ (L/hr)	4.6	i
f_m and f_e	$f_{m,1A2}$ =68%, $f_{m,3A}$ =7%, $f_{m,2E1}$ =10%, f_e =15%,	j

[a]: refers to Simcyp compound library (version 11.1).

[b]: reported value is in the range of 0.56-0.60 (Hendeles et al., 1985; St-Pierre et al., 1985) and mean value was used.

[c]: predicted from Caco-2 permeability of $25*10^{-6}$ cm/s (library) in Simcyp (version 11.1).

[d]: IR: predicted from Caco-2 permeability of $25*10^{-6}$ cm/s (library) in Simcyp (version 11.1). SR: estimated from reported $t_{1/2}$,a (Hendeles and Weinberger, 1983).

[e]: Q_{gut} model is provided in Simcyp simulator. It retains the form of the "well-stirred" liver model, but the flow term (Q_{Gut}) is a hybrid of both permeability through the enterocyte membrane and villous blood flow (Yang et al., 2007).

[f]: predicted according to Rodgers & Rowland (Rodgers and Rowland, 2007);

[g]: Reported CL_{IV} in non-pregnant, non-smokers is 3.0±0.7 L/hr (no. of studies=26) (University of Washington DiDB, http://www.druginteractioninfo.org/).

[h]: calculated by taking the product of CL_{IV} and reported mean f_e. Reported f_e ranges in 13-18% (n=22) in non-pregnant, non-smoking healthy volunteers (Tang-Liu et al., 1982; St-Pierre et al.,

1985) and 16.0 ± 3.3% (n=5) in postpartum women (Frederiksen et al., 1986) following i.v. dosing. Weighted mean f_e was used.

[i]: back-calculation from well-stirred liver model using $Q_{H,B}$ of 90L/hr.

[l]: The contribution from individual P450 obtained *in vitro* is 91.7%, 8% and 0.06% for 1A2, 2E1 and 3A, respectively (Tjia et al., 1996). However, *in vivo* DDI studies using diltizem and verapamil as the perpetrators (both are P450 3A MBI) reported AUC % change of 12-18% (Sirmans et al., 1988; Stringer et al., 1992), suggesting that P450 3A played a greater role in THEO metabolism *in vivo*. Therefore, the contribution from individual P450 (80%, 8% and 12% for 1A2, 2E1 and 3A, respectively) was adjusted accordingly. *In vivo* f_m for individual P450 was calculated by taking the product of f_m (=1-f_e) and the contribution from individual P450 .

Table 2: Summary of metoprolol (MET) drug-dependent parameters

Parameter	Value	Methods/reference
Molecular Weight	267.4	Library [a]
Log $P_{o:w}$	1.88	Library
pKa	9.75	Library
B/P Ratio	1.15	Library
$f_{u,p}$	0.88	Library
F_a	0.81	Predicted [b]
k_a (h^{-1})	0.58	Predicted [b]
F_g	0.97	Predicted by Q_{gut} model
V_{ss} (L/Kg)	3.1	Predicted [c]
CL (L/h)	55.8	Predicted via IVIVE [d]
CL_r (L/h)	4.27	e
V_{max} (µL/min/mg)	O-demethylation: $V_{max,2D6}$=300 $V_{max,3A4}$=1164 Alpha-OH: $V_{max,2D6}$=75.9 $V_{max,3A4}$=96	Optimized [f]
$K_{m,unbound}$ (µM)	O-demethylation: $K_{m,2D6}$=28.3 $K_{m,3A4}$=1162 Alpha-OH: $K_{m,2D6}$=31 $K_{m,3A4}$=874	Library
f_m and f_e (2D6 EM)	$f_{m,2D6}$ =84 %, $f_{m,3A}$ =7 %, f_e =9 %,	Predicted via IVIVE [g]

[a]: refers to Simcyp compound library (version 11.1).

[b]: predicted from human jejunum permeability (10^{-4} cm/s) (Library data) in Simcyp (version 11.1).

[c]: not reported in literature , predicted according to Rodgers & Rowland (Rodgers and Rowland, 2007).

[d]: In-vitro to in-vivo extrapolation using in vitro V_{max} and K_m and 'average' population values for liver weight and microsomal protein of 1618 g and 38.9 (mg/g liver), respectively. Reported

CL_{IV} in non-pregnant, P450 2D6 EMs and PMs is 72.5±32.2 L/hr (range 48.6-93.2 L/h) (no. of studies=3, no. of subjects=28, male only) and 30.1±8.4 L/hr (no. of studies=1, no. of subjects=3, male only) (University of Washington DiDB, http://www.druginteractioninfo.org/). Reported CL_{IV} in postpartum women is 39 ±4.8 L/hr (n=5) (Hogstedt et al., 1985).

[e]: Reported mean value in non-pregnant, P450 2D6 EMs and PMs is 4.27 L/hr (range 3.24-6.0 L/h) (no. of studies=6, no. of subjects=67) (University of Washington DiDB, http://www.druginteractioninfo.org/).

[f]: IVIVE approach using *in vitro* V_{max} determined in HLM (provided in Library) significantly under-predicted CL_{IV} and CL_{ORAL} by a factor of 2.2 and 2.3 in non-pregnant, P450 2D6 EMs. This under-prediction was also evident in non-pregnant, P450 2D6 PMs (by a factor of 3.2 and 1.4, respectively). To improve IVIVE prediction of CL, *in vivo* V_{max} for P450 2D6 and P450 3A4 was optimized by multiplying *in vitro* V_{max} by a factor of 2.

[g]: Literature $f_{m,2D6}$ =69.5-82.8% (Brown et al., 2005; Ito et al., 2005).

Table 3: Summary of Paroxetine (PAR) drug-dependent parameters

Parameter	Value	Methods/reference
Molecular Weight	329.3	Jornil
Log $P_{o:w}$	3.55	Martin et al. 2008
pKa	9.66	Martin et al. 2008
B/P Ratio	1.25	Jornil et al., 2010
$f_{u,p}$	0.05	Kaye et al., 1989
F_a	0.94	Predicted[a]
k_a (h^{-1})	1.14	Predicted[a]
F_g	0.92	Predicted by Q_{gut} model
V_{ss} (L/Kg)	12.95	Optimized [b]
$CL_{2D6\ EM}$ (L/h)	80.7	Predicted[c]
CL_r (L/h)	0.5	Sindrup et al., 1992
V_{max} (µL/min/pmol)	$V_{max,2D6}$=9.7 $V_{max,3A4}$=5.3 $V_{max,3A5}$=1.6 $V_{max,1A2}$=0.63 $V_{max,2C19}$=2.4	Jornil et al., 2010
$K_{m,unbound}$ (µM)	$K_{m,2D6}$=0.03 $K_{m,3A4}$=13.3 $K_{m,3A5}$=108 $K_{m,1A2}$=8.8 $K_{m,2C9}$=26	Jornil et al., 2010
$CL_{int,other}$ (µL/min/mg protein)	55.2	Optimized[d]
K_{inact} (2D6) (min^{-1})	0.17	Bertelsen et al., 2003
$K_{I,\ unbound}$ (2D6) (µM)	0.315	Bertelsen et al., 2003; Venkatakrishnan and Obach, 2005
K_{inact} (3A4) (min^{-1})	0.011	Obach et al., 2007
$K_{I,\ unbound}$ (3A4) (µM)	4.03	Obach et al., 2007
f_m at steady-state (2D6 EM)	$f_{m,2D6}$ =79.9 %, $f_{m,3A}$ =9.6 %, $f_{m,other}$ =9.7 %,	Predicted via IVIVE [e]

[a]: predicted from Caco-2 permeability of $17*10^{-6}$ cm/s (Jornil et al., 2010) in Simcyp (version 11.1).

[b]: V_{ss} was not reported in literature. The predicted V_{ss} according to Rodgers & Rowland is 7.5 L/Kg (Rodgers and Rowland, 2007). This value was further optimized to 12.95 L/kg by applying a global K_p scalar of 1.7, in order to improve prediction of C_{max}. Reported V_d following i.v. infusion is 17.2±9.9 L/Kg (range 8.0-28.0) (Kaye et al., 1989).

[c]: Simcyp-predicted CL in P450 2D6 EM individuals via IVIVE is 80.7±13.8 L/hr (n=100). Reported CL is 74.9±14 L/hr (range 63-91.7, n=4) following 23-28 mg IV over 30mins (Kaye 1989). The genotype of these subjects was not determined.

[d]: In P450 2D6 PM subjects, both single-dose and steady-state median CL_{oral} were significantly under-predicted by a factor of 2.9 and 3.5 respectively, using the IVIVE approach (Jornil 2010). To match single-dose and steady-state CL_{oral} in P450 2D6 PMs, an un-identified pathway ($CL_{int,other}$) was incorporated into the IVIVE model.

[e]: f_m is dose- and time-dependent. Following 20 mg SD (n=100 subjects), the predicted time-averaged mean f_m is 94.3% (2D6), 2.8% (3A4), 0.1% (1A2), 0.1% (2C19) and 2.7% (un-identified CL), respectively, in EMs. Following 20 mg QD (n=100 subjects), the predicted time-averaged mean f_m at steady-state is 80% (2D6), 9.6% (3A4), 0.5% (1A2), 0.2 % (2C19) and 9.7% ((un-identified CL), respectively, in EMs. In P450 2D6 PMs, the predicted time-averaged mean f_m is similar following 20 mg SD vs. 20 mg QD: 48.5% (3A4), 2.6% (1A2), 1.1% (2C19) and 47.5% (un-identified CL), vs. 46.9% (3A4), 2.7% (1A2), 1.1% (2C19) and 49.0% (un-identified CL).

Table 4: Summary of dextromethorphan (DEX) and dextrorphan (DXO) drug-dependent parameters

Parameter	DEX Value	Methods/reference	DXO Value	Methods/reference
Molecular Weight	271.4	Library [a]	257.4	f
Log $P_{o:w}$	3.8	Library	3.46	f
pKa	8.3	Library	9.2	g
B/P Ratio	1.32	Library	1	Assumed
$f_{u,p}$	0.5	Library	0.55	h
F_a	1.0	Library	–	–
k_a (h^{-1})	0.3	Library	–	–
F_g	0.80	Predicted by Q_{gut} model	1.0	Predicted by Q_{gut} model
V_{ss} (L/Kg)	14.45	Predicted [b]	6.78	i
CL (L/h)	103.2	Predicted	12.5	Apparent CL, Calculated [j]
CL_r (L/h)	3.6	Assumed ~ $f_{u,p}$ *GFR [c]	5	Apparent CL, Optimized [k]
$CL_{int,u}$ (µL/min/mg)	$CL_{int,u,2D6}$=760.6 $CL_{int,u,3A}$=4.3	Parameter Estimation [d]	$CL_{int,u,3A}$=0.95	l
Biliary $CL_{int,u}$ (µL/min/10^6)	–	–	0.9	m
f_m and f_e (2D6 EM)	$f_{m,2D6}$ =95.3%, $f_{m,3A}$ =0.86%, f_e =3.8%,	e	–	–

[a]: refers to Simcyp compound library (version 10).

[b]: not reported in literature , predicted according to Rodgers & Rowland (Rodgers and Rowland, 2007).

[c]: reported medians and ranges for CL_r of DEX: 9.0 L/hr (1.4 to 37 L/hr) for extensive metabolizers (Capon et al., 1996). Model-estimated CL_r were 6.5 L/hr (Abduljalil et al., 2010) and 3 L/hr (Moghadamnia et al., 2003). Given the substantial variability in literature value, CL_r of DEX was assumed to approximate $f_{u,p}$ *GFR.

[d]: $CL_{int,u,2D6}$ was estimated in Simcyp by simultaneously fitting observed C-T profiles extracted from (Abdul Manap et al., 1999; Moghadamnia et al., 2003) using an initial estimate of 253.0 (µL/min/mg) provided in compound library. $CL_{int,u,3A}$ was provided in compound library.

[e]: reported $f_{m,2D6}$ = 97% (Capon et al., 1996; Gorski et al., 2004).

[f]: http://www.chemspider.com/

[g]: reported (Kanaan et al., 2008).

[h]: reported (Lutz and Isoherranen, 2011).

[i]: calculated mean value of reported V_d in literature: range of 300 to 650 L or 4.3 to 9.3 L/Kg (assumed BW= 70 Kg) (Albers et al., 1995).
[j]: calculated mean DXO CL_{app} (= Dose*$f_{m,2D6}$ /AUC_{DXO}) was 12.5 L/hr. Dose and AUC_{DXO} (free+conjugated drug) were taken from (Capon et al., 1996; Abdul Manap et al., 1999; Gorski et al., 2004).

[k]: calculated CL_r = $Ae_{,DXO}$ /AUC_{DXO} was in the range of 5-12 L/hr. $A_{e,DXO}$ (free+conjugated drug) was calculated by Dose * % urinary recovery (reported range 40-91%) and AUC_{DXO} (free+conjugated drug) was taken from (Capon et al., 1996; Abdul Manap et al., 1999; Gorski et al., 2004). A sensitivity analysis on apparent CL_r of DXO in the range of 5-12 L/hr was conducted, and the final value (5 L/hr) was selected based on predicted $A_{e,DXO,0\text{-}24h}$ being the closest match to observed $A_{e,DXO}$ in literature (Abduljalil et al., 2010) (Fig. 5A). This CL_r corresponds to urinary recovery of 40%. A higher % urinary recovery over-predicted $A_{e,DXO}$.

[l]: taken from (Lutz and Isoherranen, 2011).

[m]: Back-calculation from Biliary CL (= CL_{app}-$CL_{m,3A}$-CL_r) and 'average' population values for liver weight and hepatocellularity of 1618 g and 117.5 (millions of cells/g liver), respectively.

Table 5: Summary of clonidine drug-dependent parameters

Parameter	Value	Methods/reference
Molecular Weight	230.1	a
Log $P_{o:w}$	1.57	b
pKa	8.05	c
B/P Ratio	1.012	d
$f_{u,p}$	0.48	e
F_a	0.98	Calculated [f]
k_a (h^{-1})	1.0	Optimized in the range of 1.0-2.3 [g]
F_g	0.99	Predicted by Q_{gut}
V_{ss} (L/Kg)	2.55	Predicted [h]
CL_{IV} (L/h)	13.6	i
CL_r (L/h)	7.0	j
$CL_{int,u}$ (µL/min/pmol of isoform)	$CL_{int,u,2D6}$= 0.32 $CL_{int,u,3A}$= 0.006 $CL_{int,u,1A2}$= 0.008	k
f_m and f_e (2D6 EM)	$f_{m,2D6}$ =33%, $f_{m,3A}$ =11%, $f_{m,1A2}$ =5%, f_e =51%,	e, l

[a]: Goodman & Gilman 10th Edition 2001.

[b]: reported (Ghasemi and Saaidpour, 2007).

[c]: reported (Cody and DeTitta, 1979).

[d]: predicted using physicochemical parameters in Simcyp. Reported B/P ratio in rodents is 1.07 (Yamahata 1996).

[e]: reported (Vanholder et al., 1988Product label for CATAPRES®).

[f]: mean reported bioavailability is 92% (range 88-96%) following a single oral dose of clonidine (Frisk-Holmberg et al., 1981; Arndts et al., 1983). Simcyp-predicted F_h is 0.95 and F_g is 0.99, therefore calculated F_a is 0.98.

[g]: reported (Frisk-Holmberg et al., 1981; Anavekar et al., 1982; Porchet et al., 1992).

[h]: predicted according to Rodgers & Rowland (Rodgers and Rowland, 2007); estimated V_{ss} value from i.v. dosing profiles is ~ 3 L/kg (Frisk-Holmberg et al., 1981). Mean K_p values determined in rodents (Conway and Jarrott, 1980; Yamahata et al., 1996) were used, as opposed to predicted K_p values, because these values were found to better characterize the biphasic distribution of clonidine in plasma following either i.v. or p.o. dosing.

[i]: mean of reported values (Frisk-Holmberg et al., 1981; Arndts et al., 1983).

[j]: calculated by taking the product of CL_{IV} and reported mean f_e (Frisk-Holmberg et al., 1981; Arndts et al., 1983; Buchanan et al., 2009).

[k]: back-calculation from hepatic CL (=CL-CL_r), f_m for individual P450 (see below), and 'average' population values for liver weight and hepatic P450 enzyme abundance of 137, 52 and 8 pmol/mg protein for P450 3A, 1A2 and 2D6, respectively.

[l]: reported f_m for individual P450 was calculated by taking the product of f_m (i.e. 1-f_e) and the contribution from individual P450 (67%, 22% and 11% for 2D6, 3A and 1A2, respectively) obtained in HLM (Claessens et al., 2010).

References

Product label for CATAPRES® (Clonidine Hydrochloride) oral tablet. http://www.accessdata.fda.gov/drugsatfda_docs/label/2012/017407s037lbl.pdf.

Abdul Manap R, Wright CE, Gregory A, Rostami-Hodjegan A, Meller ST, Kelm GR, Lennard MS, Tucker GT and Morice AH (1999) The antitussive effect of dextromethorphan in relation to CYP2D6 activity. *Br J Clin Pharmacol* **48:**382-387.

Abduljalil K, Frank D, Gaedigk A, Klaassen T, Tomalik-Scharte D, Jetter A, Jaehde U, Kirchheiner J and Fuhr U (2010) Assessment of activity levels for CYP2D6*1, CYP2D6*2, and CYP2D6*41 genes by population pharmacokinetics of dextromethorphan. *Clin Pharmacol Ther* **88:**643-651.

Abduljalil K, Furness P, Johnson TN, Rostami-Hodjegan A and Soltani H (2012) Anatomical, physiological and metabolic changes with gestational age during normal pregnancy: a database for parameters required in physiologically based pharmacokinetic modelling. *Clin Pharmacokinet* **51:**365-396.

Albers GW, Atkinson RP, Kelley RE and Rosenbaum DM (1995) Safety, tolerability, and pharmacokinetics of the N-methyl-D-aspartate antagonist dextrorphan in patients with acute stroke. Dextrorphan Study Group. *Stroke* **26:**254-258.

Anavekar SN, Jarrott B, Toscano M and Louis WJ (1982) Pharmacokinetic and pharmacodynamic studies of oral clonidine in normotensive subjects. *Eur J Clin Pharmacol* **23:**1-5.

Anderson GD (2005) Pregnancy-induced changes in pharmacokinetics: a mechanistic-based approach. *Clin Pharmacokinet* **44:**989-1008.

Arndts D, Doevendans J, Kirsten R and Heintz B (1983) New aspects of the pharmacokinetics and pharmacodynamics of clonidine in man. *Eur J Clin Pharmacol* **24:**21-30.

Borges S, Li L, Hamman MA, Jones DR, Hall SD and Gorski JC (2005) Dextromethorphan to dextrorphan urinary metabolic ratio does not reflect dextromethorphan oral clearance. *Drug Metab Dispos* **33:**1052-1055.

Brown HS, Ito K, Galetin A and Houston JB (2005) Prediction of in vivo drug-drug interactions from in vitro data: impact of incorporating parallel pathways of drug elimination and inhibitor absorption rate constant. *Br J Clin Pharmacol* **60:**508-518.

Buchanan ML, Easterling TR, Carr DB, Shen DD, Risler LJ, Nelson WL, Mattison DR and Hebert MF (2009) Clonidine pharmacokinetics in pregnancy. *Drug Metab Dispos* **37:**702-705.

Capon DA, Bochner F, Kerry N, Mikus G, Danz C and Somogyi AA (1996) The influence of CYP2D6 polymorphism and quinidine on the disposition and antitussive effect of dextromethorphan in humans. *Clin Pharmacol Ther* **60:**295-307.

Claessens AJ, Risler LJ, Eyal S, Shen DD, Easterling TR and Hebert MF (2010) CYP2D6 mediates 4-hydroxylation of clonidine in vitro: implication for pregnancy-induced changes in clonidine clearance. *Drug Metab Dispos* **38:**1393-1396.

Cody V and DeTitta GT (1979) The molecular conformation of clonidine hydrochloride, an a-adrenergic agonist *Journal of Crystal and Molecular Structure* **9:**33-43.

Conway EL and Jarrott B (1980) Clonidine distribution in the rat: temporal relationship between tissue levels and blood pressure response. *Br J Pharmacol* **71:**473-478.

Corchero J, Granvil CP, Akiyama TE, Hayhurst GP, Pimprale S, Feigenbaum L, Idle JR and Gonzalez FJ (2001) The CYP2D6 humanized mouse: effect of the human CYP2D6

transgene and HNF4alpha on the disposition of debrisoquine in the mouse. *Mol Pharmacol* **60:**1260-1267.

Cunningham FE, Baughman VL, Peters J and Laurito CE (1994) Comparative pharmacokinetics of oral versus sublingual clonidine. *J Clin Anesth* **6:**430-433.

Dickmann LJ and Isoherranen N (2012) Quantitative Prediction of CYP2B6 Induction by Estradiol During Pregnancy, Potential Explanation for Increased Methadone Clearance during Pregnancy. *Drug Metab Dispos*.

Dickmann LJ, Patel SK, Rock DA, Wienkers LC and Slatter JG (2011) Effects of interleukin-6 (IL-6) and an anti-IL-6 monoclonal antibody on drug-metabolizing enzymes in human hepatocyte culture. *Drug Metab Dispos* **39:**1415-1422.

Eyal S, Easterling TR, Carr D, Umans JG, Miodovnik M, Hankins GD, Clark SM, Risler L, Wang J, Kelly EJ, Shen DD and Hebert MF (2010) Pharmacokinetics of metformin during pregnancy. *Drug Metab Dispos* **38:**833-840.

Frederiksen MC, Ruo TI, Chow MJ and Atkinson AJ, Jr. (1986) Theophylline pharmacokinetics in pregnancy. *Clin Pharmacol Ther* **40:**321-328.

Frisk-Holmberg M, Paalzow L and Edlund PO (1981) Clonidine kinetics in man--evidence for dose dependency and changed pharmacokinetics during chronic therapy. *Br J Clin Pharmacol* **12:**653-658.

Fujimura A, Ebihara A, Ohashi K, Shiga T, Kumagai Y, Nakashima H and Kotegawa T (1994) Comparison of the pharmacokinetics, pharmacodynamics, and safety of oral (Catapres) and transdermal (M-5041T) clonidine in healthy subjects. *J Clin Pharmacol* **34:**260-265.

Gardner MJ, Schatz M, Cousins L, Zeiger R, Middleton E and Jusko WJ (1987) Longitudinal effects of pregnancy on the pharmacokinetics of theophylline. *Eur J Clin Pharmacol* **32:**289-295.

Ghasemi J and Saaidpour S (2007) Quantitative structure-property relationship study of n-octanol-water partition coefficients of some of diverse drugs using multiple linear regression. *Anal Chim Acta* **604:**99-106.

Gorski JC, Huang SM, Pinto A, Hamman MA, Hilligoss JK, Zaheer NA, Desai M, Miller M and Hall SD (2004) The effect of echinacea (Echinacea purpurea root) on cytochrome P450 activity in vivo. *Clin Pharmacol Ther* **75:**89-100.

Hamelin BA, Bouayad A, Methot J, Jobin J, Desgagnes P, Poirier P, Allaire J, Dumesnil J and Turgeon J (2000) Significant interaction between the nonprescription antihistamine diphenhydramine and the CYP2D6 substrate metoprolol in healthy men with high or low CYP2D6 activity. *Clin Pharmacol Ther* **67:**466-477.

Hendeles L, Massanari M and Weinberger M (1985) Update on the pharmacodynamics and pharmacokinetics of theophylline. *Chest* **88:**103S-111S.

Hendeles L and Weinberger M (1983) Theophylline. A "state of the art" review. *Pharmacotherapy* **3:**2-44.

Hodge LS and Tracy TS (2007) Alterations in drug disposition during pregnancy: implications for drug therapy. *Expert Opin Drug Metab Toxicol* **3:**557-571.

Hogstedt S, Lindberg B, Peng DR, Regardh CG and Rane A (1985) Pregnancy-induced increase in metoprolol metabolism. *Clin Pharmacol Ther* **37:**688-692.

Ito K, Hallifax D, Obach RS and Houston JB (2005) Impact of parallel pathways of drug elimination and multiple cytochrome P450 involvement on drug-drug interactions: CYP2D6 paradigm. *Drug Metab Dispos* **33:**837-844.

Jamei M, Dickinson GL and Rostami-Hodjegan A (2009) A framework for assessing inter-individual variability in pharmacokinetics using virtual human populations and integrating general knowledge of physical chemistry, biology, anatomy, physiology and genetics: A tale of 'bottom-up' vs 'top-down' recognition of covariates. *Drug Metab Pharmacokinet* **24:**53-75.

Jeong H (2010) Altered drug metabolism during pregnancy: hormonal regulation of drug-metabolizing enzymes. *Expert Opin Drug Metab Toxicol* **6:**689-699.

Johnson JA and Burlew BS (1996) Metoprolol metabolism via cytochrome P4502D6 in ethnic populations. *Drug Metab Dispos* **24:**350-355.

Jones DR, Gorski JC, Haehner BD, O'Mara EM, Jr. and Hall SD (1996) Determination of cytochrome P450 3A4/5 activity in vivo with dextromethorphan N-demethylation. *Clin Pharmacol Ther* **60:**374-384.

Jornil J, Jensen KG, Larsen F and Linnet K (2010) Identification of cytochrome P450 isoforms involved in the metabolism of paroxetine and estimation of their importance for human paroxetine metabolism using a population-based simulator. *Drug Metab Dispos* **38:**376-385.

Kanaan M, Daali Y, Dayer P and Desmeules J (2008) Lack of interaction of the NMDA receptor antagonists dextromethorphan and dextrorphan with P-glycoprotein. *Curr Drug Metab* **9:**144-151.

Kaye CM, Haddock RE, Langley PF, Mellows G, Tasker TC, Zussman BD and Greb WH (1989) A review of the metabolism and pharmacokinetics of paroxetine in man. *Acta Psychiatr Scand Suppl* **350:**60-75.

Ke AB, Nallan SC, Zhao P, Rostami-Hodjegan A and Unadkat JD (2012) A PBPK Model to Predict Disposition of CYP3A-metabolized Drugs in Pregnant Women: Verification and Discerning the Site of CYP3A Induction. *Clin Pharmacol Ther: Pharmacometrics & Systems Pharmacology* **1:** http://www.nature.com/psp/journal/v1/n9/index.html

Lu G, Abduljalil K, Jamei M, Johnson TN and Rostami-Hodjegan A (2012a) A Pregnancy Physiologically-Based Pharmacokinetic (p-PBPK) Model for Disposition of Drugs Metabolized by CYP1A2, CYP3A4 and CYP2D6. *British Journal of Clinical Pharmacology* **74:**873-885.

Lu G, Abduljalil K, Jamei M, Johnson TN, Soltani H and Rostami-Hodjegan A (2012b) Physiologically-based Pharmacokinetic (PBPK) Models for Assessing the Kinetics of Xenobiotics during Pregnancy: Achievements and Shortcomings. *Curr Drug Metab*.

Lutz JD and Isoherranen N (2011) Prediction of Relative In Vivo Metabolite Exposure from In Vivo Data Using Two Model Drugs: Dextromethorphan and Omeprazole. *Drug Metab Dispos*.

Moghadamnia AA, Rostami-Hodjegan A, Abdul-Manap R, Wright CE, Morice AH and Tucker GT (2003) Physiologically based modelling of inhibition of metabolism and assessment of the relative potency of drug and metabolite: dextromethorphan vs. dextrorphan using quinidine inhibition. *Br J Clin Pharmacol* **56:**57-67.

Papageorgiou I and Unadkat JD (2011) Mechanisms by which hepatic CYP3A enzymes are induced during pregnancy *ISSX, 17th North American Meeting. Atlanta, Georgia*.

Porchet HC, Piletta P and Dayer P (1992) Pharmacokinetic-pharmacodynamic modeling of the effects of clonidine on pain threshold, blood pressure, and salivary flow. *Eur J Clin Pharmacol* **42:**655-661.

Rodgers T and Rowland M (2007) Mechanistic approaches to volume of distribution predictions: understanding the processes. *Pharm Res* **24:**918-933.

Rostami-Hodjegan A, Kroemer HK and Tucker GT (1999) In-vivo indices of enzyme activity: the effect of renal impairment on the assessment of CYP2D6 activity. *Pharmacogenetics* **9:**277-286.

Rowland M, Peck C and Tucker G (2011) Physiologically-based pharmacokinetics in drug development and regulatory science. *Annu Rev Pharmacol Toxicol* **51:**45-73.

Sharma A, Pibarot P, Pilote S, Dumesnil JG, Arsenault M, Belanger PM, Meibohm B and Hamelin BA (2005) Modulation of metoprolol pharmacokinetics and hemodynamics by diphenhydramine coadministration during exercise testing in healthy premenopausal women. *J Pharmacol Exp Ther* **313:**1172-1181.

Sindrup SH, Brosen K and Gram LF (1992a) Pharmacokinetics of the selective serotonin reuptake inhibitor paroxetine: nonlinearity and relation to the sparteine oxidation polymorphism. *Clin Pharmacol Ther* **51:**288-295.

Sindrup SH, Brosen K, Gram LF, Hallas J, Skjelbo E, Allen A, Allen GD, Cooper SM, Mellows G, Tasker TC and et al. (1992b) The relationship between paroxetine and the sparteine oxidation polymorphism. *Clin Pharmacol Ther* **51:**278-287.

Sirmans SM, Pieper JA, Lalonde RL, Smith DG and Self TH (1988) Effect of calcium channel blockers on theophylline disposition. *Clin Pharmacol Ther* **44:**29-34.

St-Pierre MV, Spino M, Isles AF, Tesoro A and MacLeod SM (1985) Temporal variation in the disposition of theophylline and its metabolites. *Clin Pharmacol Ther* **38:**89-95.

Stringer KA, Mallet J, Clarke M and Lindenfeld JA (1992) The effect of three different oral doses of verapamil on the disposition of theophylline. *Eur J Clin Pharmacol* **43:**35-38.

Tang-Liu DD, Williams RL and Riegelman S (1982) Nonlinear theophylline elimination. *Clin Pharmacol Ther* **31:**358-369.

Tjia JF, Colbert J and Back DJ (1996) Theophylline metabolism in human liver microsomes: inhibition studies. *J Pharmacol Exp Ther* **276:**912-917.

Tracy TS, Venkataramanan R, Glover DD and Caritis SN (2005) Temporal changes in drug metabolism (CYP1A2, CYP2D6 and CYP3A Activity) during pregnancy. *Am J Obstet Gynecol* **192:**633-639.

Vanholder R, Van Landschoot N, De Smet R, Schoots A and Ringoir S (1988) Drug protein binding in chronic renal failure: evaluation of nine drugs. *Kidney Int* **33:**996-1004.

Venkatakrishnan K and Obach RS (2005) In vitro-in vivo extrapolation of CYP2D6 inactivation by paroxetine: prediction of nonstationary pharmacokinetics and drug interaction magnitude. *Drug Metab Dispos* **33:**845-852.

Ververs FF, Voorbij HA, Zwarts P, Belitser SV, Egberts TC, Visser GH and Schobben AF (2009) Effect of cytochrome P450 2D6 genotype on maternal paroxetine plasma concentrations during pregnancy. *Clin Pharmacokinet* **48:**677-683.

Wadelius M, Darj E, Frenne G and Rane A (1997) Induction of CYP2D6 in pregnancy. *Clin Pharmacol Ther* **62:**400-407.

Yamahata T, Minaki Y, Nishikawa H, Esumi Y, Jin Y and Takao A (1996) Metabolic Fate of Clonidine (IV): Plasma Protein Binding of Clonidine In vitro and In vivo and Transfer to Fetus and Milk in Rats after Subcutaneous Administration of Clonidine. *Drug Metab Pharmacokinet* **11:**404-410.

Yang J, Jamei M, Yeo KR, Tucker GT and Rostami-Hodjegan A (2007) Prediction of intestinal first-pass drug metabolism. *Curr Drug Metab* **8:**676-684.

Yu A and Haining RL (2001) Comparative contribution to dextromethorphan metabolism by cytochrome P450 isoforms in vitro: can dextromethorphan be used as a dual probe for both CTP2D6 and CYP3A activities? *Drug Metab Dispos* **29:**1514-1520.

FIGURE 1

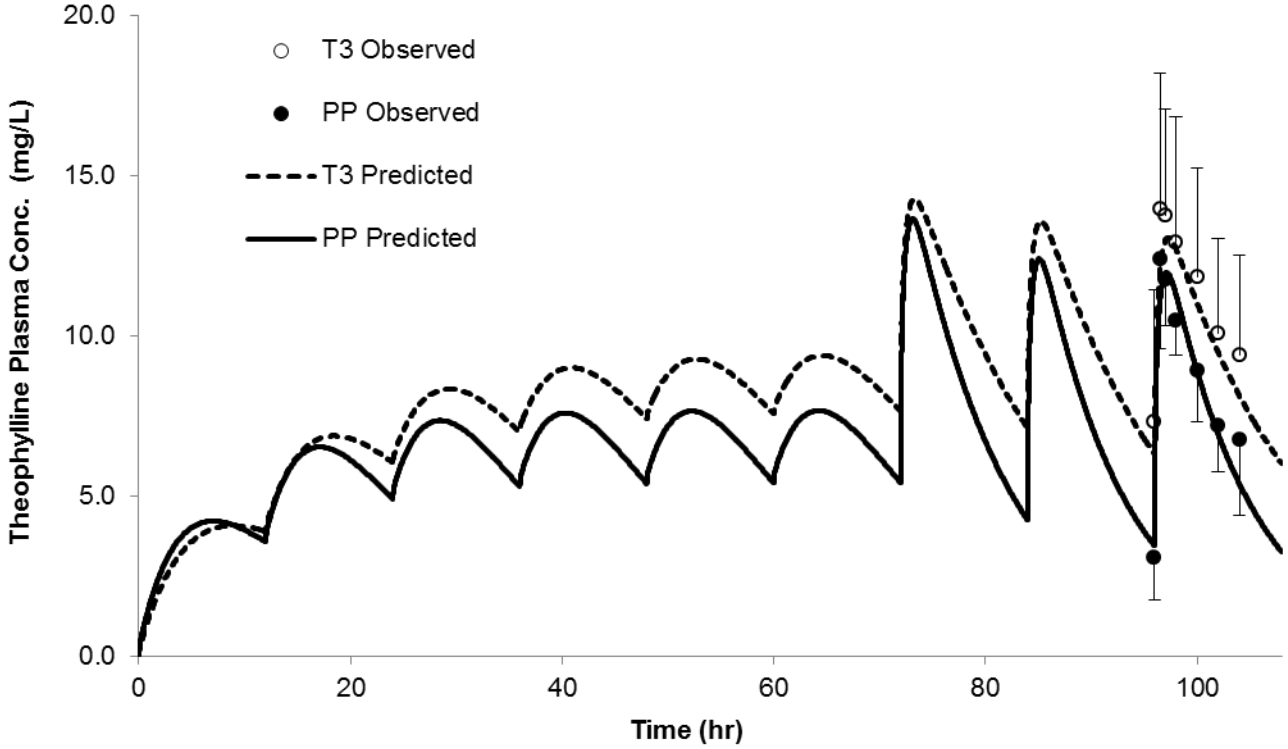
20.0
15.0
10.0
5.0
0.0
Theophylline Plasma Conc. (mg/L)
T3 Observed
PP Observed
T3 Predicted
PP Predicted
0
20
40
60
80
100
Time (hr)

FIGURE 2

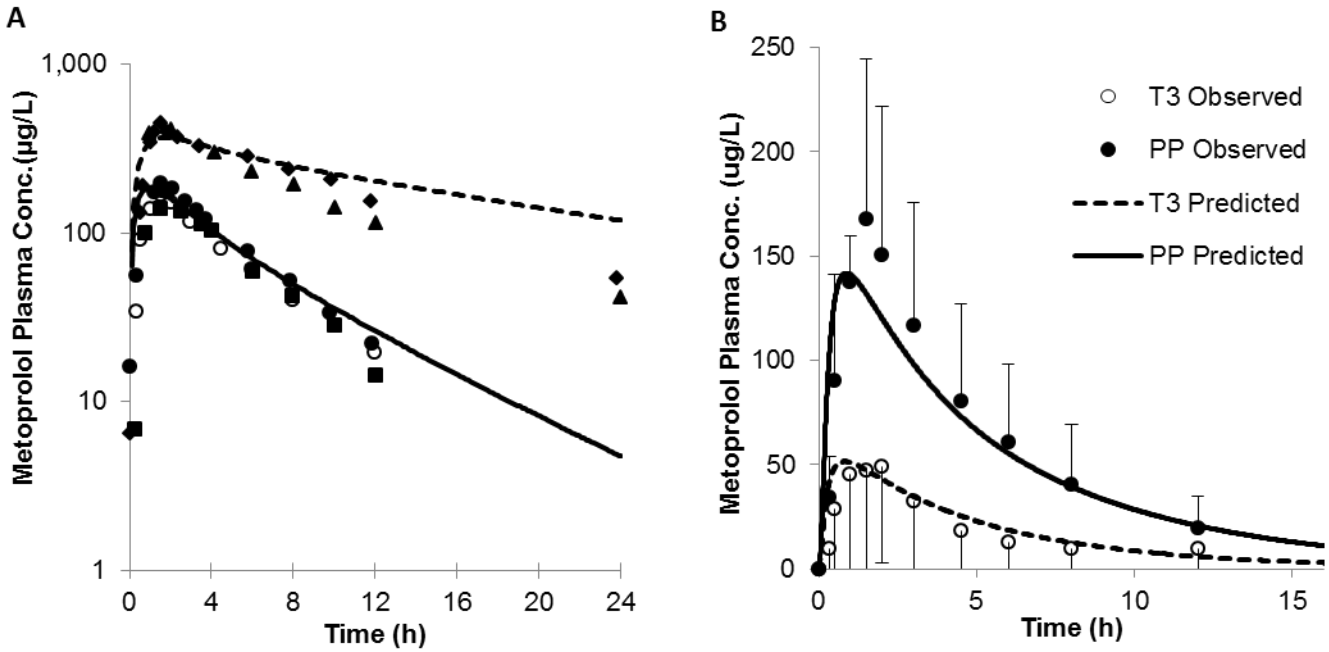
A
1,000
100
10
1
Metoprolol Plasma Conc.(µg/L)
0
4
8
12
16
20
24
Time (h)
B
250
200
150
100
50
0
Metoprolol Plasma Conc. (ug/L)
T3 Observed
PP Observed
T3 Predicted
PP Predicted
0
5
10
15
Time (h)

FIGURE 3

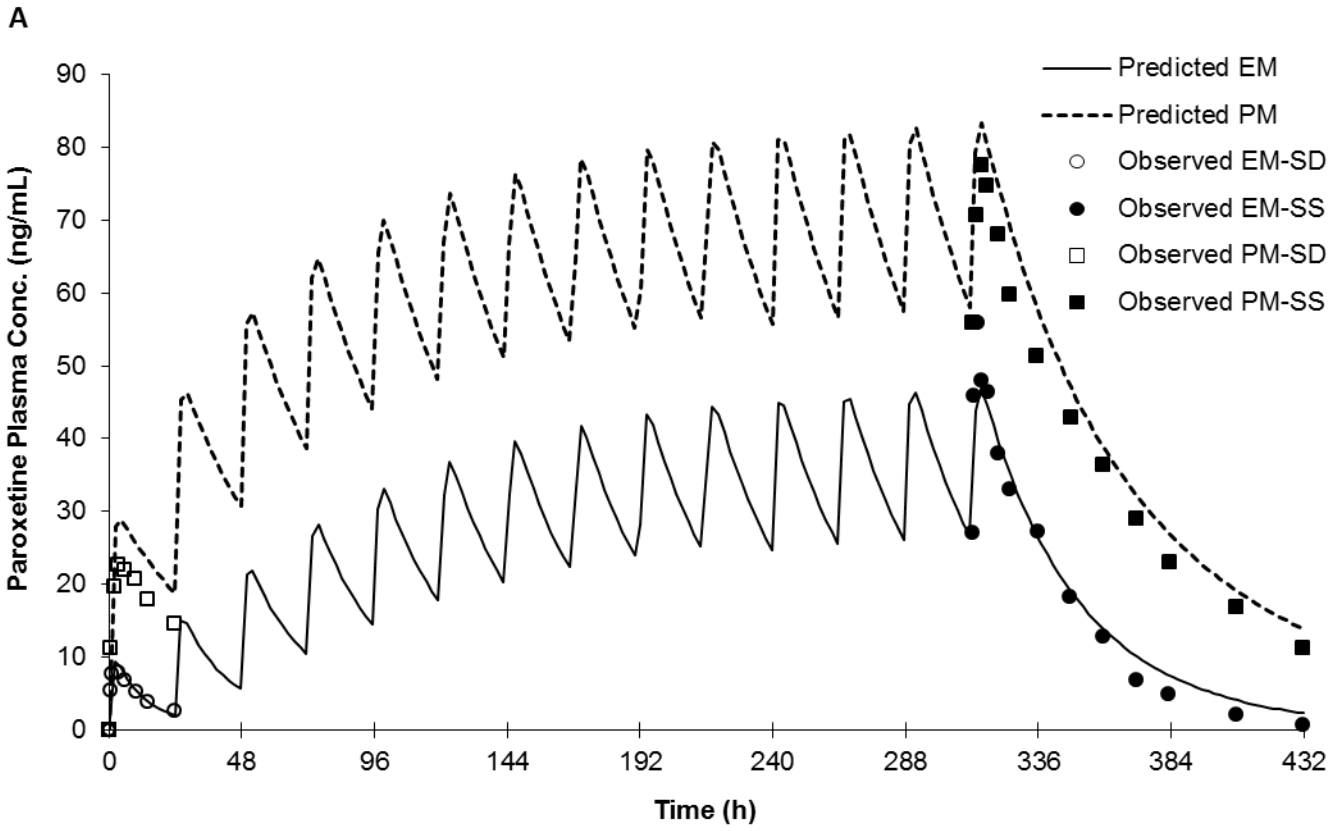
A
Predicted EM
Predicted PM
Observed EM-SD
Observed EM-SS
Observed PM-SD
Observed PM-SS
Paroxetine Plasma Conc. (ng/mL)
Time (h)
0
10
20
30
40
50
60
70
80
90
0
48
96
144
192
240
288
336
384
432

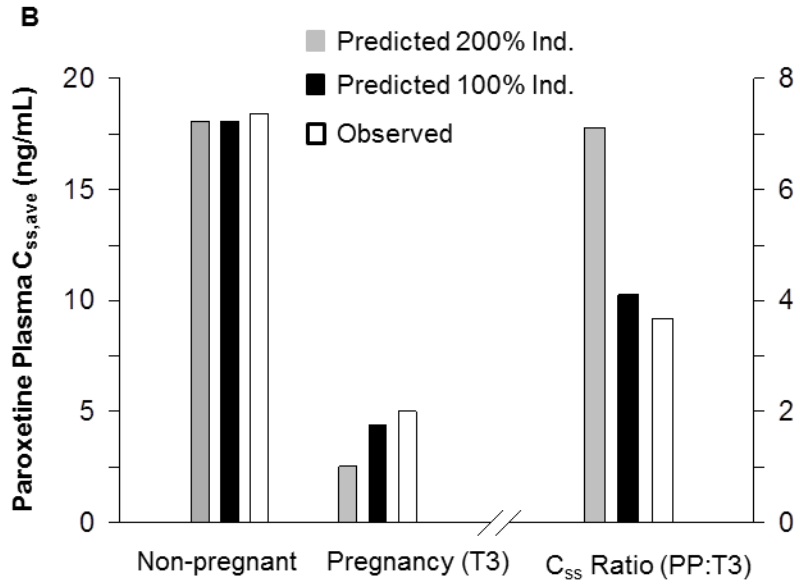
B
Predicted 200% Ind.
Predicted 100% Ind.
Observed
Paroxetine Plasma $C_{ss,ave}$ (ng/mL)
0
5
10
15
20
0
2
4
6
8
Non-pregnant
Pregnancy (T3)
C_{ss} Ratio (PP:T3)

FIGURE 4

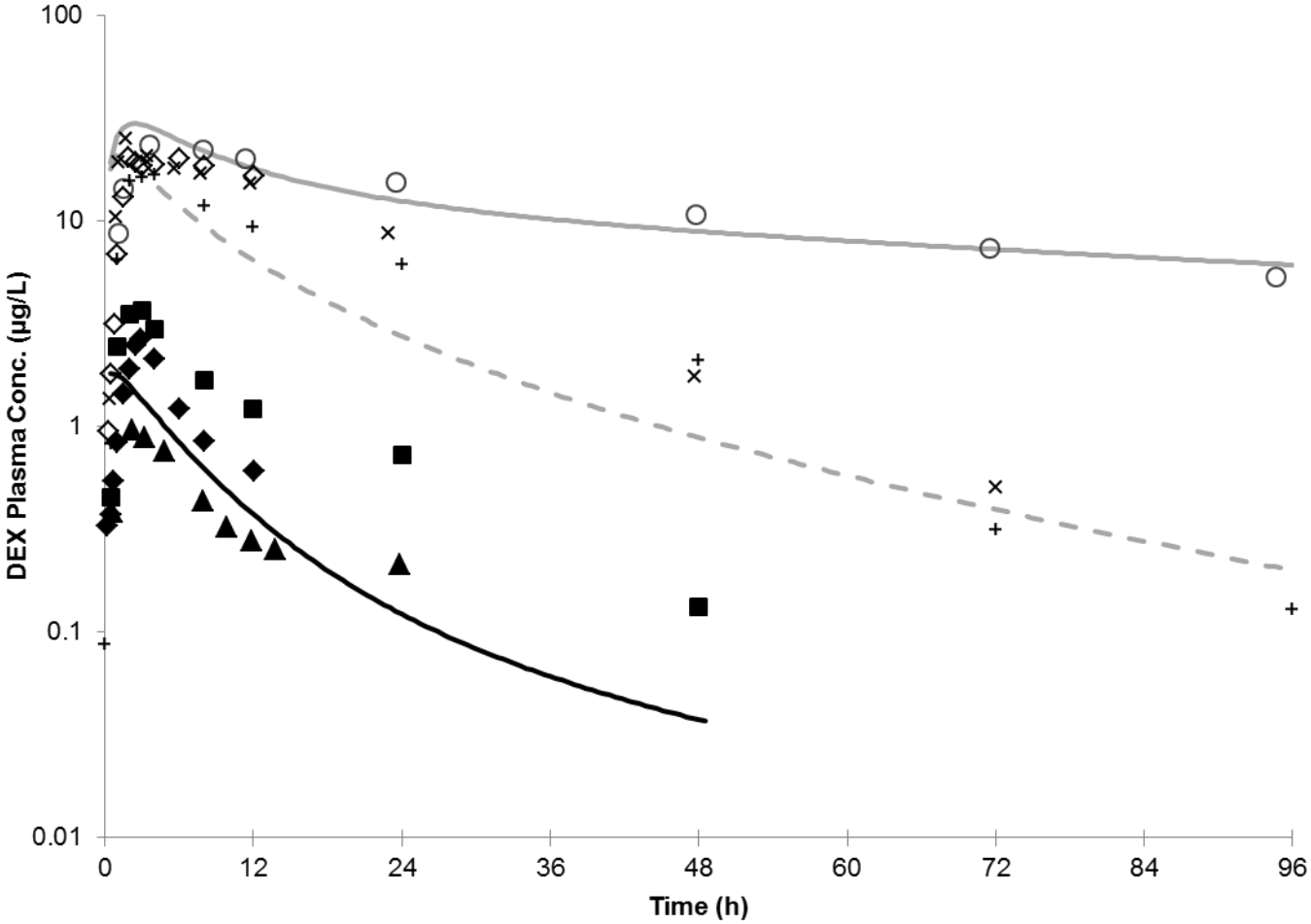

FIGURE 5

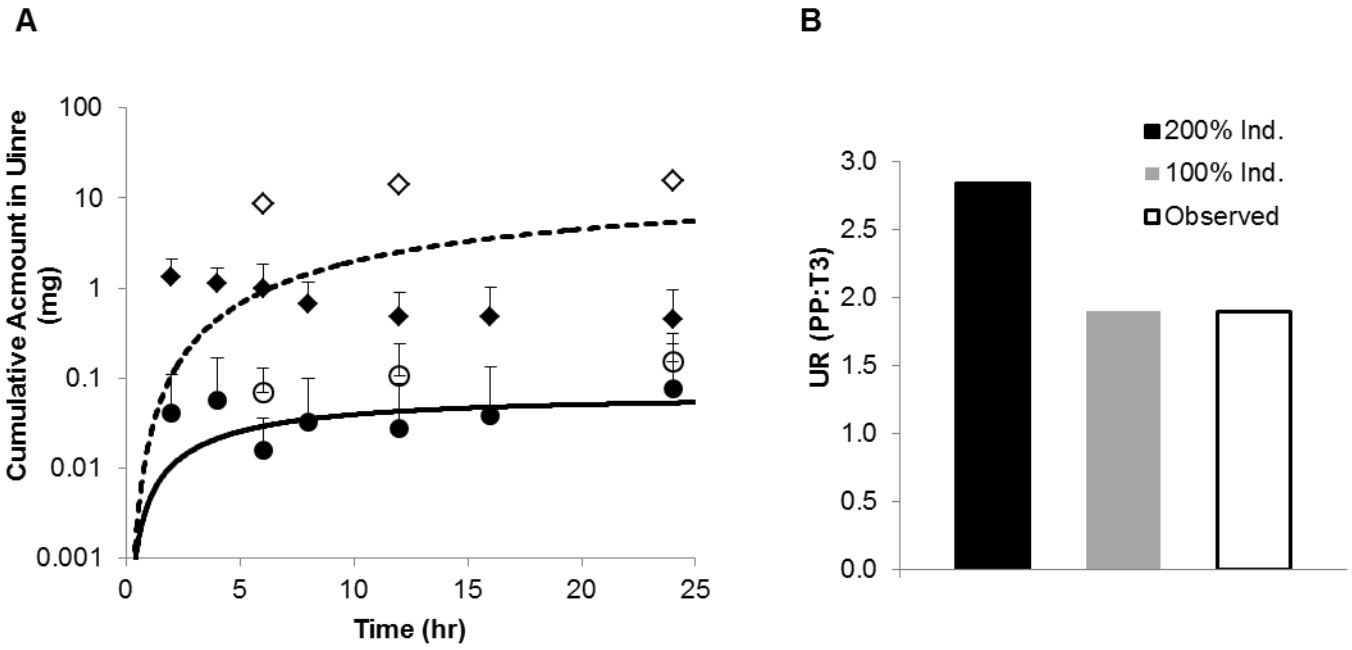
A
Cumulative Acmount in Uinre (mg)
100
10
1
0.1
0.01
0.001
0
5
10
15
20
25
Time (hr)
B
200% Ind.
100% Ind.
Observed
UR (PP:T3)
3.0
2.5
2.0
1.5
1.0
0.5
0.0

FIGURE 6

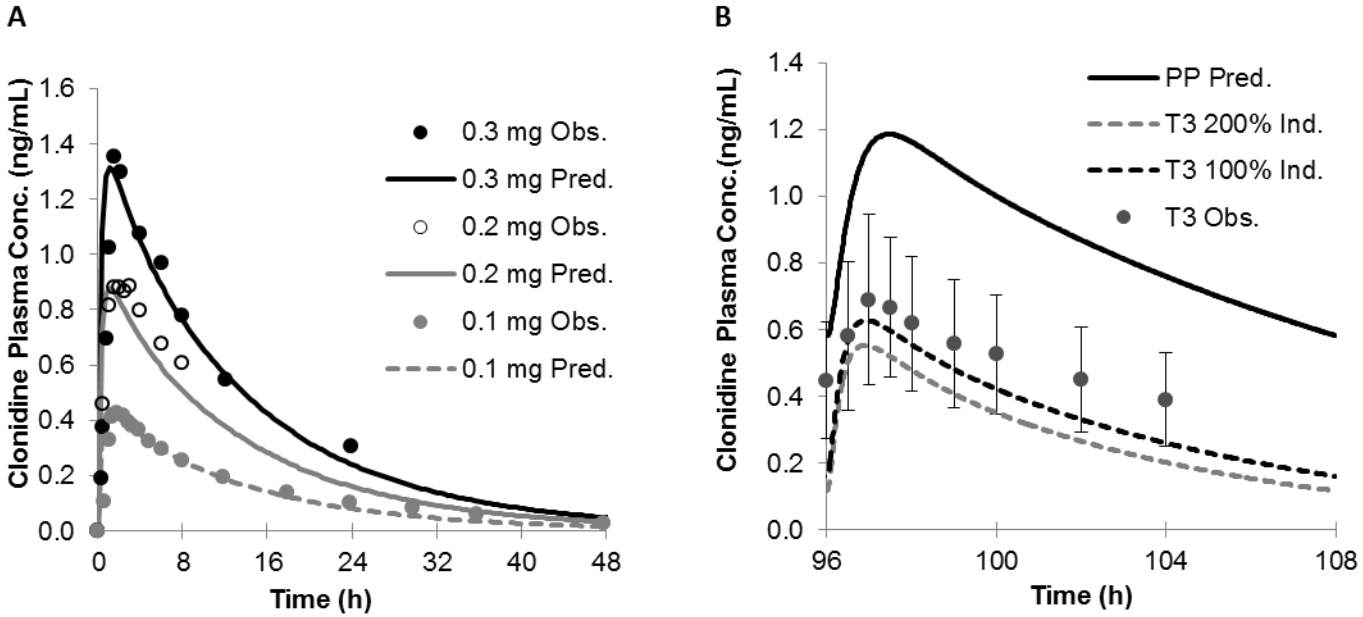
A
Clonidine Plasma Conc. (ng/mL)
1.6
1.4
1.2
1.0
0.8
0.6
0.4
0.2
0.0
0
8
16
24
32
40
48
Time (h)
0.3 mg Obs.
0.3 mg Pred.
0.2 mg Obs.
0.2 mg Pred.
0.1 mg Obs.
0.1 mg Pred.
B
Clonidine Plasma Conc.(ng/mL)
1.4
1.2
1.0
0.8
0.6
0.4
0.2
0.0
96
100
104
108
Time (h)
PP Pred.
T3 200% Ind.
T3 100% Ind.
T3 Obs.

Supplemental Materials

Supple. Table 1 Theophylline PK Parameters (259 mg p.o.) during T_3 and Postpartum			
	Observed	Predicted	Predicted/Observed
AUC_{0-8} (mg/L•hr)			
Pregnancy (T_1)	94.6[a]	109.9	1.2
Pregnancy (T_2)	98.8[a]	113.8	1.2
Pregnancy (T_3)	125.5[a]	114.3	0.9
Postpartum (PP)	93.6[b]	87.1	0.9
AUC_{PP}/AUC_{T1}	0.99	0.79	0.8
AUC_{PP}/AUC_{T2}	0.95	0.77	0.8
AUC_{PP}/AUC_{T3}	0.75	0.76	1.0
C_{max} (mg/L)			
Pregnancy (T_1)	12.9	14.6	1.1
Pregnancy (T_2)	13.0	14.7	1.1
Pregnancy (T_3)	14.0	14.3	1.0
Postpartum (PP)	12.4	13.6	1.1
$C_{max,PP}/C_{max,T1}$	0.96	0.93	1.0
$C_{max,PP}/C_{max,T2}$	0.95	0.92	1.0
$C_{max,PP}/C_{max,T3}$	0.89	0.95	1.1
$C_{min,8h}$ (mg/L)			
Pregnancy (T_1)	7.4	7.5	1.0
Pregnancy (T_2)	7.6	8.0	1.0
Pregnancy (T_3)	9.4	8.1	0.9
Postpartum (PP)	6.8	5.4	0.8
$C_{min,PP}/C_{min,T1}$	0.91	0.71	0.8
$C_{min,PP}/C_{min,T2}$	0.89	0.67	0.8
$C_{min,PP}/C_{min,T3}$	0.72	0.66	0.9

[a]: AUC estimates based on observed concentration data (Gardner et al., 1987) were generated using linear trapezoidal rule

[b]: Oral clearance (CL_{ORAL}) was found to remain suppressed during immediate postpartum period (9-13 wks PP). Therefore, AUC_{0-8} obtained during 14-58 wks postpartum was considered to represent pre-pregnancy levels.

Supple. Table 2 Metoprolol PK Parameters (100 mg p.o.)			
Non-pregnant Population			
	Obs.	Pred.	Pred./Obs.
$AUC_{0\text{-}inf}$ (µg/L•h)			
EM	895.8[a]	1087.1	1.2
PM	4062.8[a]	4507.8	1.1
AUC_{PM}/AUC_{EM}	4.5	4.1	0.9
AUC_{EM+Qd}/AUC_{EM}	3.2[b]	3.3	1.0
C_{max} (µg/L)			
EM	170.9[a]	158.7	0.9
PM	427.6[a]	313.7	0.7
$C_{max,PM}/C_{max,EM}$	2.5	2.0	0.8
$C_{min,12h}$ (µg/L)			
EM	19.2[c]	26.7	1.4
PM	133.7[d]	177.6	1.3
$C_{min,PM}/C_{min,EM}$	7.0	6.7	1.0
During T_3 and Postpartum			
	Obs. [e]	Pred. (200% P450 2D6 Ind) [f]	Pred./Obs.
$AUC_{0\text{-}inf}$ (µg/L•h)			
Pregnancy (T_3)	266.9	302.6	1.1
Postpartum (PP)	952.5	906.3	1.0
AUC_{PP}/AUC_{T3}	3.6	3.0	0.8
C_{max} (µg/L)			
Pregnancy (T_3)	49	51.8	1.1
Postpartum (PP)	168	142.7	0.8
$C_{max,PP}/C_{max,T3}$	2.4	2.8	0.8
$C_{min,12h}$ (µg/L)			
Pregnancy (T_3)	9.8	5.9	0.6
Postpartum (PP)	19.5	21.3	1.1
$C_{min,PP}/C_{max,T3}$	2.0	3.6	1.8

[a]: arithmetic mean of reported values following administration of 100mg single p.o. dose in healthy volunteers extracted from University of Washington, Metabolism & Transport Drug Interaction Database (no. of subjects =166, no. of studies=8 for the EM group and no. of subjects =20, no. of studies=3 for the PM group).

[b]: reported (Johnson and Burlew, 1996)

[c]: arithmetic mean of reported values (Hogstedt et al., 1985; Hamelin et al., 2000; Sharma et al., 2005).

[d]: arithmetic mean of reported values (Hamelin et al., 2000; Sharma et al., 2005).

[e]: arithmetic mean values reported by Hogstedt et al. (Hogstedt et al., 1985).

[f]: refers to 200% induction of P450 2D6

Supple. Table 3 Paroxetine PK Parameters in Non-pregnant Population						
Parameters	30 mg SD			30mg QD		
$AUC_{0\text{-}inf}$ or $AUC_{ss,0\text{-}tau}$ µg/L•h	Obs.[a]	Pred.	Pred./ Obs.	Obs.[a]	Pred.	Pred./ Obs.
EM	187.3	154.8	0.8	893.1	884.2	1.0
PM	1321.7	1627.9	1.2	1536.6	1703.2	1.1
AUC_{PM}/AUC_{EM}	7.1	10.5	1.5	1.7	1.9	1.1
C_{max} (µg/L)						
EM	7.9	9.1	1.2	52.4	46.9	0.9
PM	22.7	28.8	1.3	77.5	83.2	1.1
$C_{max,PM}/C_{max,EM}$	2.9	3.2	1.1	1.5	1.8	1.2
$C_{min,24h}$ (µg/L)						
EM	2.7	2.1	0.8	26.5	25.7	1.0
PM	14.5	18.9	1.3	54.2	56.5	1.0
$C_{min,PM}/C_{min,EM}$	5.4	9.1	1.7	2.0	2.2	1.1

[a]: arithmetic mean of reported values (Sindrup et al., 1992b)

Supple. Table 4	Paroxetine $C_{ss, average}$ (20mg QD) in P450 2D6 EMs during T_3 and PP				
$C_{ss, average}$ (ng/mL)	Obs. Median	Pred.[c] (200% P450 2D6 Ind) [d]	Pred. /Obs.	Pred. (100% P450 2D6 Ind) [d]	Pred. /Obs.
Non-pregnant	18.4[a]	18.1	1.0	18.1	1.0
Pregnancy (T_3)	5.0[b]	2.5	0.5	4.4	0.9
C_{ss} ratio (PP:T_3)	3.7	7.1	1.9	4.1	1.1

[a] The concentrations measured 12 hours (τ/2) after dosing were taken as an approximation to mean C_{ss} (Sindrup et al., 1992a).

[b] Reported median values (Ververs et al., 2009). Time between drug intake and sample collection varied.

[c] Predicted concentration at τ/2 was taken as an approximation to mean $C_{ss.}$

[d] Refers to 200% induction and 100% induction of P450 2D6.

Supple. Table 5 Dextromethorphan PK Parameters (30 mg p.o.) in Non-pregnant Population			
	Obs.	Pred.	Pred./ Obs.
$AUC_{0\text{-}inf}$ (µg/L•h)			
EM	16.9[a]	16.3	1.0
PM	1241.6[b]	1058.8	0.9
EM+Qd	350.8[c]	258.7	0.7
AUC_{PM}/AUC_{EM}	73.5	65.0	0.9
AUC_{EM+Qd}/AUC_{EM}	20.8	15.9	0.8
C_{max} (µg/L)			
EM	2.0[a]	1.8	0.9
PM	23.1[b]	29.7	1.29
EM+Qd	19.5[c]	21.0	1.1
$C_{max,PM}/C_{max,EM}$	12.1	16.5	1.4
$C_{max,EM+Qd}/C_{max,EM}$	10.2	11.6	1.1
$C_{min,48h}$ (µg/L)			
EM	0.2[a]	0.04	0.2
PM	10.7[b]	8.94	0.8
EM+Qd	2.0[c]	0.9	0.5
$C_{min,PM}/C_{min,EM}$	58.9	223.5	3.8
$C_{min,EM+Qd}/C_{min,EM}$	11.0	22.5	2.0

[a]: Weighted arithmetic mean of reported values following administration of 30 mg single p.o. dose (Capon et al., 1996; Abdul Manap et al., 1999; Gorski et al., 2004; Abduljalil et al., 2010)

[b]: Weighted arithmetic mean of reported values following administration of 30 mg single p.o. dose (Capon et al., 1996; Gorski et al., 2004)

[c]: Weighted arithmetic mean of reported values following administration of 30 mg single p.o. dose (Capon et al., 1996; Abdul Manap et al., 1999)

Supple. Table 6	DEX UR in 2D6 EMs during T_3 and Postpartum				
$UR_{0\text{-}24h}$ (DEX/DXO)	Obs. [a]	Pred. (200% P450 2D6 Ind)	Pred./Obs.	Pred. (100% P450 2D6 Ind)	Pred./Obs.
Pregnancy (T_3)	0.0033 (0.00147-0.0086)	0.0023 -	0.7	0.0034 -	1.0
Postpartum (PP)	0.0063 (0.0037-0.026)	0.0065 -	1.0	0.0065 -	1.0
UR_{PP}/UR_{T3}	1.9	2.9	1.5	1.9	1.0

[a]: Reported median (90% CI) following the administration of 30 mg single p.o. dose (Tracy et al., 2005)

Supple. Table 7 Clonidine PK Parameters in Non-pregnant Population			
	Obs.	Pred.	Pred./ Obs.
$AUC_{0\text{-}inf}$ (µg/L•h)			
2.35 µg/Kg i.v.	11.3[a]	12.5	1.1
1.79 µg/Kg i.v.	8.1[a]	9.5	1.2
$C_{min,\ 24h}$ (µg/L)			
2.35 µg/Kg i.v.	0.35[a]	0.156	0.4
1.79 µg/Kg i.v.	0.12[a]	0.12	1.0
$AUC_{0\text{-}inf}$ (µg/L•h)			
0.1 mg p.o.	7.3[b]	6.3	0.9
0.2 mg p.o.	14.3[c]	12.5	0.9
0.3 mg p.o.	21.5[d]	18.8	0.9
C_{max} (µg/L)			
0.1 mg p.o.	0.44[b]	0.44	1.0
0.2 mg p.o.	0.88[c]	0.88	1.0
0.3 mg p.o.	1.4[d]	1.32	0.9
$C_{min,\ 24h}$ (µg/L)			
0.1 mg p.o.	0.1[b]	0.08	0.8
0.2 mg p.o.	-	0.16	-
0.3 mg p.o.	0.3[d]	0.25	0.8

[a]: reported mean values (Frisk-Holmberg et al., 1981)

[b]: reported mean values extracted from product label for CATAPRES® (Clonidine Hydrochloride) oral tablet.

[c]: reported mean values(Porchet et al., 1992)

[d]: reported mean values (Cunningham et al., 1994)

Supple. Table 8 Clonidine PK Parameters during T_3 and Postpartum					
	Obs. [a]	Pred. (200% P450 2D6 Ind)	Pred./Obs.	Pred. (100% P450 2D6 Ind)	Pred./Obs.
$AUC_{0\text{-}tau}$ (µg/L•hr)					
Pregnancy (T_3)	5.7	4.8	0.8	5.8	1.0
Postpartum (PP)	9.6	10.4	1.1	10.4	1.1
AUC_{PP}/AUC_{T3}	1.7	2.2	1.3	1.8	1.1
C_{max} (µg/L)					
Pregnancy (T_3)	0.57	0.61	1.1	0.7	1.2
Postpartum (PP)	-	1.18	-	1.18	-
$C_{max,PP}/C_{max,T3}$	-	1.9	-	1.7	-

[a] Observed value calculated based on reported CL_{ORAL} and assumed mean dose of 0.15 mg (dose range: 0.15-0.3 mg per day) (Buchanan et al., 2009).

Chapter Three

Expansion of a PBPK Model to Predict Disposition in Pregnant Women of Drugs Cleared via Multiple CYP Enzymes, Including CYP2B6, CYP2C9 and CYP2C19

* This chapter has been submitted to the journal titled "British Journal of Clinical Pharmacology", and is formatted according to the requirements of the journal.

Expansion of a PBPK Model to Predict Disposition in Pregnant Women of Drugs Cleared via Multiple CYP Enzymes, Including CYP2B6, CYP2C9 and CYP2C19

A B Ke[1,2], S C Nallani[2], P Zhao[2], A Rostami-Hodjegan[3,4], J D Unadkat[1]

[1] Department of Pharmaceutics, University of Washington, Seattle, Washington, USA.

[2] Office of Clinical Pharmacology, Office of Translational Sciences, Center for Drug Evaluation and Research, Food and Drug Administration, Silver Spring, Maryland, USA.

[3] School of Pharmacy and Pharmaceutical Sciences, University of Manchester, Manchester, UK.

[4] Simcyp Limited (now part of Certara), Sheffield, UK.

Running title: PBPK Prediction of PK Changes during Pregnancy

Corresponding author:

Dr. Jashvant D. Unadkat

Department of Pharmaceutics

University of Washington

Box 357610

Seattle, WA 98195

Telephone: 206-543-9434

Fax: 206-543-3204

E-mail: jash@u.washington.edu

Tables: 7

Figures: 4

Abstract: 248 (250 limit)

Word count: 6743 (excluding the title page, summary, references, tables, and figures)

Abbreviations: ADME: absorption, distribution, metabolism and excretion; AUC, area under the curve; AUCR: AUC ratio; B/P: blood to plasma concentration ratio; CL: clearance; CL_r: renal clearance; $CL_{int,u}$: unbound intrinsic clearance; C_{max}: maximum plasma concentration; C_{min}: minimum plasma concentration; C_{ss}: steady-state plasma concentration; CYP: cytochrome P450; $f_{m,\ CYP}$: fraction metabolized by a specific CYP isoform; $f_{u,p}$: fraction unbound in plasma; F: bioavailability; F_a: fraction absorbed; F_g: intestinal bioavailability; F_h: hepatic bioavailability; HLM, human liver microsomes; k_a: fist order absorption rate constant; K_p, tissue-to-plasma partition coefficient; Q_{Gut}, hybrid parameter of blood flow and drug permeability; PBPK model: physiologically-based pharmacokinetic model; PP: postpartum; T_1, T_2 and T_3: 1st, 2nd and 3rd trimester; V_{ss}: volume of distribution at steady state.

STRUCTURED SUMMARY

Aim

Conducting PK studies in pregnant women is challenging. Therefore, we asked if a physiologically-based pharmacokinetic (PBPK) model could be used to predict the disposition in pregnant women of drugs cleared by multiple CYP enzymes.

Methods

We expanded and verified our previously published pregnancy PBPK model by incorporating hepatic CYP2B6 induction (based on *in vitro* data), CYP2C9 induction (based on phenytoin PK), and CYP2C19 suppression (based on proguanil PK), into the model. This model accounted for gestational age-dependent changes in maternal physiology and hepatic CYP3A, CYP1A2 and CYP2D6 activity. For verification, the pregnancy-related changes in the disposition of methadone (cleared by CYP2B6, 3A and 2C19), and glyburide (cleared by CYP3A, 2C9 and 2C19) were predicted.

Results

Predicted mean postpartum to second trimester (PP:T_2) ratios of methadone AUC, C_{max} and C_{min} were 1.9, 1.7 and 2.0, vs. observed values 2.0, 2.0 and 2.6, respectively (Pond et al.,1985). Predicted mean postpartum to third trimester (PP:T_3) ratios of methadone AUC, C_{max} and C_{min} were 2.1, 2.0 and 2.4, vs. observed values 1.7, 1.7 and 1.8, respectively. Predicted PP:T_3 ratios of glyburide AUC, C_{max} and C_{min} were 2.6, 2.2 and 7.0, vs. observed values 2.1, 2.2 and 3.2, respectively (Hebert et al., 2009).

Conclusions

Our PBPK model integrating prior physiological knowledge, *in vitro* and *in vivo* data, allowed successful

prediction of methadone and glyburide disposition during pregnancy. We propose this expanded PBPK model can be used to evaluate different dosing scenarios, during pregnancy, of drugs cleared by single or multiple CYP enzymes.

What is already known about this subject (<50 words):

- During pregnancy, changes in physiology and ADME processes can significantly affect the disposition of drugs. Such changes may require adjustments in the dosing regimen of the drug.
- Since conducting PK studies in pregnant women is challenging, alternative approaches that can predict adjustment of drug dosing regimens (if any) are highly desirable.

What this study adds (<50 words):

- We expanded and verified a novel physiologically based pharmacokinetic model, which incorporates gestational age-dependent changes in maternal physiology and major hepatic CYP enzyme activity, to predict disposition during pregnancy of drugs cleared by multiple CYP enzymes (e.g. glyburide and methadone).

Introduction

Considerable literature data demonstrate that the PK of drugs can be significantly affected by pregnancy. Such changes may lead to either under-dosing or overdosing of medication with the standard adult dose, with varying consequences for safety and efficacy [1]. For example, in pregnant opioid-dependent women, the oral clearance (CL_{ORAL}) of methadone (METH), is induced by ~105% during the second trimester (T_2) vs. postpartum (PP), and ~65% during third trimester (T_3) vs. PP [2]. Given the established link between plasma methadone concentration and the pharmacological effects [3], these changes during pregnancy may require careful evaluation of patient complaints of a dose ‘‘not holding’”. Similarly, in gestational diabetic subjects, the steady-state $AUC_{0\text{-}12}$ and C_{max} of glyburide (GLB), a drug with established plasma concentration-effect relationship at therapeutic doses [4], are 53% and 55% lower during T_3 vs. non-pregnant type 2 diabetic subjects [5]. These results suggest that patients with inadequate glucose control might benefit from increased GLB dosage. Obviously, for drugs operating at the plateau phase of the plasma concentration-effect curve, the pregnancy-induced change in their pharmacokinetics would be of less concern.

Altered drug disposition can be attributed to pregnancy-induced changes in drug absorption (e.g., gastric pH, transporters), distribution (e.g., plasma protein binding and transporters), metabolism (e.g. cytochrome P450 (CYP) metabolism) and excretion (e.g., renal secretion via transporters) (ADME). Further, data in the literature suggests that the magnitude of change in maternal hepatic enzyme activity is CYP isoform specific and gestational age dependent [6]. The underlying mechanism for the hepatic isoform-specific and gestational state specific induction during pregnancy is not fully understood. It has been postulated that the rising concentrations of

various hormones in maternal blood, including placental growth hormone, progesterone, corticosteroids and estrogens, are responsible for induction of hepatic enzyme activity [7].

Since it is logistically impossible to delineate the changes in PK of all drugs administered to pregnant women, alternative approaches such as mechanistic modeling, to predict drug disposition and adjustment of drug dosing regimens (if any) are highly desirable. These approaches, in conjunction with opportunistic PK studies in pregnant women of drugs administered for therapeutic purposes, should improve our ability to adjust drug dosing regimens for pregnant women. To this end, we have focused on a systems pharmacology approach, i.e. physiologically-based pharmacokinetic (PBPK) modeling. PBPK modeling has the advantage of incorporating both physiological parameters that are important for ADME processes and drug-specific parameters (e.g. physico-chemical and drug disposition characteristics) into a quantitative predictive model [8, 9]. A maternal PBPK model, incorporating prior physiological parameters as well as maternal hepatic CYP activity in each trimester was recently developed [10, 11]. We refined this PBPK model and showed that the PBPK model populated with CYP3A, 1A2 and 2D6 activity change, based on CL_{ORAL} of midazolam, caffeine and metoprolol, respectively, could accurately predict the disposition during pregnancy of other drugs cleared primarily by the same CYP enzyme, namely CYP3A-metabolized drug nifedipine and indinavir (CYP3A) [12], CYP1A2-metabolized drug theophylline, and CYP2D6-metabolized drug paroxetine, dextromethorphan and clonidine[13]. In the current study, we expanded and verified the established PBPK model, by incorporating CYP2B6 induction (based on *in vitro* data), CYP2C9 induction (based on phenytoin PK), and CYP2C19 suppression (based on proguanil PK). For model verification, the PBPK model was used to predict the disposition during

pregnancy of drugs cleared via these multiple CYP pathways including methadone (METH) and glyburide (GLB).

Methods

General workflow of PBPK model development and verification criterion

A general workflow of PBPK modeling and simulation of test compounds in non-pregnant subjects consisted of the following steps: 1) comparison of mean plasma concentration-time (C-T) profiles simulated using a 13-compartment full-PBPK model (Simcyp® Population-based Simulator Version 12.1, Simcyp Limited, Sheffield, UK) with those obtained from *in vivo* studies including i.v. dosing, single and multiple oral dosing (to qualify the drug-specific parameters); 2) refinement (hence referred to as modified model) of the drug-specific parameters (e.g. f_m) if the prediction in (1) above deviates significantly (<0.8-fold or >1.25-fold) from that observed. Such refinements were often based on changes in mean AUC and mean concentration-time profiles in the presence of inhibitors or genetic polymorphism of the enzymes clearing the drug; 3) populating the time-varying full PBPK model constructed in Matlab v. 7.10® (2010, Mathworks®, Natick, MA) with these qualified drug-specific parameters and pregnancy-induced CYP activity changes (see below).

Verification of the established PBPK model was primarily based on AUC because achieving equivalent drug exposure in pregnant and non-pregnant women was our primary focus. The term "verification" is used in place of "validation" to acknowledge the complexity of PBPK model that requires more than plasma data to accomplish proper validation. In addition, prediction of C_{max} and C_{min} was considered because achieving similar drug C_{max} and C_{min} may be important for some drugs where these measures are related to drug efficacy and/or toxicity. For model

verification, mean AUC, C_{max} and C_{min} of METH and GLB during pregnancy were predicted and compared with published studies in pregnant subjects. We chose the criterion of PK bioequivalence as the criterion for successful verification of the model, namely, the predicted mean population PK parameters of the drug (as described above), should fall within 80% to 125% of the observed value, i.e. $0.80 \leq pred/obs \leq 1.25$.

General pregnancy PBPK model structure and key assumptions

The general pregnancy PBPK model structure and key assumptions were described in detail previously [10, 12]. Briefly, the gestational age dependent changes in physiological parameters (e.g., cardiac output, glomerular filtrate rate, etc) were incorporated into an existing PBPK model (Jamei et al, 2009). Maternal glomerular filtration rate (GFR) was assumed to increase during pregnancy by 19%, 40% and 37% during T_1, T_2 and T_3 respectively [11]. The change in drug unbound fraction in plasma ($f_{u,p}$) during pregnancy, as a function of serum albumin or α1-AGP concentrations, was accounted for in the model as described previously [12]. The established PBPK model also assumed that hepatic CYP3A activity increased by 2.0-fold (measured by midazolam CL_{ORAL}) during T_3 [12]. The magnitude of CYP3A during T_2 was assumed to be the same as that of T_3, as suggested by similar T_2 vs. T_3 effect on indinavir CL_{ORAL} [14] . The PBPK model was further expanded to incorporate pregnancy-induced induction of CYP2B6 and CYP2C9, as well as suppression of CYP2C19 as described below. Maternal hepatic CYP2B6 was assumed to increase during pregnancy by 1.1-fold, 1.4-fold and 1.9-fold (based on *in vitro* to *in vivo* extrapolation, see results) during T_1, T_2, and T_3 respectively. Maternal CYP2C9 activity was assumed to increase by 1.4-fold, 1.5-fold and 1.6-fold (reported by phenytoin PK) during T_1, T_2 and T_3 [15, 16] (see results). Maternal CYP2C19 activity, as reported by CL_{ORAL} of the anti-

malarial agent proguanil [17, 18], was assumed to decrease by 62% and 68% during T_2 and T_3, respectively (see below). Hepatic OATP1B1 or 2B1 activity was assumed to remain constant throughout pregnancy. These changes were accomplished in Matlab v7.10®.

The mass balance differential equations (except for permeability-limited liver model) used in the model have been described previously [10, 12]. Briefly, all tissues except maternal liver were considered to be well-stirred compartments, i.e. that the unbound tissue concentration is at equilibrium with the unbound concentration in the emergent blood. The maternal liver was modeled as a permeability-limited tissue, incorporating scaled active uptake ($PS_{int,OATP}$) and scaled passive diffusion clearances (CL_{pd}) of unbound drug at the sinusoidal membrane, and scaled metabolic clearance ($CL_{int,u,h}$) of unbound drug (Eq.1-2). The liver compartment was subdivided into extracellular (EC) and intracellular compartments (IC). The EC combined tissue blood (11.5% of liver volume) and interstitial fluid (16.3% of liver volume). Biliary excretion of unchanged drug is negligible for the tested drugs and was therefore not considered in the current model.

$$V_{EC}\frac{dC_{EC,h}}{dt} = Q_{ha}C_{ab} + Q_gC_{vbg} + Q_{sl}C_{vbsl} - Q_hC_{EC} - CL_{pd}(C_{EC,h,u} - C_{IC,h,u}) - PS_{int,OATP}C_{EC,h,u} \quad \text{Eq. 1}$$

$$V_{IC}\frac{dC_{IC,h}}{dt} = PS_{int,OATP}C_{EC,h,u} + CL_{pd}(C_{EC,h,u} - C_{IC,h,u}) - CL_{int,u,h}C_{IC,h,u} \quad \text{Eq. 2}$$

For drugs that are not actively transported into the hepatocytes (such as METH and PHT), Eq.3 was used. Eq.4 was used to describe the apparent intrinsic clearance. Eq.5 was used to describe the dynamic change of the enzyme amount as a result of auto-induction by drugs such as PHT.

$$V_h\frac{dC_h}{dt} = (Q_h - Q_g - Q_{sl})C_{ab} + Q_gC_{vbg} + Q_{sl}C_{vbsl} - Q_hC_{vbh} - CL_{int,u,h}f_u\frac{C_h}{K_p} \quad \text{Eq. 3}$$

$$CL_{int,h,u} = \frac{V_{max} * A_{CYP}}{K_m + f_{u,h} * C_h} \quad \text{Eq. 4}$$

$$\frac{dA_{CYP}}{dt} = k_{deg} A_{CYP,0} - k_{deg} A_{CYP} + k_{deg} A_{CYP,0} \frac{E_{max*} f_{u,h} C_h}{EC_{50,u} + f_{u,h} C_h} \quad \text{Eq. 5}$$

where C_{ab}, C_h, C_{vbsl}, C_{vbg} and C_{vbh} represent the concentrations in the arterial blood, liver, spleen-blood, gut-blood and hepatic outlet (or liver-blood), respectively; Q_h, Q_g and Q_{sl} represent the blood flows of the liver, gut and spleen respectively; V_h, V_{EC} and V_{IC} represent the volume of the liver, extracellular compartment and intracellular compartment of the liver, respectively; f_u and $f_{u,h}$ represents the fractions unbound in plasma and liver ($f_{u,h}=f_u/K_p$ for drugs with no active uptake or efflux). $CL_{int,u,h}$, V_{max} and K_m represent the unbound hepatic intrinsic clearance, maximum velocity and the Michaelis-Menten constant for metabolism, respectively; A_{CYP} and $A_{CYP,0}$ represents the total hepatic amount of CYP isoform at a given time and at baseline. K_{deg} represents the apparent first order degradation rate constant of the CYP enzyme; $EC_{50,u}$ and E_{max} represent the unbound concentration at which 50% of maximum induction is reached, and the maximum induction potential, respectively. Pregnancy-induced change, either induction or suppression of CYP enzyme activity was reflected in unbound hepatic intrinsic clearance $CL_{int,u,h}$ for drugs with linear kinetics, or $A_{CYP,0}$ for drugs associated with saturable hepatic metabolism.

METH PBPK model construction

Methadone (METH), a drug used to treat opiate addiction, is mainly eliminated via hepatic metabolism by CYP2B6, CYP3A and CYP2C19, with a significant contribution from renal elimination (16-27%) [19, 20]. A number of studies have shown that methadone distribution

and disposition are influenced by its chirality: R-METH has lower plasma protein binding level (binding to α1-AGP), a larger volume of distribution, and higher total body clearance [21, 22]. Therefore, PBPK models for R-METH and S-METH were constructed respectively to account for the differential disposition of each enantiomer. Physiochemical and protein binding parameters (Log $P_{o:w}$, pK_a, B/P ratio, $f_{u,p}$), absorption (F_a, k_a, T_{lag}), distribution (V_{ss}), elimination (CL_{IV}) and excretion (CL_r) were obtained from literature (see Table 1). Initial scaling of *in vitro* metabolic data [19, 23] did not fully recover the observed R and S-METH metabolic clearance, CL_H. Therefore hepatic unbound intrinsic clearance $CL_{int,u}$ was back-calculated from observed CL_H (=CL_{IV}-CL_r) using well-stirred liver model. Because *in vitro* K_m for CYP2B6, CYP3A and CYP2C19 [23] is significantly greater than the therapeutic METH concentration of 1-2 μM, saturation of hepatic CYP enzymes in the clinically used dose range is unlikely. This speculation is also supported by comparable mean CL_{ORAL} following chronic dosing vs. single dosing of the racemate [20, 21, 24-26]. For these reasons saturable metabolism was not incorporated into the model. The contribution from individual CYP to total metabolic clearance obtained *in vitro* is 43.4%, 45.3% and 9.1% (R-METH), and 69.2%, 37.1% and 10.4% (S-METH), for CYP2B6, 3A and 2C19, respectively [19]. *In vivo* f_m for individual CYP was calculated by taking the product of f_m (=1-f_e) and the fractional contribution of individual CYP. Urine pH has a significant effect on renal clearance. When urine pH is below 6, the contribution of renal clearance becomes significant, accounting for around 16-27% of total body clearance [20, 27]. The average literature values for CL_r and f_e of the R-METH and S-METH were used in the final model [20, 21, 28]. The constructed drug model was verified by comparing predicted mean AUC, C_{max} and C_{min} of R-METH and S-METH following single and multiple p.o. dosing

of the racemate in non-pregnant subjects to reported literature values. The drug-dependent parameters of METH are listed in Table 1.

In vitro to in vivo extrapolation (IVIVE) of CYP2B6 induction during pregnancy

Hepatic CYP2B6 mRNA expression and enzyme activity, was shown to be induced by estradiol in a concentration-dependent manner in human hepatocytes, with EC_{50},u of 1.9±0.5 μM and E_{max} (fold-increase) of 34±22 (based on CYP2B6 mRNA expression), respectively [29]. The corresponding values based on CYP2B6 activity data are 4.1±4.1 μM and 20±21, respectively [29]. Because estradiol depletion in human hepatocytes is significant with a reported half-life of 0.57 ± 0.12 hr [30], the reported $EC_{50,u}$ was corrected for estradiol depletion by calculating the average concentration ($AUC_{0\text{-}tau}$/tau) during an incubation period of 24 hr. In the same experiment, rifampin and carbamazepine were included as positive controls. Rifampin's *in vitro* E_{max} (=9.1-fold) of CYP2B6 induction was greater than the *in vivo* E_{max} (=4 fold) as measured by hydroxybupropion formation clearance [31] . While carbamazepine's *in vitro* E_{max} (=2.2-fold) was much less than the *in vivo* E_{max} (=11.5 fold) reported by hydroxybupropion to bupropion AUC ratio [32]. IVIVE based on CYP2B6 activity data yielded similar conclusions. Given these observations, E_{max} for estradiol-mediated CYP2B6 induction was not calibrated. Based on meta-analysis of literature data, average estradiol concentration in plasma is 9.3, 33.3 and 59.6 nM during T_1, T_2 and T_3 [11]. The reported mean unbound fraction in plasma of estradiol is 2% (range 1-3%) in the non-pregnant population [33]. Estradiol mainly binds to albumin [33] and its unbound fraction in plasma is predicted to increase from the average pre-pregnancy level of 2% to 2.1%, 2.3% and 2.9% during T_1, T_2 and T_3. These correspond to unbound estradiol

concentration of 0.20, 0.76 and 1.72 nM, respectively. The magnitude of CYP2B6 induction based on CYP2B6 mRNA data was predicted using the equation 6.

$$\text{fold induction} = 1 + \frac{[I]_u \times E_{max}}{[I]_u + EC_{50}} \quad \text{Eq. 6}$$

Glyburide (GLB) PBPK model construction

GLB has dose-proportional kinetics following single and multiple p.o dosing in the clinical dose range [34]. GLB is almost exclusively cleared via hepatic metabolism (fe<0.1%) [35]. Data in literature regarding the contribution from individual CYP, particularly CYP2C9, to the metabolic clearance of GLB are inconsistent. In one study, selective inhibition studies in human liver microsomes showed that CYP3A plays a major role in GLB metabolism (~53%), followed by CYP2C9 (~28%) and CYP2C19 (<20%) [36]. In another study, using similar experimental approach, the individual CYP contribution to GLB metabolism was as follows: CYP3A (~50%)> CYP2C8 (~33%)> CYP2C19 (~17%) [37]. *In vivo* studies, on the other hand, suggested a significant role for CYP2C9 in the clearance of GLB. Single and multiple coadministration of fluvastatin (40 mg), a CYP2C9 inhibitor, increased the plasma AUC of GLB by 23% [38]. CYP2C9 is a highly polymorphic enzyme. Kirchheiner et al. showed that the total oral clearance of GLB in the CYP2C9 *3/*3 subjects (n=3) was approximately 40% of that in the CYP2C9*1/*1 subjects (n=4) [4] . Niemi et al. reported that the oral clearance of GLB in individuals heterozygous for the CYP2C9*3 allele (n=2) was 35.7% of the respective value in the CYP2C9*1/*1 subjects [39]. These clinical studies suggest the contribution of CYP2C9 to GLB metabolism *in vivo* ($f_{m,2C9}$) falls in the range of 18.6% to 63%. Considering all the *in vitro* and *in vivo* evidence, in the final GLB model, the assigned contribution from individual CYP to total GLB metabolic clearance was 50%, 30% and 20% for CYP3A, 2C9 and 2C19, respectively.

GLB has also been identified *in vitro* as a substrate of OTAP2B1 [40] and an inhibitor of OATP1B1 [41]. It is likely that GLB is also a substrate of OATP1B1, although this has not been shown in literature as of date. *In vivo*, 600-mg IV rifampin (RIF) over 30 min immediately followed by 1.25-mg oral GLB increased GLB plasma AUC by 118% and C_{max} by 81% [35]. Because RIF is a potent pan OATP inhibitor, this significant drug-drug interaction could be attributed to the inhibition of OATP2B1 and/or OATP1B1-mediated hepatic uptake clearance of GLB. These results also indicate the fraction of transport-mediated clearance towards total hepatic uptake clearance is at least 54.5%, assuming completing inhibition of OATPs by RIF.

The PBPK modeling strategy for GLB was as follows: First, the metabolic clearance of GLB (=3.6 L/hr) was predicted via IVIVE from two independent *in vitro* studies [36, 42] and similar clearance values were obtained. Definitive *in vitro* transport studies of GLB are not available, therefore the following parameters were estimated simultaneously using mean glyburide plasma pharmacokinetic data reported in subjects taking a single oral dose of 1.75-5 mg glyburide: hepatic bidirectional permeability clearance (CL_{pd}), and hepatic intrinsic uptake clearance by OATP (or the permeability surface area product, $PS_{int,OATP}$). As discussed above, both OATP2B1 and 1B1 could be important in mediating the uptake of the drug into the hepatocytes, therefore a lumped clearance $PS_{int,OATP,}$ was used. Two automated sensitivity analyses were conducted to identify the initial estimates for fitting $PS_{int,OATP}$ and CL_{pd} (Supplemental Fig.1). There are many combinations of $PS_{int,OATP}$ and CL_{pd} values that can result in AUC within the range of 0.46-0.73 ng*h/mL following 1.75 mg p.o., which is 80-125% of the mean AUC observed *in vivo* (0.58 ng*h/mL). Consequently the combination with $PS_{int,OATP} > CL_{pd}$ ($PS_{int,OATP:}$ 50 µL/min/10^6 cells; $CL_{pd:}$ 30 µL/min/10^6 cells) were selected and used as initial estimates for data fitting, as the fraction of transport-mediated clearance towards total hepatic

uptake clearance is at least 54.5% as discussed earlier. Other drug-specific parameters, including physiochemical and protein binding parameters (Log $P_{o:w}$, pK_a, $f_{u,p}$), absorption (F_a, k_a, T_{lag}), distribution (V_{ss}) and excretion (CL_r) were obtained from literature. The drug-dependent parameters of GLB are listed in Table 3. To predict the DDI between GLB and RIF, a RIF drug model provided in Simcyp simulator was updated with *in vitro* Ki of RIF against hepatic OATP2B1 or 1B1. *In vitro* Ki sourced from the online database UCSF-FDATransPortal (http://bts.ucsf.edu/fdatransportal/#content) ranged from 0.41-17 μM. Varma et al. showed using PBPK modeling, the *in vivo* Ki of rifampin as 0.41–0.6 μM, essentially the most potent *in vitro* Ki values reported, best recovered the DDI between RIF and pravastatin, a well-established substrate drug of hepatic OATP1B1[43]. Hence we used *in vivo* Ki of 0.41 μM in our prediction.

Deconvolution of the magnitude of CYP2C19 suppression during pregnancy based on proguanil PK

CYP2C19 mediates the biotransformation of the anti-malarial agent, proguanil to its active metabolite cycloguanil. Proguanil is also excreted as unchanged drug in urine (f_e = 32%) [44]. Proguanil is extensively absorbed from the gastrointestinal tract and exhibits linear pharmacokinetics over the dose range 100 mg to 400 mg [45]. The drug is 75% bound to plasma proteins and highly partitions into the red blood cells (blood to plasma concentration ratio or B/P = ~5) [46]. The CL_{ORAL} of proguanil decreases by 60% during T_2 and T_3 in patients with uncomplicated P. falciparum malaria, as compared to non-pregnant healthy subjects [17]. Possible disease effect on CL_{ORAL} of proguanil cannot be completely ruled out. In another study, where the plasma metabolic ratio of proguanil/cycloguanil was used as CYP2C19 marker, this metabolic ratio was 62% higher during T_3 vs. postpartum in subjects phenotyped as CYP2C19

extensive metabolizers [18]. The observed decrease in proguanil CL_{ORAL} during pregnancy, was then used to deconvolute the magnitude of decrease in 2C19 activity after accounting for other pregnancy related components of proguanil CL_{ORAL} (CL_r, B/P ratio and plasma protein binding). Specifically, F_a*F_G was assumed to be equal to unity and remain unchanged during pregnancy. The CL_r of proguanil greatly exceeds (> 11-fold) the renal filtration clearance ($=f_{u,p}*GFR$), suggesting proguanil is actively transported in the kidney. Because the renal transport mechanism of proguanil is unknown and because CL_r has not been assessed in pregnant women, we assumed that only the filtration clearance was increased during pregnancy. B/P ratio was predicted to decrease from baseline value of 5.0 to 4.4 during T_3 following a decrease in hematocrit value. Lastly, $f_{u,p}$ was predicted to increase from baseline value of 0.25 to 0.33 during T_3 as a function of plasma albumin concentration. Using the well-stirred liver model shown below, the deconvoluted $CL_{int,h,u}$, i.e. CYP2C19 activity, is decreased by 62% in T_2 and 68% in T_3.

$$CL_{int,h,u} = \frac{CL_{ORAL}F_aF_G - CL_r}{f_{u,p}\left(1 + \frac{CL_r}{\frac{B:P}{Q_h}}\right)} \qquad \text{Eq. 7}$$

Results

In vitro to in vivo extrapolation (IVIVE) of CYP2B6 induction during pregnancy

Using human hepatocytes, it was recently shown hepatic CYP2B6 mRNA expression and enzyme activity, can be induced by estradiol following a 48-hr incubation period, with EC_{50},u of 1.9±0.5 μM and E_{max} (fold-increase) of 34±22 (based on CYP2B6 mRNA expression), respectively [29]. The average $EC_{50,u}$ was 61.4 nM after correcting for estradiol depletion (see Methods). For reasons outlined in Methods, the E_{max} for estradiol-mediated CYP2B6 induction was not calibrated based on positive controls data including rifampin and carbamazepine. At the unbound estradiol concentration in plasma of 0.20, 0.76 and 1.72 nM, during T_1, T_2 and T_3, respectively, the predicted magnitude of CYP2B6 induction based on CYP2B6 mRNA data was 1.1-, 1.4- and 1.9-fold, respectively. The predicted magnitude based on CYP2B6 activity data was 1.0-, 1.1- and 1.3-fold, respectively. Because the increase in the rate of enzyme translation following administration of an inducer is secondary to its effect on the rate of transcription, there may be a delay, for e.g., due to turnover rate of nuclear receptors mediating the increased level of protein synthesis, between the manifestation of these two processes [47]. Considering these factors, the predicted magnitude of CYP2B6 induction based on CYP2B6 mRNA data, was used in subsequent PBPK modeling of methadone disposition.

Methadone (METH) PK Prediction in pregnancy using PBPK model incorporating CYP2B6 induction based on in vitro data

The mean AUC, C_{max} and C_{min} of R-METH and S-METH following a single p.o. dose of the racemic METH of 9.9 mg in non-pregnant subjects were quantitatively predicted by the

constructed R-METH and S-METH models (i.e., pred./obs. in the range of 0.8-1.2, Figure 1A and Table 4). At steady-state, the mean AUC, C_{max} and C_{min} of R-METH and S-METH following chronic dosing of racemic METH of 70mg Q.D. or 100 mg Q.D. were also quantitatively predicted, with the exception of $AUC_{0\text{-}tau,ss}$ (70 mg Q.D.) of S-METH and $C_{min,\ ss}$ (70 mg Q.D.) of R-METH (Figure 1B and Table 4). Nevertheless, the predictions of those were border-line acceptable with the corresponding pred./obs. of 1.26 and 0.75, respectively. Then, METH exposure in pregnant women was predicted based on the study design described [2]. In this study, the disposition of the racemic METH was studied in nine pregnant subjects who had been on METH maintenance therapy. R-METH and S-METH plasma concentrations following an average dose of 30 mg Q.D. of the racemic METH were predicted respectively, and the summed concentrations of each enantiomer were compared with the observed data (Figure 2 and Table 5). The model predicted mean AUCR (PP:T_2) of 1.9, mean C_{max} ratio (PP:T_2) of 1.8 and mean C_{min} ratio (PP:T_2) of 2.1, compared to observed mean ratios 2.0, 2.0 and 2.6, respectively. The model predicted mean AUCR (PP:T_3) of 2.1, mean C_{max} ratio (PP:T_3) of 2.0 and mean C_{min} ratio (PP:T_3) of 2.4, compared to observed mean ratios 1.7, 1.7 and 1.8, respectively. PBPK model successfully predicted racemic methadone PK during T_2, i.e. pred/obs of mean AUC, C_{max} and C_{min} in the range of 0.80-1.11 (Table 5). T_3 AUC and C_{min} were slightly under-predicted, with pred./obs. of 0.79 and 0.73, respectively. R-METH and S-METH plasma unbound fraction was predicted to increase by 23% and 25% during T_2, and 27% and 29% during T_3 vs. postpartum, as a result of reduced plasma level of AAG, the major binding protein. The reported pregnancy effect on racemic METH plasma unbound fraction was not significant, although there was a trend towards increased unbound fraction by 19-31% during pregnancy vs. postpartum. The predicted R-METH and S-METH CL_r was 1.7-fold and 1.8-fold higher

during T_3 vs. PP, as a result of increased GFR and plasma unbound fraction, comparable to the reported value of 2-fold of the racemate.

Phenytoin (PHT) prediction to inform CYP2C9 induction during pregnancy

The PHT model provided in Simcyp simulator was used without modification. The major 4-hydroxy metabolite was attributed to CYP2C9 ($f_{m,2C9}$=72%) and CYP2C19 ($f_{m,2C19}$=8%) mediated clearance, whereas the non 4-hydroxy ($f_{m,other}$=15-20%) clearance was unassigned. Furthermore, the model also accounted for saturable metabolism by CYP2C9 and 2C19, as well as auto-induction of CYP2C9 (see Table 2). To confirm *in vivo* $f_{m,2C9,}$ we predicted the effect of fluconazole inhibition (200 mg/day p.o. for 14 days) on PHT PK (250 mg/day p.o. for 4 days). The fluconazole model provided in Simcyp simulator was used without modification. The predicted PHT AUCR ($AUC_{inhibited}/AUC_{control}$) of 2.15 (data not shown) was comparable to the observed AUCR of 1.75 [48]. Furthermore, the mean AUC, C_{max}, C_{min} and $C_{pre\text{-}dose}$ of PHT (300 mg Q.D.) in non-pregnant subjects were quantitatively predicted by the PHT model (i.e., pred./obs. in the range of 0.83-1.02, Figure 3A and Table 6). In studies conducted in the pregnant subjects, PHT plasma trough concentration (i.e. $C_{pre\text{-}dose}$) is invariably used as a marker of CYP2C9 activity. Hence the change in PHT $C_{pre\text{-}dose}$ was used here to deconvolute the magnitude of increase CYP2C9 activity. In pregnant epileptic patients receiving a fixed PHT dose of 300mg daily, PHT $C_{pre\text{-}dose}$ is decreased by 43%, 51% and 61% during $T_{1,}$ T_2 and T_3, respectively[15, 16]. Through sensitivity analysis, CYP2C9 fold-induction was 1.4-, 1.5-, and 1.6-fold, during T_1, T_2 and T_3, respectively, to recover the reported changes in PHT $C_{pre\text{-}dose}$ (Figure 3B). The predicted PHT plasma unbound fraction was 15%, 26% and 30% during T_1, T_2 and T_3, compared to the reported values of 14%, 16-38% and 26-40%, respectively [16, 49].

Glyburide (GLB) PBPK model prediction incorporating OATP uptake

The constructed GLB model, accounting for metabolism by CYP3A, CYP2C9 and 2C19, as well as hepatic OATP-mediated uptake, was verified against the disposition kinetics following the administration of a single oral dose of 1.75-5 mg to non-pregnant healthy volunteers. Model-predicted $AUC_{0\text{-inf}}$, C_{max} and $C_{min,\ 12h}$ all met verification criterion, with pred./obs. in the range of 0.87-1.25 (Fig. 4A and Table 7). $C_{min,\ 24h}$ of GLB (5 mg p.o.) was under-predicted, with pred./obs. of 0.21. Following RIF treatment (600 mg i.v. over 30 min), the predicted GLB (1.25 mg p.o.) plasma AUCR and C_{max} Ratio were 1.88 and 1.47, respectively, compared to the observed ratios of 2.2 ± 0.51 and 1.8 ± 0.28, respectively[35] (Supplemental Fig. 2A). RIF plasma concentration-time profile is also in reasonable agreement with the observed data [50] (Supplemental Fig. 2B).

GLB plasma concentration-time profile following a fixed dose of 1 mg Q.D. in pregnant women was predicted based on the study design described [5]. In this study, the steady-state GLB disposition was evaluated in gestational diabetic subjects (n=40) during T_3 and compared with non-pregnant type 2 diabetic subjects (n=26). Predicted mean GLB AUCR (PP:T_3), C_{max} ratio (PP:T_3) and C_{min} ratio (PP:T_3) were 2.6, 2.2 and 7.0, compared to the observed value of 2.1, 2.2 and 3.2. Model-predicted $AUC_{0\text{-tau}}$ and C_{max} during T_3 and postpartum met verification criterion, with pred./obs. in the range of 0.87-1.05 (Fig. 4B and Table 7). $C_{min,\ 12h}$ of GLB during T_3 and postpartum was under-predicted, with pred./obs. of 0.23 and 0.49, respectively. The GLB plasma unbound fraction was predicted to increase from 1.5% to 2.1% during T_3. In comparison, the reported GLB plasma unbound fraction in gestational diabetic subjects during T_3 subjects (=1.6 ± 0.1%) is not different from that of the non-pregnant type 2 diabetic subjects (=1.5 ± 0.1%).

Discussion

Many studies in literature have utilized model (probe) drugs that report CYP enzyme activities to delineate the magnitude of change in activity of major CYP enzymes, mostly during the third trimester (e.g. caffeine for CYP1A2, metoprolol for CYP2D6, midazolam for CYP3A, phenytoin for CYP2C9) [51]. However, for hepatic CYP2B6 enzyme, such a probe drug study (e.g. bupropion) to delineate *in vivo* CYP2B6 activity during pregnancy has not been reported. Therefore, we utilized a bottom-up approach based on mechanistic studies (i.e. IVIVE). Based on gradually rising concentration of estradiol in plasma, we predicted that hepatic CYP2B6 induction during pregnancy increased gradually and peaked during T_3 at 1.9-fold of the PP value. It is noteworthy that estradiol concentrations vary considerably between individuals during pregnancy [52], and, as such, the magnitude of CYP2B6 induction could vary between women during pregnancy. For example, at the highest reported estradiol plasma concentration of ~140nM, the predicted fold-induction of CYP2B6 is 3.1-fold. We then confirmed the predicted magnitude of CYP2B6 induction *in vivo* by predicting METH disposition during pregnancy. To do so, respective METH PBPK model accounting for stereo-selective disposition of R-METH and S-METH was constructed and verified against observed PK data following single or multiple p.o. dosing of the racemate to the non-pregnant population. The PBPK model accounting for CYP2B6 induction, as well as known pregnancy effect on other clearance pathways including CYP3A, CYP2C19, and CL_r, successfully predicted METH disposition during T_2 as compared to the observed data [2]. Model prediction of METH disposition during T_3 was less robust yet border-line acceptable. We suspect this is due to that the reported mean T_2 CL_{ORAL} is 21% higher than mean T_3 CL_{ORAL}. This observed trend *in vivo* in METH CL_{ORAL} during T_2 vs. T_3, although not statistically significant, is opposite to what we predicted based on IVIVE approach.

Other clinical studies conducted in pregnant subjects on METH maintenance therapy showed a similar or greater magnitude of increment in METH CL_{ORAL} during pregnancy vs. postpartum (2.9- 3.6 fold) [53], or vs. historical controls (~1.6 fold) [54]. However because plasma concentration-time profiles were not reported in those studies, and limited sample size, these data were not used for model verification. One limitation of our study is that because METH CL_{ORAL} reports the change in multiple clearance pathways, it might not be a sensitive reporter of CYP2B6 activity. As suspected, sensitivity analysis showed CYP2B6 fold-induction in the range of 1.0-3.0 fold and 1.0-2.0 fold during T_2 and T_3, respectively, could recover the observed plasma AUC of METH during pregnancy (i.e. pred/obs within 0.80-1.25). These results also indicate that IVIVE based on CYP2B6 activity data, which predicted a smaller induction potential vs. that of mRNA data, could also recover the observed pregnancy effect on METH disposition. Future studies with probe drug bupropion during various stages of pregnancy and postpartum are highly desirable to further confirm the *in vivo* fold-induction of CYP2B6 predicted from *in vitro* data. Nevertheless, the above successful prediction of METH disposition during pregnancy shows for the first time that quantitative PK predictions of drugs cleared by multiple CYP enzymes is possible, through a PBPK model that integrates physiological changes in system dependent parameters such as CYP activity.

CYP2B6 is also an important clearance pathway for HIV drug efavirenz. *In vitro*, CYP2B6 has been identified as the main isoform metabolizing efavirenz, with smaller contributions from CYP2A6, CYP3A and UGT2B7. *In vivo*, CYP2B6 genetic variations are one of the main sources of efavirenz PK variability [55]. Interestingly, the AUC and C_{max} of efavirenz did not differ during pregnancy and postpartum in Thai population, and only $C_{min,24h}$ was lower during

the T_3 [56]. A possible explanation for the lack of pregnancy effect on efavirenz PK, at least in the Thai population, could be that the PK variability introduced by CYP2B6 genotype reduced the power of the study to detect the pregnancy effect. Auto-induction of CYP2B6 and CYP3A4 is another potential explanation. For CYP3A4, *in vitro* and *in vivo* data supports an inverse correlation between the baseline enzyme activity and the fold induction of enzyme activity, that is, the magnitude of induction depends on the baseline enzyme activity [47]. If the same holds true for CYP2B6, for an individual with high 2B6 activity pre-pregnancy (due to auto-induction), pregnancy-related increase in CYP2B6 activity may be smaller.

Estradiol (~157 nM) enhanced activities of CYP2C9 (diclofenac 4'-hydroxylation) by 1.3-2.0 fold in human hepatocytes, a magnitude comparable to that by known inducers of CYP2C9 such as phenobarbital [30]. Estradiol (100 nM) was shown to down-regulate CYP2C19 mRNA expression by ~ 30% in human hepatocytes via activation of ER [57]. These mechanistic studies provide a potential explanation for the mechanisms by which CYP2C9 is increased and CYP2C19 activity is decreased during pregnancy. However, a concentration-dependent induction or suppression relationship (i.e. EC_{50} and E_{max}) has not been established for these CYP isoforms, therefore IVIVE of the magnitude of CYP2C9 and 2C19 induction or suppression in each trimester is not possible.

To model the PK changes of CYP2C9 substrate drug GLB during pregnancy, we used probe drug PHT as the model training drug. PHT PK is complicated by two balancing factors: saturable metabolism by CYP2C9 and CYP2C19 reducing its metabolic clearance at higher concentration, and auto-induction of CYP2C9 increasing its metabolic clearance at higher

concentration. The established PHT drug model accounting for these mechanisms quantitatively predicted PHT PK, including $C_{pre\text{-}dose}$, following chronic dosing in the non-pregnant population. Numerous studies have assessed PHT $C_{pre\text{-}dose}$ in epileptic patients during pregnancy [15, 16, 49]. Although the overall trend of the change in PHT $C_{pre\text{-}dose}$ during each trimester was consistent across various studies, the exact magnitude differed. For example, Yerby et al. reported that the drop in PHT total and free concentration was 37%, 49%, 49% and 32%, 41% ,38%, respectively, during T_1, T_2 and T_3 [49]. PHT dose used during pregnancy was increased (453 mg/day) compared to postpartum (333 mg/day). We selected Tomson et al's study as the model training set because of its superior study design: a large sample size (n=29), fixed PHT dose, monotherapy, and trough sampling. Interestingly, following the same fixed dose of 300 mg/day, PHT mean $C_{pre\text{-}dose}$ during postpartum period (10.27±5.25 µg/L) reported in this study is 41% higher than the reported mean $C_{pre\text{-}dose}$ in the non-pregnant, healthy population (~7.3 µg/L, n=31) [58-60]. The difference in $C_{pre\text{-}dose}$ between epileptic patients and healthy subjects may be reflective of disease-related factors on PHT disposition. As a result of this difference, the PHT model quantitatively predicted $C_{pre\text{-}dose}$ in the non-pregnant healthy population (Table 6), but under-predicted $C_{pre\text{-}dose}$ in the pregnant epileptic patients (data not shown). However, it is expected that at steady-state, CYP2C9 activity change is proportional to the percent change in PHT $C_{pre\text{-}dose}$. Therefore, the difference in the absolute value of baseline $C_{pre\text{-}dose}$ (pred. vs. obs.) should not affect the capacity of the model to recover the change in CYP2C9 activity. The modest induction of CYP2C9 recovered from *in vivo* data is also comparable to the magnitude observed in *in vitro* studies, of 1.3-2.0 fold in human hepatocytes [30].

The commonly used proton pump inhibitors including omeprazole, lansoprazole and pantoprazole, are primarily metabolized by CYP2C19. The effect of pregnancy on the PK of these drugs has not been studied. Pregnancy-induced suppression of CYP2C19 activity was deconvoluted from the magnitude of decrease in CL_{ORAL} of proguanil after accounting for other pregnancy related components of proguanil CL_{ORAL} (see Methods). One caveat of this approach, however, is that renal clearance is a significant clearance pathway of proguanil, especially during pregnancy when CYP2C19 activity is suppressed. The pregnancy effect on CL_r of proguanil is unknown, therefore we assumed that only the filtration clearance (~10% of renal clearance) was increased during pregnancy. To definitively assess the magnitude of CYP2C19 induction during pregnancy, we propose that a PK study with the 2C19 probe omeprazole be conducted during various stages of pregnancy and postpartum in the future.

GLB has long been considered as primarily metabolized by CYP2C9. Pharmacogenetic studies appear to support this and suggest that *in vivo* CYP2C9 contributes significantly (up to 63%) to GLB metabolism, based on limited number of subjects with reduced catalytic activity of CYP2C9 [39]. However, recent *in vitro* studies [36, 42], including from our laboratory [37], suggest that CYP3A is the major isoform metabolizing GLB, contributing ~50% to GLB metabolism, followed by ~30% contribution from CYP2C9 and ~20% contribution from CYP2C19. The constructed GLB model, accounting for metabolism by these multiple CYPs, also incorporated hepatic OATP-mediated uptake in order to explain a significant DDI caused by rifampin treatment. Hepatic OATP-mediated uptake of the drug into hepatocytes is not likely to be the sole rate-limiting step of drug clearance from the body, since GLB IV clearance of 4.4 L/hr [61] can be well-estimated by metabolic clearance. Consistent with this speculation, the

estimated mean GLB sinusoidal uptake clearance of 572 L/hr (Supplemental Fig. 2C) is greater than the hepatic intrinsic metabolic clearance of 252.9 L/hr (see footnotes to Table 3). Following RIF treatment (600 mg i.v. over 30 min), GLB plasma AUCR and C_{max} ratio were well predicted by the constructed PBPK model. It is not known whether pregnancy affects hepatic OATP expression or activity, therefore no change in OATP activity was assumed in the current model. However, we conducted a sensitivity analysis to assess the impact of hepatic OATP activity on GLB plasma AUC during T_3. The latter was shown to be sensitive to change in hepatic OATP activity, when no pregnancy-related CYP induction or suppression was assumed (Supplemental Fig. 2D). Therefore, we cannot rule out the possibility that hepatic OATP activity is affected during pregnancy. GLB plasma concentration-time profile following a fixed dose of 1 mg Q.D. in pregnant women was quantitatively predicted. Because C_{max} prediction met verification criterion, the under-prediction of GLB steady-state $C_{min, 12h}$ during T_3 and postpartum could possibly be due to inadequate prediction of tissue distribution (hence the $t_{1/2}$ of drugs) which could result in inadequate prediction of C_{min}. The absorption of GLB was assumed to follow first-order kinetics with a lag time. Under this assumption, the absorption phase of GLB plasma profile following single p.o. dose in non-pregnant subjects (Fig. 4A) was adequately described. However this was not the case in pregnant subjects following multiple doses (Fig. 4B). Other absorption models, such as an inverse Gaussian density function has been used to describe GLB absorption [5]. As to what factors contribute to the apparent non-linear absorption of GLB are not clear. Saturation of intestinal transporters such as P-glycoprotein and the breast cancer resistance protein are possible explanations because GLB has been identified as a substrate for both transporters [62]. However, when evaluating GLB C_{max} in the dose range from 0.875 mg-10 mg p.o. dose in literature (University of Washington DIDB,

http://www.druginteractioninfo.org/), we did not observe dose-dependent change in C_{max} with increasing dose. Similar to METH CL_{ORAL}, because GLB CL_{ORAL} reports the change in multiple clearance pathways, it will not be a sensitive reporter of CYP2C9 activity. CYP2C9 and CYP2C19 together contribute ~50% of GLB metabolic clearance. We performed a sensitivity analysis by simultaneously varying CYP2C9 activity in the range of 1.0-fold to 3.0-fold induction, and a reduction in CYP2C19 activity of 0% to 80%, respectively. Multiple combinations of CYP2C9 and 2C19 activity change, for example, 2.7-fold induction of CYP2C9 activity coupled with 80% reduction of CYP2C19 activity, could recover the observed plasma AUC of GLB during T_3 (i.e. pred/obs within 0.80-0.93). This highlights the importance of conducting PK studies in pregnant women with well-established probe drug, to definitively delineate the change in hepatic enzyme activity during pregnancy. Nevertheless, our successful prediction of GLB AUCR (PP:T_3) during pregnancy illustrates the utility of using a PBPK model, incorporating pregnancy-dependent changes in CYP activities, to predict the disposition of a drug cleared by multiple pathways.

Conclusions

In summary, we have shown for the first time that our PBPK model: 1) can quantitatively predict the disposition of drugs during pregnancy when they are cleared via multiple CYP pathways using prior knowledge of pregnancy effect on various clearance pathways; 2) extrapolates *in vitro* data on estradiol-mediated CYP2B6 induction to its *in vivo* effect on CYP2B6 substrate drug METH; 3) allows generalization beyond model drugs studied (e.g. phenytoin, proguanil) to other drugs with well-characterized ADME characteristics (e.g. GLB). Previously, we have shown that such extrapolation can also be made for CYP3A [12], 1A2 and 2D6-metabolized

drugs [13]. Nevertheless, the magnitude of *in vivo* induction of hepatic CYP2B6 and suppression of hepatic CYP2C19 activity in pregnant women needs to be confirmed. Since conducting PK studies in pregnant women is challenging, our expanded PBPK model provides a valuable tool to evaluate different dosing regimens of drugs cleared primarily by single or multiple CYP enzymes during pregnancy. While achieving equivalent drug (total or unbound) exposure in pregnant and non-pregnant women is often the primary focus of maternal pharmacotherapy, it is equally important to carefully evaluate fetal and neonatal safety, especially for drugs such as GLB that can cross the placenta. A comprehensive fetal model could be incorporated into this PBPK model in the future to predict fetal exposure to drugs. Using such systems pharmacology approach can potentially allow us to identify drugs whose maternal-fetal PK, and therefore their efficacy and toxicity for the mother and/or the fetus, are likely to be affected by pregnancy. Conducting the trial *in silico* before its execution *in viv*o can be helpful in optimizing design of "first in pregnancy" PK study including prioritizing study period (1^{st}, 2^{nd} or 3^{rd} trimester), sample size and dosage selection. The generated information or hypotheses can be rigorously tested, and the model can be further refined as data become available from such PK studies. Ultimately, the proposed approach may help support the design of rational dosing regimen for pregnant women and their offspring.

Acknowledgements

The authors acknowledge funding from FDA Office of Women's Health and visiting fellowship from SimCYP (A.B. Ke).

Conflict of interest

All authors have completed the Unified Competing Interest form at www.icmje.org/coi_disclosure.pdf (available on request from the corresponding author) and declare: ABK had support from Office of Women's Health, US Food and Drug Administration for the submitted work; JDU was a member of the scientific advisory committee with Simcyp (now part of Certara) in the previous 3 years; no other relationships or activities that could appear to have influenced the submitted work.

List of Tables

Table 1: Summary of Methadone (MET) drug-dependent parameters

Parameter	Value	Methods/reference
Molecular Weight	309.4	a
Log $P_{o:w}$	3.93	b
pKa	9.2	a
B/P Ratio	0.75	c
$f_{u,p}$	R=0.16; S=0.12	d
F_a	0.88	e
k_a (h^{-1})	0.59	f
F_g	R=0.98; S=0.99	Predicted by Q_{gut} model [g]
T_{lag} (h)	0.295	f
V_{ss} (L/Kg)	R=6.2; S=4.7	Predicted [h]
CL_{IV} (L/h)	R=8.6; S=6.8	i
CL_r (L/h)	R=1.8; S=1.1	j
$CL_{int,u}$ (µL/min/ pmol)	R: $CL_{int,u,2B6}$=0.306 $CL_{int,u,3A}$=0.039 $CL_{int,u,2C19}$=0.078 S: $CL_{int,u,2B6}$=0.427 $CL_{int,u,3A}$=0.028 $CL_{int,u,2C19}$=0.078	k
f_m and f_e	R: $f_{m,2B6}$ =35.1%, $f_{m,3A}$ =36.6%, $f_{m,2C19}$ =7.3%, f_e =21%, S: $f_{m,2D6}$ =49.8%, $f_{m,3A}$ =26.7%, $f_{m,2C19}$ =7.5%, f_e =16%,	l,j

[a]: reported [63]

[b]: http://www.chemspider.com/Chemical-Structure.3953.html

[c]: reported value [27]

[d]: average value for R-methadone (R) and S-methadone (S) in literature [64, 65].

[e]: back-calculated from mean reported F_a*F_g (=0.78-0.79) [26] and predicted F_g (=0.98-0.99). Reported mean F is 0.82 (range 0.41-0.99) [20, 26, 66]

[f]: mean reported values [21, 67]

[g]: Q_{gut} model is provided in Simcyp simulator. It retains the form of the "well-stirred" liver model, but the flow term (Q_{Gut}) is a hybrid of both permeability through the enterocyte membrane and villous blood flow [68].

[h]: predicted according to Rodgers & Rowland [69]. Reported V_{ss} following i.v. dosing is 5.9±1.4 (R-METH) and 3.4±0.9 (R-METH) [20], or 4.74 ±1.94 L/kg (racemic METH) [26].

[i]: reported [20].

[j]: urine pH has a significant effect on renal clearance. When urine pH is below 6, the contribution of renal clearance becomes significant, accounting for around 16-30% of total body clearance [27]. Average of literature values was used [20, 21, 28].

[k]: *In vitro* HLM or recombinant CYP data [19, 23] did not fully recover observed metabolic clearance. Therefore, $CL_{int,h,u}$ for CYP2B6, 3A and 2C19 were back-calculated from hepatic CL (=CL-CL_r), f_m for individual CYP (see below), and 'average' population values for liver weight and hepatic CYP enzyme abundance of 17, 137 and 14 pmol/mg protein for CYP2B6, 3A and 2C19, respectively.

[l]: The contribution from individual CYP to total metabolic clearance obtained *in vitro* is 43.4%, 45.3% and 9.1% (R-METH), and 69.2%, 37.1% and 10.4% (S-METH), for CYP2B6, 3A and 2C19, respectively [19]. *In vivo* f_m for individual CYP was calculated by taking the product of f_m (=1-f_e) and the percent contribution from individual CYP.

Table 2: Summary of Phenytoin (PHT) drug-dependent parameters

Parameter	Value
Molecular Weight	252.28
Log $P_{o:w}$	2.47
pKa	8.15
B/P Ratio	0.61
$f_{u,p}$	0.1
F_a	0.9
k_a (h^{-1})	0.53
F_g	1.0
V_{ss} (L/Kg)	0.573
CL_{IV} (L/h)	2.07
CL_r (L/h)	0.015
V_{max} (μL/min/pmol)	$V_{max,2C9}$=0.24 $V_{max,2C19}$=1.53
K_m (μM)	$K_{m,\ 2C9}$=4.1 $K_{m,2C19}$=36.8
$CL_{int,\ other}$ (μL/min/mg)	0.97
E_{max} (CYP2C9)	1.9
EC_{50} (μM)(CYP2C9)	15.3
f_m and f_e	$f_{m,2C9}$ =72% $f_{m,2C19}$=8% $f_{m,other}$=19% f_e=1%

Table 3: Summary of Glyburide (GLB) drug-dependent parameters

Parameter	Value	Methods/reference
Molecular Weight	494.0	a
Log $P_{o:w}$	4.79	b
pKa	5.3	c
B/P Ratio	0.55	Assumed [d]
$f_{u,p}$	0.015	e
F_a	0.84	a
k_a (h^{-1})	0.756	f
T_{lag} (h)	0.39-0.46	f
F_g	0.91	Predicted by Q_{gut} model
V_{ss} (L/Kg)	0.1	Predicted [g]
CL_{IV} (L/h)	4.4	h
CL_r (L/h)	0.001	i
$CL_{int,CYP}$ (µL/min/pmol)	$CL_{int,CYP3A4}$=0.238 $CL_{int,2C9}$=0.268 $CL_{int,CYP2C19}$=0.931	j
CL_{pd} (µL/min/10^6 cells)	24	Parameter Estimation[k]
$PS_{int, OATP2B1}$ (µL/min/10^6 cells)	43.5	Parameter Estimation[k]
f_m	$f_{m,3A}$=50%, $f_{m,2C9}$ =30%, $f_{m,2C19}$=20%,	l

[a]: reported [34]

[b]: http://www.drugbank.ca/drugs/DB01016

[c]: literature value [70]

[d]: there is no evidence in literature that glyburide partitions into erythrocytes. Therefore B/P was calculated from the equation: E:P=[B:P-(1-Hct)]/Hct, where E:P refers to erythrocyte partition coefficient and Hct refers to hematocrit value (mean value of 0.45 used).

[e]: average of reported value in literature [5, 71] .

[f]: optimized in the range of 0.39-0.46 h. The reported value is 0.46 h [72]

[g]: predicted V_{ss} according to Rodgers & Rowland is 0.61 L/Kg [69]. This value was further optimized by applying a global K_p scalar of 0.1, in order to match the reported V_{ss} of 0.077 ± 0.013 L/Kg following i.v. infusion [61].

[h]: reported value is 4.4 ± 0.56 L/h (n=8) [61].

[i]: reported value [35].

[j]: back-calculation from hepatic clearance, f_m for individual CYP (see below), and 'average' population values for liver weight and hepatic CYP enzyme abundance of 137, 73 and 14 pmol/mg protein for CYP3A, 2C9 and 2C19, respectively. Hepatic intrinsic metabolic clearance (= 252.9 L/hr) was predicted using in-vitro to in-vivo extrapolation. Briefly, in vitro $CL_{int,u}$ determined in HLM [42] was scaled by 'average' population values for liver weight and microsomal protein of 1618 g and 38.9 (mg/g liver), respectively. Alternatively, in vitro V_{max} and K_m determined in recombinant CYP enzyme system [36] was scaled by 'average' population values for liver weight and respective hepatic CYP enzyme abundance as described above. Both approaches yielded similar values and the mean hepatic intrinsic clearance was used.

[k]: hepatic bidirectional permeability clearance (CL_{pd}), and hepatic intrinsic uptake clearance by OATP (or the permeability surface area product, $PS_{int,OATP}$), were estimated simultaneously using mean glyburide plasma pharmacokinetic data reported in subjects taking a single oral dose of 1.75-5 mg glyburide.

[l]: the contribution from individual CYP obtained using HLM with selective chemical inhibitors is 53%, 28% and 19% for 3A, 2C9 and 2C19, respectively [36]. In another study, the contribution from CYP3A is approximately 50%, whereas 2C8 and 2C19 combined contribute 50% [37]. However, *in vivo* DDI studies using fluvastatin as the perpetrator (a 2C9 inhibitor) reported AUC % change of 23% [38]. In addition, 2.7-fold higher glyburide AUC in subjects with *CYP2C9*1/*3* and *CYP2C9*2/*3* vs. *CYP2C9*1/*1* was observed [39]. These evidences suggest that CYP2C9 plays a significant role in glyburide metabolism *in vivo*. Therefore, the *in vitro* contribution from individual CYP was adjusted accordingly, and 50%, 30% and 20% for 3A, 2C9 and 2C19, respectively, was assigned in the final model.

Table 4: Methadone PK Parameters in Non-pregnant Healthy Volunteers							
R-Methadone				**S-Methadone**			
$AUC_{0\text{-}inf}$ ng/mL*h	Obs.	Pred.	Pred./ Obs.	**$AUC_{0\text{-}inf}$ ng/mL*h**	Obs.	Pred.	Pred./ Obs.
9.9 mg [a]	512.0	463.0	0.90	**9.9 mg** [a]	639.0	591.7	0.93
C_{max} (ng/mL)				**C_{max} (ng/mL)**			
9.9 mg	13.0	15.8	1.22	**9.9 mg**	23.1	19.5	0.85
$C_{min,\ 96h}$ (ng/mL)				**$C_{min,\ 96h}$ (ng/mL)**			
9.9 mg	1.91	1.63	0.85	**9.9 mg**	1.73	2.08	1.21
$AUC_{0\text{-}tau,ss}$				**$AUC_{0\text{-}tau,ss}$**			
70 mg Q.D. [b]	3484	3777	1.08	**70 mg Q.D.** [b]	3797	4767	1.26
100 mg Q.D. [c]	5540	5305	0.96	**100 mg Q.D.** [c]	5730	6740	1.18
$C_{max,ss}$ (ng/mL)				**$C_{max,ss}$ (ng/mL)**			
70 mg Q.D.	251	217	0.86	**70 mg Q.D.**	303	299.1	0.99
100 mg Q.D.	322	299	0.93	**100 mg Q.D.**	366	402.6	1.10
$C_{min,\ ss}$ (ng/mL)				**$C_{min,\ ss}$ (ng/mL)**			
70 mg Q.D.	148.0	110.5	0.75	**70 mg Q.D.**	146.0	140.4	0.96
100 mg Q.D.	184.5	163.1	0.88	**100 mg Q.D.**	177.0	215.2	1.22

[a]: reported mean values in subjects receiving a single oral dose of 9.9 mg racemic methadone (n=12) [20]

[b]: reported mean values normalized to a 70 mg racemic methadone daily dose (n=18) [21].

[c]: reported mean values normalized to a 100 mg racemic methadone daily dose (n=16) [25].

Table 5: Methadone PK Parameters (30 mg q.d.) during T_3 and Postpartum			
$AUC_{0\text{-}tau}$ ng/mL*h	Obs. [a]	Pred.	Pred./Obs.
Pregnancy(T_2)	1607.7	1778.7	1.11
Pregnancy(T_3)	1953.1	1539.0	0.79
Postpartum(PP)	3225.8	3298.1	1.02
AUC_{PP}/AUC_{T2}	2.0	1.9	0.92
AUC_{PP}/AUC_{T3}	1.7	2.1	1.30
C_{max} (ng/mL)			
Pregnancy(T_2)	104.3	108.9	1.04
Pregnancy(T_3)	117.7	94.5	0.80
Postpartum(PP)	204.4	190.2	0.93
$C_{max,PP}/C_{max,T2}$	2.0	1.7	0.89
$C_{max,PP}/C_{max,T3}$	1.7	2.0	1.16
$C_{min,24h}$ (ng/mL)			
Pregnancy(T_2)	42.2	51.6	1.04
Pregnancy(T_3)	60.1	43.9	0.73
Postpartum(PP)	108.3	105.6	0.98
$C_{min,PP}/C_{max,T2}$	2.6	2.0	0.94
$C_{min,PP}/C_{max,T3}$	1.8	2.4	1.33

[a]: AUC was calculated based on reported mean CL_{ORAL} and mean dose of 30 mg (n=9) [2]
C_{max} and $C_{min,24h}$ were extracted from published dose-adjusted mean concentration-time profiles.

Table 6: Phenytoin (300 mg Q.D.) PK Parameters in Non-pregnant Subjects			
	Obs.[a]	Pred.	Pred./ Obs.
$AUC_{0\text{-}tau,ss}$ (ng/mL*h)	207.6	201.6	0.97
$C_{max,ss}$ (ng/mL)	10.3	10.58	1.02
$C_{min,ss}$ (ng/mL)	7.58	6.27	0.83
$C_{pre\text{-}dose}$ (ng/mL)	7.25	6.31	0.87

[a]: arithmetic mean of reported values in non-pregnant, healthy subjects (n=31 total) receiving chronic administration of 300 mg/day [58-60]. $C_{min,ss}$ refers to the last plasma sample taken during the dosing interval and $C_{pre\text{-}dose}$ refers to the plasma trough concentration before the daily dose.

Table 7: Glyburide (p.o) PK Parameters in Non-pregnant Subjects			
1.75 mg [a]	Obs.	Pred.	Pred./ Obs.
$AUC_{0\text{-}inf}$ (ng/mL*h)	273.9	281.0	1.03
C_{max} (ng/mL)	85.8	75.0	0.87
$C_{min,12h}$ (ng/mL)	2.6	3.2	1.25
5 mg [b]			
$AUC_{0\text{-}inf}$ (ng/mL*h)	809	800.8	0.99
C_{max} (ng/mL)	109	104.8	0.96
$C_{min,\ 24h}$ (ng/mL)	5.02	1.03	0.21
Glyburide PK Parameters (1 mg b.i.d.) during T_3 and Postpartum			
$AUC_{0\text{-}tau}$ ng/mL*h	Obs. [c]	Pred.	Pred./Obs.
Pregnancy(T_3)	72	62.4	0.87
Postpartum(PP)	153	161.1	1.05
AUC_{PP}/AUC_{T3}	2.1	2.6	1.21
C_{max} (ng/mL)			
Pregnancy(T_3)	15	14.2	0.95
Postpartum(PP)	33	30.8	0.93
$C_{max,PP}/C_{max,T3}$	2.2	2.2	0.99
$C_{min,24h}$ (ng/mL)			
Pregnancy(T_3)	1.82	0.41	0.23
Postpartum(PP)	5.85	2.87	0.49
$C_{min,PP}/C_{max,T3}$	3.2	7.0	2.17

[a]: reported mean values in non-pregnant, healthy subjects with *CYP2C9*1/*1 or *1/*2* genotype (n=18 total) [39, 73]

[b]: reported mean values (n=24). The genotype of the subjects is unknown [74]

[c]: reported mean values normalized to a 1 mg b.i.d. in gestational diabetic subjects during 3rd trimester (n=40) and non-pregnant type 2 diabetic subjects (n=26) [5]. CYP2C9 genotype had no impact on GLB disposition in this study.

Legends to Figures

Figure 1. Predicted and observed plasma concentration-time profiles of methadone (METH) enantiomer R-METH and S-METH following the administration of single p.o. dose of 9.9 mg (A) and multiple p.o. dose of 70 mg/day (B) to non-pregnant subjects. The solid and dashed lines represent predicted mean R-METH and S-METH profile, respectively. Mean observed data are overlaid (●: R-METH profile; ○: S-METH profile) [20, 21]. Error bars represent standard deviations.

Figure 2. Predicted and observed plasma concentration-time profiles of racemic methadone (METH) in pregnant subjects on METH maintenance therapy of 30 mg/day. A) The solid and dashed lines represent predicted mean METH profile during postpartum (PP) and during 2nd trimester (T_2), respectively. B) The solid and dashed lines represent predicted mean METH profile during postpartum and during 3rd trimester (T_3), respectively. Mean observed data are overlaid (●: postpartum profile; ○: T_2 or T_3 profile)[2]. Error bars represent standard deviations.

Figure 3 Predicted and observed phenytoin (PHT) plasma concentration following multiple p.o. dose of 300 mg/day. A) Predicted (solid line) and observed (symbols) [58, 60, 75] PHT plasma concentration-time profiles following chronic dosing of 300 mg/day (p.o.) in non-pregnant healthy subjects. B) The grey bars represent predicted percent decrease in PHT trough concentration ($C_{pre\text{-}dose}$), and the white bars represent observed mean percent decrease in PHT $C_{pre\text{-}dose}$ in pregnant women during pregnancy (T_1, T_2 and T_3) vs. postpartum [16].

Figure 4. A) Predicted and observed plasma concentration-time profiles of glyburide (GLB) after administration of a single oral dose of 1.75-5 mg to non-pregnant subjects. The black and grey solid lines represent predicted mean profile in subjects receiving 1.75 mg and 5 mg, respectively. Mean observed data after the administration of 1.75 mg GLB (● and ○) [39, 73] and 5 mg GLB (♦) [74] are overlaid. B) Predicted and observed plasma concentration-time profiles of glyburide (GLB) following chronic dosing of 1 mg/day (p.o.) during 3rd trimester (T_3) and postpartum. The solid and dashed lines represent predicted mean GLB profile during postpartum and during T_3, respectively. Mean observed data [5] are overlaid (●: non-pregnant type 2 diabetic subjects profile or T2DM; ○: gestational diabetic subjects T_3 profile or GDM). Error bars represent standard deviations.

FIGURE 1

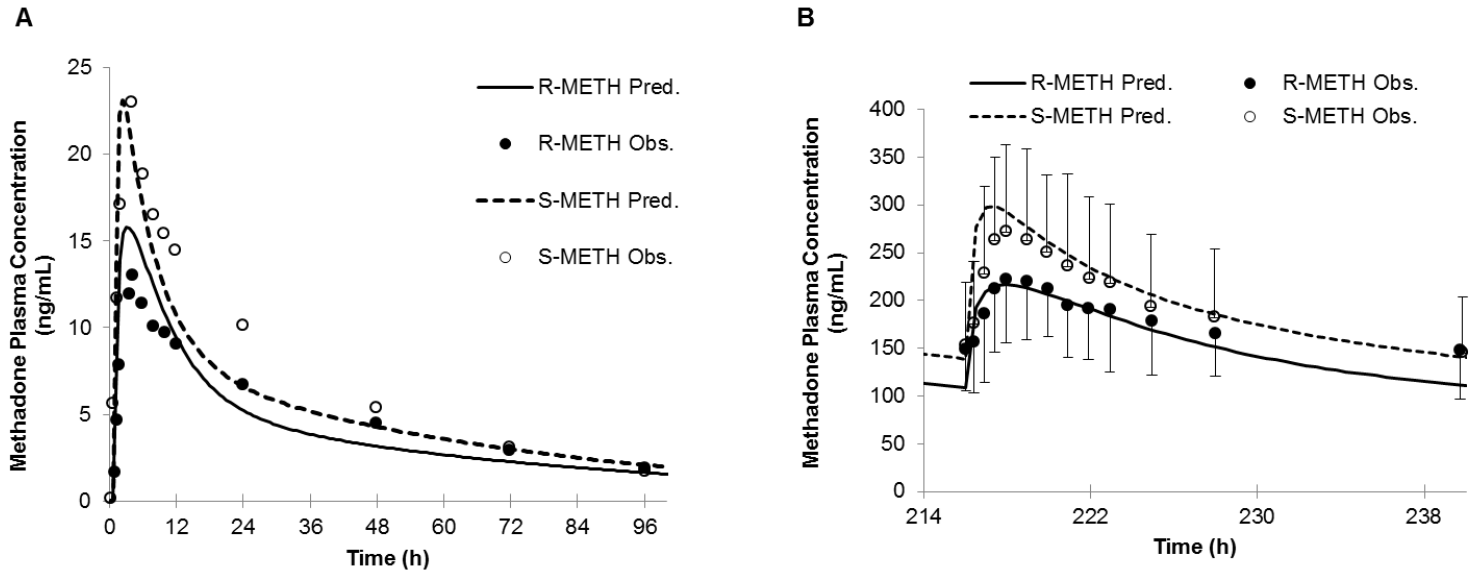
A
Methadone Plasma Concentration (ng/mL)
25
20
15
10
5
0
0
12
24
36
48
60
72
84
96
Time (h)
R-METH Pred.
R-METH Obs.
S-METH Pred.
S-METH Obs.
B
Methadone Plasma Concentration (ng/mL)
400
350
300
250
200
150
100
50
0
214
222
230
238
Time (h)
R-METH Pred.
R-METH Obs.
S-METH Pred.
S-METH Obs.

FIGURE 2

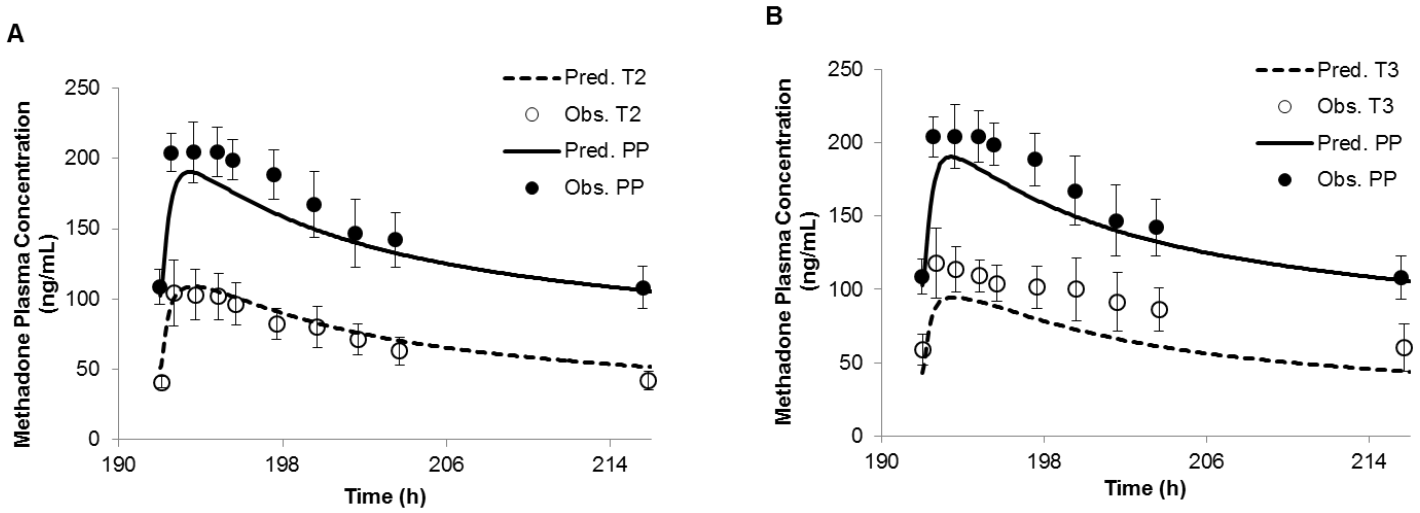
A
Methadone Plasma Concentration (ng/mL)
250
200
150
100
50
0
190
198
206
214
Time (h)
Pred. T2
Obs. T2
Pred. PP
Obs. PP
B
Methadone Plasma Concentration (ng/mL)
250
200
150
100
50
0
190
198
206
214
Time (h)
Pred. T3
Obs. T3
Pred. PP
Obs. PP

FIGURE 3

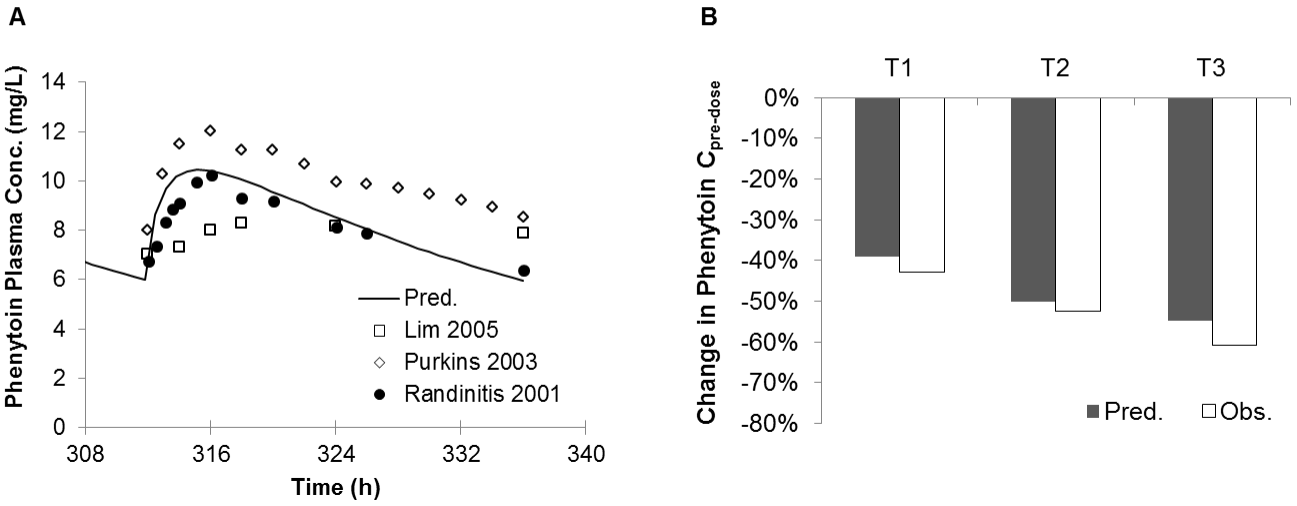
A
Phenytoin Plasma Conc. (mg/L)
14
12
10
8
6
4
2
0
308
316
324
332
340
Time (h)
Pred.
Lim 2005
Purkins 2003
Randinitis 2001
B
Change in Phenytoin Cpre-dose
T1
T2
T3
0%
-10%
-20%
-30%
-40%
-50%
-60%
-70%
-80%
Pred.
Obs.

FIGURE 4

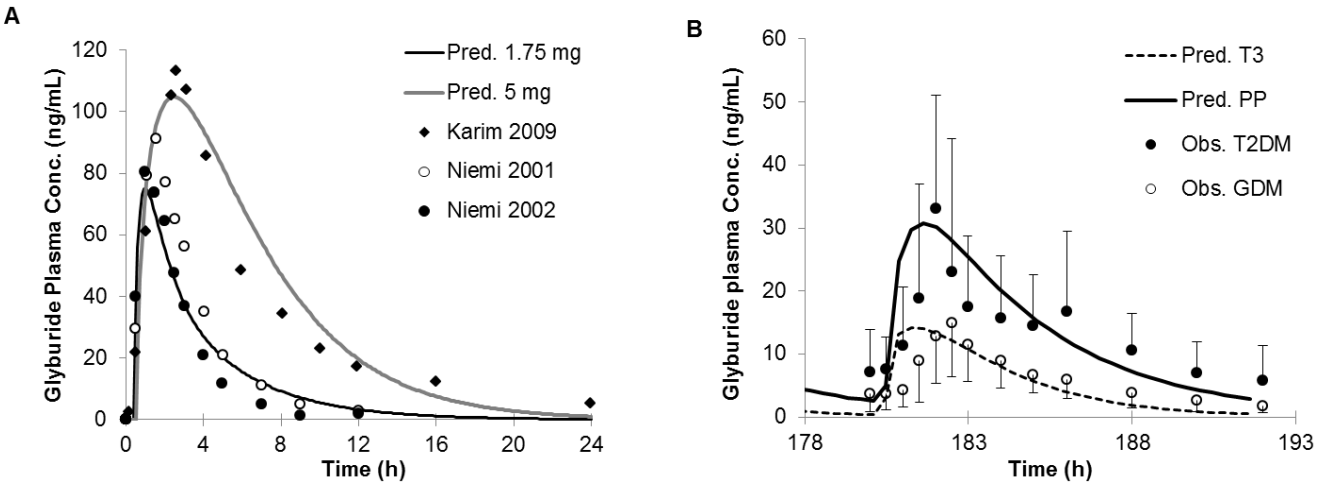
A
Glyburide Plasma Conc. (ng/mL)
Time (h)
Pred. 1.75 mg
Pred. 5 mg
Karim 2009
Niemi 2001
Niemi 2002
B
Glyburide plasma Conc. (ng/mL)
Time (h)
Pred. T3
Pred. PP
Obs. T2DM
Obs. GDM

REFERENCES

1. van Hasselt JG, Andrew MA, Hebert MF, Tarning J, Vicini P, Mattison DR. The Status of Pharmacometrics in Pregnancy: Highlights from the 3(rd) American Conference on Pharmacometrics. Br J Clin Pharmacol 2012.
2. Pond SM, Kreek MJ, Tong TG, Raghunath J, Benowitz NL. Altered methadone pharmacokinetics in methadone-maintained pregnant women. J Pharmacol Exp Ther 1985; 233: 1-6.
3. Shiran MR, Lennard MS, Iqbal MZ, Lagundoye O, Seivewright N, Tucker GT, Rostami-Hodjegan A. Pharmacokinetic-pharmacodynamic modeling of mood and withdrawal symptoms in relation to plasma concentrations of methadone in patients undergoing methadone maintenance treatment. J Clin Psychopharmacol; 32: 666-71.
4. Kirchheiner J, Brockmoller J, Meineke I, Bauer S, Rohde W, Meisel C, Roots I. Impact of CYP2C9 amino acid polymorphisms on glyburide kinetics and on the insulin and glucose response in healthy volunteers. Clin Pharmacol Ther 2002; 71: 286-96.
5. Hebert MF, Ma X, Naraharisetti SB, Krudys KM, Umans JG, Hankins GD, Caritis SN, Miodovnik M, Mattison DR, Unadkat JD, Kelly EJ, Blough D, Cobelli C, Ahmed MS, Snodgrass WR, Carr DB, Easterling TR, Vicini P. Are we optimizing gestational diabetes treatment with glyburide? The pharmacologic basis for better clinical practice. Clin Pharmacol Ther 2009; 85: 607-14.
6. Hodge LS, Tracy TS. Alterations in drug disposition during pregnancy: implications for drug therapy. Expert Opin Drug Metab Toxicol 2007; 3: 557-71.
7. Jeong H. Altered drug metabolism during pregnancy: hormonal regulation of drug-metabolizing enzymes. Expert Opin Drug Metab Toxicol 2010; 6: 689-99.
8. Rowland M, Peck C, Tucker G. Physiologically-based pharmacokinetics in drug development and regulatory science. Annu Rev Pharmacol Toxicol 2011; 51: 45-73.
9. Jamei M, Dickinson GL, Rostami-Hodjegan A. A framework for assessing inter-individual variability in pharmacokinetics using virtual human populations and integrating general knowledge of physical chemistry, biology, anatomy, physiology and genetics: A tale of 'bottom-up' vs 'top-down' recognition of covariates. Drug Metab Pharmacokinet 2009; 24: 53-75.
10. Lu G, Abduljalil K, Jamei M, Johnson TN, Rostami-Hodjegan A. A Pregnancy Physiologically-Based Pharmacokinetic (p-PBPK) Model for Disposition of Drugs Metabolized by CYP1A2, CYP3A4 and CYP2D6. British Journal of Clinical Pharmacology 2012; 74: 873-85.
11. Abduljalil K, Furness P, Johnson TN, Rostami-Hodjegan A, Soltani H. Anatomical, physiological and metabolic changes with gestational age during normal pregnancy: a database for parameters required in physiologically based pharmacokinetic modelling. Clin Pharmacokinet 2012; 51: 365-96.
12. Ke AB, Nallan SC, Zhao P, Rostami-Hodjegan A, Unadkat JD. A PBPK Model to Predict Disposition of CYP3A-metabolized Drugs in Pregnant Women: Verification and Discerning the Site of CYP3A Induction. *Clin Pharmacol Ther: Pharmacometrics & Systems Pharmacology* 2012; 1: http://www.nature.com/psp/journal/v1/n9/index.html
13. Ke AB, Nallan SC, Zhao P, Rostami-Hodjegan A, Isoherranen N, Unadkat JD. A PBPK Model to Predict Disposition of P450 2D6 and P450 1A2 Metabolized Drugs in Pregnant Women. *submitted*. Drug Metab Dispos 2012.
14. Cressey TR, Best BM, Achalapong J, Stek A, Wang J, Chotivanich N, Yuthavisuthi P, Suriyachai P, Prommas S, Shapiro DE, Watts DH, Smith E, Capparelli E, Kreitchmann R, Mirochnick M. Reduced indinavir exposure during pregnancy. Br J Clin Pharmacol 2013.
15. Tomson T, Lindbom U, Ekqvist B, Sundqvist A. Epilepsy and pregnancy: a prospective study of seizure control in relation to free and total plasma concentrations of carbamazepine and phenytoin. Epilepsia 1994; 35: 122-30.
16. Tomson T, Lindbom U, Ekqvist B, Sundqvist A. Disposition of carbamazepine and phenytoin in pregnancy. Epilepsia 1994; 35: 131-5.

17. McGready R, Stepniewska K, Edstein MD, Cho T, Gilveray G, Looareesuwan S, White NJ, Nosten F. The pharmacokinetics of atovaquone and proguanil in pregnant women with acute falciparum malaria. Eur J Clin Pharmacol 2003; 59: 545-52.
18. McGready R, Stepniewska K, Seaton E, Cho T, Cho D, Ginsberg A, Edstein MD, Ashley E, Looareesuwan S, White NJ, Nosten F. Pregnancy and use of oral contraceptives reduces the biotransformation of proguanil to cycloguanil. Eur J Clin Pharmacol 2003; 59: 553-7.
19. Totah RA, Sheffels P, Roberts T, Whittington D, Thummel K, Kharasch ED. Role of CYP2B6 in stereoselective human methadone metabolism. Anesthesiology 2008; 108: 363-74.
20. Kharasch ED, Hoffer C, Whittington D, Walker A, Bedynek PS. Methadone pharmacokinetics are independent of cytochrome P4503A (CYP3A) activity and gastrointestinal drug transport: insights from methadone interactions with ritonavir/indinavir. Anesthesiology 2009; 110: 660-72.
21. Foster DJ, Somogyi AA, Dyer KR, White JM, Bochner F. Steady-state pharmacokinetics of (R)- and (S)-methadone in methadone maintenance patients. Br J Clin Pharmacol 2000; 50: 427-40.
22. Eap CB, Buclin T, Baumann P. Interindividual variability of the clinical pharmacokinetics of methadone: implications for the treatment of opioid dependence. Clin Pharmacokinet 2002; 41: 1153-93.
23. Totah RA, Allen KE, Sheffels P, Whittington D, Kharasch ED. Enantiomeric metabolic interactions and stereoselective human methadone metabolism. J Pharmacol Exp Ther 2007; 321: 389-99.
24. Cao YJ, Smith PF, Wire MB, Lou Y, Lancaster CT, Causon RC, Bigelow GE, Martinez E, Fuchs EJ, Radebaugh C, McCabe S, Hendrix CW. Pharmacokinetics and pharmacodynamics of methadone enantiomers after coadministration with fosamprenavir-ritonavir in opioid-dependent subjects. Pharmacotherapy 2008; 28: 863-74.
25. Liu P, Foster G, Labadie R, Somoza E, Sharma A. Pharmacokinetic interaction between voriconazole and methadone at steady state in patients on methadone therapy. Antimicrob Agents Chemother 2007; 51: 110-8.
26. Kharasch ED, Hoffer C, Whittington D, Sheffels P. Role of hepatic and intestinal cytochrome P450 3A and 2B6 in the metabolism, disposition, and miotic effects of methadone. Clin Pharmacol Ther 2004; 76: 250-69.
27. Garrido MJ, Troconiz IF. Methadone: a review of its pharmacokinetic/pharmacodynamic properties. J Pharmacol Toxicol Methods 1999; 42: 61-6.
28. Boulton DW, Arnaud P, DeVane CL. Pharmacokinetics and pharmacodynamics of methadone enantiomers after a single oral dose of racemate. Clin Pharmacol Ther 2001; 70: 48-57.
29. Dickmann LJ, Isoherranen N. Quantitative Prediction of CYP2B6 Induction by Estradiol During Pregnancy, Potential Explanation for Increased Methadone Clearance during Pregnancy. Drug Metab Dispos 2012.
30. Choi SY, Koh KH, Jeong H. Isoform-specific Regulation of Cytochromes P450 Expression by Estradiol and Progesterone. Drug Metab Dispos 2012.
31. Kirby BJ, Collier AC, Kharasch ED, Whittington D, Thummel KE, Unadkat JD. Complex Drug Interactions of the HIV Protease Inhibitors 3: Effect of Simultaneous or Staggered Dosing of Digoxin and Ritonavir, Nelfinavir, Rifampin or Bupropion. Drug Metab Dispos 2012.
32. Ketter TA, Jenkins JB, Schroeder DH, Pazzaglia PJ, Marangell LB, George MS, Callahan AM, Hinton ML, Chao J, Post RM. Carbamazepine but not valproate induces bupropion metabolism. J Clin Psychopharmacol 1995; 15: 327-33.
33. Product label for **Activella** ® (estradiol/norethindrone acetate) tablets. http://www.accessdata.fda.gov/drugsatfda_docs/label/2006/022001lbl.pdf.
34. GLIMEL® (glibenclamide) Tablets Product Label. http://www.pbs.gov.au/meds%2Fpi%2Fafpglime10808.pdf.
35. Zheng HX, Huang Y, Frassetto LA, Benet LZ. Elucidating rifampin's inducing and inhibiting effects on glyburide pharmacokinetics and blood glucose in healthy volunteers: unmasking the differential effects of enzyme induction and transporter inhibition for a drug and its primary metabolite. Clin Pharmacol Ther 2009; 85: 78-85.

36. Zharikova OL, Fokina VM, Nanovskaya TN, Hill RA, Mattison DR, Hankins GD, Ahmed MS. Identification of the major human hepatic and placental enzymes responsible for the biotransformation of glyburide. Biochem Pharmacol 2009; 78: 1483-90.
37. Zhou L, Naraharisetti SB, Liu L, Wang H, Lin YS, Isoherranen N, Unadkat JD, Hebert MF, Mao Q. Contributions of human cytochrome P450 enzymes to glyburide metabolism. Biopharm Drug Dispos 2010; 31: 228-42.
38. Appel S, Rufenacht T, Kalafsky G, Tetzloff W, Kallay Z, Hitzenberger G, Kutz K. Lack of interaction between fluvastatin and oral hypoglycemic agents in healthy subjects and in patients with non-insulin-dependent diabetes mellitus. Am J Cardiol 1995; 76: 29A-32A.
39. Niemi M, Cascorbi I, Timm R, Kroemer HK, Neuvonen PJ, Kivisto KT. Glyburide and glimepiride pharmacokinetics in subjects with different CYP2C9 genotypes. Clin Pharmacol Ther 2002; 72: 326-32.
40. Satoh H, Yamashita F, Tsujimoto M, Murakami H, Koyabu N, Ohtani H, Sawada Y. Citrus juices inhibit the function of human organic anion-transporting polypeptide OATP-B. Drug Metab Dispos 2005; 33: 518-23.
41. Hirano M, Maeda K, Shitara Y, Sugiyama Y. Drug-drug interaction between pitavastatin and various drugs via OATP1B1. Drug Metab Dispos 2006; 34: 1229-36.
42. Naritomi Y, Terashita S, Kagayama A. Identification and relative contributions of human cytochrome P450 isoforms involved in the metabolism of glibenclamide and lansoprazole: evaluation of an approach based on the in vitro substrate disappearance rate. Xenobiotica 2004; 34: 415-27.
43. Varma MV, Lai Y, Feng B, Litchfield J, Goosen TC, Bergman A. Physiologically based modeling of pravastatin transporter-mediated hepatobiliary disposition and drug-drug interactions. Pharm Res 2012; 29: 2860-73.
44. Funck-Brentano C, Becquemont L, Lenevu A, Roux A, Jaillon P, Beaune P. Inhibition by omeprazole of proguanil metabolism: mechanism of the interaction in vitro and prediction of in vivo results from the in vitro experiments. J Pharmacol Exp Ther 1997; 280: 730-8.
45. Product label for MALARONE ® (250 mg Atovaquone + 100 mg Proguanil Hydrochloride) Tablets. http://www.gsk.ca/english/docs-pdf/Malarone_PM_EN_20071102.pdf.
46. Wattanagoon Y, Taylor RB, Moody RR, Ochekpe NA, Looareesuwan S, White NJ. Single dose pharmacokinetics of proguanil and its metabolites in healthy subjects. Br J Clin Pharmacol 1987; 24: 775-80.
47. Almond LM, Yang J, Jamei M, Tucker GT, Rostami-Hodjegan A. Towards a quantitative framework for the prediction of DDIs arising from cytochrome P450 induction. Curr Drug Metab 2009; 10: 420-32.
48. Blum RA, Wilton JH, Hilligoss DM, Gardner MJ, Henry EB, Harrison NJ, Schentag JJ. Effect of fluconazole on the disposition of phenytoin. Clin Pharmacol Ther 1991; 49: 420-5.
49. Yerby MS, Friel PN, McCormick K, Koerner M, Van Allen M, Leavitt AM, Sells CJ, Yerby JA. Pharmacokinetics of anticonvulsants in pregnancy: alterations in plasma protein binding. Epilepsy Res 1990; 5: 223-8.
50. Lau YY, Huang Y, Frassetto L, Benet LZ. effect of OATP1B transporter inhibition on the pharmacokinetics of atorvastatin in healthy volunteers. Clin Pharmacol Ther 2007; 81: 194-204.
51. Anderson GD. Pregnancy-induced changes in pharmacokinetics: a mechanistic-based approach. Clin Pharmacokinet 2005; 44: 989-1008.
52. O'Leary P, Boyne P, Flett P, Beilby J, James I. Longitudinal assessment of changes in reproductive hormones during normal pregnancy. Clin Chem 1991; 37: 667-72.
53. Wolff K, Boys A, Rostami-Hodjegan A, Hay A, Raistrick D. Changes to methadone clearance during pregnancy. Eur J Clin Pharmacol 2005; 61: 763-8.
54. Jarvis MA, Wu-Pong S, Kniseley JS, Schnoll SH. Alterations in methadone metabolism during late pregnancy. J Addict Dis 1999; 18: 51-61.

55. Siccardi M, Almond L, Schipani A, Csajka C, Marzolini C, Wyen C, Brockmeyer NH, Boffito M, Owen A, Back D. Pharmacokinetic and pharmacodynamic analysis of efavirenz dose reduction using an in vitro-in vivo extrapolation model. Clin Pharmacol Ther 2012; 92: 494-502.
56. Cressey TR, Stek A, Capparelli E, Bowonwatanuwong C, Prommas S, Sirivatanapa P, Yuthavisuthi P, Neungton C, Huo Y, Smith E, Best BM, Mirochnick M. Efavirenz pharmacokinetics during the third trimester of pregnancy and postpartum. J Acquir Immune Defic Syndr 2012; 59: 245-52.
57. Mwinyi J, Cavaco I, Pedersen RS, Persson A, Burkhardt S, Mkrtchian S, Ingelman-Sundberg M. Regulation of CYP2C19 expression by estrogen receptor alpha: implications for estrogen-dependent inhibition of drug metabolism. Mol Pharmacol 2010; 78: 886-94.
58. Lim ML, Min SS, Eron JJ, Bertz RJ, Robinson M, Gaedigk A, Kashuba AD. Coadministration of lopinavir/ritonavir and phenytoin results in two-way drug interaction through cytochrome P-450 induction. J Acquir Immune Defic Syndr 2004; 36: 1034-40.
59. Randinitis EJ, Alvey CW, Koup JR, Rausch G, Abel R, Bron NJ, Hounslow NJ, Vassos AB, Sedman AJ. Drug interactions with clinafloxacin. Antimicrob Agents Chemother 2001; 45: 2543-52.
60. Purkins L, Wood N, Ghahramani P, Love ER, Eve MD, Fielding A. Coadministration of voriconazole and phenytoin: pharmacokinetic interaction, safety, and toleration. Br J Clin Pharmacol 2003; 56 Suppl 1: 37-44.
61. Rydberg T, Jonsson A, Melander A. Comparison of the kinetics of glyburide and its active metabolites in humans. J Clin Pharm Ther 1995; 20: 283-95.
62. Pollex EK, Anger G, Hutson J, Koren G, Piquette-Miller M. Breast cancer resistance protein (BCRP)-mediated glyburide transport: effect of the C421A/Q141K BCRP single-nucleotide polymorphism. Drug Metab Dispos; 38: 740-4.
63. DISKETS® (Methadone Hydrochloride) Tablets Product Label. http://www.accessdata.fda.gov/drugsatfda_docs/label/2008/017058s019lbl.pdf.
64. Eap CB, Cuendet C, Baumann P. Binding of d-methadone, l-methadone, and dl-methadone to proteins in plasma of healthy volunteers: role of the variants of alpha 1-acid glycoprotein. Clin Pharmacol Ther 1990; 47: 338-46.
65. Gerber JG, Rosenkranz S, Segal Y, Aberg J, D'Amico R, Mildvan D, Gulick R, Hughes V, Flexner C, Aweeka F, Hsu A, Gal J. Effect of ritonavir/saquinavir on stereoselective pharmacokinetics of methadone: results of AIDS Clinical Trials Group (ACTG) 401. J Acquir Immune Defic Syndr 2001; 27: 153-60.
66. Dale O, Sheffels P, Kharasch ED. Bioavailabilities of rectal and oral methadone in healthy subjects. Br J Clin Pharmacol 2004; 58: 156-62.
67. Wolff K, Rostami-Hodjegan A, Hay AW, Raistrick D, Tucker G. Population-based pharmacokinetic approach for methadone monitoring of opiate addicts: potential clinical utility. Addiction 2000; 95: 1771-83.
68. Yang J, Jamei M, Yeo KR, Tucker GT, Rostami-Hodjegan A. Prediction of intestinal first-pass drug metabolism. Curr Drug Metab 2007; 8: 676-84.
69. Rodgers T, Rowland M. Mechanistic approaches to volume of distribution predictions: understanding the processes. Pharm Res 2007; 24: 918-33.
70. Savolainen J, Jarvinen K, Taipale H, Jarho P, Loftsson T, Jarvinen T. Co-administration of a water-soluble polymer increases the usefulness of cyclodextrins in solid oral dosage forms. Pharm Res 1998; 15: 1696-701.
71. Obach RS, Lombardo F, Waters NJ. Trend analysis of a database of intravenous pharmacokinetic parameters in humans for 670 drug compounds. Drug Metab Dispos 2008; 36: 1385-405.
72. Rydberg T, Jonsson A, Karlsson MO, Melander A. Concentration-effect relations of glibenclamide and its active metabolites in man: modelling of pharmacokinetics and pharmacodynamics. Br J Clin Pharmacol 1997; 43: 373-81.
73. Niemi M, Backman JT, Neuvonen M, Neuvonen PJ, Kivisto KT. Effects of rifampin on the pharmacokinetics and pharmacodynamics of glyburide and glipizide. Clin Pharmacol Ther 2001; 69: 400-6.

74. Karim A, Laurent A, Munsaka M, Wann E, Fleck P, Mekki Q. Coadministration of pioglitazone or glyburide and alogliptin: pharmacokinetic drug interaction assessment in healthy participants. J Clin Pharmacol 2009; 49: 1210-9.
75. Randinitis EJ, Koup JR, Rausch G, Abel R, Bron NJ, Hounslow NJ, Vassos AB, Sedman AJ. Clinafloxacin pharmacokinetics in subjects with various degrees of renal function. Antimicrob Agents Chemother 2001; 45: 2536-42.

Supplemental Figure 1. Changes in glyburide AUC (1.75 mg p.o.) as a function of hepatic bidirectional permeability clearance (CL_{pd}), and hepatic intrinsic uptake clearance by OATP ($PS_{int,OATP}$). There are many combinations of $PS_{int,OATP}$ and CL_{pd} values that can result in AUC within the range of 0.46-0.73 ng*h/mL following 1.75 mg p.o., which is 80-125% of the mean AUC observed *in vivo* (0.58 ng*h/mL). Consequently, $PS_{int,OATP} > CL_{pd}$ ($PS_{int,OATP:}$ 50 µL/min/10^6 cells; $CL_{pd:}$ 30 µL/min/10^6 cells) were selected and used as initial estimates for data fitting.

Supplemental Figure 2. A) Predicted plasma concentration-time profiles of GLB after administration of a single oral dose of 1.25 mg to non-pregnant subjects, in the presence and absence of rifampin (RIF) treatment (600 mg i.v.) (control: solid line; RIF treatment: dashed line). B) Predicted (solid line) and observed (●) [50] plasma concentration-time profiles of rifampin (600 mg i.v. over 30-min infusion). C) Predicted time course of GLB hepatic sinusoidal uptake clearance in the presence and absence of RIF treatment (control: solid line; RIF treatment: dashed line). D) Change in GLB AUC (1 mg/day p.o.) during T_3 as a function of hepatic OATP activity. While hepatic OATP activity was increased up to 10-fold of the value used in the final GLB model, pregnancy-induced changes in CYP activities were ignored. The dashed line represents the mean observed value.

SUPPLE FIGURE 1

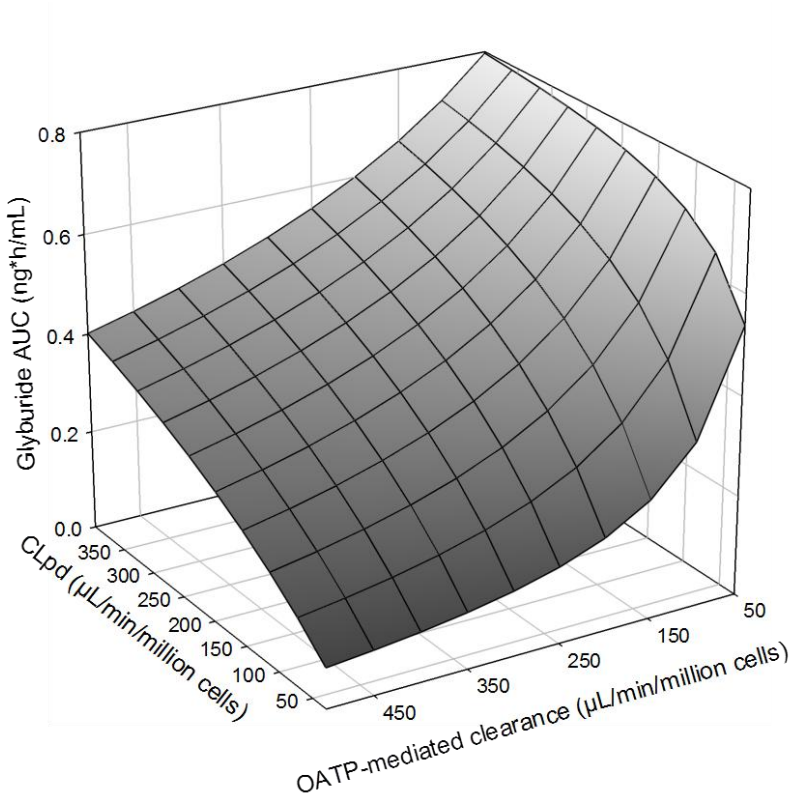

SUPPLE FIGURE 2

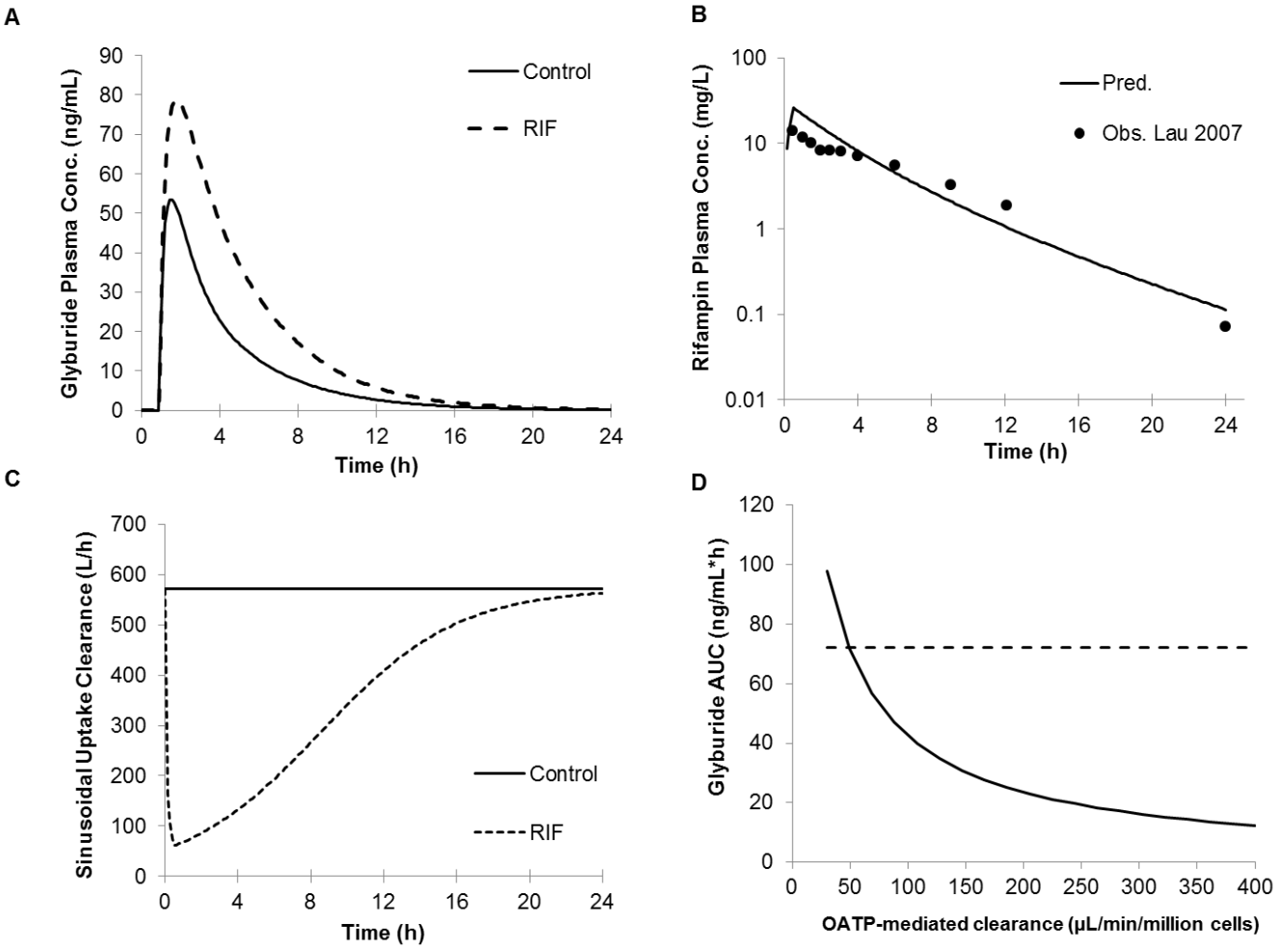

Chapter Four

Modeling the Cyclosporine A inhibition of Distribution of the P-glycoprotein PET ligand, [^{11}C]-Verapamil, into the Maternal Brain and Fetal Liver of the Pregnant Non-Human Primate: Impact of Tissue Blood Flow and Site of Inhibition

*This chapter has been accepted for publication in the journal titled "Journal of Nuclear Medicine", and is formatted according to the requirements of the journal.

Modeling the Cyclosporine A inhibition of Distribution of the P-glycoprotein PET ligand, [^{11}C]-Verapamil, into the Maternal Brain and Fetal Liver of the Pregnant Non-Human Primate: Impact of Tissue Blood Flow and Site of Inhibition

Short running title: Verapamil Transport across BBB and BPB

Alice Ban Ke[1], Sara Eyal[1*], Francisco S. Chung[1+], Jeanne M. Link[2], David A. Mankoff[2$], Mark Muzi [2] and Jashvant D. Unadkat[1]

[1]Department of Pharmaceutics, University of Washington, Seattle, Washington [2]Division of Nuclear Medicine, University of Washington, Seattle, Washington

Address correspondence to:

Dr. Jashvant D. Unadkat

Department of Pharmaceutics

University of Washington

Box 357610

Seattle, WA 98195

Telephone: 206-543-9434

Fax: 206-543-3204

E-mail: jash@u.washington.edu

First author:

Alice Ban Ke

Ph.D. candidate

Department of Pharmaceutics

University of Washington

Box 357610

Seattle, WA 98195

Telephone: 206-685-0902

E-mail: banke@uw.edu

(Abstract Word Count 301)

(Manuscript Text Word Count: 4836)

(Total Word Count 6998)

This study was supported by National Institute of Health grants U10HD047892 (OPRU network), P50HD044404, GM032165 and RR00166.

*Current affiliation: Institute of Drug Research, School of Pharmacy, The Hebrew University, Jerusalem, Israel

[+]Current affiliation: Department of Biochemistry and Molecular Biology, College of Medicine, University of the Philippines Manila, Philippines.

[$]Current affiliation: Division of Nuclear Medicine, Department of Radiology, University of Pennsylvania.

ABSTRACT

Through PET imaging, our laboratory has studied the dynamic biodistribution of [^{11}C]-verapamil, a P-gp substrate, in the pregnant non-human primate, *M. nemestrina*. To gain detailed insight into the kinetics of verapamil transport across the blood-brain barrier (BBB) and the blood-placenta barrier (BPB), we analyzed these dynamic biodistribution data by compartmental modeling.

Methods Thirteen pregnant macaques (gestational age, 71-159 d; term, 172 d) underwent PET imaging with [^{11}C]-verapamil before and during cyclosporine (CsA; a P-gp inhibitor) infusion (6, 12 or 24 mg/kg/h). Dynamic [^{11}C]-verapamil brain or fetal liver (reporter of placental P-gp function) activity were assessed by a one-tissue (1C) or two-tissue compartment (2C) model.

Results The 1C model best explained the observed brain and fetal liver distribution of [^{11}C]-radioactivity. When P-gp was completely inhibited, the brain and fetal liver distribution clearance (K_1) approximated tissue blood flow (Q), i.e. extraction ratio, ER = (K_1/Q) was ~1, indicating that in the absence of P-gp function, the distribution of [^{11}C]-verapamil radioactivity into these compartments is limited by blood-flow. The potency of CsA to inhibit P-gp was tissue independent (maternal BBB IC_{50}: 5.67 ± 1.07 μM vs. BPB IC_{50}: 7.63 ± 3.16 μM).

Conclusions We propose that on deliberate or inadvertent P-gp inhibition, the upper boundary of increase in human brain (or fetal) distribution of lipophilic drugs such as verapamil will be limited by tissue blood flow. This finding provides a means to predict the magnitude of P-gp based drug interactions at the BBB and BPB when only the drug's baseline (i.e in the absence of P-gp inhibition) distribution across these barriers is

available through PET imaging. Our data suggest that P-gp based drug interactions at the human BBB and BPB can be clinically significant, particularly for those P-gp substrate drugs where P-gp plays a significant role in excluding the drug from these privileged compartments.

Key Words: P-glycoprotein; blood-brain barrier; blood-placenta barrier; PET imaging.

INTRODUCTION

Based on rodent studies, the multidrug-resistance protein, P-glycoprotein (P-gp) is considered to be the most important efflux transporter at the blood-brain barrier (BBB), because of its high level of expression at the luminal membrane in brain capillary endothelial cells and its ability to exclude a wide variety of drugs and endogenous substances from the central nervous system (CNS) (*1*). Drug removal protects the CNS from potential neurotoxic effects, but also prevents effective pharmacotherapy of neurological diseases. These rodent studies have also shown that P-gp is highly expressed at the blood-placenta barrier (BPB), where it limits drug delivery to the fetus (e.g. HIV protease inhibitors) (*2*). Alternatively, the barrier may protect the fetus from toxicity of maternal cancer chemotherapy (*3*).

While these rodent studies have demonstrated significant P-gp activity at the BBB and BPB, it is not clear whether the same magnitude of activity is present at the human BBB and BPB. We and others have begun to address this question through measurement of P-gp activity at the human BBB, in the presence and absence of P-gp inhibitors, using various P-gp PET ligands (e.g. [^{11}C]-verapamil), and inhibitors (e.g. cyclosporine A - CsA, tariquidar) (*4-7*). However, for ethical reasons it is not possible to conduct such studies to determine the magnitude of P-gp activity at the human BPB. Moreover, complete inhibition of P-gp at the human BBB (and possibly BPB) with the prototypic P-gp inhibitor, CsA, is not possible due to potential toxicity of this inhibitor when administered at doses necessary to produce such an effect (*8*). Therefore, we conducted [^{11}C]-verapamil dynamic biodistribution studies in a representative animal model, the

pregnant non-human primate, *M. nemestrina*, where it is possible to administer doses of CsA that can completely inhibit P-gp. We published the non-parametric analysis of the results of these whole-body PET imaging studies and showed an increased distribution (as measured by $AUC_{tissue}/AUC_{plasma}$) of [^{11}C]-radioactivity across the BBB and the BPB, with minimal or no changes in distribution of [^{11}C]-radioactivity into other organs such as the maternal liver, spleen and kidneys (*9, 10*). To gain detailed insight into the transport kinetics of [^{11}C]-verapamil radioactivity into macaque tissues with and without P-gp modulation, we analyzed these macaque data using compartmental modeling.

Our human PET study examining inhibition of P-gp at the BBB using [^{11}C]-verapamil as a model P-gp substrate and CsA as a model P-gp inhibitor showed that inhibition of P-gp increased the plasma (or blood) to brain distribution clearance (K_1) of [^{11}C]-verapamil radioactivity rather than the efflux rate constant k_2 (*6*). Moreover, by examining regional P-gp activity at the BBB with [^{11}C]-verapamil and CsA we showed that in the absence of functional P-gp activity (e.g. pituitary), the distributional clearance (K_1) of lipophilic P-gp ligands (such as verapamil) into the brain is limited by delivery (i.e., by regional cerebral blood flow or rCBF) (Q) (*7*). Hence, we proposed that the extraction ratio ($ER= K_1 /Q$) is a better index, compared with K_1, of P-gp activity. In the presence of P-gp, the brain ER of lipophilic ligands like [^{11}C]-verapamil can be low and therefore the blood-flow dependence of tracer distribution (K_1) into the tissue may not be apparent. However, ER of these tracers can increase substantially once P-gp activity is inhibited and consequently, the delivery of P-gp substrates can become perfusion-dependent (*11*). Our ability to completely inhibit P-gp by CsA in the macaque provided us an opportunity

to test the hypothesis that, as is the case in humans, inhibition of P-gp at both the BBB and BPB in the macaque is reported by [^{11}C]-verapamil K_1 (and ER) and not k_2. And, that the upper boundary of K_1 of a lipophilic P-gp ligand (e.g. [^{11}C]-verapamil) is limited by tissue blood flow. Several groups have shown that inhibition of P-gp may be tissue-dependent (*12*). Based on these data, we also asked if CsA inhibition of P-gp at the BBB and the BPB in the macaque is tissue-dependent.

Therefore, the goals of our investigation were three-fold: First, to confirm, through compartmental modeling, that inhibition of P-gp at both the BBB and BPB in the macaque is reported by [^{11}C]-verapamil K_1 and ER and not k_2. Second, to address whether the magnitude of K_1 of a lipophilic drug (e.g. verapamil), in the absence of P-gp function, is limited by tissue blood flow. Third, to determine if the *in vivo* potency (IC_{50}) of P-gp inhibition by CsA at both the BBB and BPB is tissue-dependent.

MATERIALS AND METHODS

PET Imaging

All experimental procedures were approved by the University of Washington Animal Care Committee. The study design (Fig. 1) has been previously published (*9, 10*) and is briefly summarized in Supplemental Methods. Blood and plasma radioactivity from [^{15}O]-water, [^{11}C]-verapamil and [^{11}C]-CO substudies, was measured by a gamma counter (Cobra Counter; Packard Corporation, Meriden, Conn). Plasma [^{11}C]-verapamil and metabolite concentrations were determined by solid phase extraction/HPLC analysis as previously described (*13*).

Model Input Function

Briefly, metabolite assays of plasma after [^{11}C]-verapamil administration resulted in 3 fractions: unchanged verapamil, D617/D717 (formed by dealkylation, henceforth referred to as D617), and other metabolites (formed by N-demethylation, referred to as polar metabolites) (*13*). An exponential function was fitted to these metabolite analysis data to derive the fraction of verapamil, D617 and polar metabolites in arterial plasma (Supplemental Fig. 1A), as described previously (*6*). These analyses were used to provide a metabolite-corrected input function (C_{VER}, unchanged verapamil; $C_{VD,}$ combined activity of verapamil and D617) used for compartmental modeling (Supplemental Fig. 1B). For animals (macaque 4, 5 and 15) where plasma verapamil and metabolites profiles were not determined, a population (mean) metabolite fraction curve, generated from the animals where these curves were available, was used. In pilot studies, the blood:plasma ratio of [^{11}C]-verapamil radioactivity was found to be 1.0.

Hence, input function based on plasma concentration measurements were considered to be equivalent to those based on blood concentration measurements.

Verapamil Compartmental Modeling

Either a 1-compartment (1C) or 2-compartment model (2C) was fitted to the [^{11}C]-verapamil data (*6*). The estimated model parameters included delay, K_1, k_2 in a 1C model and K_1, k_2, k_3 and k_4 in a 2C model. The correction for vascular space activity in brain tissue ROIs and fetal liver ROIs was done by fixing V_b to values measured directly from the tissue blood volume analysis from [^{11}C]-CO PET study, similar to that described previously (*6*). The average V_b for maternal brain was 0.044 ml/g and for fetal liver was 0.10 ml/g.

The time delay between the plasma input function and the tissue activity curve were estimated as part of model optimization. Model parameters were estimated by minimizing the weighted residual sum of the square error (WRRS) between the model solution and the PET measurements, where the residuals were weighted by the best possible weighting scheme, i.e. inverse of constant variance of the tissue activity (i.e., uniform weighting, standard deviation was equal to 5% of average tissue activity) over time (*14*). Goodness of fit of the models to the data was evaluated using the Akaike information criterion (AIC) and Schwarz Criterion (SC), and visual inspection of the model fits and residual plots.

Tissue and plasma area under the concentration-time curves (AUC) of total [^{11}C]-radioactivity were previously reported (*9*). The ratio of the vascular volume-corrected tissue AUC and plasma AUC, designated as AUCR, was calculated and used as an additional index of P-gp activity.

Tissue Blood Flow Estimation

Cerebral and placental blood flow rates were estimated using a one-compartment model as previously described (*6*). Unlike humans, macaques have bidiscoidal placenta composed of primary and secondary discs. Due to limited resolution of the MRI images obtained in the current study, it was not possible to identify both primary and secondary discs on these images. Therefore, placental blood flow was estimated following a manual adjustment of [^{15}O]-water radioactivity in the placenta by a factor of 2, on the basis that primary and secondary discs have similar size and perfusion level (*15*).

Estimation of the Potency of CsA to Inhibit P-gp

Using nonlinear regression (WinNonlin 5.2; Pharsight Corporation, Mountain View, CA), sigmoidal E_{max} model was fitted to the percentage change in ER as a function of increasing inhibitor concentration to estimate the E_{max}, the IC_{50}, and the Hill coefficient (γ).

Statistical Analysis

Data are expressed as mean ± SD. Statistical analysis was performed using GraphPad Prism 5.0 (GraphPad software, La Jolla, CA). Either repeated-measures analysis of variance, followed by Bonferroni's test for multiple comparisons, or the paired *t* test was used for statistical comparison between different kinetic models whenever appropriate. CsA-induced changes in kinetic parameters were evaluated using the paired *t* test. The significance level was set at $P < .05$.

RESULTS

Animals

The demographics of animals are summarized in Table 1 and previously (*9*, *10*). In this data set, we included one animal (macaque 4) which was not previously reported that received a lower CsA infusion rate (6 mg/kg/h). The average CsA blood concentration achieved in this animal was 2.9 μM. In the animals administered 12 mg/kg/h and 24 mg/kg/h, the average CsA blood concentrations achieved were 7.0±2.0 μM (range 4.7-10.0 μM) and 21.6±3.3 μM (range 17.9-25.8 μM) respectively. Of the thirteen pregnant macaques, data from one animal (macaque 10) were excluded from subsequent kinetic analysis due to unusually low arterial blood tracer concentrations but expected tissues concentrations resulting in [^{11}C]-verapamil K_1 estimates that were physiologically unrealistic. For another animal (macaque 12), only maternal brain image data were used because image artifacts due to retained radioactivity in the maternal bladder, did not allow quantification of radioactivity in the fetal liver. Therefore, maternal brain uptake was evaluated in twelve animals and fetal liver radioactivity uptake was evaluated in eleven animals.

Distribution of [^{11}C]-verapamil into maternal brain

We evaluated the performance of 1C and 2C models with respect to their ability to fit [^{11}C]-verapamil radioactivity distribution into the brain before and during inhibition of macaque BBB P-gp with CsA (Fig. 2A shows the profiles for macaque 7), in order to arrive at the most appropriate model to estimate the distribution of [^{11}C]-verapamil radioactivity across the macaque BBB as opposed to the human BBB.

To determine the influence of tracer metabolism on the estimation of kinetic parameters, several arterial input functions including or excluding metabolites were evaluated (see Methods). Based on the comparison of AIC values and visual inspection of the model fit, the 2C model using C_{VER} as the input function with the lowest AIC values was considered to be most appropriate for describing 0-45 min brain dynamic data in macaques (see Supplemental Results). Although the 2C model has the advantage of separating initial transport rates (K_1, k_2) from the rate constants associated with tissue binding (k_3,k_4), the latter were estimated with poor confidence (COV% of the estimates of 30-200%). Therefore, we investigated the 1C model. Similar to our previous kinetic analysis with human [^{11}C]-verapamil brain dynamic data (*6*), we found that a 1C model showed a poor model fit for during-CsA brain time-activity curve from 0 to 45 min (Fig. 2B, the $1C_{45}$ model fit with C_{VER} as the input function is shown). However, 1C model using only the first 9 min of the data yielded good model fits (Fig. 2B, $1C_9$). The COV% of the parameter estimates for $1C_9$ model was 1-5% for K_1 and 4-18% for k_2. Lastly, estimates of K_1 were highly correlated between the $1C_9$ and $2C_{45}$ models ($r = 0.96$, $n = 12$, $p<0.0001$).

Since 1C model appeared to be adequate to assess K_1 using only the first 9 min of the brain uptake curve, we also evaluated the goodness of fit when different input functions were used for this model (Fig. 2D). Arterial input functions including or excluding metabolites had negligible impact on model fits for pre-CsA tissue time-activity curves (Table 2: $p=0.149$ for C_{VER} vs. $C_{VD,}$ $p=0.131$ for C_{TOTAL} vs. $C_{VER,}$ $n=12$). However, during P-gp inhibition by CsA, models using C_{VD} or C_{TOTAL} as the input function

performed slightly (but significantly) better than C_{VER} (Table 2), as assessed by goodness of fit ($p=0.002$ for C_{VER} vs. C_{VD}, $p=0.02$ for C_{TOTAL} vs. C_{VER}). However, neither K_1 values (pre and during-CsA) nor the percentage change in K_1 differed significantly when different input functions were used ($p>0.22$ in all comparisons).

Based on the results of model characterization, as in humans, the 1C model applied to the first 9 min of brain dynamic data using C_{VER} as the input function was the simplest and most parsimonious model to estimate K_1 and k_2 for the distribution of [^{11}C]-verapamil radioactivity across the macaque BBB. As expected, P-gp inhibition during CsA treatment (CsA concentration: 14.3±6.4 μM, range 7.8-21.0 μM) increased K_1 of [^{11}C]-verapamil radioactivity into the brain by 372±193% (range 170-645%, n=6, data from two animals were excluded from this comparison, see below), and K_1 approached rCBF (Q) at maximal inhibition (Table 3). At a lower CsA blood concentration (4.7±1.4 μM, range 2.9-6.2 μM), the observed increase in K_1 was smaller (120±110%, range 28-270%, Table 3). Estimates of cerebral blood flow were 0.92±0.30 and 0.90±0.24 ml/min/g with and without CsA treatment respectively, in animals with higher CsA concentrations (n=6, Table 3). The extraction ratio (i.e. K_1/Q or ER) increased from 0.23±0.05 (n=6) and approached unity (1.0±0.19, n=6) in animals with higher CsA blood concentrations (Table 3). The percentage change in ER of [^{11}C]-verapamil radioactivity into the brain was linearly correlated with percentage change in flow-normalized AUCR (i.e. AUCR/Q) ($r=0.80$, $p=0.002$, Fig. 3A), whereas the correlation between k_2 and AUCR was much weaker ($r=0.14$, $p=0.29$, Fig. 3B). In addition, the change in k_2 (-7 ± 33%, data not

shown) was much less than the ~300% observed in AUCR and was not statistically significant (P>0.05, pre-CsA vs. during-CsA).

Distribution of [^{11}C]-verapamil into fetal liver

In contrast to maternal brain, a shorter duration of the tissue scans up to 9 min for fetal liver was not considered because it failed to estimate the efflux rate constant k_2 with acceptable precision (COV% > 200%). Representative fetal liver time-activity curves for [^{11}C]-verapamil before and during CsA treatment are shown in Fig. 4A. An example of the fit of the 1C model up to 20 min and 45 min of during-CsA dynamic data is shown in Fig. 4B and 4C (also see Supplemental Results).

Despite the difference in the extent of verapamil metabolism at 20 min (~70%) versus 45 min (~85%), the model using C_{VER} as the input function consistently yielded lower AIC values than that of C_{VD} and C_{TOTAL} in describing both pre and during-CsA dynamic feta liver curves (Table 2), and the difference was supported by visual inspection of the model fit (Fig. 4B and 4C). Similar to the brain model, the input function did not impact K_1 estimations. Although truncated fetal liver data set from 0 to 20 min seemed to be adequate to estimate K_1, the estimates for k_2 were associated with a much larger variability (COV% of 20-80%) compared to that of the full-duration data (COV%<20%). Therefore, a 1C model was fitted to the fetal liver data up to 45 min using C_{VER} as the input function to estimate K_1 and k_2 for each animal. P-gp inhibition during CsA treatment (CsA blood concentration: 14.3±6.4 μM, range 7.8-21.0 μM) increased the fetal liver K_1 of [^{11}C]-verapamil radioactivity by 174±75% (range 79%-259%, n=4, data

from three animals were excluded from this comparison, see below) (Table 3). Placental blood flow estimates were 0.84±0.20 and 0.68±0.21 ml/min/g with and without CsA treatment respectively, in animals with higher CsA concentrations (n=4, Table 3). The ER increased from 0.20±0.10 to 0.68±0.36 in animals with higher CsA blood concentrations (n=4, data from three animals were excluded from this comparison, see below) (Table 3). Similar to maternal brain, the change in k_2 (-2 ± 32%, data not shown) was much less than the ~120% difference in fetal liver uptake of radioactivity expressed as AUCR and was not significantly different (p = 0.32) pre-CsA vs. during-CsA. Five out of eleven animals had a negative percentage change in k_2. The percentage change in the ER of [^{11}C]-verapamil radioactivity by the fetal liver was highly correlated with the percentage change in AUCR/Q (r=0.92, p<0.0001, Fig. 3C), whereas the correlation between k_2 and AUCR was weaker (r=0.56, p=0.25, Fig. 3D).

The potency of CsA to inhibit P-gp at the maternal BBB and the BPB

ER was used as a measure of P-gp activity at the BBB and BPB. We observed a bimodal relation in maternal brain and placental P-gp inhibition by CsA. After an initial increase in the ER as the blood CsA concentration increased, further increase in CsA blood concentrations (> 20 µM), resulted in a decrease in the ER (Fig. 5A and 5B). The animals showing this behavior at the higher CsA blood concentrations (> 20 µM), were excluded when estimating the potency of CsA to inhibit P-gp (IC_{50}) using the sigmoidal E_{max} model. Similar CsA IC_{50} values were obtained in different tissues (IC_{50_BBB} = 5.67 ± 1.07 µM versus IC_{50_BPB} = 7.63 ± 3.16 µM). The E_{max} and Hill coefficient (γ) for P-gp inhibition at the BBB (E_{max} = 386 ± 79%; γ = 4.01±

2.09) and BPB (E_{max} = 387 ± 119%; γ = 1.73± 0.74) was not significantly different ($p > 0.05$; Fig. 5A and 5B).

DISCUSSION

We report here for the first time a detailed kinetic analysis of the distribution of verapamil, a P-gp substrate, into the maternal brain and fetal compartment of the pregnant non-human primate, *M. nemestrina*. We and others have previously shown that inhibition of P-gp at the BBB results in increased distributional clearance (K_1) across the human BBB, with little or no change in the efflux rate constant k_2 (*6, 16*). Here we asked if this was true for inhibition of P-gp at the macaque BBB and BPB.

As we have reported before, the vast majority of radioactivity in the fetal compartment was concentrated in the fetal liver, with trace amount in the extrahepatic fetal tissues (*9*). Hence, the fetal liver served as a readily identifiable reporter of placental transfer of [^{11}C]-radioactivity and therefore placental P-gp activity. In contrast, the shape and location of the placenta makes it difficult to reliably identify and quantify tissue radioactivity. Given the high blood content of the placenta (~ 50% of placenta is maternal or fetal blood), reliable estimate of P-gp activity by measuring changes in placental radioactivity was not possible. This limitation may also impact accurate determination of placental blood flow. Nonetheless, our estimates of placental blood flow were comparable to placental perfusion rates obtained by contrast-enhanced ultrasound technique in pregnant macaques (*15*).

As in humans, verapamil is metabolized in macaques and the rate of metabolism is faster but unaffected by gestational age or CsA administration (*9, 10*). To determine the influence of tracer metabolism on kinetic parameter estimation, we compared three

different input functions including C_{TOTAL} (total plasma activity), C_{VER} (unchanged verapamil) and C_{VD} (combined activity of verapamil and D617) for modeling analysis. The rationale for this comparison was that D617 is a P-gp substrate (*17*) and therefore its transport might be kinetically indistinguishable from the transport of verapamil; and at the end of 40 min, a large fraction of the circulating total radioactivity (~35%) is composed of polar metabolites (likely not P-gp substrates) which could diffuse across the BBB (or BPB) as they do in rodents (*18*). We note that significant plasma concentrations of both D617 and polar metabolites are present late after tracer administration and therefore had minimal influence on K_1 estimated using $1C_9$ or $2C_{45}$ models, because K_1 is most influenced by initial tissue concentrations. In contrast, these metabolites could affect estimates of k_2 and tissue binding (k_3 and k_4), which is exactly what we observed (see Table 2). To our surprise, including D617 into the input function did not markedly improve goodness of fit (i.e. AIC and SC) of either $1C_9$ model or $2C_{45}$ model (or $1C_{45}$ for fetal liver), to the pre-CsA and during-CsA brain or fetal time-activity curves. We speculate that in macaques, D617 (or a different metabolite that elutes in the same fractions as D617) does not enter the brain in significant quantity in the presence or absence of P-gp activity. Interestingly, Verbeek et al. have shown that in rodents, [^{11}C]-D617 has lower affinity to P-gp than verapamil (*19*). Taken together, the 1C model with C_{VER} as the input function was identified to be the most appropriate model to explain the observed maternal brain and fetal distribution of [^{11}C]-radioactivity data up to 9 min and 45 min, respectively. In the presence of CsA, consistent with the change in AUCR, K_1 of [^{11}C]-verapamil radioactivity into the maternal brain and the fetal liver was significantly increased while k_2 was not. Based on the above kinetic analyses we conclude that, as is

the case at the human BBB, inhibition of P-gp at the BBB and the BPB in the macaque is reported by an increase in [^{11}C]-verapamil K_1 and not k_2.

The ER provides a measure of the ability of each tissue/organ to extract the tracer and serves as an overall measure of the permeability of the BBB and BPB. The excellent correspondence of the change in verapamil ER following P-gp inhibition to flow-normalized AUCR of maternal brain and fetal liver supports the above argument. As per our hypothesis, when P-gp was completely inhibited by CsA, the ER of [^{11}C]-radioactivity by both the brain and the placenta approximated unity (i.e., K_1 approximated blood flow).

The concept that for lipophilic drugs the upper boundary of K_1 is perfusion is important to allow estimation of the dynamic range in brain exposure following maximal P-gp inhibition at the human BBB. Estimating this dynamic range is important to allow prediction of the magnitude of drug interaction likely to occur at the BBB when P-gp is deliberately or inadvertently inhibited. This can be done only when the upper boundary for the brain distribution of the drug is known. However, currently this upper boundary is not possible to obtain as approved drugs (e.g. CsA) that are P-gp inhibitors cannot be safely administered to completely inhibit P-gp at the human BBB. More selective and potent 2nd and 3rd generation inhibitors of P-gp have been developed (e.g. tariquidar) but are not approved as drugs. Since the lower boundary of brain penetration is dictated by the net permeability of the compound, and the upper boundary dictated by tissue perfusion, probes associated with a higher baseline brain distribution (in the absence of P-gp inhibition) would be expected to be associated with a smaller increase in brain

distribution when P-gp is maximally inhibited compared with drugs with lower baseline brain distribution. For example, the PET ligands, verapamil and N-desmethyl-loperamide (dLOP) are both lipophilic compounds (*20, 21*). However, the differential permeability of these two P-gp probes is evident in the 4-6 fold difference in mean baseline K_1 values (0.035-0.06 ml/min/g for verapamil vs. 0.015 ml/min/g for dLOP in humans; 0.26 ml/min/g for verapamil vs. 0.04 ml/min/g for dLOP in macaques) (*5, 7, 11, 22*). The higher baseline ER in the macaques as compared to that in humans is consistent with the observation that P-gp expression in the macaques is lower (macaque vs. human: 4.71 ± 1.30 vs. 6.06 ± 1.69 fmol/µg protein) (*23, 24*) and rCBF in the pregnant macaques is higher (macaque vs. human: 0.5-1.2 ml/min/g (from this study) vs. 0.3-0.5 ml/min/g (*7, 11*)). Therefore, we predict that dLOP is excluded from the brain by P-gp to a greater extent than verapamil and as a result the increase in brain exposure of dLOP on complete P-gp inhibition would be greater than that of verapamil. Data in the literature support this speculation. Following P-gp inhibition by tariquidar (6 mg/kg), the increase (though not necessarily the maximal increase) in the brain distribution of [^{11}C]-verapamil (reported by K_1) was 2.5-fold, while it was 4-fold for [^{11}C]-dLOP (*5, 11*).

Our previous analysis of these pregnant macaque data using AUCR as an index of P-gp activity concluded that P-gp activity in maternal brain and in the placenta increases with gestational age (*10*). In the present study, using ER as an index of P-gp activity, although there was a similar trend of greater change in brain and placental ER as gestational age increased , none of these between-group differences were statistically significant (for the brain, p=0.178 or the fetal liver, p=0.548). This difference is likely

due to the fact that the ER takes into account the variation in tissue blood flow, whereas the AUCR does not. The concentration-dependent inhibition of P-gp (i.e. increase in [^{11}C]-verapamil ER) by CsA in the brain and the placenta was bimodal. In the lower range of CsA blood concentrations, as expected, the brain and placental ER increased with increase in CsA concentration. However, in the higher range of CsA blood concentrations (> 20 μM), there was a decrease in ER. This bi-modality in CsA inhibition in both tissues suggests that, at the higher CsA blood concentrations, mechanisms other than inhibition of P-gp (e.g. inhibition of influx transporters) are responsible for [^{11}C]-verapamil distribution into these tissues. At the BBB, our assumption of P-gp specificity of verapamil and CsA is not unreasonable given the known functional efflux transporters expressed at this location. *In-vitro* cellular uptake experiments have shown that verapamil is not a substrate for organic anion transporting polypeptide (OATP) brain isoforms 1A2 and 2B1 (personal communication, Dr. Yurong Lai, Pfizer). However, we cannot rule out the possibility that in the placenta, verapamil and CsA could interact through other transporters present there (*25*).

There is increasing evidence that P-gp inhibition appears to be tissue- and species-specific. For example, peripheral P-gp activities in the rodents or humans, such as those in testes and lymphocytes, have different sensitivity to P-gp inhibitors than does P-gp at the BBB (*12, 26*). Although the mechanisms underlying this differential sensitivity are not yet fully understood, the higher expression of P-gp at the BBB compared with other tissues (*27*) is thought to lower the competitive inhibitor concentration at the site of inhibition relative to that in the plasma. As a result higher plasma concentrations are

required to inhibit P-gp at the BBB resulting in higher IC_{50} value. However, in the current study, a more specific measure of P-gp inhibition, namely ER, suggested no distinctive difference in the potency of CsA inhibiton (IC_{50}) of P-gp expressed at the BBB and BPB. When corrected for protein binding, the *in vivo* unbound IC_{50} at the macaque BBB or BPB was in reasonable agreement with *in vitro* IC_{50} (*8*). In addition, the potency of CsA to inhibit macaque P-gp (IC_{50} of 5.67± 1.07 μM) at the BBB is similar to that at the rat BBB (7.2 ± 0.5 μM), suggesting no marked species differences in the ability of CsA to inhibit BBB P-gp in rats and humans. This finding supports our contention that the rat serves as an excellent model to predict P-gp based interactions provided the differences in cerebral blood flow are taken into consideration. On complete inhibition of P-gp, a much more profound increase in brain exposure (~12.9 fold) of verapamil at the rodent BBB (*8, 18*) is likely due to the greater cerebral blood flow in rodents. In small animals, using [^{14}C]-iodoantipyrine autoradiography (*28, 29*), CBF was estimated at 0.5-2.4 ml/min/g across different brain regions. The CBF measured by PET in non-pregnant macaques ranged between 0.3-0.6 ml/min/g (*22*). The mean value of CBF in rodents is almost twice as high as that in macaques, which could explain a 2.5-fold greater effect in the rat in the brain distribution of verapamil as a result of complete P-gp inhibition. Therefore, the rodent P-gp knockout models can overestimate the maximum potential for P-gp-mediated drug interactions at the human BBB.

CONCLUSION

Our results support the hypothesis that, in the absence of functional P-gp, tissue blood flow limits the distributional clearance of [^{11}C]-verapamil across the macaque BBB and BPB. Our results also highlight the importance of utilizing flow-normalized K_1 or ER as a measure of P-gp activity at the BBB and BPB. And, the measure can provide a means to predict the magnitude of P-gp based drug interactions at the BBB and BPB when only the baseline (i.e. in the absence of P-gp inhibition) distribution across these barriers is available through PET imaging. In addition, the *in vivo* potency (IC_{50}) of P-gp inhibition by CsA at both the BBB and BPB is not tissue-dependent. Given that the non-human primate is probably the most relevant model for predicting likely tissue exposure levels in humans, it is reasonable to speculate that P-gp based drug interactions at the human BBB and BPB can be clinically significant, particularly for those P-gp substrate drugs where P-gp plays a significant role in excluding the drug from these privileged compartments. Deliberate circumvention of P-gp (by selective non-toxic inhibitors) at the BBB and BPB could increase drug delivery to the CNS and the fetus, for example in the treatment of brain tumors and fetal arrhythmia (*30*).

ACKNOWLEDGEMENT

This study was supported by National Institute of Health grants U10HD047892 (OPRU network), P50HD044404, GM032165 and RR00166.

DISCLOSURE/CONFLICT OF INTERESTS

The authors declared no conflict of interest.

REFERENCES

1. Eyal S, Hsiao P, Unadkat JD. Drug interactions at the blood-brain barrier: fact or fantasy? *Pharmacol Ther.* 2009;123:80-104.

2. Smit JW, Huisman MT, van Tellingen O, Wiltshire HR, Schinkel AH. Absence or pharmacological blocking of placental P-glycoprotein profoundly increases fetal drug exposure. *J Clin Invest.* 1999;104:1441-1447.

3. Ceckova-Novotna M, Pavek P, Staud F. P-glycoprotein in the placenta: expression, localization, regulation and function. *Reprod Toxicol* 2006;22:400-410.

4. Sasongko L, Link JM, Muzi M, et al. Imaging P-glycoprotein transport activity at the human blood-brain barrier with positron emission tomography. *Clin Pharmacol Ther.* 2005;77:503-514.

5. Bauer M, Zeitlinger M, Karch R, et al. Pgp-mediated interaction between (R)-[11C]verapamil and tariquidar at the human blood-brain barrier: a comparison with rat data. *Clin Pharmacol Ther.* 2012;91:227-233.

6. Muzi M, Mankoff DA, Link JM, et al. Imaging of cyclosporine inhibition of P-glycoprotein activity using 11C-verapamil in the brain: studies of healthy humans. *J Nucl Med.* 2009;50:1267-1275.

7. Eyal S, Ke B, Muzi M, et al. Regional P-Glycoprotein activity and inhibition at the human blood-brain barrier as imaged by positron emission tomography. *Clin Pharmacol Ther.* 2010;87:579-585.

8. Hsiao P, Bui T, Ho RJ, Unadkat JD. In vitro to in vivo prediction of P-glycoprotein based drug interactions at the human and rodent blood-brain barrier. *Drug Metab Dispos.* 2008 36:481-484.

9. Eyal S, Chung FS, Muzi M, et al. Simultaneous PET imaging of P-glycoprotein inhibition in multiple tissues in the pregnant nonhuman primate. *J Nucl Med.* 2009;50:798-806.

10. Chung FS, Eyal S, Muzi M, et al. Positron emission tomography imaging of tissue P-glycoprotein activity during pregnancy in the non-human primate. *Br J Pharmacol.* 2010;159:394-404.

11. Kreisl WC, Liow JS, Kimura N, et al. P-glycoprotein function at the blood-brain barrier in humans can be quantified with the substrate radiotracer 11C-N-desmethyl-loperamide. *J Nucl Med.* 2010;51:559-566.

12. Wagner CC, Bauer M, Karch R, et al. A pilot study to assess the efficacy of tariquidar to inhibit P-glycoprotein at the human blood-brain barrier with (R)-11C-verapamil and PET. *J Nucl Med.* 2009;50:1954-1961.

13. Unadkat J, Chung F, Sasongko L, et al. Rapid solid-phase extraction method to quantify [^{11}C]-verapamil, and its [^{11}C]-metabolites, in human and macaque plasma. *Nucl Med Biol.* 2008;35:911-917.

14. Yaqub M, Boellaard R, Kropholler MA, Lammertsma AA. Optimization algorithms and weighting factors for analysis of dynamic PET studies. *Phys Med Biol.* 2006;51:4217-4232.

15. Keator CS, Lindner JR, Belcik JT, Bishop CV, Slayden OD. Contrast-enhanced ultrasound reveals real-time spatial changes in vascular perfusion during early implantation in the macaque uterus. *Fertil Steril.* 2011;95:1316-1321 e1311-1313.

16. Kannan P, John C, Zoghbi SS, et al. Imaging the function of P-glycoprotein with radiotracers: pharmacokinetics and in vivo applications. *Clin Pharmacol Ther.* 2009;86:368-377.

17. Pauli-Magnus C, von Richter O, Burk O, et al. Characterization of the major metabolites of verapamil as substrates and inhibitors of P-glycoprotein. *J Pharmacol Exp Ther.* 2000;293:376-382.

18. Hsiao P, Sasongko L, Link JM, et al. Verapamil P-glycoprotein transport across the rat blood-brain barrier: cyclosporine, a concentration inhibition analysis, and comparison with human data. *J Pharmacol Exp Ther.* 2006;317:704-710.

19. Verbeek J, Syvanen S, Schuit RC, et al. Synthesis and preclinical evaluation of [(11)C]D617, a metabolite of (R)-[(11)C]verapamil. *Nucl Med Biol.* 2012;39:530-539.

20. Waterhouse RN. Determination of lipophilicity and its use as a predictor of blood-brain barrier penetration of molecular imaging agents. *Mol Imaging Biol.* 2003;5:376-389.

21. Lazarova N, Zoghbi SS, Hong J, et al. Synthesis and evaluation of [N-methyl-11C]N-desmethyl-loperamide as a new and improved PET radiotracer for imaging P-gp function. *J Med Chem.* 2008;51:6034-6043.

22. Liow JS, Kreisl W, Zoghbi SS, et al. P-Glycoprotein Function at the Blood-Brain Barrier Imaged Using 11C-N-Desmethyl-Loperamide in Monkeys. *J Nucl Med.* 2009;50:108-115.

23. Ito K, Uchida Y, Ohtsuki S, et al. Quantitative membrane protein expression at the blood-brain barrier of adult and younger cynomolgus monkeys. *J Pharm Sci.* 2011;100:3939-3950.

24. Uchida Y, Ohtsuki S, Katsukura Y, et al. Quantitative targeted absolute proteomics of human blood-brain barrier transporters and receptors. *J Neurochem.* 2011;117:333-345.

25. Prouillac C, Lecoeur S. The role of the placenta in fetal exposure to xenobiotics: importance of membrane transporters and human models for transfer studies. *Drug Metab Dispos.*38:1623-1635.

26. Choo EF, Kurnik D, Muszkat M, et al. Differential in vivo sensitivity to inhibition of P-glycoprotein located in lymphocytes, testes, and the blood-brain barrier. *J Pharmacol Exp Ther* 2006;317:1012-1018.

27. Tachibana T, Kitamura S, Kato M, et al. Model analysis of the concentration-dependent permeability of P-gp substrates. *Pharm Res.* 2010;27:442-446.

28. Nakao Y, Itoh Y, Kuang TY, Cook M, Jehle J, Sokoloff L. Effects of anesthesia on functional activation of cerebral blood flow and metabolism. *Proc Natl Acad Sci U S A.* 2001;98:7593-7598.

29. Ohno K, Pettigrew KD, Rapoport SI. Local cerebral blood flow in the conscious rat as measured with 14C-antipyrine, 14C-iodoantipyrine and 3H-nicotine. *Stroke.* 1979;10:62-67.

30. Maeno Y, Hirose A, Kanbe T, Hori D. Fetal arrhythmia: prenatal diagnosis and perinatal management. *J Obstet Gynaecol Res.* 2009;35:623-629.

TABLE 1 Demographics of Pregnant, Non-human Primates at Time of PET Study

CsA dose	**12 mg/kg/h**			**24 mg/kg/h**			
Study No.	**Gestational Age (days)**	**Age(y)**	**Body weight (kg)**	**Study No.**	**Gestational Age (days)**	**Age(y)**	**Body weight (kg)**
5	81	14.5	7.4	6	71	9.7	7.7
14	66	9	7.3	8	72	12.5	9.1
15	55	7.02	7.2	10	96	9.5	8.7
7	159	14.5	10.3	12	85	8	6.8
17	138	8	9.3	11	155	12.5	8.2
19	145	8.7	7.6	13	155	8	7.6
4*	122	7.3	9.8				

Full term for *M. nemestrina* is ~172 days. CsA, cyclosporine A. * CsA dose for this animal was 6 mg/kg/h.

TABLE 2 Parameter Estimates and AIC Values When a One-Tissue (1C) Model was Fitted to the [^{11}C]-verapamil Dynamic Biodistribution Data

	K_1 (mL · min^{-1} · g^{-1})		k_2 (min^{-1})		AIC		paired *t*-test comparisons of AIC values (p-value) **		
Input function	Pre CsA	During CsA	Pre CsA	During CsA	Pre CsA	During CsA	Pre CsA	During CsA	Comparisons
Maternal Brain* (n=12)									
C_{VER}	0.264 ± 0.116	0.777 ± 0.196	0.119 ± 0.034	0.084 ± 0.027	41.9±20.2	-1.14 ± 10.63	0.149	0.002	C_{VER} vs. C_{VD}
C_{VD}	0.263 ± 0.116	0.791± 0.178	0.141 ± 0.050	0.09 ± 0.036	41.5±19.6	-5.64 ± 8.88	0.251	0.631	C_{VD} vs. C_{TOTAL}
C_{TOTAL}	0.223 ± 0.079	0.854 ± 0.183	0.162 ± 0.048	0.140 ± 0.034	38.2±17.4	-6.16 ± 9.84	0.131	0.021	C_{TOTAL} vs. C_{VER}
Fetal Liver^{+} (n=11)									
C_{VER}	0.206 ± 0.121	0.413 ± 0.175	0.035 ± 0.020	0.033 ± 0.009	173.5±33.5	153.9±36.8	0.035	0.11	C_{VER} vs. C_{VD}
C_{VD}	0.232 ± 0.171	0.444± 0.206	0.074 ± 0.040	0.086 ± 0.025	187.6±32.7	173.3±39.3	0.02	0.013	C_{VD} vs. C_{TOTAL}
C_{TOTAL}	0.207 ± 0.068	0.452 ± 0.179	0.099 ± 0.048	0.105 ± 0.028	189.7±34.7	175.9±38.5	0.024	0.04	C_{TOTAL} vs. C_{VER}

Data are given as mean ± SD. *9 min tissue-activity data $^{+}$45 min tissue-activity data

**Comparison of the SC values resulted in similar p values.

TABLE 3 [^{11}C]-Verapamil radioactivity K_1, Q and ER Estimates Grouped by CsA Blood Concentration

CsA Conc. (μM)	**No. of**	**Before CsA**			**During CsA**			**% Change due to CsA**		
Mean ± SD (Range)	**Animals**	K_1	Q	ER	K_1	Q	ER	K_1	Q	ER
Maternal brain										
4.7±1.4 (2.9-6.2)	4	0.35±0.19	0.74±0.14	0.49±0.24	0.64±0.18	0.83±0.21	0.84±0.40	120±110%	12±8%	99±98%
14.3±6.4 (7.8-21.0)	6	0.20±0.07	0.92±0.30	0.23±0.05	0.87±0.20	0.90±0.24	1.0±0.19	372±193%	0±20%	361±123%
Fetal Liver										
4.7±1.4 (2.9-6.2)	4	0.17±0.09	0.67±0.22	0.28±0.19	0.36±0.18	0.72±0.25	0.55±0.33	115±28%	9±17%	102±54%
14.3±6.4 (7.8-21.0)	4	0.15±0.03	0.84±0.20	0.20±0.10	0.43±0.17	0.68±0.21	0.68±0.36	174±75%	-18±22%	238±61%

Data are given as mean ± SD. K_1 and Q are in units of $mL \cdot min^{-1} \cdot g^{-1}$

FIGURE LEGENDS

FIGURE 1. Schematic of the PET protocol.

FIGURE 2. Brain time-activity curves for [^{11}C]-verapamil before and during CsA treatment. A) Representative curves illustrate the difference in brain uptake of [^{11}C]-radioactivity before and during administration of CsA in non-human primates (macaque 7 as an example). B) A one-tissue compartment (1C) or a two-tissue compartment (2C) model was fitted to 45 min ($1C_{45}$ and $2C_{45}$) or the initial 9 min ($1C_9$) of during-CsA brain time-activity curve (C_T). C_{VER} was used as the arterial input function. C) A 1C model was fitted to the initial 9 min of during-CsA brain time-activity curve (C_T). C_{VER}, C_{VD} or C_{TOTAL} were used as the arterial input functions.

FIGURE 3. The percentage change in the brain ER of [^{11}C]-verapamil radioactivity A) was linearly correlated with percentage change in flow-normalized brain AUCR (AUCR/Q) ($r=0.80$, $p=0.002$), whereas B) the correlation between brain k_2 and AUCR was much weaker ($r=0.14$, $p=0.29$). Similarly, the percentage change in fetal liver ER of [^{11}C]-verapamil radioactivity C) was highly correlated with percentage change in fetal liver AUCR/Q ($r=0.92$, $p<0.0001$), whereas D) the correlation between fetal liver k_2 and AUCR was weaker ($r=0.56$, $p=0.25$).

FIGURE 4. Fetal liver time-activity curves for [^{11}C]-verapamil before and during CsA treatment. A) Representative curves illustrate the difference in fetal liver uptake of [^{11}C]-

radioactivity before and during the administration of CsA in non-human primates (macaque 13 is shown as an example). B) A 1C model was fitted to during-CsA time-activity curve (C_T) up to 20 min. C_{VER}, C_{VD} or C_{TOTAL} were used as the model input functions. C) A 1C model was fitted to during-CsA time-activity curve (C_T) up to 45 min. Model input functions used were similar to those in panel B.

FIGURE 5. Inhibition of P-gp (as measured by ER) at the BBB (A) and BPB (B) increased as CsA blood concentration increased up to ~20 µM. Future increases in CsA blood concentration resulted in a decrease in ER. Therefore, when estimating the potency of CsA to inhibit P-gp (IC_{50}) using the sigmoidal E_{max} model, data points shown as open circles were excluded. The potency (IC_{50}) for P-gp inhibition at the BBB and BPB were similar (IC_{50_BBB}= 5.67 ± 1.07 µM versus IC_{50_BPB}= 7.63 ± 3.16 µM), as was the E_{max} for P-gp inhibition (E_{max_BBB}= 386 ± 79% versus E_{max_BPB}= 387 ± 119%). Estimated Hill coefficient (γ) for P-gp inhibition at the BBB and BPB were γ =4.01± 2.09 and 1.73± 0.74 respectively. Filled circles: observed data points; Open circles: data points excluded from this analysis; Solid line: predicted values.

FIGURE 1.

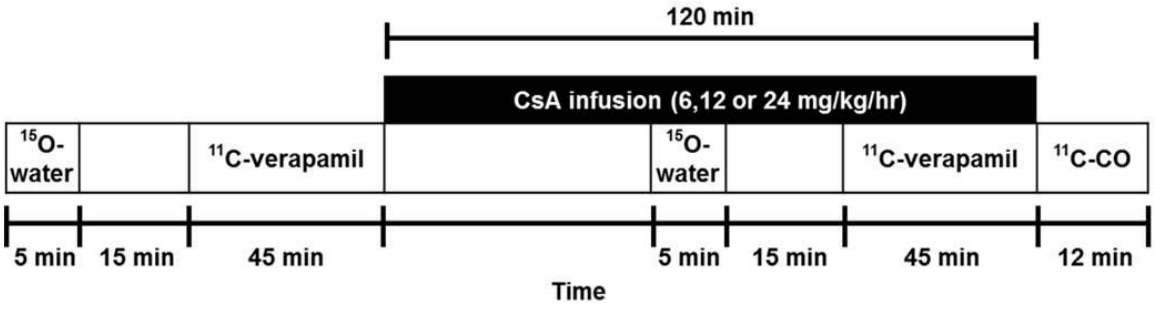

Tracer	Route of administration	Time frames of image acquisition (seconds)	Arterial blood sampling (after tracer injection)
^{15}O-water (45-76 MBq/kg)	Intravenous bolus	15 x 3, 10 x 6, 21 x 9	15, 30, 45, 60, 90, 120, 180, 300 s
^{11}C-verapamil (14-75 MBq/kg)	Intravenous infusion over 1 min	12 x 10, 6 x 30, 4 x 60, 2 x 180, 6 x 300	0, 15, 30, 45, 60 s, 2, 4, 8, 14, 20, 30, 40 min
^{11}C-CO (7-93 MBq/kg)	Inhalation	240, 480	6, 8, 10 min

FIGURE 2.

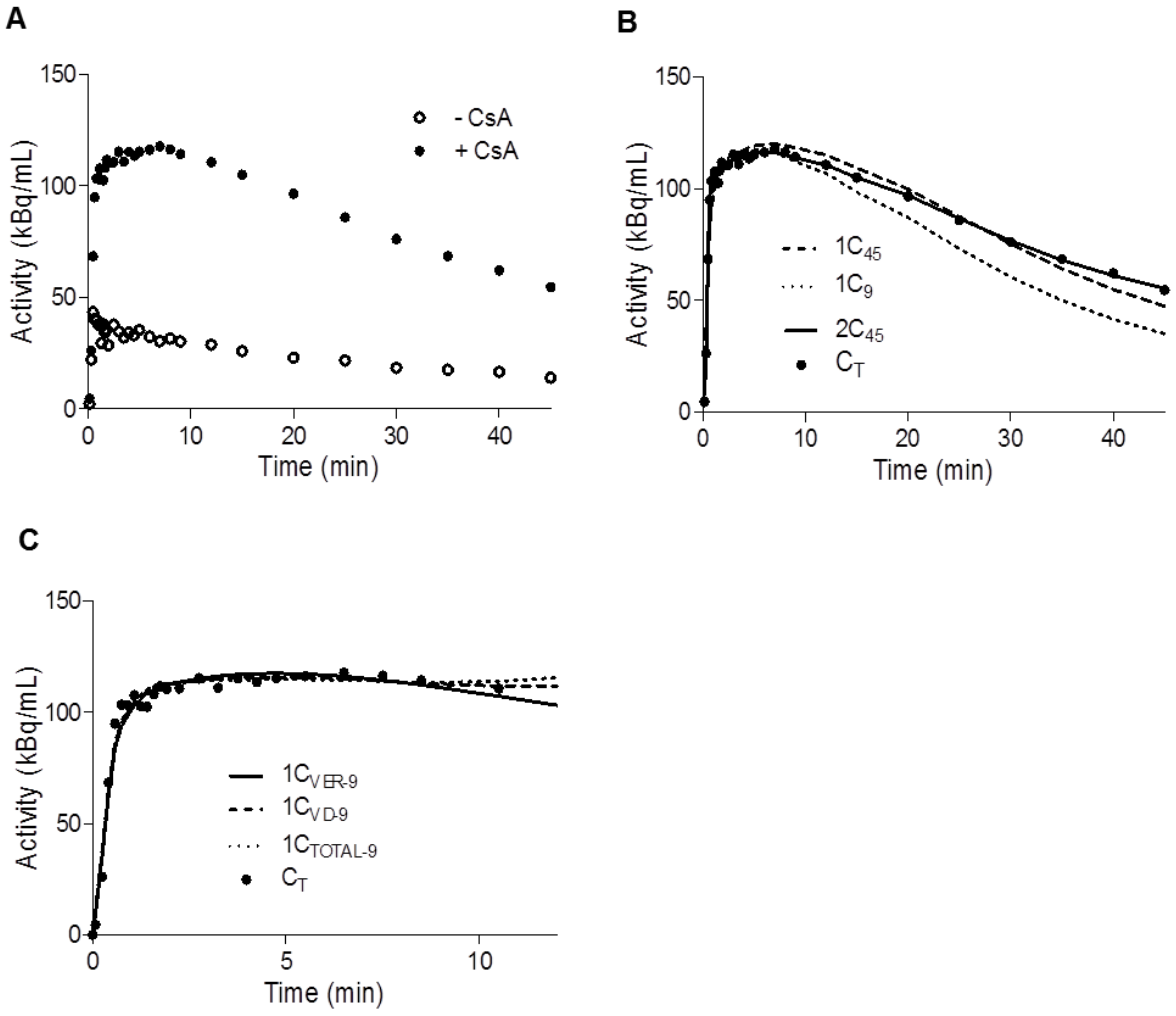
A
150
100
50
0
Activity (kBq/mL)
0
10
20
30
40
Time (min)
- CsA
+ CsA
B
150
100
50
0
Activity (kBq/mL)
0
10
20
30
40
Time (min)
1C45
1C9
2C45
CT
C
150
100
50
0
Activity (kBq/mL)
0
5
10
Time (min)
1CVER-9
1CVD-9
1CTOTAL-9
CT

FIGURE 3.

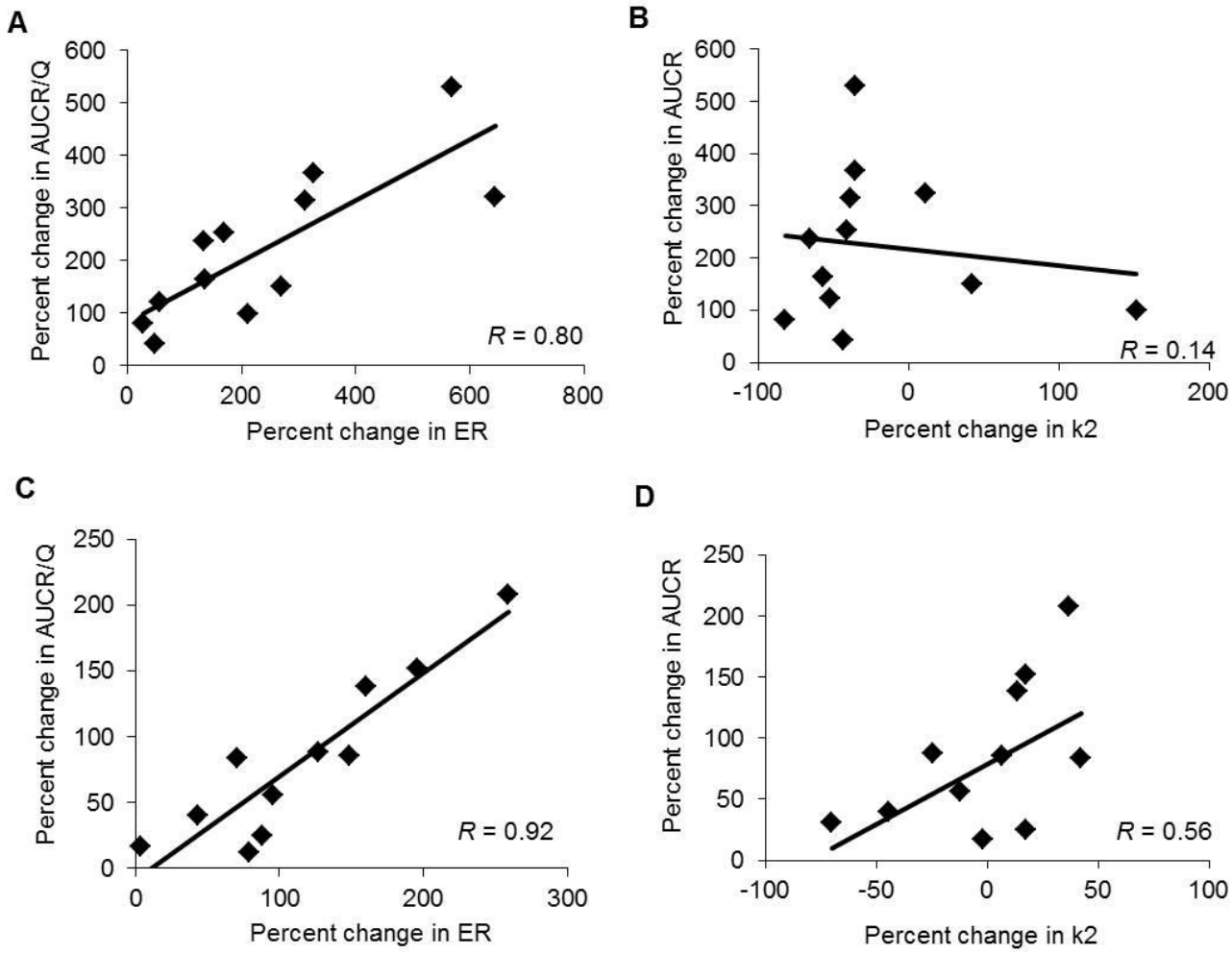
A
Percent change in AUCR/Q
Percent change in ER
R = 0.80
B
Percent change in AUCR
Percent change in k2
R = 0.14
C
Percent change in AUCR/Q
Percent change in ER
R = 0.92
D
Percent change in AUCR
Percent change in k2
R = 0.56

FIGURE 4.

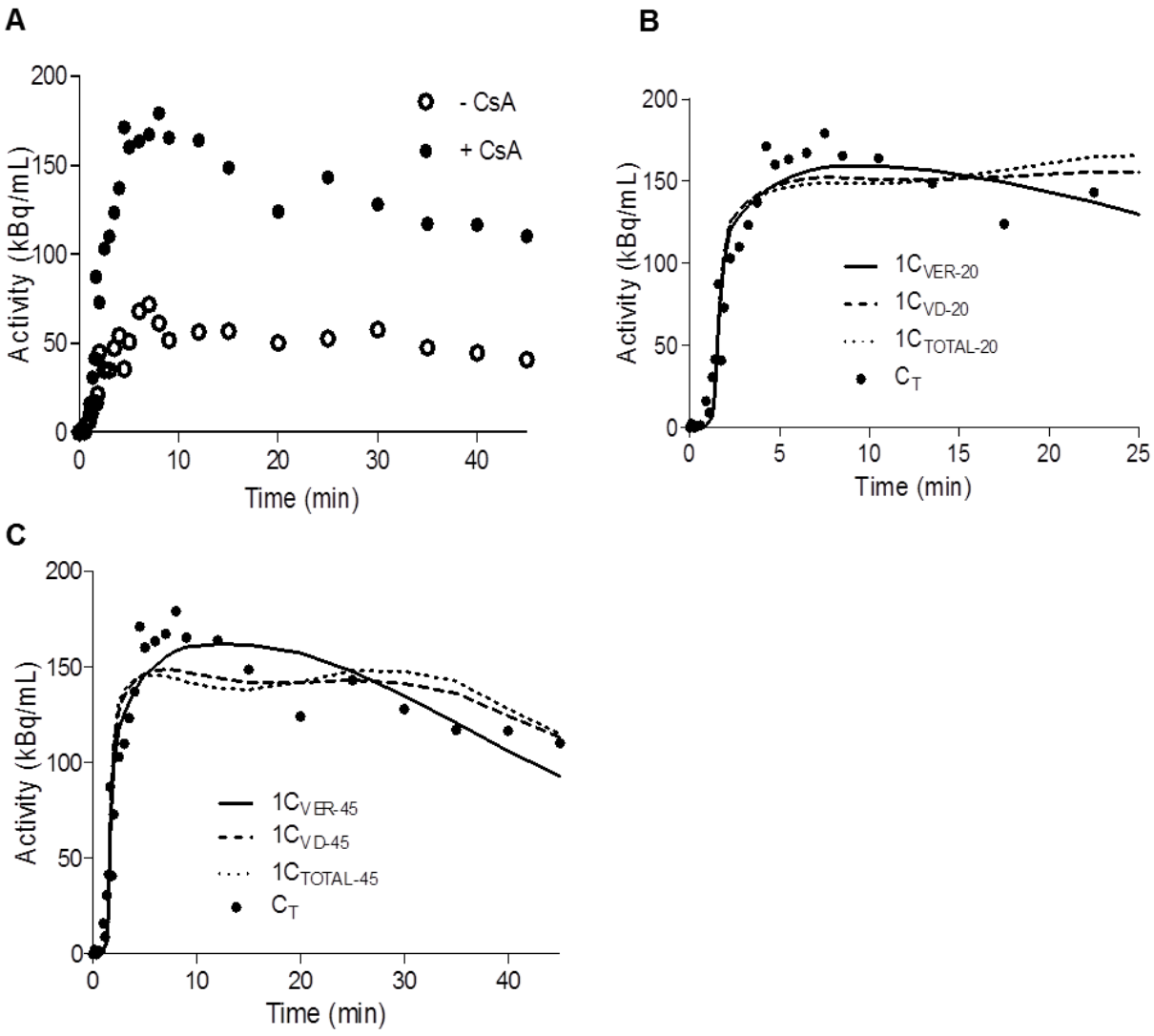
A
200
150
100
50
0
Activity (kBq/mL)
0
10
20
30
40
Time (min)
- CsA
+ CsA
B
200
150
100
50
0
Activity (kBq/mL)
0
5
10
15
20
25
Time (min)
1C VER-20
1C VD-20
1C TOTAL-20
C T
C
200
150
100
50
0
Activity (kBq/mL)
0
10
20
30
40
Time (min)
1C VER-45
1C VD-45
1C TOTAL-45
C T

FIGURE 5.

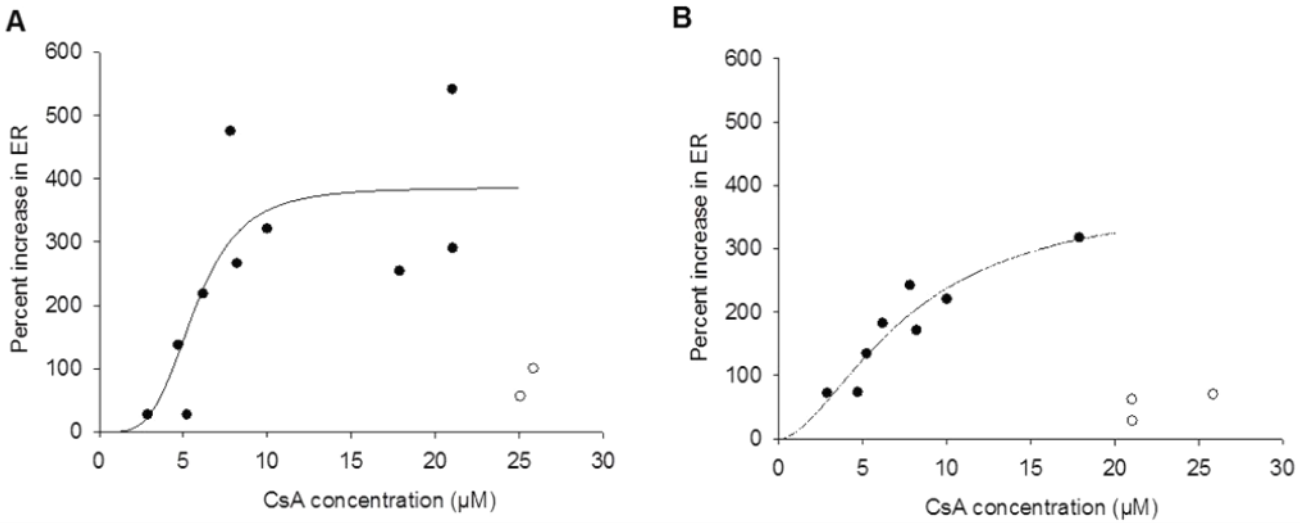
A
B
Percent increase in ER
CsA concentration (μM)
0
100
200
300
400
500
600
0
5
10
15
20
25
30

SUPPLEMENTAL FIGURE 1.

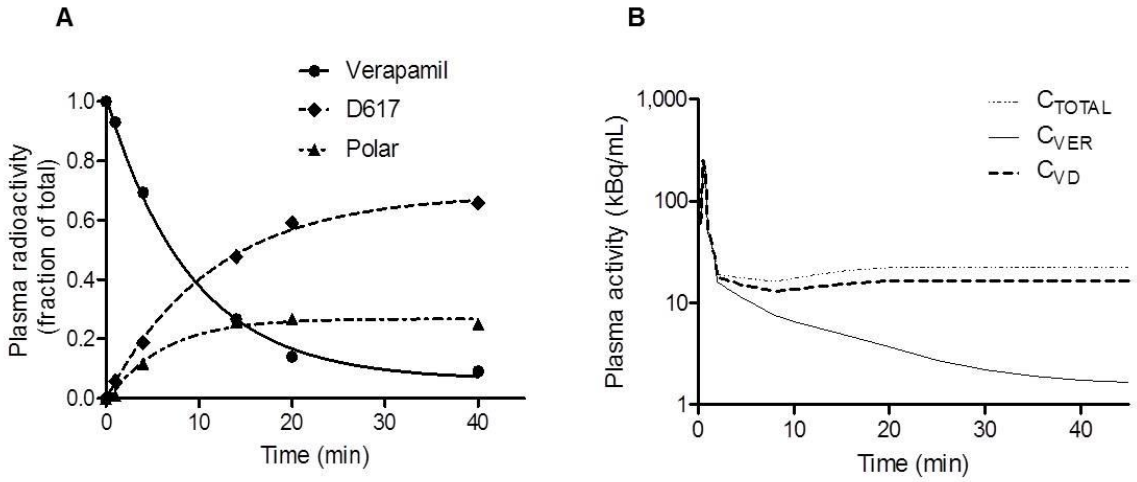

SUPPLEMENTAL FIGURE 2.

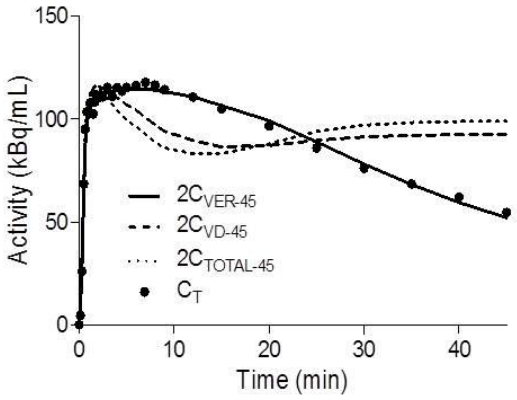

Conclusion Chapter

Conclusion

Modeling and simulation of PK and PD of drugs in pregnancy is well recognized as an unmet need in the scientific community. The long-term objective of my research proposal was to quantitatively predict maternal-fetal drug disposition during pregnancy, utilizing PBPK modeling and simulation based on mechanistic studies. There have been significant developments in PBPK models for the average or special populations over the past decade, as well as our understanding of the profound physiological and metabolic changes which occur during pregnancy. The interdisciplinary collaboration between the University of Washington, the Food and Drug Administration and Simcyp Limited has presented me a unique opportunity to integrate available knowledge and prior information together with experimental data into a generic and flexible PBPK model to predict maternal exposure to drugs (and their metabolites) during the course of pregnancy. To the best of our knowledge, the proposed PBPK model for the pregnant population is the first generic (not drug or gestational-age specific) PBPK model to allow evaluation of different dosing regimens of drugs, cleared via a single or multiple P450 enzyme(s), throughout pregnancy. To date, we have expanded, refined and validated an established PBPK model by predicting the disposition of drugs cleared primarily by CYP3A (midazolam, nifedipine, indianvir), CYP1A2 (theophylline), CYP2D6 (metoprolol, paroxetine, dextromethorphan, clonidine), CYP2C9 (phenytoin), or those cleared by multiple CYP enzymes (glyburide, methadone). As described in great detail in chapters 1-3, we populated the PBPK model with probe drug data delineating the hepatic CYP enzyme activity during pregnancy, and validated the model performance for non-probe drugs associated with well-characterized ADME characteristics and cleared primarily by the same CYP enzyme as the probe drug. The refined PBPK model

assuming 99% induction of hepatic CYP3A during the third trimester (T_3) based on midazolam data, quantitatively predicted T_3- induced change in the disposition of other CYP3A-metabolized drugs, nifedipine and indinavir (chapter 1). The PBPK model assuming 65% suppression of hepatic CYP1A2 during T_3 based on caffeine data, successfully predicted theophylline disposition during T_3 (chapter 2). We defined the range of CYP2D6 induction during T_3 to be 100% to 200% through modeling metoprolol, paroxetine and dextromethorphan disposition during pregnancy. (chapter 2). Due to lack of probe drug study for CYP2B6, we incorporated CYP2B6 induction by estradiol based on *in vitro* to *in vivo* extrapolation. The expanded PBPK model assumed 1) hepatic CYP2B6 induction of 40% and 90% during T_2 and T_3, respectively; 2) hepatic CYP2C9 (based on phenytoin data) induction of 50% and 60% during T_2 and T_3, respectively; 3) hepatic CYP2C19 (based on proguanil data) suppression of 62% and 68% during T_2 and T_3, respectively. Based on the expanded model, the disposition of methadone (cleared by CYP3A, 2B6 and 2C19) and glyburide (cleared by CYP3A, 2C9 and 2C19) during T_2 and/or T_3 was successfully predicted (chapter 3).

Moreover, our PBPK approach to modeling drug disposition in pregnancy allowed us to bridge knowledge gaps that are not currently addressed or are difficult to test through clinical studies in this special population. For example, discerning the site (hepatic, intestinal, or both) of CYP3A induction in pregnancy. For drugs predominantly cleared by CYP3A, the site of CYP3A induction during pregnancy is expected to have differential impact on pregnancy induced change in AUC. Our sensitivity analysis suggests that the observed change in systemic exposure to midazolam, nifedipine and indinavir was mostly driven by an induction of hepatic 3A activity, with modest to little contribution from intestinal 3A induction. Based on this finding, and our observation that

hepatic, but not intestinal, luciferase activity is increased by pregnancy in the CYP3A4-promoter-luciferase transgenic mice, we propose that human pregnancy induces hepatic, and not intestinal, CYP3A activity. Further, this research helps shed light on knowledge gaps that warrant further studies. For example, there are certain limitations of published CYP2D6 probe drug studies including limited sample size, lack of concentration-time profile, or the use of urinary metabolic ratio as an index of enzyme activity. To definitively assess the magnitude of CYP2D6 induction during pregnancy, we propose that a PK study with the most sensitive 2D6 probe dextromethorphan, where the plasma concentration-time profile of dextromethorphan as opposed to single time-point concentration is measured, be conducted during various stages of pregnancy and postpartum. In the absence of such data, we can only conclude that the CYP2D6 induction during T_3 ranges from 100% to 200%. Because methadone CL_{ORAL} reports the change in multiple clearance pathways, it might not be a sensitive reporter of *in vivo* CYP2B6 activity. Future studies with CYP2B6 probe drug bupropion during various stages of pregnancy and postpartum are highly desirable to further refine the *in vivo* fold-induction of CYP2B6 predicted from *in vitro* data.

To fully populate the PBPK model, more probe drug studies to delineate the longitudinal changes of other CYPs and UGTs are warranted. Examples may include omeprazole, repaglinide and chlorzoxazone PK studies to assess the effect of pregnancy on CYP2C19, 2C8 and CYP2E1 activity *in vivo*. For the majority of the probe drug studies conducted in pregnant women, data are obtained only in the third trimester. This issue stems from the limitation that some probe drugs cannot be safely administered to pregnant women during early gestation if they are not used for therapeutic purposes. We have proposed an alternative approach to predict the magnitude of

enzyme induction or suppression in earlier trimesters, through mechanistic studies with human hepatocytes incubated with corresponding concentration of specific hormones in plasma observed during each trimester. This approach has been shown to successfully predict CYP3A and CYP2B6 induction in the third trimester, and can be expanded to study other CYP isoforms. Currently, we have incorporated into the PBPK model known knowledge of pregnancy effect on renal transporter organic cation transporter 2 and renal P-glycoprotein, based on metformin and digoxin data. Future studies should extend to other important renal transporters such as organic anion transporters. Understanding the effect of pregnancy on the expression/activity of hepatic transporters, organic anion-transporting polypeptide 1B1 and 1B3 (OATP), is important when uptake of the drug into hepatocytes is the rate-limiting step of its clearance. Statins are probe drugs for OATPs but they are contraindicated in pregnant women. In future, newly-identified probe drugs for OATPs that are not contraindicated in pregnancy should be evaluated.

Further expansion of the established PBPK model for the pregnant population can consist of the following aspects. First, the pregnancy effect on UGT1A1, 1A4 and 2B7 can be incorporated into the existing model, when appropriate scaling factors for UGT enzymes in hepatic and extra-hepatic tissues becomes available. Population variability in the predicted drug exposure measures can also be incorporated, when necessary data on the variability (and covariance) in the system- and drug-dependent parameters are better defined. Eventually, the creation and validation of a "virtual pregnant population" integrated into a predictive PBPK platform can be used, prior to clinical investigations, to evaluate different dosing regimens in pregnant women for drugs (and their metabolites) cleared primarily via single or mixed CYP or UGT metabolism.

The coupled maternal-fetal physiology imposes additional concerns for both efficacy and safety of treatment. Recommendation of dose adjustment in this population should also be carefully evaluated in terms of assessing the risk of fetal exposure to drugs administered to the mother. Fetal exposure to drugs not only depends on maternal pharmacokinetics, but also depends on placental passage of drugs. My research focused on understanding the contribution of the placental efflux transporter, P-glycoprotein (P-gp), to drug distribution into the fetus *in vivo*, as a first step towards quantitative prediction of fetal-to-maternal drug concentration ratios. Only recently it has become possible to evaluate P-gp activity *in vivo* when positron emission tomography (PET) imaging probe [^{11}C]-verapamil was developed. Although the noninvasive measurement by PET of placental P-gp function in humans is not possible due to fetal radiation exposure, the pregnant macaque provides a physiologically relevant model for studying the contribution of P-gp to drug distribution into the fetus. We applied compartmental modeling to analyze the dynamic whole-body biodistribution data obtained in pregnant macaques (chapter 4). Our results support the hypothesis that, in the absence of functional P-gp, tissue blood flow limits the distributional clearance of [^{11}C]-verapamil across the macaque blood-brain barrier and blood-placental barrier. Our results also highlight the importance of utilizing flow-normalized K_1 or extraction ratio as a measure of P-gp activity expressed in the brain and the placenta. Using this index of P-gp activity, although we observed a trend of greater change in brain and placental extraction ratio as gestational age increased from mid-gestation to late-gestation , the differences were not statistically significant. This indicates P-gp activity in maternal brain and in the placenta does not appear to increase with gestational age in pregnant macaques. The implication of this work is that when modeling maternal-to-fetal transfer of drugs, P-gp mediated efflux clearance of drugs can be considered to be independent of gestational age, provided that macaque

data is representative of human data. The latter can be confirmed in the near future, by quantifying the absolute quantity of P-gp in human placental tissue of various gestational ages, owing to the recent advancement in LC-MS methods for protein quantification.

Increasing knowledge base of placental transport of drugs would be especially helpful in the utility of PBPK models in further exploration of fetal exposure *in silico.* Specifically, we have proposed to estimate the net *in vivo* maternal-fetal placental clearance of the drug via placental transporters involved by scaling *in vitro* transport data to the whole organ level. The current maternal PBPK model includes a simple fetal distribution model with no fetal elimination. It can be extended to a more comprehensive fetal model populated with literature values of fetal physiological parameters. The initial goal of fetal model assessment can be modest, that is, to accurately classify drugs into three categories: low (<0.2), intermediate (0.2-0.6) or high (>0.6) fetal-to-maternal concentration ratios at steady-state.

In conclusion, we demonstrated through this research, that by integrating prior physiological knowledge, preclinical data and clinical data to quantify anticipated PK changes of drugs during pregnancy, the PBPK approach allows extrapolation beyond model drugs studied to other drugs with well-characterized ADME characteristics. Conducting the trial *in silico* before its execution *in viv*o can also be helpful in optimizing design of "first in pregnancy" PK study including prioritizing study period (first, second and third trimester), sample size and dosage selection. The established maternal PBPK model has the potential to be expanded to assess fetal exposure to drugs administered to the mother. Using such systems pharmacology approach can potentially allow us to identify drugs whose maternal-fetal PK, and therefore their efficacy and toxicity for

the mother and/or the fetus, are likely to be affected, as well as predict the extent of this effect by pregnancy. Ultimately, the generated information will support the design of rational dosing regimen for pregnant women and their unborn child.